НАЦІОНАЛЬНА АКАДЕМІЯ НАУК УКРАЇНИ
НАВЧАЛЬНО-НАУКОВИЙ КОМПЛЕКС
«ІНСТИТУТ ПРИКЛАДНОГО СИСТЕМНОГО АНАЛІЗУ»
НАЦІОНАЛЬНОГО ТЕХНІЧНОГО УНІВЕРСИТЕТУ УКРАЇНИ
«КИЇВСЬКИЙ ПОЛІТЕХНІЧНИЙ ІНСТИТУТ ІМЕНІ ІГОРЯ СІКОРСЬКОГО»

СИСТЕМНІ ДОСЛІДЖЕННЯ ТА ІНФОРМАЦІЙНІ ТЕХНОЛОГІЇ

МІЖНАРОДНИЙ НАУКОВО–ТЕХНІЧНИЙ ЖУРНАЛ

№ 3 2024

ЗАСНОВАНО У ЛИПНІ 2001 р.

АДРЕСА РЕДАКЦІЇ:
03056, м. Київ,
просп. Перемоги, 37, корп. 35,
ННК «ІПСА» КПІ ім. Ігоря Сікорського
Тел.: **204-81-44**; факс: **204-81-44**
E-mail: journal.iasa@gmail.com
http://journal.iasa.kpi.ua

У номері:

NATIONAL ACADEMY OF SCIENCES OF UKRAINE
EDUCATIONAL AND SCIENTIFIC COMPLEX
«INSTITUTE FOR APPLIED SYSTEM ANALYSIS»
OF THE NATIONAL TECHNICAL UNIVERSITY OF UKRAINE
«IGOR SIKORSKY KYIV POLYTECHNIC INSTITUTE»

SYSTEM RESEARCH AND INFORMATION TECHNOLOGIES

INTERNATIONAL SCIENTIFIC AND TECHNICAL JOURNAL

№ 3 2024

IT IS FOUNDED IN JULY 2001

THE EDITION ADDRESS:

03056, Kyiv,
av. Peremogy, 37, building 35,
Institute for Applied System Analysis
at the Igor Sikorsky Kyiv Polytechnic Institute
Phone: **204-81-44**; Fax: **204-81-44**
E-mail: journal.iasa@gmail.com
http://journal.iasa.kpi.ua

In the issue:

Шановні читачі!

Навчально-науковий комплекс «Інститут прикладного системного аналізу» Національного технічного університету України «Київський політехнічний інститут імені Ігоря Сікорського» видає міжнародний науково-технічний журнал

«СИСТЕМНІ ДОСЛІДЖЕННЯ ТА ІНФОРМАЦІЙНІ ТЕХНОЛОГІЇ».

Журнал публікує праці теоретичного та прикладного характеру в широкому спектрі проблем, що стосуються системних досліджень та інформаційних технологій.

Провідні тематичні розділи журналу:

Теоретичні та прикладні проблеми і методи системного аналізу; теоретичні та прикладні проблеми інформатики; автоматизовані системи управління; прогресивні інформаційні технології, високопродуктивні комп'ютерні системи; проблеми прийняття рішень і управління в економічних, технічних, екологічних і соціальних системах; теоретичні та прикладні проблеми інтелектуальних систем підтримання прийняття рішень; проблемно і функціонально орієнтовані комп'ютерні системи та мережі; методи оптимізації, оптимальне управління і теорія ігор; математичні методи, моделі, проблеми і технології дослідження складних систем; методи аналізу та управління системами в умовах ризику і невизначеності; евристичні методи та алгоритми в системному аналізі та управлінні; нові методи в системному аналізі, інформатиці та теорії прийняття рішень; науково-методичні проблеми в освіті.

Головний редактор журналу — науковий керівник ННК «ІПСА» КПІ ім. Ігоря Сікорського, академік НАН України Михайло Захарович Згуровський.

Журнал «Системні дослідження та інформаційні технології» включено до переліку наукових фахових видань України (категорія «А»).

Журнал «Системні дослідження та інформаційні технології» входить до таких наукометричних баз даних: Scopus, EBSCO, Google Scholar, DOAJ, Index Copernicus, реферативна база даних «Україніка наукова», український реферативний журнал «Джерело», наукова періодика України.

Статті публікуються українською та англійською мовами.

Журнал рекомендовано передплатити. **Наш індекс 23918.** Якщо ви не встигли передплатити журнал, його можна придбати безпосередньо в редакції за адресою: 03056, м. Київ, просп. Перемоги, 37, корп. 35.

Завідувачка редакції **С.М. Шевченко**
Редакторка **Р.М. Шульженко**
Молодша редакторка **Л.О. Тарин**
Комп'ютерна верстка, дизайн **А.А. Патіохи**
Рішення Національної ради України з питань телебачення і радіомовлення №1794 від 21.12.2023. Ідентифікатор медіа R30-02404

Підписано до друку 28.09.2024. Формат 70×108 1/16. Папір офс. Гарнітура Times.
Спосіб друку – цифровий. Ум. друк. арк. 14,411. Обл.-вид. арк. 28,56. Наклад 94 пр. Зам. № 11/04

Національний технічний університет України
«Київський політехнічний інститут імені Ігоря Сікорського»
Свідоцтво про державну реєстрацію: ДК № 5354 від 25.05.2017 р.
просп. Перемоги, 37, м. Київ, 03056.
ФОП Пилипенко Н.М., вул. Мічуріна, б. 2/7, м. Київ, 01014. тел. (044) 361 78 68.
Виписка з Єдиного державного реєстру № 2 070 000 0000 0214697 від 17.05.2019 р.

Dear Readers!

Educational and Scientific Complex «Institute for Applied System Analysis» of the National Technical University of Ukraine «Igor Sikorsky Kyiv Polytechnic Institute» is published of the international scientific and technical journal

«SYSTEM RESEARCH AND INFORMATION TECHNOLOGIES».

The Journal is printing works of a theoretical and applied character on a wide spectrum of problems, connected with system researches and information technologies.

The main thematic sections of the Journal are the following:

Theoretical and applied problems and methods of system analysis; theoretical and applied problems of computer science; automated control systems; progressive information technologies, high-efficiency computer systems; decision making and control in economic, technical, ecological and social systems; theoretical and applied problems of intellectual systems for decision making support; problem- and function-oriented computer systems and networks; methods of optimization, optimum control and theory of games; mathematical methods, models, problems and technologies for complex systems research; methods of system analysis and control in conditions of risk and uncertainty; heuristic methods and algorithms in system analysis and control; new methods in system analysis, computer science and theory of decision making; scientific and methodical problems in education.

The editor-in-chief of the Journal is scientific director of the Institute for Applied System Analysis at the Igor Sikorsky Kyiv Polytechnic Institute, academician of the NASU Michael Zaharovich Zgurovsky.

The articles to be published in the Journal in Ukrainian and English languages are accepted. Information printed in the Journal is included in the Catalogue of periodicals of Ukraine.

СИСТЕМНІ ДОСЛІДЖЕННЯ ТА ІНФОРМАЦІЙНІ ТЕХНОЛОГІЇ

3 • 2024

ЗМІСТ

SYSTEM RESEARCH AND INFORMATION TECHNOLOGIES

3 • 2024

CONTENT

UDC 004.8:336
DOI: 10.20535/SRIT.2308-8893.2024.3.01

IMPROVING THE ACCURACY OF NEURAL NETWORK EXCHANGE RATE FORECASTING USING EVOLUTIONARY MODELING METHODS

S.S. FEDIN

Abstract. A set of models of feedforward neural networks is created to obtain operational forecasts of the time series of the hryvnia/dollar exchange rate. It is shown that using an evolutionary algorithm for the total search of basic characteristics and a genetic algorithm for searching the values of the matrix of neural network weight coefficients allows optimizing the configuration and selecting the best neural network models according to various criteria of their training and testing quality. Based on the verification of forecasting results, it is established that the use of neural network models selected by the evolutionary modelling method increases the accuracy of forecasting the hryvnia/dollar exchange rate compared to neural network models created without the use of a genetic algorithm. The accuracy of the forecasting results is confirmed by the method of inverse verification using data from different retrospective periods of the time series using the criterion of the average absolute percentage error of the forecast.

Keywords: exchange rate, genetic algorithm, evolutionary modeling, neural network, optimization, forecasting, accuracy, time series.

INTRODUCTION

In the foreign and domestic practice of financial analysis and forecasting, artificial intelligence information technologies are widely used, which are currently an integral auxiliary tool in the process of making managerial decisions in the field of economics and finance [1]. The use of these technologies, in particular, contributes to the successful solution of the tasks of forecasting currency and stock exchange rates, assessing the risk of financial and banking operations, analyzing and forecasting market indicators, credit ratings of businesses etc. [1–3].

Management of economic entities, including financial systems, is carried out under conditions of uncertainty, which necessitates the use of methods of obtaining information on economic indicators to make a reasonable judgment about possible future states of the system or alternative ways and timing of their implementation. Future uncertainty cannot be completely eliminated, so the main task of decision-making under uncertainty is to find “good” or “best” decisions from a range of alternatives.

One of the tools in the process of making such decisions is the forecasting methodology [4; 5]. The need to use different forecasting methods is caused by the fact that in the context of nonlinear dynamic processes of financial markets, determining their future states is a difficult task, but obtaining reliable information about the value of financial indicators is a key aspect of supporting decision-making at a certain point in time.

According to the results of independent studies confirms the assumption that the time series of financial indicators, in particular, stock prices and exchange rates, are characterized by nonlinear trends at different periods of retrospection [6–9]. The dynamics of exchange rates is characterized by complex nonlinear dependencies with a high level of noise and veiled periodic components with variable amplitude, which causes the presence of heterogeneous components in the time series and does not allow for the selection of a single model structure for the entire time series data set [10]. Thus, at different periods of retrospection, the structure of the model (the nature of the trend) changes, this increases the degree of information uncertainty and reduces the reliability of forecasting. The solution to this problem requires the use of artificial intelligence methods, including neural networks and evolutionary modeling.

A common characteristic of these non-parametric information processing methods is the ability to recognize patterns — trends based on the generalization of input information [11]. The ability to model nonlinear processes and adaptability allow the use of neural networks and evolutionary algorithms in solving various forecasting problems in the face of noisy input data [12; 13]. In addition, compared to classical analytical models, neural networks allow obtaining reliable forecast estimates for non-stationary and periodic time series of financial indicators [11].

Thus, the use of neural network and evolutionary forecasting methods can be viewed as a generalization of traditional approaches to solving the urgent problem of recognizing trends in the time series of exchange rates and timely management decision-making.

PROBLEM DEFINITION

To build a multilayer feedforward neural network, let us assume that the set of training sample examples is represented by data vectors (X, Y), the structure of which determines the number of inputs N and outputs M of the neural network, where $X = (x_1, x_2, \ldots, x_N)$ is the value of the input vector, and $Y = (y_1, y_2, \ldots, y_M)$ — the desired (actual or reference) values of the output vector.

Then the process of training a neural network as a dynamic system consists in achieving such a state of the network in which the differences between all output Y' and the desired values of the training sample vectors Y do not exceed the value of the error δ, which is determined in advance and calculated in a certain way. In this case, the task of training a neural network is to determine the values of all its characteristics, so that when any vector X from the set of training examples (X, Y) is fed to the input, the neural network output for a given set of weight coefficients W is the vector $Y'(W) = \{y'_1(W), y'_2(W), \ldots, y'_M(W)\}$, which differs from the reference vector Y by no more than value of error δ.

In this case, the objective function (training criterion) will be the error $\delta_{\max}(W)$ — the maximum difference between Y' and Y for all vectors of the training set containing *n* elements. The minimum value of the error δ will allow obtaining the maximum training accuracy of the neural network model.

The objective function is represented as the sum of the squares of deviations of the values Y from the values Y', obtained by the dynamic process of propagation of training sample examples from the inputs to the outputs of the neural network

$$\delta(W) = \frac{1}{2}\left\|Y - Y_i'(W)\right\|^2 = \frac{1}{2}\sum_{k=1}^{M}(Y_k - Y_k'(W))^2 \ . \qquad (1)$$

Then the iterative process of finding the weights of inter-neuronal connections W of the neural network that would satisfy the given value of criterion (1) can be carried out by the gradient descent method based on the dependence

$$W(n+1) = W(n) - \eta \cdot \mathrm{grad}_W \delta(W(n)) \ , \qquad (2)$$

where η is the step size (error correction rate coefficient).

To obtain an estimate of the learning criterion (1) and find the vector weights of the neural network (2), the Back Propagation of Error algorithm can be used. The disadvantage of this algorithm is that it can only find local minimum of the objective function (1). Since the task of finding the characteristics of a neural network that satisfies the condition $\delta(W_{\max}) = 0$ for real data is unattainable and is usually not set, the optimal solution turns into the search for a better or rational solution [14]. An effective way to find such a solution is to use the mathematical apparatus of genetic algorithms, the functioning of which is based on the mechanisms of natural evolution using selection and crossover operators of parental individuals, mutation of offspring and assessment of their fitness [12; 15–17]. Since all of these operators are collectively aimed at improving each individual, the preliminary results of the genetic algorithm will be iterative improvements in the solution population compared to the initial population, the size of which remains constant. The resulting neural network individual differs from its parent(s) and may be more or less adapted to transmit genetic information (chromosomes) to subsequent generations, which is characterized by an estimate of the fitness function. The chromosome of an individual consists of neurons — genes, each of which is represented by a set of values of its input weights [16; 18].

Let us represent individuals as a vector containing meaningful "genetic" information in the form of input and output weights of the neural network $W = (W_{inp}, W_{hid}^{j}, W_{out})$, where W_{inp} — is the vector of input weights of the neural network; W_{hid}^{j} — is the vector of weights between the *j*-th and (*j*+1)-th hidden layers of a multilayer neural network; W_{out} — is the vector of output weights of a neural network; $j = \overline{1...k-1}$, where *k* is the number of hidden layers. The dimension of W is equal to $(N+1)J_1 + J_1J_2 + ... + J_{k-1}J_k + J_kM$, where J_j is the number of neurons in the *j*-th hidden layer [19].

Then, the task of building a complete neural network can be solved in two stages, each of which requires the use of a specific genetic algorithm, namely:

– a total search for the basic characteristics of the neural network topology, i.e. determining the number of hidden layers *k* and neurons in each hidden layer *J* (Fig. 1);

– optimization of the neural network configuration by determining the "best" combination of the values of the weight coefficients W of all inter-neuronal connections (Fig. 2).

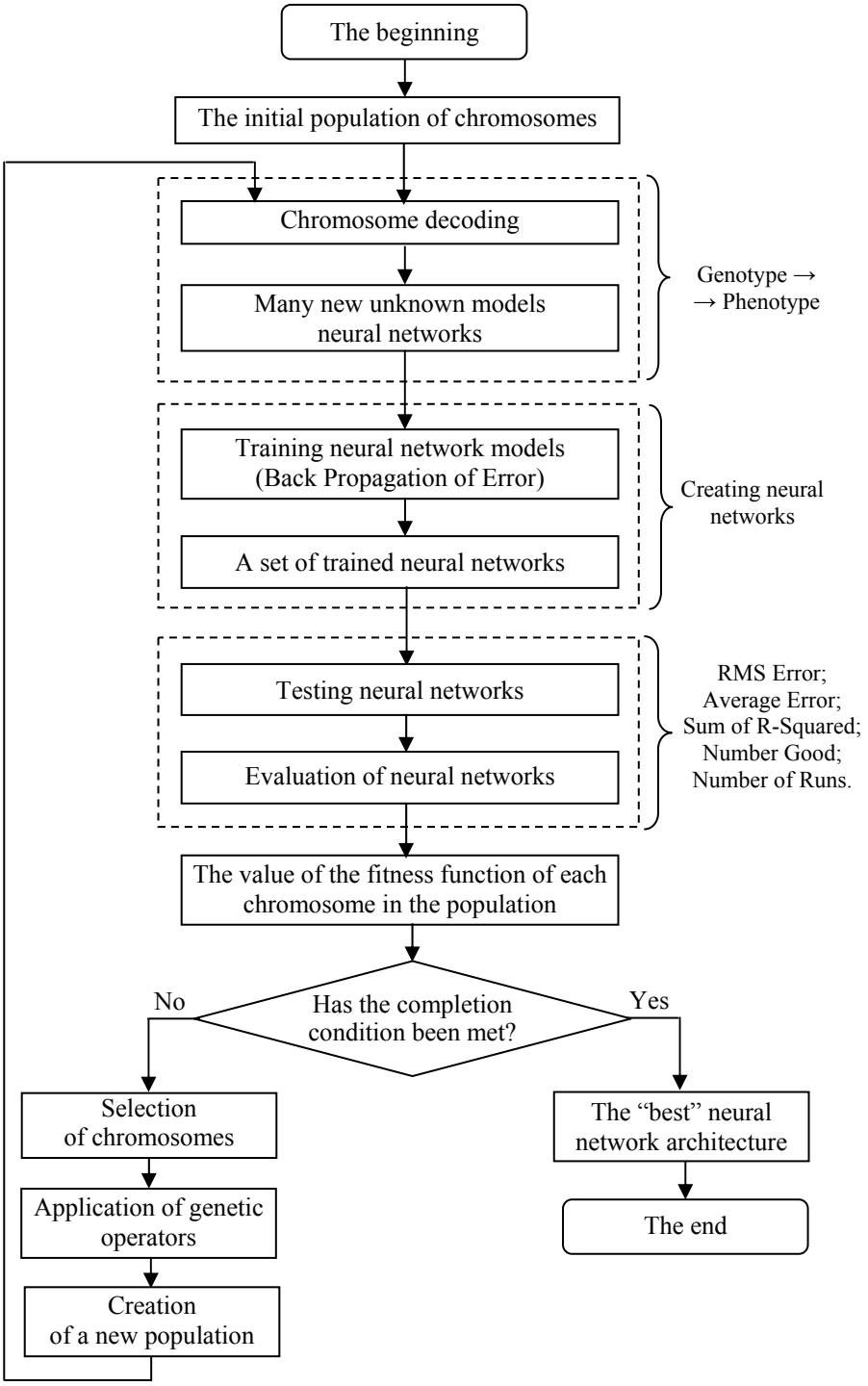

Fig. 1. Flowchart of the genetic algorithm for finding the neural network topology — evolution of architectures

Let us present four fitness functions (Table 1) for their sequential application in the genetic algorithm for optimizing the configuration of a neural network model (Fig. 2).

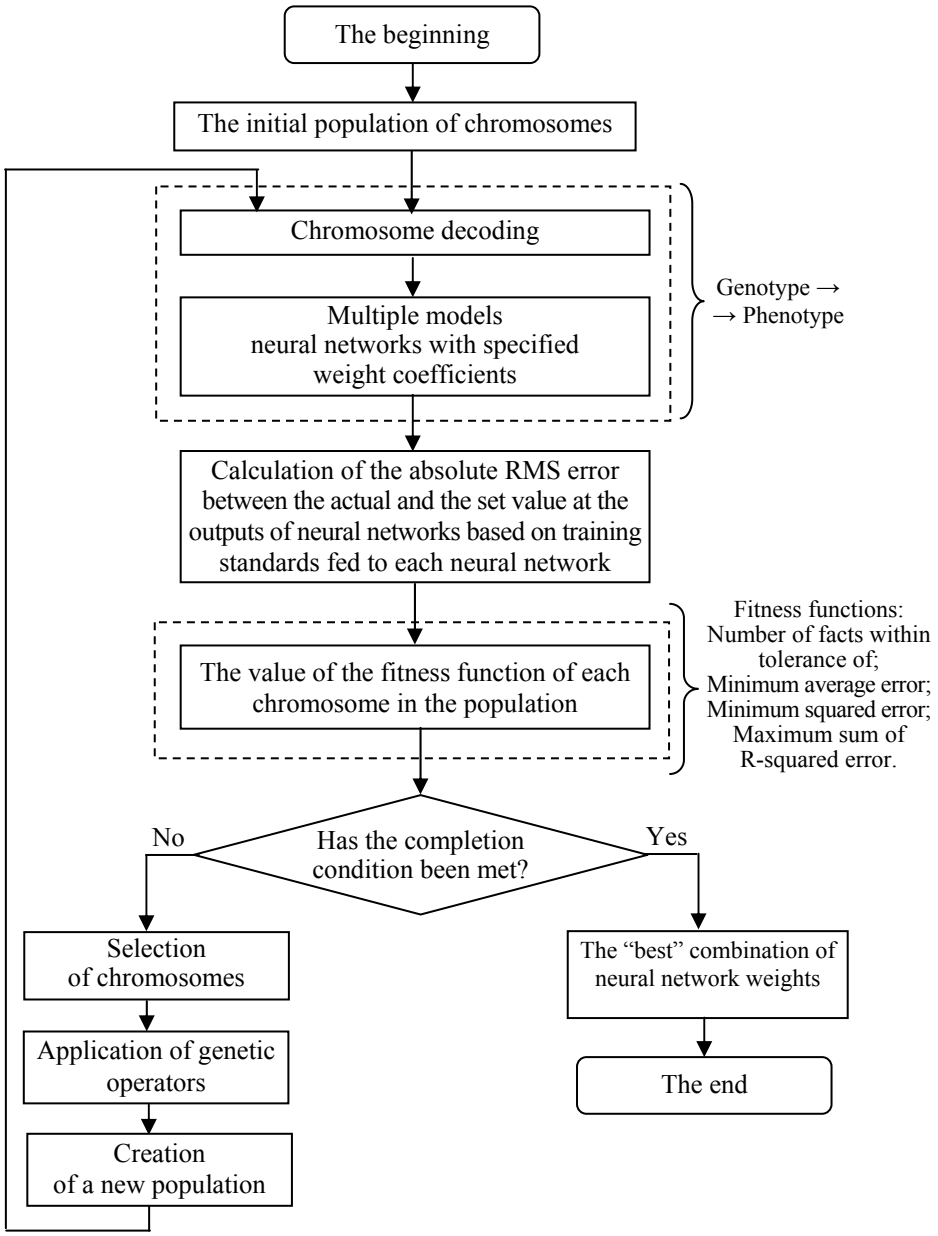

Fig. 2. Flowchart of the genetic algorithm for finding the weighting matrix of a neural network — evolution of weights

In accordance with the value of one of the selected fitness functions (Table 1), the genetic algorithm (Fig. 2) allows iteratively improving the population of neural network individuals and determining the neural network configuration that corresponds to the minimum error value (1), which can ultimately contribute to improving the accuracy of operational forecasting of time series of exchange rates.

Table 1. Types of fitness functions for the genetic algorithm for finding the matrix of neural network weighting coefficients (evolution of weights)

Criterion	Type of fitness function
Number of facts within the tolerance of	$Y' \in Y \pm TOL(Y_{\max} - Y_{\min})$, (3) where TOL is the accuracy parameter of neural network training and testing
Minimum average error	$\max(1 - Avg\ Error)$, (4) where $Avg\ Error = \frac{1}{n}\sum_{i=1}^{n}\lvert Y_i' - Y_i\rvert$.
Minimum squared error	$\max(1 - RMS\ Error)$, (5) where $RMS\ Error = \frac{1}{n}\sqrt{\sum_{i=1}^{n}(Y_i' - Y_i)^2}$
Maximum sum of R-squared error	$\max(\sum R^2)$, (6) where $R^2 = \frac{\left[n\sum_{i=1}^{n}(Y_i'Y_i) - \sum_{i=1}^{n}Y_i'\sum_{i=1}^{n}Y_i\right]^2}{\left[n\sum_{i=1}^{n}(Y_i')^2 - \left(\sum_{i=1}^{n}Y_i'\right)^2\right]\left[n\sum_{i=1}^{n}(Y_i)^2 - \left(\sum_{i=1}^{n}Y_i\right)^2\right]}$.

RESEARCH OBJECTIVE

This study is dedicated to improve the accuracy of neural network forecasting of the exchange rate of the currency pair hryvnia/dollar through the use of a genetic algorithm that allows to optimizing the configuration and perform an evolutionary search for the best neural networks models according to a given criterion of the quality of their training and testing.

LITERATURE REVIEW

The studies of S.A. Ayvazyan, I.G. Lukyanenko, L.I. Krasnikova, P.I. Bidyuk, O.V. Polovtsev, I.V. Baklan, V.M. Rifa, J. Johnston, J. DiNardo, G.E.P. Box, G.M. Jenkins demonstrate that the use of time series analysis methods is one of the most common approaches to forecasting the development of economic systems and processes, evaluating alternative economic strategies, as well as managing economic and financial risks [20–26].

It is known that the purpose of time series analysis is to obtain useful information from an ordered sequence of real numbers x_t, $t = 1,2,\ldots,T$, which are the results of observations of a certain value, based on a certain mathematical model [11; 27]. Such a model should explain the essence of the dynamic process, in particular, describe the nature of the data, which can be random, stationary, non-stationary, or periodic [27]. Time series of currency exchange rates or stock price movements usually contain random fluctuations and noise in varying proportions [11]. Therefore, the quality of the model is largely determined by its ability to approximate the regular (predictable) structure of the time series, separating

it from the noise. To solve this problem, methods of statistical analysis of time series are effective, including linear autoregressive moving average models (ARMA), ARMA+trend models, and methods of forecasting nonlinear processes, which include artificial neural networks [9]. The peculiarity of using neural network models is the ability to reproduce any dependence of the form $\hat{x}_t = f(x_{t-1}, x_{t-2}, ..., x_{t-p}) + \varepsilon_t$ with a continuous function f based on the delay vector between current and past data $(x_{t-1}, x_{t-2}, \ldots, x_{t-p})$ in *n*-dimensional space of time-shifted values [11; 19].

However, under conditions of uncertainty of the future situation, associated, for example, with changes in the nature of the trend of financial indicators at different time intervals, the task of fully building a neural network model is complex both in terms of its dimensionality and in terms of ensuring the accuracy of the model during training and testing. One of the effective ways to solve this problem is to combine neural networks and genetic algorithms to find the best solution from a number of alternatives in the argument search space and determine the extremum of the objective function of the learning error (1) [12; 14]. This combination can be auxiliary when (methods are applied sequentially one after the other) or equal (simultaneous application of both methods, for example, to find the weights of inter-neural connections) [28; 29].

It is assumed that in the face of changing trends in financial indicators, the use of the principle of equal combination of a genetic algorithm and a feedforward neural network will optimize the machine learning process and, as a result, improve the accuracy of approximating the regular component of the exchange rate time series in the selected observation interval.

Thus, conducting a study aimed at ensuring the accuracy of neural network forecasting of non-stationary time series by using genetic algorithms in optimizing the training process of multilayer neural networks is an urgent scientific and practical task.

MATERIALS AND METHODS

As the initial data for creating neural network forecasting models, we used factual data of the time series of the official hryvnia exchange rate against the US dollar, which were borrowed from the government electronic resource [30]. To assess the accuracy of the forecast, the principle of simulation forecasting was applied, since the actual value of the hryvnia exchange rate in relation to the one-day forecast advance period, i.e. Tuesday 06.10.2020, is known and amounts to 28.4009 hryvnia per 1 dollar. In determining the dimension of the neural network training sample, we used the methods of spectral and autocorrelation analysis of time series data, as well as the method of a branched delay line, according to which the architecture of the feedforward neural network allows us to model any finite time dependence of the following form [11]

$$Y(t) = F[X(t), X(t-1), ..., X(t-p)]. \quad (7)$$

The spectral analysis shows that the frequency of the first harmonic is approximately zero (Fig. 3, *a*). This indicates the absence of periodicity in the regular component of the time series, and, as a result, the appropriateness of setting the forecast advance period to correspond to the daily change in the

hryvnia/dollar exchange rate. The result of the autocorrelation analysis (Fig. 3, *b*) characterizes the non-stationary of the hryvnia exchange rate time series, since the maximum value of the autocorrelation coefficient corresponds to the first lag (time series shift), so the use of feedforward neural networks is an appropriate way to obtain an operational simulation forecast. The observation period, which is one week and corresponds to the number of inputs of the neural network training sample, was determined taking into account the lag for which the autocorrelation coefficient exceeds 0.85 (Fig. 3, *b*) [31].

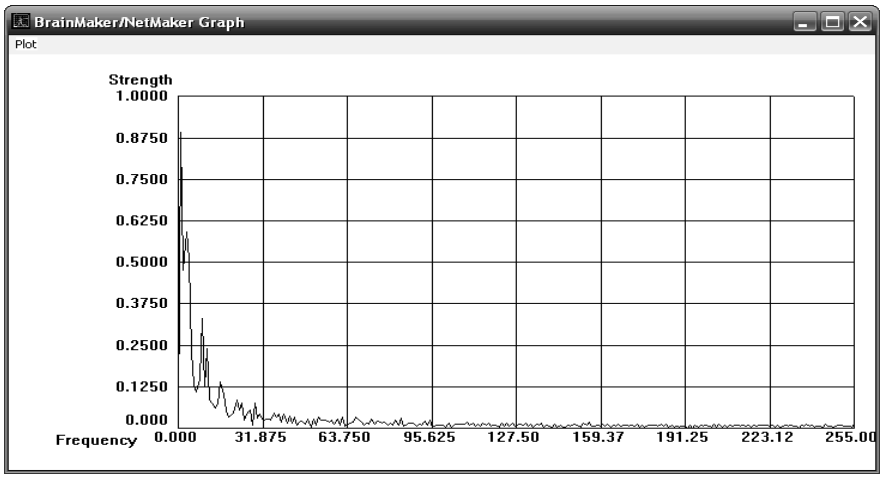

a

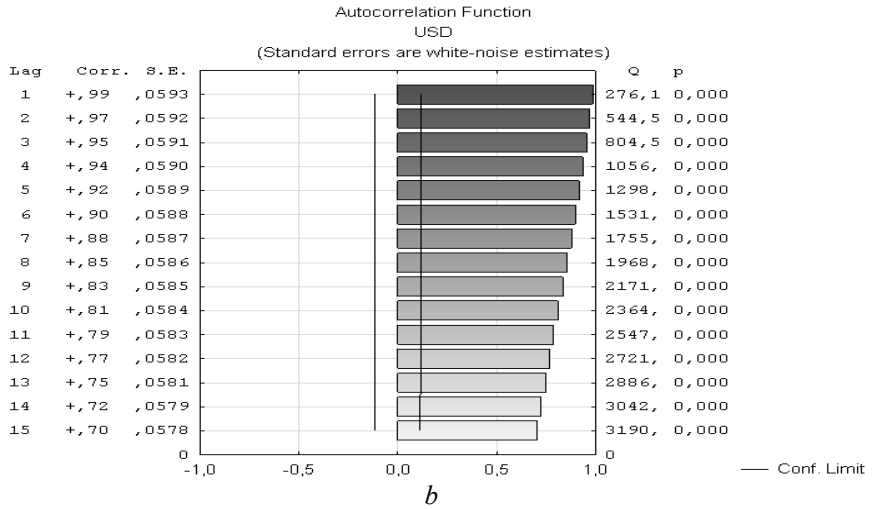

b

Fig. 3. Results of spectral analysis of the time series in NetMaker (*a*); autocorrelation analysis of the time series in STATISTICA 10 (*b*)

Thus, in accordance with (7) and based on the obtained estimates of the time series autocorrelation coefficients (Fig. 3, *b*), the training set of $n = 274$ examples has a dimension consisting of seven inputs (Input) USD1 $(t-7)$, USD2 $(t-6)$,...,USD7 $(t-1)$ and one output (Pattern) USD8 (t). Testing of the USD_11.net neural network model with the 7:10:1 architecture, trained in the BrainMaker Professional system for 67 epochs of training (Run), showed that all 27 facts of the test sample (10% of the number of examples of the training sam-

ple) are classified as Good, i.e., within the tolerance range when condition (3) is met for the value of the TOL parameter $= 0.10$ [31]. The result of the simulation neural network forecasting was obtained using a training example that characterizes the last week of the observation period before Tuesday 06.10.2020 (t), i.e. the value of the hryvnia exchange rate from 29.09.2020 $(t-7)$ to 05.10.2020 $(t-1)$. To ensure the convergence of the results of neural network forecasting, training and testing of models with the 7:10:1 architecture was repeated $L = 5$ times with the value of the TOL parameter $= 0.10$. The evaluation of the results of testing neural network models (Table 2) and the accuracy of the simulation forecast for Tuesday 06.10.2020 (Table 3) was carried out according to the criterion of the mean absolute percentage error (*MAPE*)

$$MAPE = \frac{100}{n}\sum_{i=1}^{n}\frac{\left|Y_i' - Y_i\right|}{Y_i}, \tag{8}$$

where Y', Y are respectively the predicted (Out) and actual (Ptn) values of the i-th example selected for testing, $i = 1,\ldots,n$.

Table 2. The value of the *MAPE* criterion, %, based on the results of testing USD neural network models created in BrainMaker Professional

USD_11.net	USD_12.net	USD_13.net	USD_14.net	USD_15.net
0.784	0.761	0.822	0.726	0.664

The analysis of the data presented in Table 2 shows that for the test sample, the value of the *MAPE* criterion is in the range (0.664...0.822%), and the lowest value of this criterion corresponds to the USD_15.net neural network model (Table 3).

Table 3. Evaluation of the accuracy of forecasting results using neural network models created in BrainMaker Professional

Model	Run	Good	Result	*MAPE*, %
USD_11.net	67	27	27.875	1.85
USD_12.net	129	27	27.912	1.72
USD_13.net	83	27	27.888	1.81
USD_14.net	98	27	27.878	1.84
USD_15.net	62	27	27.883	1.82

The analysis of the data presented in Table 3 shows a high speed of neural network training (Run parameter) and finding all the facts of the test sample within the training tolerance (Good parameter) in accordance with condition (3). At the same time, the interval of the *MAPE* criterion is (1.72...1.85%), the lowest value of which corresponds to the USD_12.net model.

Attempts to create neural network models with a further reduction of the training tolerance allowed us to establish that for a sample of initial data when the value of the TOL parameter is set to 0.06, the machine learning process using the Back Propagation of Error algorithm in the BrainMaker Professional system does not converge. Therefore, the task of improving the accuracy of neural network forecasting of the hryvnia/dollar exchange rate was solved by evolutionary modeling in the Genetic Training Option (GTO) software using genetic algorithms

(Figs. 1, 2) and a smaller training tolerance compared to the models presented in Table 3. At the same time, the assumption of increasing the accuracy of neural network forecasting can be confirmed by fulfilling the following condition

$$\max_{L} MAPE^{\,\mathrm{GTO}\,l} < \min_{L} MAPE^{\,\mathrm{USD}\,l}, \qquad (9)$$

where is the l-th model of a neural network created with (GTO_l) and without (USD_l) genetic algorithm, $l = 1,\ldots,L$.

CONDUCTING COMPUTATIONAL EXPERIMENTS USING EVOLUTIONARY MODELING METHODS

The experimental studies were devoted to confirming the assumption that it is possible to improve the accuracy of neural network forecasting by using evolutionary modeling methods. Computational experiments were carried out according to a methodology that includes two stages, namely:

1) use of genetic algorithms in GTO (Figs. 1, 2) for the neural network model formed in BrainMaker Professional with randomly selected weights;

2) using the BrainMaker Professional system to automatically complete the machine learning process.

The use of the total search algorithm in GTO (Fig. 1) with a change in the TOL parameter and a given range of the number of neurons in the hidden layer of the neural network allowed us to obtain the result of training the neural network population (Fig. 4) and the model of the neural network GTO.net, all the facts of the test sample of which, according to condition (3), are within the training tolerance Good = 27.

Genetic Training Option

File Optimize Sort

Network file: USD_11.def Total Iterations = 40

Optimization Results

Iteration	StartTol	EndingTol	Hidden1	Run	Good	AvgError	RMSError	hh:mm:ss	R*:USD8	Bad:USD8
1	0.1000	0.0400	1	1000	16	0.0365	0.0456	00:00:16	0.9758	11
2	0.1100	0.0400	1	1000	21	0.0290	0.0410	00:00:16	0.9807	6
3	0.1000	0.0500	1	1000	21	0.0365	0.0456	00:00:16	0.9758	6
4	0.1100	0.0500	1	1000	24	0.0290	0.0410	00:00:16	0.9807	3
5	0.1000	0.0400	2	1000	15	0.0359	0.0449	00:00:15	0.9757	12
6	0.1100	0.0400	2	1000	19	0.0335	0.0452	00:00:15	0.9804	8
7	0.1000	0.0500	2	1000	22	0.0359	0.0449	00:00:15	0.9757	5
8	0.1100	0.0500	2	1000	21	0.0335	0.0452	00:00:16	0.9804	6
9	0.1000	0.0400	3	1000	19	0.0320	0.0382	00:00:23	0.9844	8
10	0.1100	0.0400	3	1000	23	0.0200	0.0286	00:00:40	0.9893	4
11	0.1000	0.0500	3	1000	23	0.0320	0.0382	00:00:15	0.9844	4
12	0.1100	0.0500	3	1000	24	0.0200	0.0286	00:00:40	0.9893	3
13	0.1000	0.0400	4	1000	18	0.0327	0.0393	00:00:23	0.9815	9
14	0.1100	0.0400	4	1000	20	0.0274	0.0319	00:00:19	0.9869	7
15	0.1000	0.0500	4	1000	22	0.0327	0.0393	00:00:23	0.9815	5
16	0.1100	0.0500	4	1000	24	0.0274	0.0319	00:00:36	0.9869	3
17	0.1000	0.0400	5	1000	20	0.0269	0.0355	00:00:30	0.9833	7
18	0.1100	0.0400	5	1000	23	0.0251	0.0359	00:00:16	0.9848	4
19	0.1000	0.0500	5	1000	24	0.0269	0.0355	00:00:38	0.9833	3
20	0.1100	0.0500	5	1000	25	0.0251	0.0359	00:00:16	0.9848	2
21	0.1000	0.0400	6	1000	21	0.0260	0.0316	00:00:16	0.9882	6
22	0.1100	0.0400	6	1000	25	0.0219	0.0273	00:00:21	0.9906	2
23	0.1000	0.0500	6	1000	25	0.0260	0.0316	00:00:16	0.9882	2
24	0.1100	0.0500	6	1000	26	0.0219	0.0273	00:00:16	0.9906	1
25	0.1000	0.0400	7	1000	24	0.0215	0.0288	00:00:16	0.9900	3
26	0.1100	0.0400	7	1000	24	0.0199	0.0267	00:00:17	0.9908	3
27	0.1000	0.0500	7	1000	25	0.0215	0.0288	00:00:16	0.9900	2
28	0.1100	0.0500	7	1000	26	0.0199	0.0267	00:00:17	0.9908	1
29	0.1000	0.0400	8	1000	18	0.0325	0.0382	00:00:17	0.9888	9
30	0.1100	0.0400	8	1000	23	0.0252	0.0319	00:00:16	0.9869	4
31	0.1000	0.0500	8	1000	21	0.0325	0.0382	00:00:17	0.9888	6
32	0.1100	0.0500	8	1000	25	0.0252	0.0319	00:00:17	0.9869	2
33	0.1000	0.0400	9	1000	19	0.0277	0.0326	00:00:17	0.9873	8
34	0.1100	0.0400	9	1000	23	0.0245	0.0336	00:00:16	0.9853	4
35	0.1000	0.0500	9	1000	23	0.0277	0.0326	00:00:16	0.9873	4
36	0.1100	0.0500	9	1000	24	0.0245	0.0336	00:00:17	0.9853	3
37	0.1000	0.0400	10	1000	23	0.0223	0.0275	00:00:16	0.9906	4
38	0.1100	0.0400	10	1000	23	0.0202	0.0256	00:00:16	0.9924	4
39	0.1000	0.0500	10	1000	26	0.0223	0.0275	00:00:17	0.9906	1
40	0.1100	0.0500	10	1000	24	0.0202	0.0256	00:00:16	0.9924	3

Fig. 4. The result of GTO at the stage of total search for the basic characteristics of the neural network when ordering the population of models by the criterion of the number of neurons of the hidden layer Hidden 1

The main purpose of the GTO.net model, whose training was completed at the minimum value of the TOL parameter=0.056≤0.060, is to be used to perform crossover and mutation operators using the two best models that form the initial population of neural networks (Fig. 4). In the process of implementing genetic operators, in particular, it was assumed that each neural network would be trained for 100 epochs (Run) and 30 generations would be changed. To evaluate the neural network's adaptability, we used the results of both training and testing of the already trained neural network model. At the same time, 50% of all neurons were subjected to crossover and 10% to mutation. It was also assumed that the neurons were directly crossed by 50% and 25% using a uniform and normal random variable distribution law, respectively. The mutation of neurons was carried out in the same proportion as when performing the crossover operator. The fitness (quality) of the neural network model was assessed by one of the four GTO statistical criteria (Table 1).

The result of evaluating the quality of training for the 30 formed neural networks according to criterion (5), ordered from the highest to the lowest value, showed that the neural network model corresponding to the value $\max(1 - RMS\ Error) = 0.9735$ is the "best". The application of the created neural network model allowed us to obtain the forecast value of the exchange rate for Tuesday 06.10.20, which is equal to 28.071 hryvnias per 1 dollar. The final result of the genetic algorithm is the automatic saving of the five best out of 30 neural network models GTO001.net, GTO002.net, GTO003.net, GTO004.net, GTO005.net with a TOL value of 0.056. Evaluation of the results of testing the models created using the genetic algorithm and the accuracy of neural network forecasting according to criterion (8) is presented in Table 4 and Table 5, respectively.

Table 4. The value of the *MAPE* criterion, %, based on the results of testing USD neural network models created in GTO

GTO001.net	GTO002.net	GTO003.net	GTO004.net	GTO005.net
0.349	0.348	0.369	0.357	0.388

The analysis of the data presented in Table 4 shows that for the test sample, the value of the *MAPE* criterion is in the range (0.348...0.388%), and the lowest value of this criterion corresponds to the GTO002.net neural network model. Thus, based on a comparison of the results in Table 2 and Table 4, condition (9) is proved to be met.

Table 5. Evaluation of the accuracy of forecasting results using neural network models created by evolutionary modeling methods using GTO software and BrainMaker Professional system

Model	Run	Good	Result	*MAPE*, %
GTO001.net	100	27	28.071	1.16
GTO002.net	100	27	28.075	1.15
GTO003.net	100	27	28.077	1.14
GTO004.net	100	27	28.063	1.19
GTO005.net	100	27	28.082	1.12

The analysis of the data presented in Table 5 shows that at the same speed of the neural network model training process ($\text{Run} = 100$), all the facts of the test

sample in accordance with condition (3) are within the training tolerance ($Good = 27$). At the same time, the result of the evaluation of criterion (8) is in the interval (1.12...1.15%), the lowest value of which corresponds to the GTO005.net neural network model.

Comparison of the results in Table 3 and Table 5 shows that the accuracy of the point forecast of the hryvnia exchange rate obtained using neural network models created by evolutionary modeling methods is higher than that of models created without the use of a genetic algorithm. To exclude the possibility of obtaining a random result of neural network forecasting using evolutionary modeling methods and to confirm the convergence of the neural network training and testing process, computational experiments in GTO were repeated five times using different statistical criteria: RMS Error; Average Error; Sum of R-Squared; Number Good; Number of Runs (Fig. 1).

Thus, at the first stage of applying the GTO evolutionary algorithm to find the basic characteristics and obtain the initial population of neural networks, in addition to the result with a different number of neurons in one hidden layer (Fig. 4), we obtained five more variants of ordering the initial population of neural network individuals. Thus, given the Hidden 1 ordering criterion, the total number of computational experiments was six. At the second stage, for the obtained six variants of the initial population of neural networks and four criteria (3)–(6), we repeated computational experiments to assess the adaptability of neural network models when optimizing their configuration using a genetic algorithm (Fig. 2).

RESULTS OF COMPUTATIONAL EXPERIMENTS

An assessment of the accuracy of the results of the daily forecasting of the hryvnia/dollar exchange rate for Tuesday 06.10.2020, obtained on the basis of neural network models created using a genetic algorithm, is presented in Tables 6–9 and Figs. 5–8.

Table 6. *MAPE* values, % for neural network models created on the basis of the criterion Number of facts within tolerance of

Ordering criterion	Model				
	GTO001	GTO002	GTO003	GTO004	GTO005
Hidden 1	1.34	1.24	1.20	1.14	1.11
RMS Error	1.34	1.12	1.15	1.25	1.18
Average Error	1.19	1.25	1.28	1.28	1.24
Sum of R-Squared	1.34	1.12	1.16	1.14	1.23
Number Good	1.19	1.32	1.21	1.22	1.15
Number of Runs	1.19	1.15	1.26	1.17	1.14

Table 7. *MAPE* values, % for neural network models created on the basis of the criterion Minimum average error

Ordering criterion	Model				
	GTO001	GTO002	GTO003	GTO004	GTO005
Hidden 1	1.24	1.19	1.19	1.23	1.26
RMS Error	1.23	1.22	1.26	1.23	1.26
Average Error	1.22	1.26	1.16	1.23	1.14
Sum of R-Squared	1.28	1.19	1.16	1.25	1.15
Number Good	1.17	1.13	1.31	1.25	1.28
Number of Runs	1.26	1.24	1.27	1.26	1.22

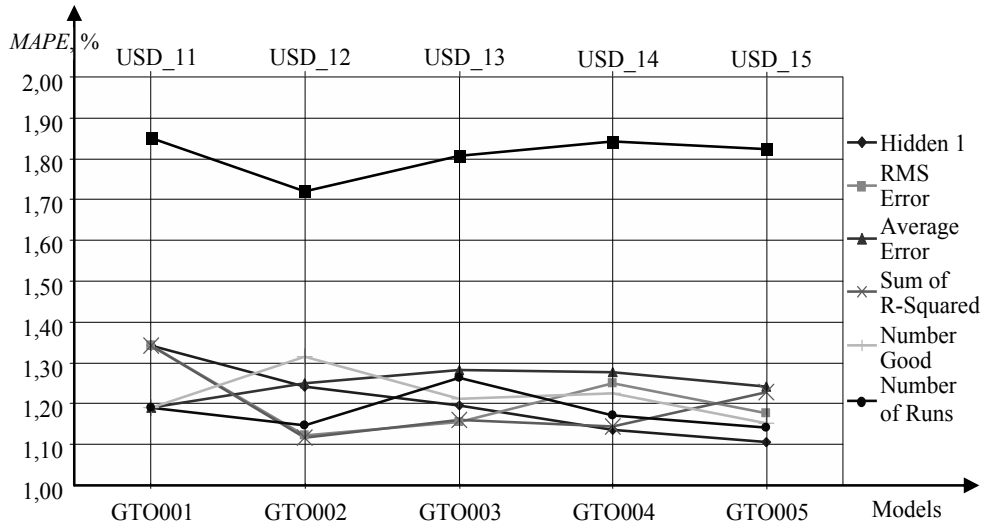

Fig. 5. MAPE values for forecasting the hryvnia exchange rate using five USD neural network models and five GTO neural network models created on the basis of the criterion Number of facts within tolerance of

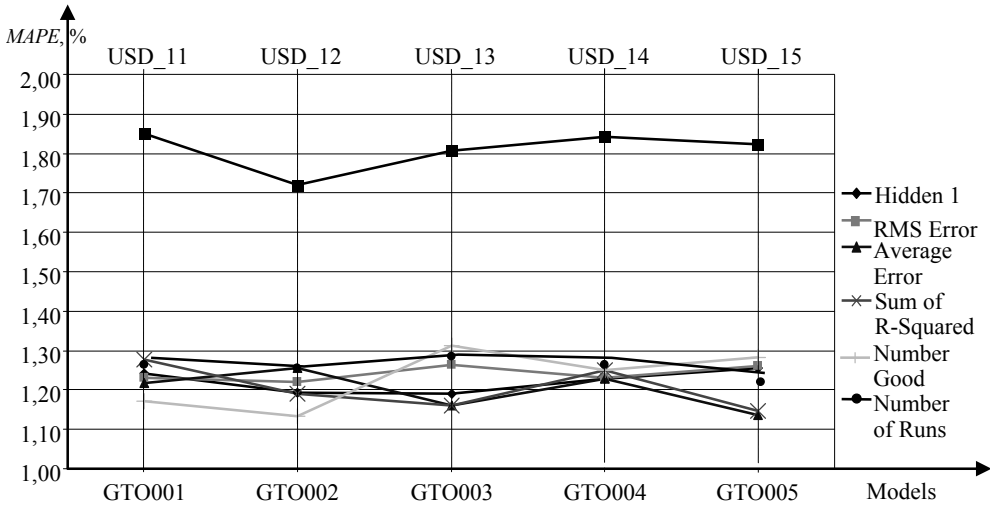

Fig. 6. MAPE values for forecasting the hryvnia exchange rate using five USD neural network models and five GTO neural network models created on the basis of the criterion Minimum average error

Table 8. *MAPE* values, % for neural network models created on the basis of the criterion Minimum squared error

Ordering criterion	**Model**				
	GTO001	GTO002	GTO003	GTO004	GTO005
Hidden 1	1.16	1.15	1.14	1.19	1.12
RMS Error	1.20	1.25	1.28	1.24	1.27
Average Error	1.20	1.15	1.22	1.27	1.18
Sum of R-Squared	1.22	1.18	1.24	1.17	**1.12**
Number Good	1.20	1.16	1.26	1.15	1.20
Number of Runs	1.13	1.17	1.18	1.17	1.15

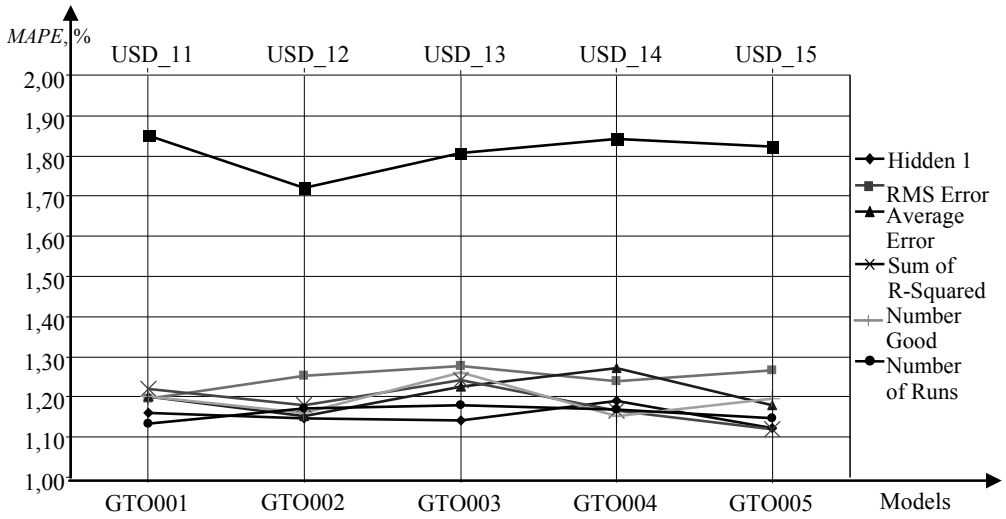

Fig. 7. MAPE values for forecasting the hryvnia exchange rate using five USD neural network models and five GTO neural network models created on the basis of the criterion Minimum squared error

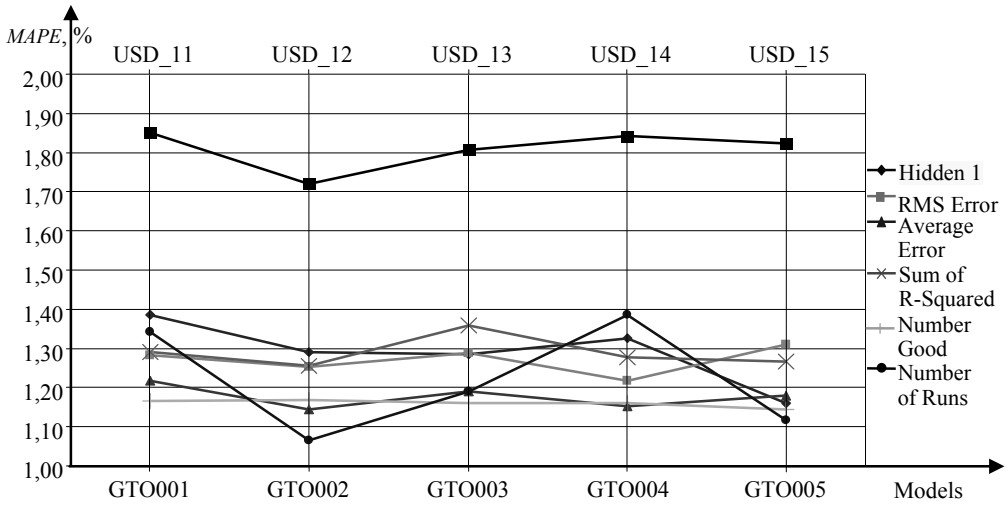

Fig. 8. MAPE values for forecasting the hryvnia exchange rate using five USD neural network models and five GTO neural network models created on the basis of the criterion Maximum sum of R-squared error

Table 9. *MAPE* values, % for neural network models created on the basis of the criterion Maximum sum of R-squared error

Ordering criterion	Model				
	GTO001	GTO002	GTO003	GTO004	GTO005
Hidden 1	1.39	1.29	1.28	1.33	1.16
RMS Error	1.28	1.25	1.29	1.22	1.31
Average Error	1.22	1.14	1.19	1.15	1.18
Sum of R-Squared	1.29	1.26	1.36	1.28	1.27
Number Good	1.17	1.17	1.16	1.16	1.14
Number of Runs	1.34	1.07	1.19	1.39	1.12

DISCUSSION OF THE OBTAINED RESULTS

Data analysis (Tables 6–9, Figs. 5–8) shows that the intervals of MAPE values for neural network models trained according to criteria (3)–(6) are, respectively: (1.11…1.34%); (1.13…1.31%); (1.12…1.28%); (1.07…1.39%), and for neural network models trained without the use of a genetic algorithm (1.72…1.85%) (Table 3).

Thus, on the basis of six computational experiments, the convergence of the process of re-training, testing and selection of the best neural network models was confirmed, and it was found that any of the 120 neural network models $(5 \times 6 \times 4 = 120)$ created by evolutionary modelling methods can improve the accuracy of the daily forecast of the hryvnia/dollar exchange rate (Figs. 6–9). Since the smallest interval of the *MAPE* value (1,12…1,28%) meets the criterion (5) — Minimum squared error (Table 8), the forecasting results with a one-week advance warning period were obtained using the best model of the GTO005.net neural network (Table 10) for the Sum of R-Squared ordering criterion (*MAPE*=1,12%, Table 8).

Table 10. The result of forecasting the hryvnia exchange rate using neural network models based on the criterion Minimum squared error

Ordering criterion	Model				
	GTO001	GTO002	GTO003	GTO004	GTO005
Hidden 1	28.071	28.075	28.077	28.063	28.082
RMS Error	28.061	28.045	28.038	28.049	28.041
Average Error	28.060	28.074	28.053	28.040	28.066
Sum of R-Squared	28.054	28.066	28.048	28.070	**28.083**
Number Good	28.060	28.071	28.043	28.074	28.061
Number of Runs	28.079	28.068	28.066	28.069	28.075

The GTO005.net model (Table 10) is characterized by the lowest forecast error value $|\Delta| = 0.318$, where $|\Delta|$ is the a posteriori value of the deviation of the forecast value of the hryvnia/dollar exchange rate of 28.083 from the actual value of 28.4009 hryvnia per 1 dollar. The results of the estimates for the weekly forecast lead time obtained using the most accurate neural network model USD_12.net (Table 3), which was created without the use of a genetic algorithm, and the selected most accurate model GTO005.net are shown in Table 11.

Table 11. Evaluation of the neural network forecasting result with a warning period of one week from 07.10.2020 to 13.10.2020

Date	Hryvnia exchange rate	USD_12.net	GTO005.net	$MAPE_{USD\_12}$	$MAPE_{GTO005}$
07.10.2020	28.364	27.913	28.082	1.590	0.994
08.10.2020	28.324	27.916	28.099	1.440	0.794
09.10.2020	28.284	27.921	28.096	1.282	0.663
10.10.2020	28.284	27.925	28.079	1.268	0.723
11.10.2020	28.284	27.913	28.058	1.310	0.798
12.10.2020	28.210	27.903	28.052	1.088	0.559
13.10.2020	28.248	27.895	28.055	1.250	0.684

Taking into account all the values of the weekly forecast lead time for the USD_12.net and GTO005.net models (Table 11), the estimated mean absolute

percentage error (8) is 1.318% and 0.745%, respectively. Thus, for the GTO005.net model, the *MAPE* estimate is approximately 1.77 times lower than the *MAPE* estimate for the USD_12.net model. Thus, the analysis of the results obtained (Table 11), as well as in the case of the daily point forecast, shows that the accuracy of the weekly forecast of the hryvnia/dollar exchange rate has improved.

The adequacy of the results was checked, as well as the reliability and validity of the neural network forecast was assessed using the inverse verification method on a new retrospective period of the hryvnia/dollar exchange rate time series — from 02.10.2023 to 19.03.2024. To obtain a weekly forecasting result based on the data of the observation period from 02.10.2023 to 12.03.2024, the neural network was trained in the GTO system using the Sum of R-Squared ordering criterion at the stage of total search for its basic characteristics, and the Minimum squared error criterion to select the best neural network models (5). The evaluation of the obtained forecasting result is shown in Table 12.

Table 12. Evaluation of the result of neural network forecasting with a warning period of one week from 13.03.2024 to 19.03.2024

Date	Hryvnia exchange rate	GTO_USD.net	$MAPE_{GTO\_USD}$
13.03.2024	38.4924	38.379	0.295
14.03.2024	38.7878	38.399	1.002
15.03.2024	38.6854	38.518	0.433
16.03.2024	38.6854	38.453	0.601
17.03.2024	38.6854	38.451	0.606
18.03.2024	38.7998	38.499	0.775
19.03.2024	38.9744	38.526	1.150

The estimate of the *MAPE* criterion, taking into account all values of the weekly forecast advance period for the GTO_USD.net model (Table 12), is 0.695%, which is less than the value of 0.745% for the GTO005.net model (Table 11). At the same time, the test of the statistical hypothesis that there is no significant difference between $MAPE_{GTO005}$ and $MAPE_{GTO\_USD}$, which was performed in STATISTICA 10 based on a *t*-test for independent variables ($p \approx 0.696 > 0.05$), confirms the reliability of the result of improving the accuracy of the neural network forecast (Fig. 9).

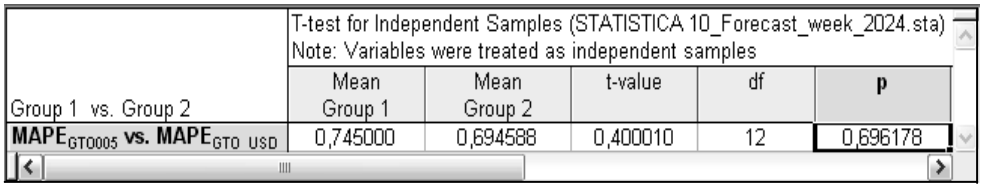

Fig. 9. Screenshot of the result of testing the statistical hypothesis that there is no significant difference in the *MAPE* estimates for the GTO005.net and GTO_USD.net models

Thus, the analysis of all the results obtained for different periods of retrospection of the time series of the hryvnia/dollar exchange rate under the condition of changing the nature of its trend confirms the reliability of the results obtained and allows us to recommend the use of evolutionary modeling methods in training and optimizing feedforward neural networks to improve the accuracy of operational neural network forecasting of time series of exchange rates.

CONCLUSIONS

1. In order to obtain an operational forecast of the hryvnia/dollar exchange rate with a one-day and one-week lead time for different observation periods in 2020 and 2024, feedforward neural network models with the Back Propagation of Error learning algorithm were developed using the BrainMaker Professional system and the Genetic Training Option software.

2. Computational experiments have shown that the use of a genetic algorithm in training neural networks can improve the accuracy of operational forecasts by optimizing the configuration and carrying out an evolutionary search for the best neural network models in accordance with a given criterion for the quality of their training and testing compared to neural network models created without the use of a genetic algorithm. The validity of the obtained forecast results is confirmed by assessing their reliability by the method of inverse verification carried out for different retrospective periods of the hryvnia/dollar exchange rate using the statistical criterion *MAPE*.

REFERENCES

1. Hidayat Muhammad, Defitri Siska Yulia, and Hilman Haim, "The Impact of Artificial Intelligence (AI) on Financial Management," *Management Studies and Business Journal (PRODUCTIVITY)*, vol. 1 (1), pp. 123–129, 2024.
2. Agrawal Ajay, Gans Joshua, and Goldfarb Avi, *Artificial intelligence in the service of business. How machine prediction helps to make decisions*. M.: Mann, Ivanov & Ferber, 2019, 336 p.
3. V.V. Pryimuk, "Implementation of artificial intelligence in the financial activity of the enterprise," *Collection of scientific works of the State Tax University*, 2023 (1), pp. 183–198.
4. B.E. Grabovetskyi, *Economic Forecasting and Planning: a textbook*. K.: Centre for Educational Literature, 2003, 188 p.
5. "*Prognostics. Terms and definitions*. Committee for Scientific and Technical Terminology, issue 109. M.: Nauka, 1990, 56 p.
6. John T. Barkoulas, Anthony G. Barilla, and William Wells, "Long-memory exchange rate dynamics in the euro era," *Chaos, Solitons & Fractals*, vol. 86 (C), pp. 92–100, 2016.
7. Yu-chin Chen, Kwok Ping Tsang, "What Does the Yield Curve Tell Us about Exchange Rate Predictability?" *The Review of Economics and Statistics*, vol. 95, pp. 185–205, 2013.
8. A.A. Chistyakova, B.V. Shamsha, "Information technology for forecasting non-stationary time series using singular spectral analysis," *East European Journal of Advanced Technologies*, no. 2/4 (68), pp. 24–30, 2014.
9. P.I. Bidyuk, I.V. Baklan, and V.I. Lytvynenko, *Modelling and forecasting of nonlinear dynamic processes*. K.: EKMO, 2004, 120 p.
10. A.A. Chistyakova, "Development of methods for analysing heterogeneous dynamics series based on statistical characteristics," *East European Journal of Advanced Technologies*, no. 5/4 (71), pp. 35–43, 2014.
11. D.-E. Bastens, W.-M. Van den Berg, and D. Wood, *Neural Networks and Financial Markets: Decision Making in Trading Operations*. M.: TVP Scientific Publishing House, 1997, 236 p.
12. D. Rutkovskaya, M. Pilinsky, and L. Rutkovsky, *Neural Networks, Genetic Algorithms and Fuzzy Systems*; Translated from Polish by I.D. Rudinsky. M.: Hotline-Telecom, 2004, 452 p.
13. Andreas S. Weigend, Bernardo A. Huberman, and David E. Rumelhart, "Predicting the future: a connectionist approach," *International Journal of Neural Systems*, vol. 01, no. 03, pp. 193–209, 1990.
14. V.V. Korneev, A.F. Gareev, S.V. Vasyutin, and V.V. Raikh, *Databases. Intelligent information processing*. M.: Nolige, 2000, 352 p.
15. L.A. Gladkov, V.V. Kureichik, and V.M. Kureichik, *Genetic algorithms*; 2nd ed. M.: Fizmatlit, 2006, 320 p.
16. V.F. Sytnyk, M.T. Krasnyuk, *Intelligent data analysis (data mining)*. K.: KNEU, 2007, 376 p.
17. N.M. Kussul, A.Y. Shelestov, and A.M. Lavreniuk, *Intelligent computing: a textbook*. K.: Naukova Dumka, 2006, 186 p.

18. "Genetic Training Option," *California Scientific Software*. Nevada City, CA 95959, 1996, 54 p.
19. 19. P.I. Bidyuk, O.I. Savenkov, and I.V. Baklan, *Time series: modelling and forecasting*. K.: EKMO, 2004, 144 p.
20. S.A. Aivazyan, V.S. Mkhitaryan, *Applied Statistics and Fundamentals of Econometrics*. M.: UNITY, 1998, 1006 p.
21. I.G. Lukianenko, L.I. Krasnikova, *Econometrics: a textbook*. K.: Znannya Society, KOO, 1998, 494 p.
22. P.I. Bidyuk, O.V. Polovtsev, *Analysis and Modelling of Economic Processes in Transition*. K.: NTUU "KPI", 1999, 230 p.
23. P.I. Bidyuk, I.V. Baklan, and V.N. Rifa, "Systematic approach to the construction of a egression model on time series," *Systemic Research and Information Technology*, no. 3, pp. 114–131, 2002.
24. J. Johnston, J. DiNardo, *Econometric methods*. New York: McGraw-Hill, 2007, 531 p.
25. G.E.P. Box, G.M. Jenkins, *Time Series Analysis: Forecasting and Control*. San Francisco: Holden-Day, 1976, 575 p.
26. G.E.P. Box, G.M. Jenkins, and G.C. Reinsel, *Time Series Analysis: Forecasting and Control*; 4th ed. US: John Wiley & Sons., 2008, 784 p.
27. Y.P. Lukashin, *Adaptive methods of short-term forecasting of time series: a textbook*. M.: Finance and Statistics, 2003, 416 p.
28. Z. Guo, R.E. Uhrig, "Use of genetic algorithms to select inputs for neural network," *Proceedings of International Workshop on Combinations of Genetic Algorithms and Neural Networks, COGAN-92*, pp. 223–234, 1992.
29. D. Whitley, T. Starkweather, and C. Bogart, "Genetic algorithms and neural networks: Optimising connections and connectivity," *Parallel Computing*, vol. 14, issue 3, pp. 347–361, 1990.
30. *National Bank of Ukraine. Official exchange rate of the hryvnia against foreign currencies. US dollar.* [website]. Available: https://bank.gov.ua/ua/markets/ exchangerate-chart?cn%5B%5D=USD (accessed 21.04.2024)
31. S.S. Fedin, *Artificial Intelligence Systems and Data Analysis Technologies: Workshop*; 2nd ed. K.: Interservice, 2021, 848 p.

Received 02.04.2024

INFORMATION ON THE ARTICLE

Serhii S. Fedin, ORCID: 0000-0001-9732-632X, National Transport University, Ukraine, e-mail: sergey.fedin1975@gmail.com

ПІДВИЩЕННЯ ТОЧНОСТІ НЕЙРОМЕРЕЖЕВОГО ПРОГНОЗУВАННЯ ВАЛЮТНОГО КУРСУ МЕТОДАМИ ЕВОЛЮЦІЙНОГО МОДЕЛЮВАННЯ / С.С. Федін

Анотація. Створено комплекс моделей прямошарових нейронних мереж для отримання оперативних прогнозів часового ряду валютного курсу гривні/долара. Показано, що використання еволюційного алгоритму тотального пошуку базових характеристик і генетичного алгоритму пошуку значень матриці вагових коефіцієнтів нейромереж дає змогу оптимізувати конфігурацію та відібрати кращі нейромережеві моделі за різними критеріями якості їх навчання та тестування. На основі верифікації результатів прогнозування встановлено, що використання відібраних методом еволюційного моделювання нейромережевих моделей дозволяє підвищити точність прогнозу курсу гривні/долара порівняно з нейромережевими моделями, які були створені без застосування генетичного алгоритму. Достовірність одержаних результатів прогнозування підтверджено методом інверсної верифікації за даними різних ретроспективних періодів часового ряду з використанням критерію середньої абсолютної відсоткової похибки прогнозу.

Ключові слова: валютний курс, генетичний алгоритм, еволюційне моделювання, нейронна мережа, оптимізація, прогнозування, точність, часовий ряд.

UDC 519.81
DOI: 10.20535/SRIT.2308-8893.2024.3.02

DETERMINATION OF THE GENERALIZED OPTIMALITY CRITERIA FOR SELECTING CIVILIAN SHELTER FACILITIES FROM ATTACKS BY BALLISTIC (CRUISE) MISSILES AND KAMIKAZE DRONES IN URBANIZED AREAS

V. YAKOVENKO, N. FURMANOVA, I. FLYS, O. MALYI, O. FARAFONOV, H. MOROZ

Abstract. The object of the study is the planning of the selection of civilian shelter from attacks by ballistic (cruise) missiles and kamikaze drones in urbanized areas. A generalized model for assessing the choice of civilian shelter facilities has been developed by applying linear forms of factor linkage in combination with a generalized optimality criterion in the form of a linear combination of local criteria. The multivariate regression analysis method was chosen to study the correlation between the generalized criterion and the observed feature. A generalized criterion for the optimal choice of civilian shelter facilities from attacks by ballistic (cruise) missiles and kamikaze drones in urbanized areas is calculated in the form of regression coefficients. The criterion can facilitate a simplified determination of the generalized indicator of a linear model for planning the protection of civilians in cities outside the area of hostilities. The initial data is a set of physical (technical) states of shelters with a list of values and features sufficient to assess their resistance to high dynamic loads.

Keywords: optimality criterion, civilian shelter facilities, weighting factor, missile attacks.

INTRODUCTION

The long-term evolution of the modern world hegemony of the rule of international norms and humanity has failed completely. It was completely levelled after the Russian Federation (RF) unleashed its so-called “aggression” against the sovereign state of Ukraine [1]. After all, a war in the centre of Europe on such a scale since the end of the Second World War is the trigger for the first shot of a new global war. Consequently, the dictators felt the complete amorphousness of global institutions, as well as the meaninglessness of any commitments and international treaties [2–4]. Thus, the beginning of Russia’s aggression against Ukraine was carried out using several indirect levers of pressure: political, financial and economic, media, human and military [5, 6]. Subsequently, hybridity grew into the so-called “special military operation” (SMO), a striking feature of which is a categorical violation of all international legal norms [7] and crimes against civilians. This raises the logical question of the safety of children, women, and the

elderly living in peaceful towns and villages, but suffering from regular air attacks by enemy forces using cruise (ballistic) missiles and attack kamikaze drones.

The world has a vast experience of successfully solving various complex problems, but humanity is losing the war to brazen terrorism. The protection of civilians in urbanized areas that are not involved in hostilities remains a serious problem. Protecting ordinary citizens from missile and kamikaze drones attacks, developing infrastructure that will protect them not only from death but also from injury - these are questions that needed to be answered yesterday. It is necessary to immediately create a fund for protective structures throughout the country without exception.

Ukraine can learn from the experience of other countries. Israel, for example, has many mobile shelters [8], especially in cities with short daylight hours in the south in the form of bus stops or just separate blocks. The main types of Israeli shelters are:

- protected rooms (mamads), which in peacetime are used by Israelis as ordinary living quarters;
- a folding bomb shelter that can fit in a room and unfold in a few minutes in an apartment or house;
- strengthening socially important facilities, including bus stops and schools;
- temporary bell-shaped fortifications for a limited number of people that can be placed in open space or near roads;
- sewerage pipes as storage facilities, which are laid near houses in several-metre-long lines.

In addition, Israel has a concept of protected space in the form of places that were not designed as shelters, but can be used in the absence of better alternatives. In general, such places mean any premises that are separated from the street by more than two walls and do not have windows according to the rule of two walls. This can significantly reduce the number of casualties even in the context of mass attacks [9] and when using fragmentation and high-explosive shells that have a high degree of damage to objects [10–12]. Thus, there is real experience in protecting civilians from missile and UAV attacks. However, any country keeps its experience in planning the choice of defences secret. The impression that it is easy to choose certain protective structures is superficial, as, as a rule, separate unrelated local tasks are solved. There is no comprehensive approach to achieving the overall goal, so developing approaches to decision-making on the choice of civilian shelter facilities from missile and kamikaze drones attacks is an urgent task.

LITERATURE ANALYSIS AND PROBLEM STATEMENT

Global weapons manufacturers are increasingly paying attention to limiting the unexpected lethality of their weapons by “scalping” the enemy [13]. However, this does not apply to the military and political leadership of the Russian Federation. In the current realities of the so-called undeclared wars, civilians are an integral part of these confrontations, and the use of UAVs for inflicting damage is constantly increasing.

Article [14] discusses the current threats of kamikaze dronesand methodologies for assessing these threats, and proposes modelling the UAV threat through an attack protection tree. Study [15] analyses in depth the use of UAVs in modern confrontations and cyberattacks, and considers countermeasures based on the

technical limitations and shortcomings of the aircraft. However, these works do not address the issue of assessing the protection of shelter facilities.

Civilian sheltering facilities play an important role in protecting people from enemy aggression and should therefore be considered an effective security measure. The article [16] discusses some strategic considerations of passive protection in the design and planning of urban shelters, in particular for countries with a critical strategic and sensitive location and exposed to threats from expansionist states. A comprehensive analysis of shelters, taking into account their actual state, is proposed in [17]. In 2022, the State Fire Service of Poland conducted an inventory of shelters for the population and posted an app with information on their location and class. However, the authors note that the created database is incomplete and often the data provided is not true. Therefore, it is proposed to create an interdepartmental group of professionals to develop criteria for assessing the suitability and protection of shelters from various types of impacts (military operations, man-made accidents, environmental disasters, etc.).

Israel's use of civilian shelter facilities is a part of a defence system, another component of which is the Iron Dome, a missile defence system deployed around Israel's major urbanized areas. It was created to provide citizens with greater protection from enemy missile attacks. The study [18] examined how civilians' experience with the Iron Dome system affects their perceptions of its reliability, their trust in it, their attitudes towards enemy missile alerts, and their decision to stay in the ADS. Although the study takes into account various indicators of reliability, the focus is on the perception of the proposals from the automated decision-making system by the population.

A similar issue is raised by [19], which analyses the results of the erroneous perception of the probability of being hit by ballistic missiles, as demonstrated by the operator of an automated air defence system. This study confirms the need to develop a comprehensive approach to threat assessment and recommendations for actions without or with minimised operator involvement.

A major study [20] was commissioned by the United States Air Force Europe (USAFE). It addresses a number of issues related to protection against cruise and ballistic missiles and UAVs, including the analysis of shelters and recommendations for their modernisation. However, the work is analytical in nature and does not raise the issue of collecting general information and selecting the optimal civilian shelter facilities.

The importance of research on the development of decision support systems is confirmed by [21], which describes an experiment on the implementation of such a system within a defence operation. However, the modelling is based on the results of a reconnaissance model of UAVs, which is the subject of a significant part of the paper.

Thus, there are many works that solve individual problems of using civilian shelter facilities from missile and kamikaze drones attacks, but there is no comprehensive approach to achieving the overall goal. Therefore, there is a need to develop a methodological approach to analysing the initial data with the selection of an optimality criterion. It should approximate the determination of the generalisation of the indicator of the linear planning model for selecting facilities of sheltering the civilian population from attacks by ballistic (cruise) missiles and kamikaze drones in urbanized areas.

PURPOSE AND OBJECTIVES OF THE STUDY

The purpose of the study is to develop a mathematical approach that will improve the efficiency and accuracy of decision-making on the choice of civilian shelter

facilities from attacks by ballistic (cruise) missiles and kamikaze drones in urbanized areas. This will provide an opportunity to improve the safety of civilians in cities and towns outside the combat zone.

The following tasks were set to achieve this goal:

- to develop a generalised model for assessing the selection of civilian shelter facilities against attacks by ballistic (cruise) missiles and kamikaze drones s in urbanized areas;
- determine the vectors of weighting coefficients of the proposed model;
- to justify the choice of a method for studying the correlation between a generalised criterion and an observable feature.

MATERIALS AND METHODS OF RESEARCH

The object of the study is to plan the choice of civilian shelter facilities from attacks by ballistic (cruise) missiles and kamikaze drones in urbanized areas. The essence of the proposed approach is to adapt the existing mathematical apparatus to the real conditions of operational decision-making by applying a generalised optimality criterion. The weighting criteria make it possible to determine how relevant individual means are in a particular situation, which will increase the efficiency of planning the selection of the civilian shelter facilities.

The following research methods were chosen:

- generalization — to formulate an indicator of a linear model for planning the protection of civilians from attacks by ballistic (cruise) missiles and kamikaze drones in urbanized areas;
- classification — to identify and substantiate the main factors affecting the feasibility of using and the effectiveness of the protective properties of the protective equipment in a given situation;
- analysis — to determine the criteria that can be used when deciding on the choice of civilian shelter facilities from attacks by ballistic (cruise) missiles and kamikaze drones in urbanized areas;
- regression analysis — to study the correlation between the generalised criterion and the observed feature;
- synthesis — to develop a model for assessing the effectiveness of civilian shelter facilities.

The mathematical modelling was carried out using ASNA software (Ukraine), which provides a formalised representation of the structure and behaviour of a system engineering object.

RESULTS OF RESEARCH ON THE MATHEMATICAL APPARATUS FOR ASSESSING THE EFFECTIVENESS OF CIVILIAN SHELTER FROM MISSILE AND UAV ATTACKS

Development of a generalised model for assessing the choice of shelter from missile and UAV attacks

Decisions on the choice of civilian shelter should be made taking into account all the above criteria and in accordance with national and international standards. The standards for this type of structure should also be taken into account.

The optimal criteria for the selection of a civilian protective structure may vary depending on the specific conditions and missile attacks. However, in general, there are several criteria that can be used when deciding on the selection of civilian protective equipment:

- effectiveness of civilian shelter facilities: it is important that the type of structures and method of their application are designed to protect people without injury or maim from the fragmentation and blast effects of ballistic (cruise) missiles and enemy UAVs;
- minimizing collateral damage during relocation to a shelter: it is important to take into account possible collateral damage based on the density of civilian areas and the availability of convenient routes to access protective shelters;
- minimizing collateral damage in the event of a direct hit by both aircraft and their bulky fragments after being shot down by air defence forces. It is important to take into account possible cases of hitting these structures and provide them with medical supplies to provide first aid to the victims. It is also advisable to place signalling devices to notify the State Emergency Service and medical teams of damage to the civilian shelter facilities;
- consideration of the specifics of the environment in urbanised areas. Consideration should be given to the weather, time of day, terrain, built-up and illumination of the area, the presence of parked cars on the way to the civilian shelter facilities, the average length of the journey and other conditions that may impede rapid movement;
- cost-effectiveness: the cost of sheltering civilians, the ability of industry to meet the needs of the population in a short time, and the cost of their maintenance and upkeep should be taken into account.

In general, the choice of civilian shelter in urbanized areas should be based on tools that can describe the degree of realisation of their potential capabilities (Fig. 1).

The analysis of Fig. 1 indicates a factor that affects the optimisation of decisions. This may be the so-called wide range of protective structures from various manufacturers. However, its main role is to implement simple concepts — preserving not only civilian lives, but also health in the full sense of the word. After all, the existing standards are more general [22] and do not fully reveal the essence of protecting citizens from missile threats [23] or the threat of using kamikaze drones . Therefore, in order to determine the criterion for the optimal selection of an air defence system against attacks by ballistic (cruise) missiles and kamikaze drones in urbanized areas, it is necessary to understand the relationship between the nature of the attacks and the capabilities of the civilian shelter facilities. For the practical implementation of the above, it is possible to use linear forms of factor relationship in combination with a generalised optimality criterion in the form of a linear combination of local criteria [24–26]:

$$F(x)=a_1 f_1(x)+...+a_i f_i(x)+...+a_K f_K(x), \qquad (1)$$

where a_i are the weighting coefficients for local optimality criteria; i is the index of the local criterion $(1,2,...,K)$.

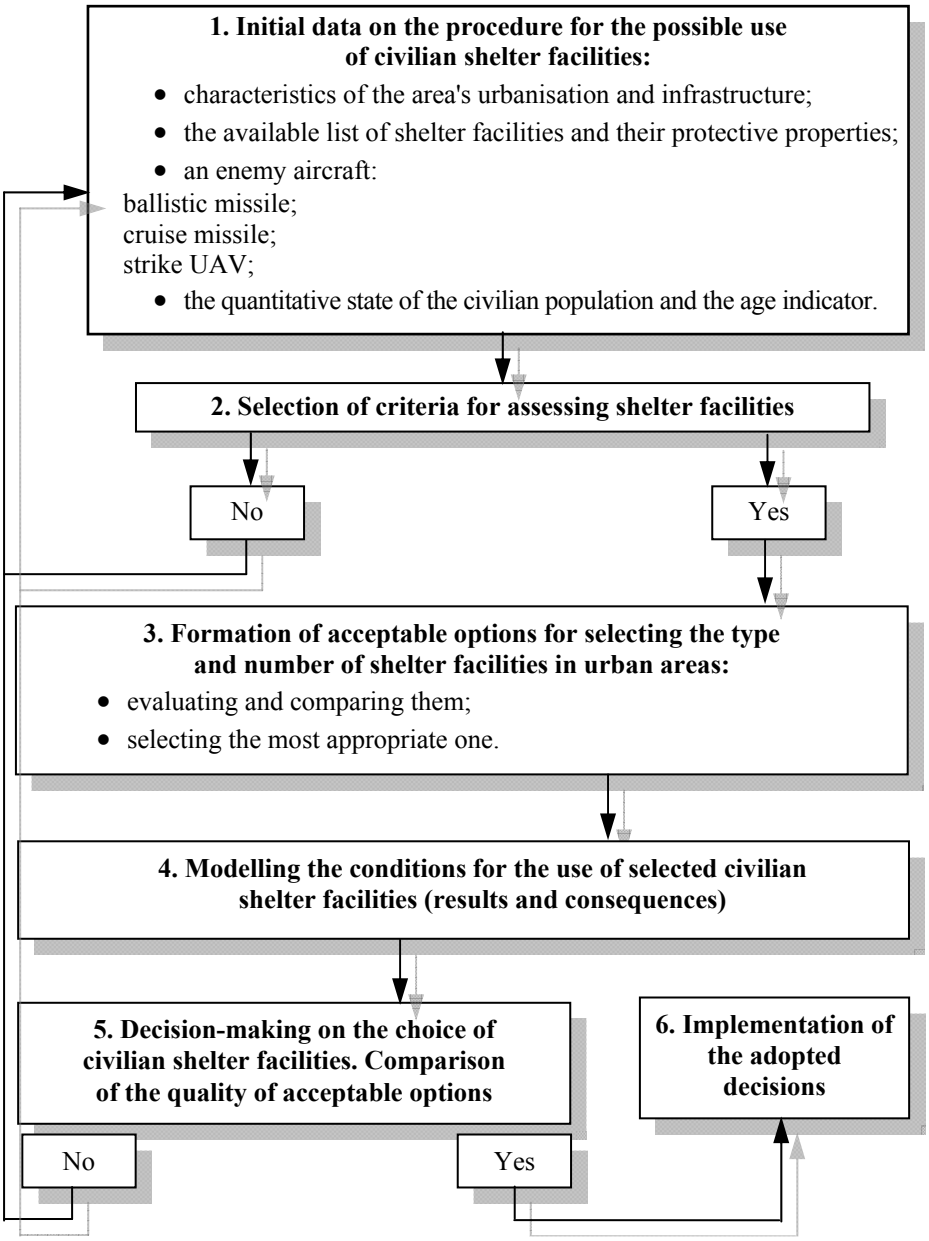

Fig. 1. Flowchart of the model for assessing the effectiveness of the use of civilian shelter facilities

Determination of the weighting vectors of the proposed model

To determine the vector $\overline{a}$ of weighting coefficients, it is possible to apply an approach with the selection of a certain local criterion as an indicator (basic optimality criterion) $f_i(x)$. Then, the dependence of the remaining criteria $(K-1)$ on the given one can be represented as [27; 28]:

$$f_i(x) = a_1^* f_1(x) + \ldots + a_{i-1}^* f_{i-1}(x) + a_{i+1}^* f_{i+1}(x) + \ldots + a_K^* f_K(x). \qquad (2)$$

Based on the method of multivariate regression analysis and using dependence (2), $\bar{a}^0$ will look like this [29–31]:

$$f_i(x)=a_1^0 f_1(x)+...+a_{i-1}^0 f_{i-1}(x)+a_{i+1}^0 f_{i+1}(x)+...+a_K^0 f_K(x).$$

Then the optimisation criterion in the linear model will be applied in the following interpretation:

$$F(x)=f_i(x)=a_1^0 f_1(x)+...+a_{i-1}^0 f_{i-1}(x)+a_{i+1}^0 f_{i+1}(x)+...+a_K^0 f_K(x).$$

Some local criteria $k_1 < k$ (time to move to shelters) should be minimised as much as possible, and the rest (number of civilian shelter facilities, their degree of protection) should be maximised:

$$F(x) = -\sum_{i=1}^{k_1} a_i^0 f_i(x) + \sum_{i=k_1+1}^{K} a_i^0 f_i(x) \to \max,$$

either:

$$F(x)=\sum_{i=1}^{k_1} a_i^0 f_i(x) - \sum_{i=k_1+1}^{K} a_i^0 f_i(x) \to \min.$$

This approach is associated with the rapidity and unpredictability of attacks, as well as possible sudden changes in the situation.

Selecting a method for studying the correlation between a generalised criterion and an observable feature

To study the effectiveness of the relationship between the generalised criterion $F(x)$ and the observational feature $f_i\ (i=\overline{1,K})$ as the weighting factor a_i $(i=\overline{1,K})$ of the function of the form (2), it is possible to apply the method of multivariate regression analysis:

$$F(x,a)=a_0+a_1 f_1(x)+...+a_j f_j(x)+...+a_m f_m(x),$$

where *m* is the number of parameters under study, *units*.

In this case, the level of regression is described by the values of $a_0, a_1,\ldots,a_m$ and the final variance. Replacing the values of $a_0, a_1,\ldots,a_m$ with their estimates, and $f_j(x)$ with f_j, the regression equation will take the form:

$$F(x)=b_0+b_1 f_1+...+b_j f_j+...+b_m f_m.$$

The initial data for calculating the coefficients $b_0, \ldots,b_m$ are a sample from a multidimensional population in the form of the matrix f and the vector $\overline{F}$ [32–34]:

$$f=\begin{vmatrix} f_{11} & f_{21} & f_{j1} & f_{m1} \\ f_{12} & f_{22} & f_{j2} & f_{m2} \\ \cdots & \cdots & \cdots & \cdots \\ f_{1n} & f_{2n} & f_{jn} & f_{mn} \end{vmatrix}, \quad \overline{F}=\begin{vmatrix} F_1 \\ F_2 \\ \cdots \\ F_n \end{vmatrix}.$$

For the convenience of selecting the civilian shelter facilities through $\bar{f}_j$, it is advisable to define the *j*-th vector as the column f of the matrix

$\bar{f}_j = \{f_{j1}, f_{j2}, ...f_{jn}\}$, and through $\bar{f}_i$ to calculate the *i*-th vector as a row of the corresponding matrix $\bar{f}_i = \{f_{1i}, f_{2i}, ..., f_{mi}\}$:

$$\begin{cases} nb_0 + b_1\sum_{i=1}^{n} f_{1i} + ... + b_m\sum_{i=1}^{n} f_{mi} = \sum_{i=1}^{n} F_i; \\ b_0\sum_{i=1}^{n} f_{1i} + b_1\sum_{i=1}^{n} f_{1i}f_{1i} + ... + b_m\sum_{i=1}^{n} f_{1i}f_{mi} = \sum_{i=1}^{n} f_{1i}F_i; \\ ..... \\ b_0\sum_{i=1}^{n} f_{mi} + b_1\sum_{i=1}^{n} f_{1i}f_{mi} + ... + b_m\sum_{i=1}^{n} f_{mi}f_{mi} = \sum_{i=1}^{n} f_{mi}F_i. \end{cases} \quad (3)$$

Despite the fact that this system can be calculated by any method of linear algebra, in conditions of limited time indicators, the inverse matrix method can be used when selecting civilian shelter facilities, expressing through b_j $(j = 1,2,\ldots,m)$ [35–37].

Substituting the equation of the form (3) into the other expressions of the system, we define the coefficient matrix by C with the unknown parameters $b_1, b_2, \ldots, b_m$ and the substitution of b_0. The inverse matrix can be defined by C^{-1}, respectively, the element located at the intersection of the *i-th* row and the *j-th* column by c_{ij}^{-1}:

$$b_j = \sum_{i=1}^{n} c_{ij}^{-1}(f_{ji}F_i - n\bar{f}_j\overline{F}). \quad j = 1,2,...,m, \quad b_0 = \overline{F} - b_1\bar{f}_1 - ... - b_j\bar{f}_j - ... - b_m f_m.$$

The estimate of the final variance s_{qp}^2 is the expression:

$$s_{KH}^2 = \frac{\sum_{i=1}^{n}[F_i - F(f_i)]^2}{n - m - 1},$$

where F_i is the measured value of the performance attribute; $F(f_i)$ is the value of the outcome variable calculated according to the regression equation.

To statistically substantiate the conclusion $t = \left|\frac{b_j}{s_{b_j}}\right|$ each of the coefficients $(j = 0,1,2,...,m)$ is different from zero (significance of the regression coefficient estimates) and is calculated by the expression [38, 39]:

$$\begin{cases} s_{b_0} = \dfrac{s_{KH}}{\sqrt{\dfrac{1}{n} + \sum_{j,k=1}^{n} \bar{f}_j\bar{f}_k c_{ij}^{-1}}}, \\ \qquad\qquad i = 1,2,...,n, \quad j \neq k. \\ s_{b_j} = \dfrac{s_{KH}}{\sqrt{c_{jj}^{-1}}}, \end{cases} \quad (4)$$

In accordance with the given significance level χ and the number of degrees of freedom $k = n - m - 1$, the critical value of $t_{\chi k}$ is as follows:

$t > t_{\chi k}$, the null hypothesis that the regression coefficient is equal to zero is rejected and considered significant;

$t < t_{\chi k}$, the estimate of the regression coefficient will be insignificant.

Due to the regression analysis, the expression for the generalised optimality criterion will be as follows:

$$F(x) = b_0 + b_1 f_1(x) + ... + b_{m'} f_{m'}(x),$$

where $m' < m$ — regression coefficients may be insignificant.

The multivariate regression analysis method was chosen due to its following advantages:

- allows for easy interpretation of the impact of individual independent variables on the dependent variable; regression coefficients help to understand how much the dependent variable changes when the unit of the independent variable changes, while holding other variables constant;
- linear regression is a relatively simple and well-studied model, which makes it a reasonable choice for the first analysis of data;
- If the relationship between the variables is basically linear, then linear regression can provide fairly accurate results;
- it can help to identify statistically significant relationships between variables and highlight important factors;
- it is possible to analyze the influence of one factor while others are fixed, which helps to understand how variables interact with each other.

To conduct the analysis, it is proposed to determine the values of the weighting coefficients for various attributes (Table).

Characteristics and common features of the object influencing on results

Type	**Characteristics and common features**
Characteristics of urbanized areas	local centre
	centre of the periphery
	commercial district
	residential area
	industrial area
	neighbourhood
Planning of urban streets and their importance	rectangular
	radiated
	beam
	beam-ring
	contour shaped
	wrong
	combined planning
	linear
Characteristics of buildings by size	small buildings (area is less than 180 m^2)
	medium-sized buildings (area from 180 m^2 to 2000 m^2)
	large buildings (area from 2000 m^2 to 4000 m^2)
	massive buildings (area exceeds 4000 m^2)
Characteristics of buildings by height	low-rise (up to 3 floors inclusive, with a building height of up to 9 m)
	multi-storey (up to 9 floors inclusive, with a building height of 9 m to 26.5 m)
	Increased-storey (up to 16 floors inclusive, with a height of 26.5 m to 47 m)
	high-rise (more than 16 floors, with a height of more than 47 m)

Continued Table

Type	**Characteristics and common features**		
Construction materials	Wood		
	Brick		Brick buildings
			Buildings with box walls
	Reinforced concrete		
	Steel or metal		Frame houses with heavy walls
			Frame houses with lightweight walls
Type of facilities that can be used as a civilian shelter	Special purpose buildings		Storage
			Anti-radiation (anti-chemical) shelter
	Dual-purpose buildings		
	Prefabricated modular civil defence structures		
	Rapidly built modular storage facilities		
	External enclosing structures of modular type prefabricated radiation protection shelters		
	The simplest shelters		
An enemy aircraft	Ballistic missile (rocket) Cruise missile Strike UAV	Initial effect of the explosion	light flash
			sound effect
		Impact of the explosion (impact on surrounding infrastructure)	Brisant effect
			blast effect
			thermal effect
			fragmentation effect
			Secondary fragmentation effect of the destroyed object (breaking up the fragmentation mass of the aircraft)
		Explosion residual effects (dispersion and impact of explosive particles and detonation products)	Impact of explosive particles on the environment
			Impact of particles of the object's fragmentation shell on the environment
			The impact of particles of the destroyed object on the environment
Quantitative state of the civilian population	Total quantity and ratio of urban and rural residents		
Age structure of the population	Total quantity and ratio of people of different age groups		
Description and population of the settlement	A farmstead (a house for 1 family, with accompanying buildings, in rural areas) — up to 25 people		
	Village (small community registered in rural areas) — from 100 to 1000 people		
	Urban-type settlements — from 1,000 to 10,000 people		
	Small towns — up to 50 thousand people		
	Average city — from 50 thousand to 250 thousand people		
	Large city — from 250,000 to 500,000 people		
	Large city — from 500,000 to 1 million people		
	Millionaire city — more than 1 million people		

The concepts in Table have the following meaning.

Dual-purpose structures are ground or underground structures or their separate parts that are designed or adapted for use for their main functional purpose,

including for the protection of the population, and in which conditions for the temporary stay of people are created.

Quick-build civil protection structures of modular type should ensure protection of the population to be sheltered from the estimated impact of destruction means in accordance with ДБН В.2.2-5 within the normative time established in accordance with ДБН В.1.2-4.

Quick-build modular storage facilities must provide protection against:

- exposure to excessive pressure at the front of an airborne shock wave of at least 100 kPa;
- local and general effects of conventional munitions (small arms, fragments of hand grenades, artillery ammunition and aerial bombs).

External enclosing structures of prefabricated modular radiation protection shelters should provide protection of the public against:

- local and general effects of conventional munitions (small arms, fragments of hand grenades, artillery ammunition and aerial bombs);
- exposure to external ionising radiation and excessive pressure of the airborne shock wave front, depending on the location.

The simplest shelters are fortifications or basements, or other underground structures where people can temporarily stay in order to reduce the combined damage from hazards and from the effects of munitions during a special period.

To understand the destructive effect of aircraft even after they are shot down in the air, we will model this process. After an aircraft is detonated in the air, the explosion products, expanding to a value equal to 10–12 charge radii before atmospheric pressure is restored, will displace the air adjacent to them, compressing it and setting it in motion. However, the expansion process will not end there. By inertia, it will increase to a value close to 20 charge radii. At this point, the layer of compressed air is detached from the explosion products and, due to the energy it receives, continues to move independently at supersonic speed, representing the so-called air shock wave. The latter captures significant masses of air as it moves. Thus, the enlarged air moves behind the shock wave front, leaving behind a region of rarefaction where the pressure drops below atmospheric pressure.

As the energy of the shock wave moves away from the centre of the explosion, it is dispersed spherically in the environment, heating the air. Thus, the pressure amplitude (jump) gradually decreases with increasing distance from the centre of the explosion, and the velocity at the wave front decreases, becoming the speed of sound. As a result, the shock wave gradually fades away. However, the depth of the wave, namely the time of its overpressure action, increases with distance from the centre of the explosion [40].

The shock wave from an aircraft crash reaches the ground and is reflected from it and moves towards the centre of the explosion as a reflected shock wave. As it moves in the air, which is thinned and heated by the previous shock (incident) wave, its speed is greater than the speed of the incident shock wave, and at a distance approximately equal to the height of the explosion, the reflected shock wave catches up with the incident shock wave and, merging with it, forms the so-called main shock wave, which carries.

Thus, when an aircraft is shot down, the reflected wave will usually move along with the main wave with the pressure at its front close to the main wave. Therefore, there is a common assumption that the shock wave from a ground explosion of an aircraft and the shock wave from its impact within the irregular reflection zone are zones of increased pressure hypothetically created by a double

mass charge. This will be true when calculating the dynamic loads of the rigid surfaces of the civilian shelter facilities. However, when calculating non-rigid surfaces, it is advisable to take into account the correction factor with the charge mass.

Coefficients are assigned to the input values, and the ASNA software determines the weight of each value through mathematical modelling. This can take into account mutual exclusions or complementarities in the Kolmogorov–Chapman system of equations on which the selected software is based.

Using the systems engineering approach, it is possible to obtain calculations for systems that do not yet exist, when reference values are not yet available. The methodology allows values to be obtained if specific values are provided, such as concrete thickness, reinforcement diameter, etc.

Based on the values given in Table, we calculated and obtained graphs (Figs. 2–5), which allow us to conclude that the results obtained are adequate to the values obtained by other scientists [41].

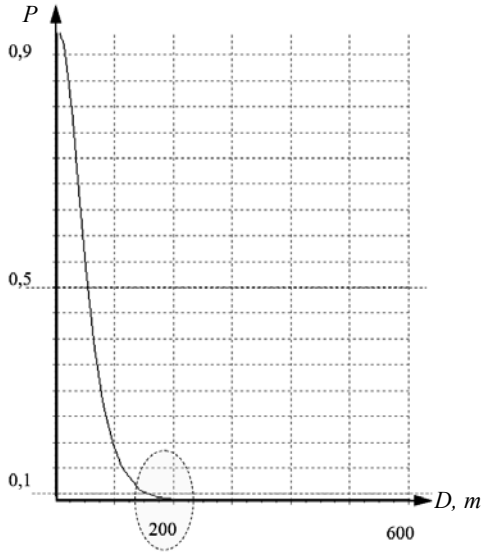

Fig. 2. Diagram of the location of the civilian shelter facilities from the residence of citizens

The analysis of Fig. 2 shows that the distance (*D*) of the location of the control centre from the dwellings should not exceed 200 m. Depending on the time of day (day, night), weather conditions (slippery road in winter, heavy rain in summer), presence of children under 6 years old in the family, elderly people over 60 years old, people with different health conditions, the time for moving increases. Therefore, the location of a civilian shelter facilities against aircraft strikes at a distance of more than 200 m reduces the likelihood of protecting people from damage of varying degrees.

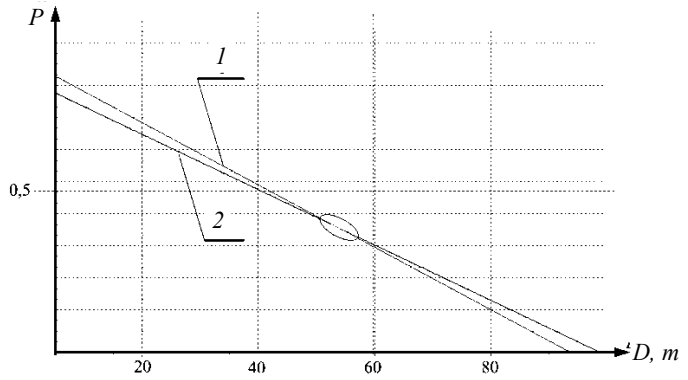

Fig. 3. Graph of the probability of damage versus wall thickness of typical civilian shelter facilities (*1*) and non-typical civilian shelter facilities (*2*)

The authors of this paper argue that structures of different types in the form of civilian shelter facilities can be combined as typical and non-typical. The analysis of Fig. 3 shows that the degree of protection of typical and atypical objects with wall thicknesses from 20 mm to 60 mm steel equivalent, depending on its ability to withstand shock waves and fragments of different fractions, has virtually the same properties of 54 mm thickness.

Analysis of Fig. 4 shows the following. Regardless of the type of shelter, during the open impact of a warhead (within 50 kg) of a Shahed UAV (Russian analogue is the "Герань-2"), the probability of sustaining damage at the level of 0.5 in the form of acubarotrauma of varying degrees or other injuries is within 34 m. In other words, the protection against direct impact of a Shahed-type kamikaze drones on Mamad-type premises without additional obstacles in the form of building walls or other structures (objects) is close to that of specially equipped premises. The placement of the civilian shelter facilities directly in the room allows to reduce the time for movement, i.e. staying in the unprotected area.

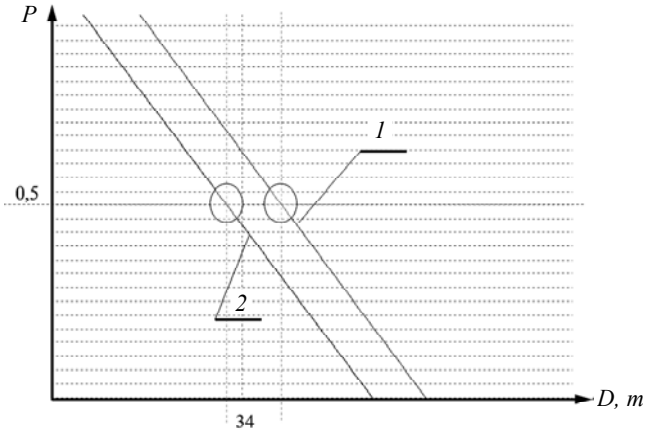

Fig. 4. Diagram of comparative characteristics of protective properties of civilian shelter facilities in the form of special rooms (*2*) and rooms of the "mamad" type (*1*)

An analysis of Fig. 5 shows that, regardless of the type of settlement, when

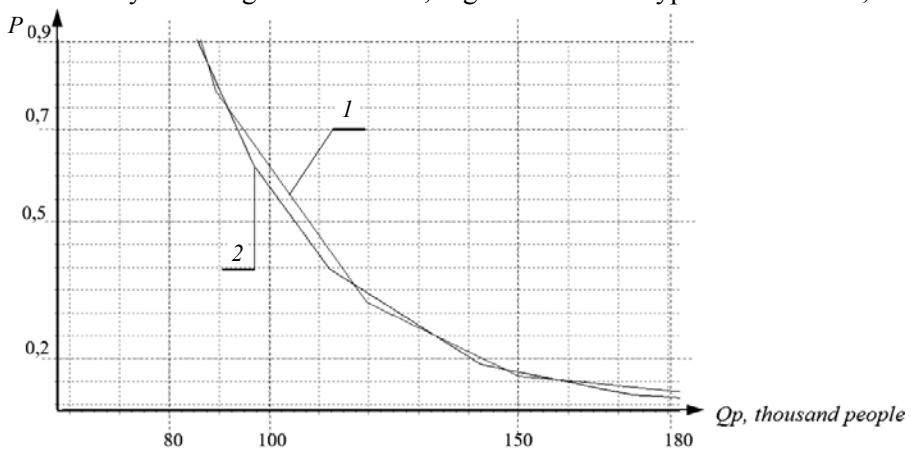

Fig. 5. Graph of the dependence of the protective properties of the civilian shelter facilities on the number of civilians in need of protection

the population is 87.000 or more, and despite the uniformity of the warning, the number of collective-type civilian shelter facilities is significantly reduced. The authors deliberately did not take into account cities with a population of more

than one million people, because in these cities the communication infrastructure and the sense of danger are more developed than in much smaller towns and villages, where people's confidence in their own safety is based mainly on the principle of self-complacency. Those settlements with a population of less than 87.000 should be considered according to a different principle or be merged into certain structures. This is because it is difficult to assess the feasibility of building civilian shelter facilities for a population of up to 10.000 inhabitants without taking into account economic indicators. Private households allow for the construction of various types of structures where it would be possible to hide from enemy aircraft.

DISCUSSION OF THE RESULTS OF THE STUDY OF THE CRITERION FOR THE OPTIMAL CHOICE OF CIVILIAN SHELTER FACILITIES

This paper calculates a generalised criterion for the optimality of the selection of civilian shelter facilities in the form of regression coefficients (4). It is based on the developed model for assessing the effectiveness of the use of civilian protective equipment, the flowchart of which is shown at Fig. 1. The optimality criterion is capable of determining a generalised indicator of a linear model for selecting civilian shelter facilities during attacks by ballistic (cruise) missiles and kamikaze drones in urbanized areas.

The essence of the proposed approach is to adapt the existing mathematical apparatus to the real conditions of operational decision-making through the use of a generalised optimality criterion. The weighting criteria make it possible to determine how relevant individual facilities are in a particular situation, which will increase the efficiency of planning the selection of civilian shelter facilities during attacks by ballistic (cruise) missiles and kamikaze drones s in urbanized areas.

In order to select sheltering civilians from attacks, it is necessary to have a set of physical (technical) states of civilian shelter facilities with a set of values and signs sufficient to assess their reliability. This necessitates the creation and implementation of a new system of concepts based on a more detailed accounting of the results of civilian protection. In turn, this to some extent limits the applicability of the research results and requires preliminary data preparation for their use.

A similar study [42], which analysed the use of tunnels as civilian shelter facilities, is based on the use of hierarchy analysis. This requires users to perform a large number of pairwise comparisons and importance assessments. For large and complex problems, this can be a time-consuming and confusing process. Paper [43] uses a stepwise weighting factor analysis to develop a model for rapidly assessing the vulnerability of office buildings to explosion. However, this multicriteria decision-making method may not be sufficiently transparent about how it arrives at the final rankings and decisions. This can be a concern in situations where stakeholders need to understand the reasoning behind decisions. The research presented in this paper does not have these shortcomings. Its peculiarity is the focus on applying the choice of the civilian shelter facilities in urbanized areas, which leads to the inclusion of a significant number of indirect indicators in the calculation.

The advantages of the proposed approach are as follows:

- versatility: the generalised optimality criterion can be applied to different types of civilian shelter facilities in the context of attacks by ballistic (cruise) missiles and kamikaze drones s in urbanized areas;

- time and resource savings: compared to traditional assessment methods, the time and resources required to assess the suitability of civilian shelter facilities against ballistic (cruise) missile and kamikaze drones attacks can be reduced;
- decision-making support: application of the generalised optimality criterion can help to make a rational decision on the informed choice of civilian shelter facilities with objective data and conclusions obtained also on the basis of mathematical models on the course of possible consequences.

The limitation of this study is that the proposed solutions address only a few types of possible causes of damage (ballistic missile, cruise missile or kamikaze drones and do not include fragmentation and high-explosive projectiles.

Some possible disadvantages may include:

- subjectivity of the choice of criteria: the choice of criteria used in the model can be subjective and dependent on the researcher, which can lead to incorrect or biased results;
- increased requirements for input data: the development and application of the model may require a significant amount of data that may be difficult to obtain or process.

Increasing the protection of the population can be achieved by creating a fund of protective structures and, on its basis, informing the population about the optimal choice of civilian shelter facilities.

A fund of civilian shelters can be created by:

- implementation of the provisions of the sections (schemes) of engineering and technical measures for civil protection of urban planning and design documentation of construction projects in terms of construction (adaptation) of protective and dual-purpose structures;
- integrated development of the underground space of cities and other settlements to accommodate social, industrial and economic facilities;
- creation and registration of existing dual-purpose structures and simple shelters, other operated facilities, including underground and above-ground buildings, mine and other workings and underground cavities;
- construction of quick-build protective structures and arrangement of the simplest shelters during the special period;
- proactive acquisition (manufacture) and maintenance in peacetime of special designs of quick-build shelters, including block-modular type, ready for installation and use.

Public awareness will be based on the data on the protective structures fund. It can take various forms: posting information on a website or physical objects, development of an application for mobile phones that will take into account a person's location and distance to nearby civilian shelter facilities, etc. This is planned to be put into practice in the course of further research and experiments.

Along with the results obtained, the authors of this paper consider it expedient to use the experience of Israel, which consists in partial abandonment of the so-called "public" shelters in the future and transition to "individual" shelters in the homes of Ukrainian citizens. First, the flight time of ballistic missiles is measured in minutes. Secondly, there is a problem of ignoring air raid warnings among the public. Thirdly, the maintenance of collective civilian shelter facilities is a rather cumbersome task even for Israel.

Thus, blindly and thoughtlessly copying the experience of other countries is a futile exercise. After all, from the mentality of the population, traditions and

geographical location to the enemy, all of which impose significant limitations on someone else's experience. Therefore, it is important to evaluate and take into account the results of others, but the main thing is to create our own authentic model of protecting civilians from missile and Kamikaze drones . Moreover, such work should be carried out on an ongoing basis and not just for years, but for decades.

CONCLUSIONS

1. A generalised model for assessing the use of civilian shelter facilities selecting has been developed by applying linear forms of factor linkage in combination with a generalised optimality criterion in the form of a linear combination of local criteria.

2. The vectors of weighting coefficients of the proposed model were determined, taking into account their peculiarities in the context of attacks by ballistic (cruise) missiles and kamikaze drones in urbanized areas.

3. The method of multivariate regression analysis was chosen as a method of studying the correlation between the generalised criterion and the observed feature. Its advantages are the interpretability of the impact of individual independent variables on the dependent variable, ease of use, good handling of linear dependencies and the ability to detect changes, as well as relatively simple modelling of the influence of variables on each other.

Conflict of interest. The authors declare that there are no conflicts of interest in this research, including financial, special nature, authorship or any other nature that could affect the research and the results presented in this article.

Finance. The investigation was carried out without financial support.

Data availability. Data will be given for the connected power supply.

REFERENCES

1. A. Goncharova, Y. Fursa, O. Kryzhevska, L. Zolota, and I.P. Hrybachova, "Inheritance in the occupied territories and in the area of antiterrorism operation: the experience of Ukraine," *Amazonia Investiga*, vol. 11, no. 50, pp. 55–65, 2022. doi: https://doi.org/10.34069/AI/2022.50.02.6
2. Andrew Monaghan, "The 'War' in Russia's 'Hybrid Warfare'," *Parameters*, vol. 45, no. 4, 2015. doi: https://doi.org/10.55540/0031-1723.2987
3. O. Shevchuk, N. Mentuh, "Legal aspects of professional preparation of anti-terrorist operation," *Actual problems of law*, no. 3, pp. 96–99, 2018. doi: https://doi.org/10.35774/app2017.03.096
4. A. Loishyn, I. Tkach, M. Tkach, and V. Shevchuk, "Analysis and systematization of approaches to understanding the concept of "hybrid war"," *Journal of Scientific Papers "Social Development and Security"*, *11*(1), pp. 145–162, 2021. doi: https://doi.org/10.33445/sds.2021.11.1.15
5. M. Kyzym, V. Khaustova, and V. Shlykova, "War in Ukraine: Analysis of the Prerequisites, Lessons of the Infighting, and Conclusions for the Future," *The Problems of Economy*, no. 2(52), pp. 47–57, 2022. doi: https://doi.org/10.32983/2222-0712-2022-2-47-57
6. L.A. Moniz Bandeira, "Ukrainian Separatists and the War in Donbass," in *The World Disorder*. Springer, Cham, 2019. doi: https://doi.org/10.1007/978-3-030-03204-3_20
7. M. Zabrodskyi, J. Watling, O.V. Danylyuk, and N. Reynolds, *Preliminary lessons in conventional warfighting from Russia's invasion of Ukraine: February-July 2022.* London: Royal United Services Institute, 2022. Available: https://static.rusi.org/359-SR-Ukraine-Preliminary-Lessons-Feb-July-2022-web-final.pdf

8. Y. Elster, A. Zussman, and N. Zussman, "Effective Counter-Terrorism: Rockets, Iron Dome, and the Israeli Housing Market," *Journal of Policy Analysis and Management*, 38(2), pp. 308–337, 2019. doi: https://doi.org/10.1002/pam.22114
9. L. Zucker, E.H. Kaplan, "Mass casualty potential of Qassam rockets," *Studies in Conflict & Terrorism*, 37(3), pp. 258–266, 2014. doi: https://doi.org/10.1080/1057610X.2014.872024
10. V. Yakovenko, B. Volochiy, N. Furmanova, I. Savina, and O. Malyi, "Application of states and transitions graph for developing the model of the process of shelling a mobile armored target," *Proceedings - 16th International Conference on Advanced Trends in Radioelectronics, Telecommunications and Computer Engineering, TCSET 2022*, pp. 727–732. doi: https://doi.org/10.1109/TCSET55632.2022.9766916
11. V. Yakovenko et al., "Determining the components of the structuralautomatic model of firing a single target in armor protection with fragmentation-beam projectiles of directed action in a series of three shots based on the reference graph of states," *Eastern-European Journal of Enterprise Technologies*, vol. 5, no. 3(119), pp. 29–41, 2022. doi: https://doi.org/10.15587/1729-4061.2022.266275
12. V. Yakovenko, et al., "Building a model of the process of shooting a mobile armored target with directed fragmentation-beam shells in the form of a discrete-continuous stochastic system," *Eastern-European Journal of Enterprise Technologies*, vol. 6, no. 4(114), pp. 51–63, 2021. doi: https://doi.org/10.15587/1729-4061.2021.245703
13. M. Graswald, R. Gutser, J. Breiner, F. Grabner, T. Lehmann, and A. Oelerich, "Defeating Modern Armor and Protection Systems," *Proceedings of the 2019 15th Hypervelocity Impact Symposium, Destin, FL, USA. April 14–19, 2019*. V001T03A004. ASME. doi: https://doi.org/10.1115/HVIS2019-050
14. M.S. Ismail, A. Ahmad, S. Ismail, and N.M.M. Yusop, "A review on Unmanned Aerial Vehicle (UAV) threats assessments," in *AIP Conference Proceedings*, vol. 2617, no. 1, 2022. doi: https://doi.org/10.1063/5.0119703
15. J.P. Yaacoub, H. Noura, O. Salman, and A. Chehab, "Security analysis of drones systems: Attacks, limitations, and recommendations," *Internet of Things*, *11*, 100218, 2020. doi: https://doi.org/10.1016/j.iot.2020.100218
16. A. Shakibamanesh, "Public shelters: Towards secure urban planning and designing in terms of passive defense," *Geografia*, 11(3), 2015. Available: http://journalarticle.ukm.my/9219/1/1x.geografia-mac15-amir-bi-edam.pdf
17. W. Harmata, Z. Szcześniak, M. Sobiech, and A. Baryłka, "Ad hoc hiding places as part of collective protection," *Inżynieria Bezpieczeństwa Obiektów Antropogenicznych*, (2), pp. 26–41, 2023. doi: https://doi.org/10.37105/iboa.173
18. G. Cohen-Lazry, T. Oron-Gilad, "Is staying out of bomb-shelters a human-automation interaction issue?," *Technology in Society*, 47, pp. 25–30, 2016. doi: http://dx.doi.org/10.1016/j.techsoc.2016.08.002
19. H. Medema, H. Blackman, K. Savchenko, and R. Boring, "Human reliability considerations from the Hawaii ballistic missile alert event," *Probabilistic Safety Assessment and Management PSAM 14, September 2018, Los Angeles, CA*. Available: https://scholarworks.boisestate.edu/research_development_pubs/8/
20. Alan J. Vick, Sean M. Zeigler, Julia Brackup, and John Speed Meyers, "Air Base Defense. Rethinking Army and Air Force Roles and Functions," *RAND*, 2020. Available: https://www.rand.org/pubs/research_reports/RR4368.html
21. J. Drozd, "Experiment of the tactical decision support system within company defensive operation," in *Modelling and Simulation for Autonomous Systems: 5th International Conference, MESAS 2018, Prague, Czech Republic, October 17–19, 2018, Revised Selected papers 5,* pp. 544–552. Springer International Publishing. doi: https://doi.org/10.1007/978-3-030-14984-0_40
22. M. Pydko, "Aktualnist tsyvilnoho zakhystu naselennia zhytlovoi zabudovy v mistakh Ukrainy," *Mistobuduvannia ta terytorialne planuvannia*, 83, pp. 254–265, 2023. doi: https://doi.org/10.32347/2076-815x.2023.83.254-265

23. T. Zhydkova, S. Chepurna, "Orhanizatsiia zakhystu tsyvilnoho naselennia v bahatopoverkhovykh zhytlovykh budynkakh," *Mistobuduvannia ta terytorialne planuvannia*, 80, pp. 191–202, 2022. doi: https://doi.org/10.32347/2076-815x.2022.80.191-202
24. Z. Kingston, M. Moll, and L.E. Kavraki, "Sampling-based methods for motion planning with constraints," *Annual review of control, robotics, and autonomous systems*, 1, pp. 159–185, 2018. doi: https://doi.org/10.1146/annurev-control-060117-105226
25. Ulus Firdevs, *Algorithms for Vector Optimization Problems Princeton*. NJ: Princeton University, 2015. Available: http://arks.princeton.edu/ark:/88435/dsp01n009w461x
26. R. Mathar, G. Alirezaei, E. Balda, and A. Behboodi, *Fundamentals of data analytics: With a view to machine learning*, pp. 1–127, 2020. doi: https://doi.org/10.1007/978-3-030-56831-3
27. F. Bendaoud, "Multicriteria optimization methods for network selection in a heterogeneous environment," *Intelligent network management and control: Intelligent security, multi-criteria optimization, cloud computing, internet of vehicles, intelligent radio*, pp. 89–115, 2021. doi: https://doi.org/10.1002/9781119817840.ch4
28. D.S. Kim, T.S. Phạm, and N.V. Tuyen, "On the existence of Pareto solutions for polynomial vector optimization problems," *Mathematical Programming*, 177(1-2), pp. 321–341, 2019. Available: https://link.springer.com/article/10.1007/s10107-018-1271-7
29. N. Gunantara, "A review of multi-objective optimization: Methods and its applications," *Cogent Engineering*, 5(1), 1502242, 2018. doi: https://doi.org/ 10.1080/ 23311916.2018.1502242
30. L. Bottou, F.E. Curtis, and J. Nocedal, "Optimization methods for large-scale machine learning," *SIAM review*, 60(2), pp. 223–311, 2018. doi: https://doi.org/10.1137/ 16M1080173
31. P.E. Gill, W. Murray, and M.H. Wright, *Classics in Applied Mathematics. Practical Optimization*. 2019. doi: https://doi.org/10.1137/1.9781611975604
32. A. Matsumoto, *Optimization and dynamics with their applications: Essays in honor of Ferenc Szidarovszky*, pp. 1–344, 2017. doi: https://doi.org/10.1007/978-981-10-4214-0
33. B. Orazbayev et al., *System concept for modelling of technological systems and decision making in their management*, pp. 1–180, 2021. doi: https://doi.org/10.15587/978-617-7319-34-3
34. T.C. Hu, A.B. Kahng, *Linear and integer programming made easy*, pp. 1–143, 2016. doi: https://doi.org/10.1007/978-3-319-24001-5
35. V.M. Hlushkov, V.S. Mykhailevych, V.L. Volkovych, and H.A. Dolenko, "K voprosu systemnoi optymyzatsyy v mnohokryteryalnykh zadachakh lyneinoho prohrammyrovanyia," *Kybernetyka*, 3, pp. 4–8, 1982.
36. L. Csirmaz, "Using multiobjective optimization to map the entropy region," *Computational Optimization and Applications*, 63(1), pp. 45–67, 2016. doi: https://doi.org/10.1007/s10589-015-9760-6
37. P. Gupta, M.K. Goyal, S. Chakraborty, and A.A. Elngar, *Machine learning and optimization models for optimization in cloud*, pp. 1–204, 2022. doi: https://doi.org/10.1201/9781003185376
38. J. Jahn (Ed.), *Vector optimization*. Berlin: Springer, 2009, pp. 2327–4697. Available: https://link.springer.com/book/10.1007/978-3-642-02886-1
39. O.T. Altinoz, *Optimal controller parameter tuning from Multi/Many-objective optimization algorithms*. 2019. doi: https://doi.org/10.1007/978-3-030-25446-9_3
40. A.V. Ishchenko, M.V. Kobets, *Means and methods of detecting explosive substances and devices in the fight against terrorism: educational and practical manual*. K.: National Academy of Internal Affairs of Ukraine, 2015, 144 p.
41. Mahdi Modiri, Ali Mohammad, and Ali Rezaei Moghaddam, "Spatial Organizing and Distribution of Gas Stations Following Urban Passive Defense Approach (Case

Study: Gas Stations of Mashhad Metropolis)," *Urban Management*, no. 44, pp. 39–52, 2016.

42. J. Nakhaei, M. Bitarafan, and S. Lale Arefi, "Choosing the best urban tunnels as safe space in crisis using AHP method: a case study in Iran," *Journal of Architecture and Urbanism*, 39(2), pp. 149–160, 2015. doi: https://doi.org/10.3846/ 20297955.2015.1056439
43. J. Nakhaei, M. Bitarafan, S. Lale Arefi, and O. Kapliński, "Model for rapid assessment of vulnerability of office buildings to blast using SWARA and SMART methods (a case study of swiss re tower)," *Journal of Civil Engineering and Management*, 22(6), pp. 831–843, 2016. doi: https://doi.org/10.3846/ 13923730.2016.1189457

Received 01.09.2023

INFORMATION ON THE ARTICLE

Vadim V. Yakovenko, ORCID: 0000-0001-8591-6998, Odesa Military Academy, Ukraine, e-mail: yakob@ukr.net

Nataliia I. Furmanova, ORCID: 0000-0002-8670-2948, Zaporizhzhia Polytechnic National University, Ukraine, e-mail: nfurmanova@gmail.com

Ihor M. Flys, ORCID: 0000-0001-6334-0027, Hetman Petro Sahaidachnyi National Army Academy, Ukraine, e-mail: 9imf61@gmail.com

Oleksandr Yu. Malyi, ORCID: 0000-0002-8457-8154, Zaporizhzhia Polytechnic National University, Ukraine, e-mail: docsasha2@gmail.com

Oleksii Yu. Farafonov, ORCID: 0000-0001-5963-5033, Zaporizhzhia Polytechnic National University, Ukraine, e-mail: farafon@zntu.edu.ua

Harri V. Moroz, ORCID: 0000-0003-4636-4961, Zaporizhzhia Polytechnic National University, Ukraine, e-mail: garrymrz206@gmail.com

ВИЗНАЧЕННЯ УЗАГАЛЬНЕНОГО КРИТЕРІЮ ОПТИМАЛЬНОСТІ ВИБОРУ ЗАСОБІВ УКРИТТЯ ЦИВІЛЬНОГО НАСЕЛЕННЯ ВІД АТАК БАЛІСТИЧНИМИ (КРИЛАТИМИ) РАКЕТАМИ ТА УДАРНИМИ БЕЗПІЛОТНИМИ ЛІТАЛЬНИМИ АПАРАТАМИ В УРБАНІЗОВАНИХ РАЙОНАХ / В.В. Яковенко, Н.І. Фурманова, І.М. Флис, О.Ю. Малий, О.Ю. Фарафонов, Г.В. Мороз

Анатоція. Об'єктом дослідження є планування вибору засобів укриття цивільного населення від атак балістичними (крилатими) ракетами та ударними безпілотними літальними апаратами (БпЛА) в урбанізованих районах. Розроблено узагальнену модель оцінювання вибору засобів укриття цивільного населення шляхом застосування лінійних форм зв'язку факторів у поєднанні з узагальненим критерієм оптимальності у вигляді лінійної комбінації локальних критеріїв. Як метод дослідження кореляції між узагальненим критерієм та спостережною ознакою обрано метод багатовимірного регресійного аналізу. Розраховано узагальнений критерій оптимальності вибору засобів укриття цивільного населення від атак балістичними (крилатими) ракетами та ударними БпЛА в урбанізованих районах у вигляді коефіцієнтів формування регресії. Критерій здатен сприяти спрощеному визначенню узагальненого показника лінійної моделі планування захисту мирних громадян у містах поза межами бойових дій. Вихідними даними є набір фізичних (технічних) станів укриттів з переліком величин і ознак, достатніх для оцінювання їх стійкості до високих динамічних навантажень.

Ключові слова: критерій оптимальності, засоби укриття цивільного населення, ваговий коефіцієнт, ракетні атаки.

UDC 004.056.55+004.421.5
DOI: 10.20535/SRIT.2308-8893.2024.3.03

DATA SCRAMBLER KNIGHT TOUR ALGORITHM

V.V. ROMANUKE, S.A. YAREMKO, O.M. KUZMINA, H.A. YEHOSHYNA

Abstract. Nowadays, data scrambling remains a vital technique to protect sensitive information by shuffling it in a way that makes it difficult to decipher or reverse-engineer while still maintaining its usability for legitimate purposes. As manipulating the usability of the scrambled data remains a challenge on the background of risking losing data and getting them re-identified by attackers, scrambling and descrambling should be accomplished faster by not increasing data loss and re-identification risks. A scrambling algorithm must have a linear time complexity, still shuffling the data to minimize the risks further. A promising approach is based on the knight open tour problem, whose solutions appear like a random series of knight positions. Hence, a knight open tour algorithm is formalized, by which the knight seems to move chaotically across the chessboard. The formalization is presented as an indented pseudocode to implement it efficiently, whichever programming language is used. The output is a square matrix representing the knight open tour. Based on the knight tour matrix, data scrambler and descrambler algorithms are presented in the same manner. The algorithms have a linear time complexity. The knight-tour scrambling has a sufficiently low guess probability if an appropriate depth of scrambling is used, where the data is re-scrambled repetitively. The scrambling depth is determined by repetitive application of the chessboard matrix, whose size usually increases as the scrambling is deepened. Compared to the pseudorandom shuffling of the data along with storing the shuffled indices, the knight-tour descrambling key is stored and sent far simpler yet ensures proper data security.

Keywords: data scrambling, knight open tour problem, linear time complexity, guess probability, scrambling depth.

INTRODUCTION

Data scrambling, also known as data obfuscation or data anonymization, is a technique used to protect sensitive information by altering or shuffling it in a way that makes it difficult to decipher or reverse-engineer while still maintaining its usability for legitimate purposes [1; 2]. Data scrambling is an essential component of data protection strategies, helping organizations safeguard sensitive information while still benefiting from its utility [3; 4]. Scrambling is similar to encryption and ciphering, but these techniques differ in their fundamental approaches and purposes [5; 6].

Scrambling is a data protection technique that aims to balance data privacy with usability by partially obscuring data, making it reversible in most cases [7]. Encryption, on the other hand, focuses on data confidentiality by converting it into ciphertext, which is typically not usable without decryption [8]. Ciphering is a broader term that encompasses both scrambling and encryption, as it refers to the process of transforming data to protect its confidentiality or privacy [9]. While scrambling may involve various transformations, such as shuffling, substitution, or masking, to make the data less readable [10], encryption is primarily used to

secure data by converting it into a ciphertext using cryptographic algorithms [8; 11; 12]. Encrypted data is typically not usable or meaningful without the corresponding decryption key, as it appears as random ciphertext [5; 6; 9; 11].

The choice between scrambling and encryption depends on the specific use case and requirements regarding data protection and usability. The main purposes of data scrambling are data privacy and compliance. It protects, for example, personal identification data, financial records, proprietary business data, from unauthorized access or disclosure. Data scrambling helps organizations comply with data protection regulations and privacy laws, such as GDPR or HIPAA [13; 14], which require the safeguarding of sensitive data.

One common method of data scrambling is shuffling data using an appropriate algorithm [15]. Knowing this particular algorithm allows descrambling the scrambled data. Other methods are masking that replaces parts of sensitive data with placeholders or pseudonyms, tokenization that replaces sensitive data with tokens or references, which are meaningless without the associated mapping, and data perturbation [16; 17]. The latter is a technique that adds random noise or perturbation to numerical data to protect its privacy while preserving statistical properties.

Data scrambling is successfully used in secure storage, where data at rest is protected from unauthorized access in databases, file systems, or backups. Data sharing is another use case, where organizations share data with third parties for analysis or collaboration without revealing sensitive details. In addition, scrambled data can be used in non-production and test environments to simulate real data without exposing sensitive information [1; 2; 4; 7; 10].

The development of data scrambling includes understanding data sensitivity priority, strengthening encryption, selecting appropriate anonymization techniques based on the specific data and use case, and continuously monitoring and auditing data scrambling processes to ensure their effectiveness and compliance. However, determining a balance between data protection and data usability is challenging [18]. The other two main challenges are data loss and re-identification risks [19; 20]. Thus, improper implementation of data scrambling techniques can lead to data loss or degradation of data quality. Besides, which is the most important and where ones must be the most cautious, attackers may still re-identify individuals or sensitive data if not properly scrambled [21].

While scrambling is frequently used for images due to its visual nature, it is not limited to images and can be applied effectively to text and numerical data as well to protect sensitive information while maintaining data usability [22]. This is often seen in scenarios like redacting personally identifiable information in documents or anonymizing user-generated content in social media moderation [8; 9; 13; 23], academic performance [24], and recommender system profiles [25]. Numerical data, such as financial records, health records, or scientific research data, may also require protection through scrambling techniques [26; 27]. This is essential for compliance with data privacy regulations like GDPR or HIPAA [13; 14].

PROBLEM STATEMENT

As manipulating the usability of the scrambled data remains a challenge on the background of risking to lose data and get them re-identified by attackers, scrambling and descrambling should be accomplished faster by not increasing data loss

and re-identification risks. A scrambling algorithm must be of a linear time complexity still shuffling the data so that to further minimize the risks. A promising approach is based on the knight open tour problem [28; 29] whose solutions appear like a random series of knight positions. The goal of the research is to apply this property of the solutions to data scrambling. For achieving the goal, the following five tasks are to be fulfilled:

1. To formalize a knight open tour algorithm, by which the knight is seemed to move chaotically across the chessboard. The formalization is to be presented as an indented pseudocode to efficiently implement it, whichever programming language is used. The output is a square matrix representing the knight open tour.

2. To algorithmize a data scrambler and descrambler based on the knight tour matrix. Both the algorithms must be given as indented pseudocodes.

3. To estimate the time complexity of the algorithms. In addition, to compare their performance to other approach of scrambling by shuffling the data, including the probability of illegitimately descrambling by attackers.

4. To discuss the significance and practical applicability of the suggested knight open tour algorithm. The proper contribution to the field of data scrambling should be emphasized.

5. To conclude on the suggestion and findings along with mentioning a possibility to extend and advance the research.

KNIGHT TOUR MATRIX

The directions the knight can move on the chessboard are completely described by the horizontal and vertical sets

$$S_{\text{hor}} = \{s_l^{(\text{hor})}\} = \{-2, -1, 1, 2, -2, -1, 1, 2\} \tag{1}$$

and

$$S_{\text{vert}} = \{s_l^{(\text{vert})}\} = \{1, 2, 2, 1, -1, -2, -2, -1\}. \tag{2}$$

Sets (1) and (2) are such that

$$s_l^{(\text{hor})} = s_{l+4}^{(\text{hor})} \quad \forall l = \overline{1, 4},$$

and

$$s_l^{(\text{vert})} = -s_{l+4}^{(\text{vert})} \quad \forall l = \overline{1, 4}.$$

If the knight starts its open tour at horizontal position x and vertical position y on a chessboard of size $M \times M$, the knight open tour algorithm finds a sequence of the remaining $M^2 - 1$ chessboard positions that constitute the tour. The sequence is written by the set of integers from 1 to M^2, where 1 corresponds to the starting position of the knight. These integers are put on the chessboard, forming thus an $M \times M$ matrix

$$\mathbf{B}_M = K(M, x, y) = [b_{rt}]_{M \times M}, \tag{3}$$

where $b_{rt} \in \{\overline{1, M^2}\}$ and $K(M, x, y)$ is the algorithm mapping the size of the chessboard and the knight starting position into matrix $\mathbf{B}_M$ by (3).

While the knight tour problem is NP-hard in general [28], there is a number of heuristic algorithms that allow finding a solution in linear time — that is, in a

time amount proportional to number M^2. One of such heuristics is the Warnsdorff's rule [30; 31]. This rule finds a single solution. According to the Warnsdorff's rule, the knight is moved so that it always proceeds to the position from which the knight will have the fewest onward moves. The priority queue of available neighbors is stored as a set

$$Q = \{[q_{w1} \quad q_{w2}]\}_{w=1}^{W},\ W \in \mathrm{N} \cup \{0\}. \tag{4}$$

The algorithm is presented as an indented pseudocode (Algorithm 1), where set (4) dynamically changes its size inside the outer loop.

Algorithm 1. The Warnsdorff's rule indented pseudocode

for $k = 1$ with step 1 to $k = M^2$ do
  $b_{yx} = k$, $Q = \varnothing$
  for $l = 1$ with step 1 to $l = M$ do
    $m_{\text{hor}} = x + s_l^{(\text{hor})}$, $m_{\text{vert}} = y + s_l^{(\text{vert})}$
    if $m_{\text{hor}} \geqslant 1$ and $m_{\text{hor}} < M + 1$ and $m_{\text{vert}} \geqslant 1$ and $m_{\text{vert}} < M + 1$
      if $b_{m_{\text{vert}} m_{\text{hor}}} = 0$
        $c = 0$
        for $u = 1$ with step 1 to $u = M$ do
          $g_{\text{hor}} = m_{\text{hor}} + s_u^{(\text{hor})}$, $g_{\text{vert}} = m_{\text{vert}} + s_u^{(\text{vert})}$
          if $g_{\text{hor}} \geqslant 1$ and $g_{\text{hor}} < M + 1$ and $g_{\text{vert}} \geqslant 1$ and $g_{\text{vert}} < M + 1$
            if $b_{g_{\text{vert}} g_{\text{hor}}} = 0$ then $c^{(\text{obs})} = c$,
            $c = c^{(\text{obs})} + 1$
        if $Q = \varnothing$ then $Q = \{[c \quad l]\}$
        else
          if $q_{w1} > c$ then $Q^{(\text{obs})} = Q$, $Q = \{[c \quad l], Q^{(\text{obs})}\}$
          else
            if $q_{w1} = c$
              if $q_{w2} > l$ then $Q^{(\text{obs})} = Q$,
              $Q = \{[c \quad l], Q^{(\text{obs})}\}$
              else $Q^{(\text{obs})} = Q$,
              $Q = \{Q^{(\text{obs})}, [c \quad l]\}$
            if $q_{w1} < c$ then $Q^{(\text{obs})} = Q$,
            $Q = \{Q^{(\text{obs})}, [c \quad l]\}$
  if $Q \neq \varnothing$ then $l^* = q_{12}$, $x^{(\text{obs})} = x$, $x = x^{(\text{obs})} + s_{l^*}^{(\text{hor})}$, $y^{(\text{obs})} = y$,
  $y = y^{(\text{obs})} + s_{l^*}^{(\text{vert})}$
  else break

The knight open tour resulting from Algorithm 1 mostly seems to be rather chaotic. An example of the tour for 16×16 chessboard is shown in Fig. 1, where the entries of the knight tour matrix $\mathbf{B}_{16}$ are also given (odd and even numbers

differ in their color). Some traceries are still noticeable, though. Especially near the margins — where the knight has fewer possibilities to move onward.

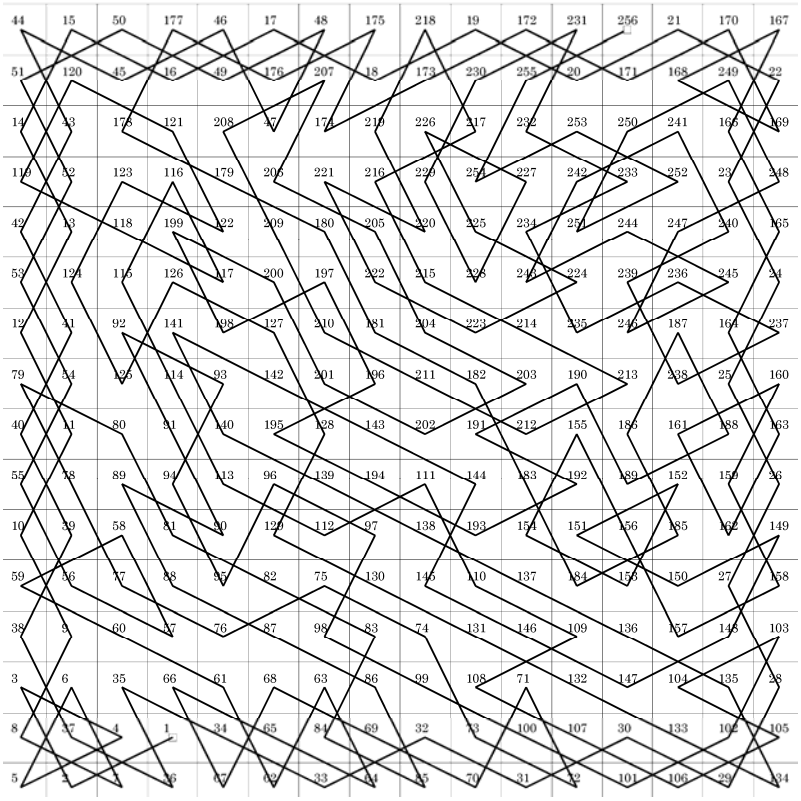

Fig. 1. A knight open tour built by the Warnsdorff's rule algorithm for 16×16 chessboard

When we have two-dimensional data of N points in each dimension, it can be formally presented as a square matrix

$$\mathbf{D}=[d_{ij}]_{N\times N}, \tag{5}$$

where d_{ij} is either real or complex number. In particular, if $M=N$, the data in matrix (5) can be scrambled using the pattern of the knight tour matrix (3) by just shuffling the entries of $\mathbf{D}$ in accordance with $\mathbf{B}_M$. When $M\neq N$, we can shuffle not an entry but an $a\times a$ square of a^2 entries, where $a=\dfrac{N}{M}$ and it obviously must be integer. This is the core of the algorithm for data scrambling and descrambling based on the knight tour matrix (3).

DATA SCRAMBLER AND DESCRAMBLER

A data scrambler is an operator that maps data matrix (5) using the knight tour matrix (3) into an $N\times N$ matrix

$$\mathbf{H}=F(\mathbf{D},\mathbf{B}_M)=[h_{ij}]_{N\times N}. \tag{6}$$

Operator $F(\mathbf{D}, \mathbf{B}_M)$ in (6) is realized by a data scrambler algorithm (Algorithm 2), which, using matrices $\mathbf{D}$ and $\mathbf{B}_M$, dynamically builds an $M^2 \times 1$ array

$$\mathbf{Q}_{\text{square}} = [q_{k1}^{(\text{square})} \quad q_{k2}^{(\text{square})}]_{M^2 \times 1} \tag{7}$$

containing coordinates of successive positions to shuffle.

Algorithm 2. A data scrambler by (6) using the knight open tour matrix (3)

for $l = 1$ with step 1 to $l = M$ do

for $u = 1$ with step 1 to $u = M$ do

$k = (l-1) \cdot M + u$, $q_{k1}^{(\text{square})} = l$, $q_{k2}^{(\text{square})} = u$

for $l = 1$ with step 1 to $l = M$ do

for $u = 1$ with step 1 to $u = M$ do

$k = b_{lu}$, $l_{\text{scr}} = q_{k1}^{(\text{square})}$, $u_{\text{scr}} = q_{k2}^{(\text{square})}$

$h_{i^* j^*} = d_{i^{**} j^{**}}$ for $i^* = (l-1) \cdot a + m$, $j^* = (u-1) \cdot a + m$, $m = \overline{1, a}$

$i^{**} = (l_{\text{scr}} - 1) \cdot a + m$, $j^{**} = (u_{\text{scr}} - 1) \cdot a + m$

It is worth noting that the data can be a three-dimensional matrix as well. Then the data scrambler algorithm processes the third-dimension layers in parallel, using, for instance, the data vectorization approach [32]. Thus, the color image in Fig. 2 is scrambled by using an ordinary chessboard matrix $\mathbf{B}_8$ with its

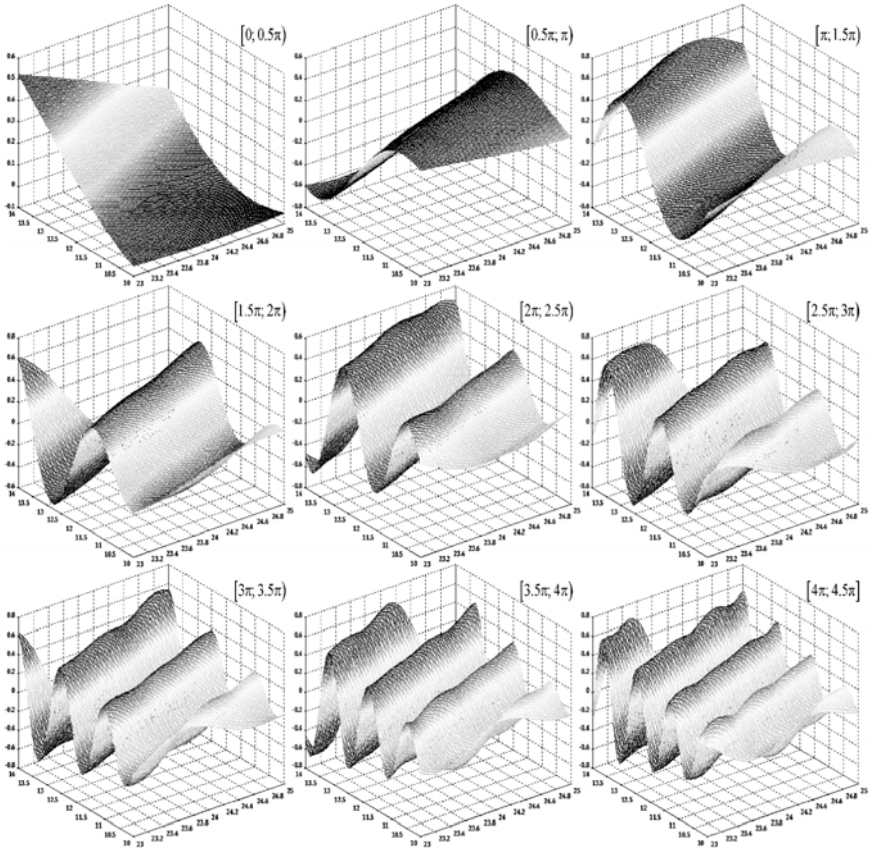

Fig. 2. The image of data of a $4096 \times 4096 \times 3$ array (the image is taken from [33])

starting position $\{7, 6\}$ ($x = 6$, $y = 7$). The scrambled image is shown in Fig. 3. In this scientific-data-like example, the scrambling result may not seem that convincing, but the mosaic in Fig. 3 is nonetheless pretty hard to assemble it back to the original image in Fig. 2. Nevertheless, many mosaic squares contain parts of consistent information. This is due to every mosaic square is a 512×512 color image.

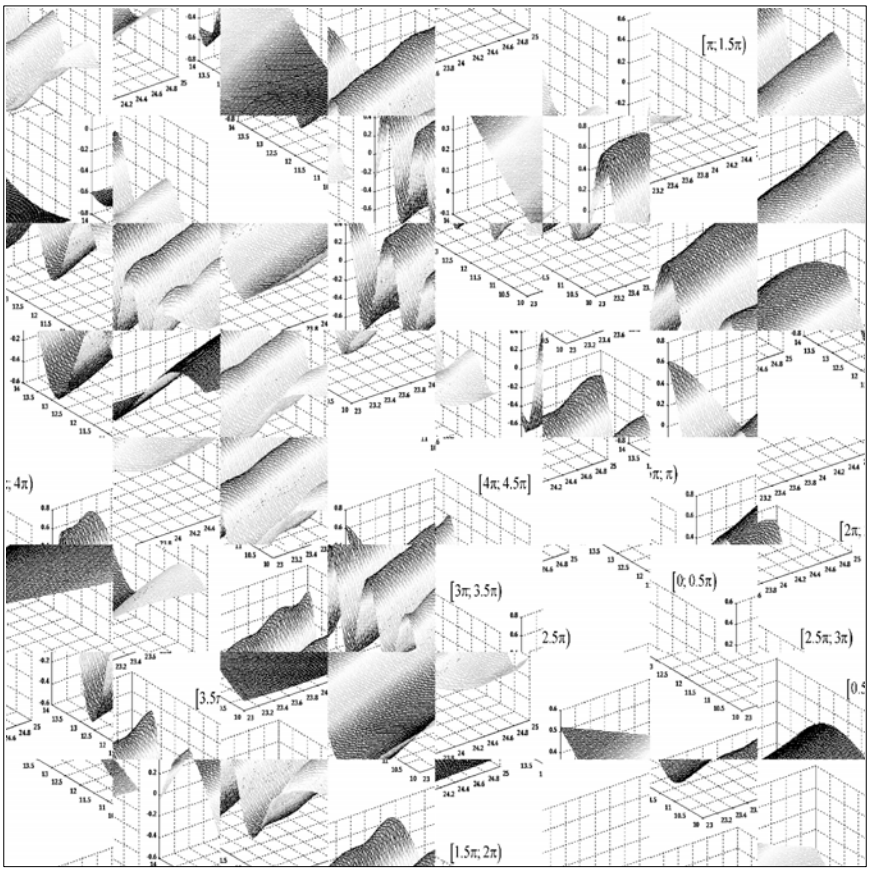

Fig. 3. The scrambled image in Fig. 2 by using $\mathbf{B}_8$ with its starting position $\{7, 6\}$

To decrease the data readability, the size of the chessboard should be increased. On the other hand, the scrambler can be applied once again to the scrambled data. Thus, Fig. 4 presents a result of scrambling the scrambled image in Fig. 3 by using matrix $\mathbf{B}_{16}$ with its starting position $\{7, 12\}$ ($x = 12$, $y = 7$). Now the readability of the image parts is lower, although many parts and their local information are still distinguishable. However, assembling the mosaic in Fig. 4 back to the original image is much more difficult compared to the mosaic in Fig. 3.

Indeed, the mapping of data (5) by (6) and (3) is a very simple approach whose guess probability is M^{-2}. To go deeper in scrambling, consider its depth Θ, where $\Theta \in \mathrm{N} \bigcup \{0\}$, and an additional sequence of integers $\{M_\gamma\}_{\gamma=1}^{\Theta}$, where usually

$$M < M_\gamma < M_{\gamma+1} \text{ by } \gamma = \overline{1, \Theta - 1}. \qquad (8)$$

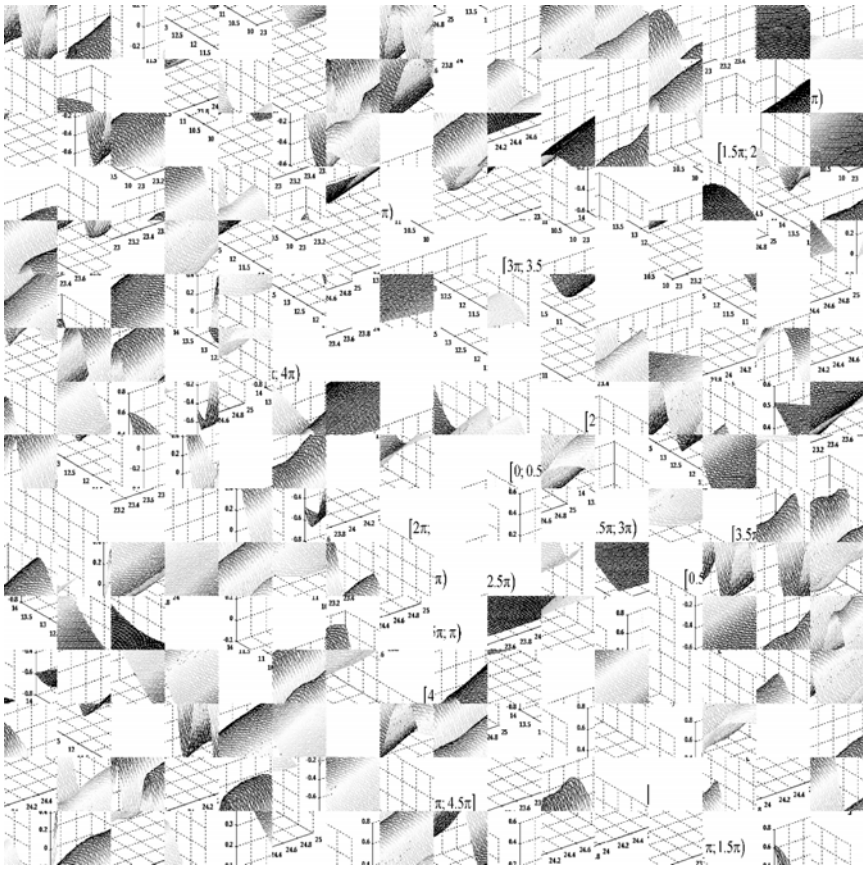

Fig. 4. The scrambled image in Fig. 3 by using $\mathbf{B}_{16}$ with its starting position $\{7,12\}$

Then the scrambling of depth Θ is recursively fulfilled as

$$\mathbf{H}_{\gamma+1} = F(\mathbf{H}_{\gamma}, \mathbf{B}_{M_\gamma}) \text{ for } \gamma = \overline{1,\Theta} \tag{9}$$

by $\mathbf{H}_1 = \mathbf{H}$. The case $\Theta = 0$ is the simplest possible scrambling here. Overall, there are $\Theta + 1$ transformations by operator F. They result in a set $\{\mathbf{H}_\gamma\}_{\gamma=1}^{\Theta+1}$ of scrambled data matrices. The last matrix in this set, $\mathbf{H}_{\Theta+1}$, is the final result of the data scrambling of depth Θ. The guess probability herein becomes equal to

$$\left(M^2 \cdot \prod_{\gamma=1}^{\Theta} M_\gamma^2 \right)^{-1}. \tag{10}$$

So, the image in Fig. 4 is the scrambling result of depth 1, and its guess probability is

$$(M^2 \cdot M_1^2)^{-1} = (8^2 \cdot 16^2)^{-1} = 2^{-14} = 0.00006103515625.$$

Going deeper by using matrix $\mathbf{B}_{32}$ with its starting position $\{6,21\}$ ($x = 21$, $y = 6$) further strengthens the encryption (Fig. 5) decreasing the guess probability by 1024 times.

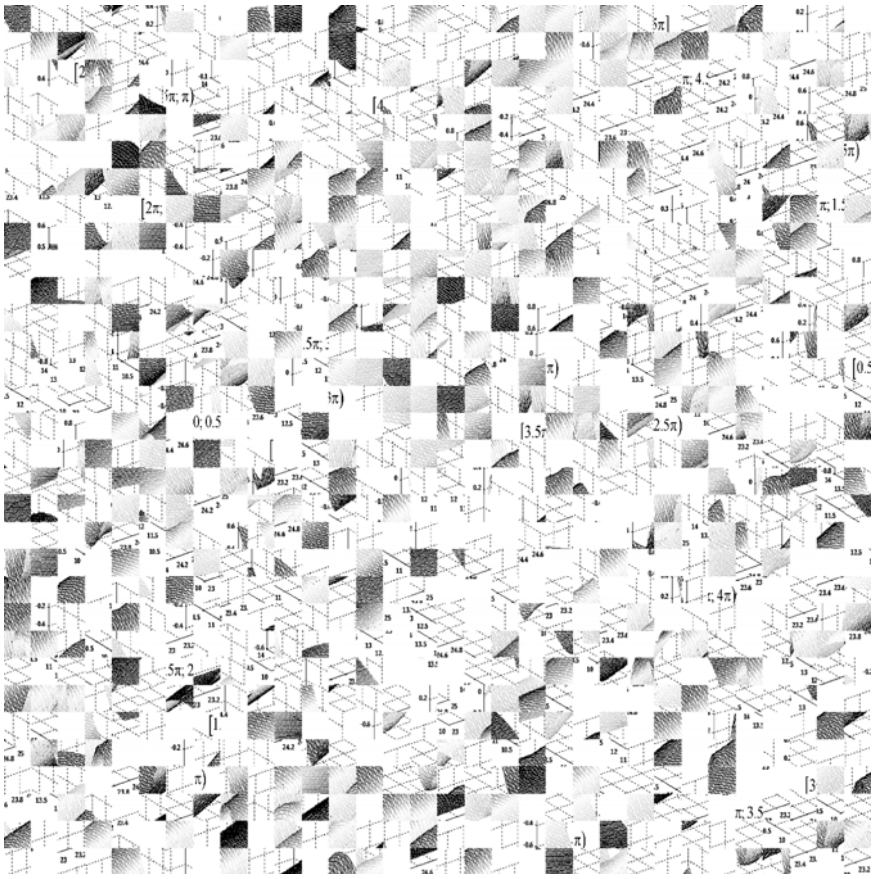

Fig. 5. The scrambled image in Fig. 4 (depth 2) by using $\mathbf{B}_{32}$ with its starting position $\{6, 21\}$, where the guess probability is $2^{-24} = 0.000000059604644775390625$

Herein, while obeying inequality (8), conditions

$$M_{\gamma+1} = 2 \cdot M_{\gamma} \text{ by } \gamma = \overline{1, \Theta - 1} \text{ and } M_1 = 2 \cdot M \tag{11}$$

are followed. This is convenient to establish the guess probability such as it is desired to be. Scrambling to depth 3 (Fig. 6), where matrix $\mathbf{B}_{64}$ has its starting position $\{3, 46\}$ ($x = 46$, $y = 3$), makes the guess practically impossible within a reasonable amount of time (unless the latest advanced computational techniques are applied, like, e. g., quantum computing):

$$(M^2 \cdot M_1^2 \cdot M_2^2 \cdot M_3^2)^{-1} = (8^2 \cdot 16^2 \cdot 32^2 \cdot 64^2)^{-1} = 2^{-36} =$$

$$= \frac{1}{68719476736} < 1.5 \cdot 10^{-11}.$$

Besides, while the usability is maintained, the data in Fig. 6 is not readable even partially — every mosaic square is just a 64×64 color image.

Fig. 7 shows that at depth 4 for this particular example the scrambled image is perceived as noise. Every mosaic square is just a 32×32 color image. The guess probability is 16384 times lower than that for the scrambled image in Fig. 6:

$$(M^2 \cdot M_1^2 \cdot M_2^2 \cdot M_3^2 \cdot M_4^2)^{-1} = (8^2 \cdot 16^2 \cdot 32^2 \cdot 64^2 \cdot 128^2)^{-1} = 2^{-50} =$$

$$= \frac{1}{1125899906842624} < 8.9 \cdot 10^{-16}.$$

The data readability is nearly at naught. Therefore, Fig. 7 is the final result of scrambling the data in Fig. 2.

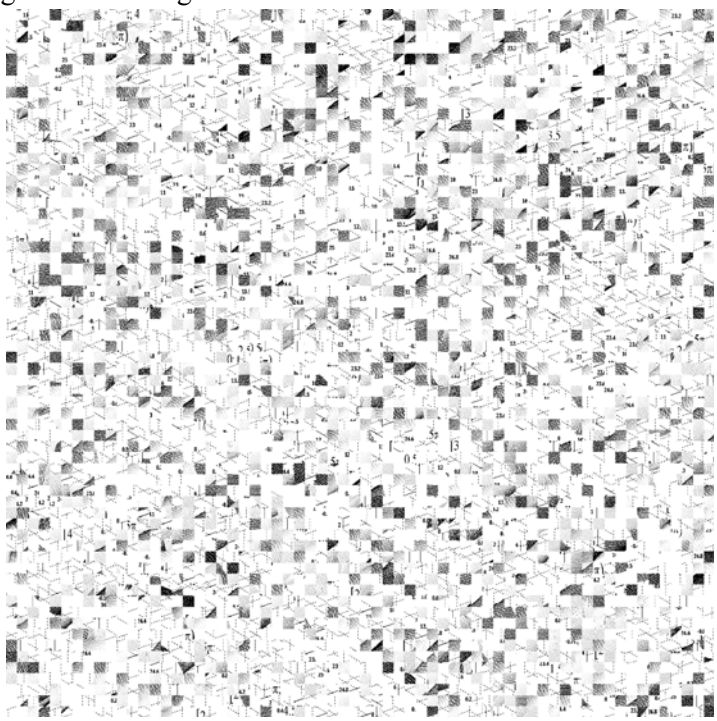

Fig. 6. The scrambled image in Fig. 5 (depth 3) by using $\mathbf{B}_{64}$ with its starting position $\{3, 46\}$, where the guess probability is 2^{-36}

Fig. 7. The scrambled image in Fig. 6 (depth 4) by using $\mathbf{B}_{128}$ with its starting position $\{6, 36\}$, where the guess probability is 2^{-50}

A data descrambler is an operator that maps scrambled data matrix (6) using the knight tour matrix (3) back into matrix (5):

$$\mathbf{D}= G(\mathbf{H}, \mathbf{B}_M)\,. \tag{12}$$

Operator $G(\mathbf{H}, \mathbf{B}_M)$ in (12) is realized by a data descrambler algorithm (Algorithm 3), which, using matrices $\mathbf{H}$ and $\mathbf{B}_M$, dynamically builds array (7).

Algorithm 3. A data descrambler by (7) using the knight open tour matrix (3)

for $l=1$ with step 1 to $l=M$ do

  for $u=1$ with step 1 to $u=M$ do

    $k=(l-1)\cdot M+u$, $q_{k1}^{(\text{square})}=l$, $q_{k2}^{(\text{square})}=u$

for $l=1$ with step 1 to $l=M$ do

  for $u=1$ with step 1 to $u=M$ do

    $k=b_{lu}$, $l_{\text{scr}}=q_{k1}^{(\text{square})}$, $u_{\text{scr}}=q_{k2}^{(\text{square})}$

    $d_{i^{**}j^{**}}=h_{i^*j^*}$ for $i^*=(l-1)\cdot a+m$, $j^*=(u-1)\cdot a+m$, $m=\overline{1,a}$

    $i^{**}=(l_{\text{scr}}-1)\cdot a+m$, $j^{**}=(u_{\text{scr}}-1)\cdot a+m$

The descrambling of depth Θ is recursively fulfilled as

$$\mathbf{H}_{\Theta-\gamma+1}=G(\mathbf{H}_{\Theta-\gamma+2}, \mathbf{B}_{M_{\Theta-\gamma+1}}) \text{ for } \gamma=\overline{1,\Theta}\,. \tag{13}$$

Obviously, there are $\Theta+1$ transformations by operator G restoring the backward set of scrambled data matrices $\{\mathbf{H}_{\Theta-\gamma+1}\}_{\gamma=1}^{\Theta}$. The last matrix in this set, $\mathbf{H}_1=\mathbf{H}$, is put into operator (12) and then the final result of the data descrambling is obtained.

Henceforth, the data scrambler by (6) and (9) requires knowing $\Theta+1$ chessboard matrices

$$\{\mathbf{B}_M, \{\mathbf{B}_{M_\gamma}\}_{\gamma=1}^{\Theta}\} \tag{14}$$

whose sizes obey inequality (8) or, in particular, the doubling by (11). This ensures the guess probability equal to (10) or, if the doubling by (11) is used, the guess probability equal to

$$\left(M^2\cdot(2M)^2\cdot\prod_{\gamma=2}^{\Theta}(2M_{\gamma-1})^2\right)^{-1}=\left(M^2\cdot 4M^2\cdot\prod_{\gamma=2}^{\Theta}4M_{\gamma-1}^2\right)^{-1}=$$

$$=\left(\sqrt{4^{\Theta(\Theta+1)}}M^{2\cdot(\Theta+1)}\right)^{-1}. \tag{15}$$

Each of matrices (14) is defined by its size and the starting position of the knight. Therefore, the data scrambler is defined by the sizes and starting positions

$$\{M, \{M_\gamma\}_{\gamma=1}^{\Theta}\} \text{ and } \{\{y,x\}, \{y_\gamma, x_\gamma\}_{\gamma=1}^{\Theta}\}, \tag{16}$$

respectively. Consequently, the data descrambler by (12) and (13) is defined by sets (16). Knowing (16) allows descrambling data in matrix $\mathbf{H}_{\Theta+1}$ without any data losses.

KNIGHT-TOUR SCRAMBLING VERSUS SHUFFLER SCRAMBLING

It is obvious that, despite a linear time complexity, too deep scrambling may take significant amounts of time. However, the deep scrambling is really needful only for decreasing the guess probability as much as possible. In other situations, the data scrambler can be applied just once to produce a scrambled data matrix of sufficiently low readability. For example, the data image in Fig. 2 scrambled with a matrix $\mathbf{B}_{128}$ looks blurred (Fig. 8) and its scientific data is not readable almost much as the image in Fig. 7, although the guess probability is just 2^{-14} (relatively, it is pretty high).

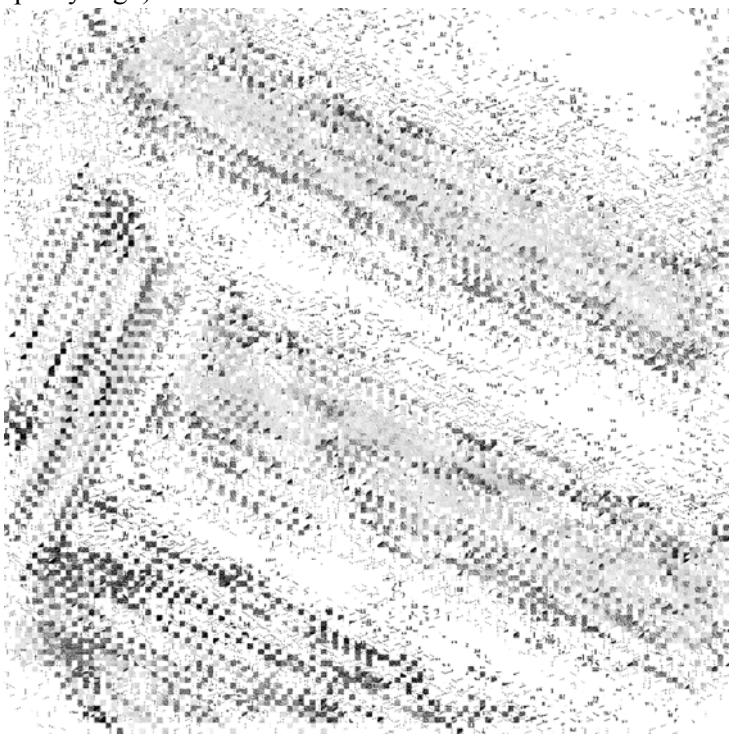

Fig. 8. The scrambled image in Fig. 2 by using the chessboard matrix of size 128 (the zero depth of scrambling, $\Theta = 0$), where the guess probability is the same as for the scrambled image in Fig. 4 with the scrambling depth 1

Could the same effect be when, instead of the data scrambler knight tour algorithm, a more random and less sophisticated approach is used? For instance, such an approach is the pseudorandom shuffling of the data along with storing the shuffled indices. The shuffler scrambling is defined just by an $N \times N$ matrix

$$\mathbf{S} = [\sigma_{ij}]_{N \times N} \tag{17}$$

of randomly permutated unique N^2 integers from 1 to N^2. Then the shuffler scrambling and descrambling algorithms are those Algorithms 2 and 3, respectively, where only $a = 1$ and matrix (17) is used instead of matrix (3). The guess probability in this case is N^{-2} as the shuffler algorithm is presumed to be known and it can be defined by the position of an integer value from 1 to N^2.

Obviously, if the knight-tour scrambling is of depth 0, then the shuffler scrambling results in a lower guess probability unless $M = N$:

$$M^{-2} > N^{-2} \text{ for } M < N .$$

However, as the scrambling is developed deeper, the guess probability may significantly drop, as it has been demonstrated above by Figs. 4–7.

Consider a range of the data set size as follows:

$$N \in \{2^3, 2^4, 2^5, 2^6, 2^7, 2^8\} = \{8, 16, 32, 64, 128, 256\} . \quad (18)$$

Then data matrix (5) with integers

$$d_{ij} \in [0; 255] \subset \mathbf{Z}$$

is re-generated for 100 repetitions for each of the six values of N in (18). The depth of scrambling is

$$\Theta = \log_2 N - 3 .$$

So, the knight-tour data scrambler is applied as deep as possible, i. e.

$$\{M, \{M_\gamma\}_{\gamma=1}^{\Theta}\} = \{8, \{2^{\gamma+3}\}_{\gamma=1}^{\Theta}\} = \{8, \{2^{\gamma+3}\}_{\gamma=1}^{\Theta-1}, N\} .$$

That is, the knight tour matrix $\mathbf{B}_{M_\Theta} = \mathbf{B}_N$, whichever N is. This is expectedly the worst-case scenario with respect to the computation time of the knight-tour data scrambler compared to the shuffler. Table 1 presents statistics after averaging over the 100 repetitions of the knight-tour data scrambler versus shuffler. The similarity index ratio is calculated as the ratio of the averaged similarity rate by the knight-tour data scrambler to the averaged similarity rate by the shuffler, where the averaged similarity rate is calculated as the element-wise number of coincidences in matrices $\mathbf{D}$ and the scrambled data matrix divided by N^2. The knight-tour-scrambling guess probability herein is calculated by (15). The statistics remain almost the same for any other 100-repetition generations. Although the knight-tour-to-shuffler time ratios reveal some favorability of the shuffler computation time, the shuffler is a far less reliable scrambler due to its guess probability is too high compared to the knight-tour-scrambling guess probability. Besides, the knight-tour-to-shuffler similarity index ratio confirms that the knight-tour data scrambler produces a scrambled object which resembles the original less than a scrambled object by the shuffler resembles it.

Table 1. Knight-tour scrambling versus shuffler scrambling

N	Knight-tour-to-shuffler scrambling time ratio	Knight-tour-to-shuffler descrambling time ratio	Similarity index ratio	Knight-tour-scrambling guess probability	Shuffler-scrambling guess probability
8	0.5797	1.1134	0.2308	$8^{-2} = 2^{-6} = 0.015625$	0.015625
16	1.3375	1.3913	1.0055	$8^{-2} \cdot 16^{-2} = 2^{-14} = 6.103515625 \cdot 10^{-5}$	0.00390625
32	1.3805	1.416	0.7135	$8^{-2} \cdot 16^{-2} \cdot 32^{-2} = 2^{-24} < 6 \cdot 10^{-8}$	$9.765625 \cdot 10^{-4}$
64	1.3392	1.3928	0.9337	$8^{-2} \cdot 16^{-2} \cdot 32^{-2} \cdot 64^{-2} = 2^{-36} < 1.5 \cdot 10^{-11}$	$2.44140625 \cdot 10^{-4}$
128	1.2306	1.2232	0.995	$2^{-50} < 8.9 \cdot 10^{-16}$	$6.103515625 \cdot 10^{-5}$
256	1.1258	1.1157	1.0079	$2^{-66} < 1.4 \cdot 10^{-20}$	$1.52587890625 \cdot 10^{-5}$

Consider another series of 100 simulations for the knight-tour data scrambler. Let

$$N \in \{2^3, 2^4, 2^5, 2^6, 2^7, 2^8, 2^9, 2^{10}\} = \{8, 16, 32, 64, 128, 256, 512, 1024\} \quad (19)$$

and the remaining simulation parameters be the same. Let the depth be varied from 0 to 5. Then, for each repetition, there is an instance of some size in (19) and $\Theta \in \{\overline{0, 5}\}$. The averaged interrelation between scrambling and descrambling computation times is shown in Table 2. The interrelation varies within 20 % on average for any other 100-repetition generations. The knight-tour data descrambler seemingly operates faster owing to the memory allocation and code compilation that are done following the scrambling.

Table 2. Knight-tour scrambling-to-descrambling time ratio

N	**Depth of scrambling**					
	0	1	2	3	4	5
8	0.9248					
16	1.0638	1.0302				
32	1.0756	1.0231	1.056			
64	1.0765	1.0578	1.039	1.0206		
128	1.151	1.179	1.1399	1.0888	1.0859	
256	1.1518	1.361	1.3882	1.3129	1.102	1.0409
512	1.2119	1.5472	1.6715	1.732	1.42	1.1119
1024	1.1883	1.6135	1.8532	2.0819	1.9851	1.3881

Obviously, as the size of the data matrix increases, the computation time grows. Table 3 shows the computation time relative growth with respect to the computation time taken to scramble with a chessboard matrix of size N. At the first glance, there is a quadratic time complexity with respect to size N along each column, but the real size of the algorithm input is N^2, so Table 3 confirms a linear time complexity of Algorithm 2. So does Table 4 showing the computation time relative growth with respect to the computation time taken to descramble with a chessboard matrix of size N. However, it is worth noting that Algorithm 3 being of a linear time complexity seems to be faster (this is clearly seen when Table 4 is cell-by-cell compared to Table 3). This effect has been already explained above — the data descrambler by Algorithm 3 virtually utilizes the memory preallocation and code pre-compilation, done for Algorithm 2 in this case.

Table 3. Knight-tour scrambling time relative growth as N increases

N	**Depth of scrambling**					
	0	1	2	3	4	5
8	1					
16	0.5562	1				
32	0.4834	1.0351	1			
64	0.5661	1.1575	1.1084	1		
128	1.0355	1.832	1.5465	1.2523	1	
256	2.7697	4.2452	2.86	1.8061	1.1855	1
512	9.1934	12.8017	7.7231	3.8901	1.8098	1.1376
1024	35.2239	42.9207	23.9562	11.245	4.1936	1.5951

Table 4. Knight-tour descrambling time relative growth as N increases

N	**Depth of scrambling**					
	0	1	2	3	4	5
8	1					
16	0.4835	1				
32	0.4156	1.0423	1			
64	0.4863	1.1273	1.1265	1		
128	0.832	1.6007	1.4327	1.174	1	
256	2.2238	3.2135	2.1756	1.4041	1.1681	1
512	7.0152	8.524	4.8793	2.2924	1.3839	1.0649
1024	27.412	27.4043	13.6509	5.5127	2.2939	1.1961

Another important property is how the computation time grows as the scrambling depth is increased. Table 5 shows the computation time relative growth with respect to the scrambling depth. It appears that the data scrambler has a quadratic time complexity with respect to the scrambling depth. Roughly the same time complexity is observed for the data descrambler (Table 6). This is particularly explained with that the chessboard matrix size is increased twice along a dimension, i. e. it is increased fourfold if to count its entries.

Table 5. Knight-tour scrambling time relative growth as the depth is increased

N	**Depth of scrambling**					
	0	1	2	3	4	5
8	1					
16	1	3.57				
32	1	4.2513	15.4973			
64	1	4.0595	14.6675	59.8536		
128	1	3.5128	11.1889	40.9824	202.9467	
256	1	3.0433	7.7362	22.0973	89.947	782.9858
512	1	2.7648	6.2936	14.3384	41.3688	268.3466
1024	1	2.4194	5.0952	10.8178	25.0193	98.2041

Table 6. Knight-tour descrambling time relative growth as the depth is increased

N	Depth of scrambling					
	0	1	2	3	4	5
8	1					
16	1	3.6864				
32	1	4.4696	15.785			
64	1	4.1312	15.1969	63.1311		
128	1	3.4293	11.2978	43.3244	215.123	
256	1	2.5756	6.4187	19.3856	94.0116	866.4042
512	1	2.1657	4.5632	10.0329	35.3074	292.477
1024	1	1.7818	3.2672	6.1745	14.9772	84.0675

The knight-tour scrambling similarity index showing the unit-normalized part of the number of coincidences in the data matrix and the scrambled data matrix appears to be quite stable regardless of the data set size and the scrambling

depth (Table 7). The scrambling similarity index scarcely exceeds 0.5 %. The average similarity index varies within 20 % on for any other 100-repetition generations. A maximum variation is spotted at a 53 % rate.

Table 7. Knight-tour scrambling similarity index

N	Depth of scrambling					
	0	1	2	3	4	5
8	0.0033					
16	0.0037	0.0043				
32	0.0041	0.0041	0.0051			
64	0.0038	0.0038	0.0048	0.0041		
128	0.0039	0.0039	0.0048	0.0041	0.004	
256	0.0039	0.0039	0.0048	0.0042	0.0039	0.004
512	0.0039	0.0039	0.0049	0.0041	0.0039	0.0039
1024	0.0039	0.0039	0.0049	0.0041	0.0039	0.0039

The final remark of the knight-tour scrambling versus shuffler scrambling relates to the descrambling key. While the knight-tour data descrambler must hold the $\Theta+1$ sizes and starting positions (16), its memory size requirement is very low. In the double precision format, it is just

$$8\cdot 3\cdot(\Theta+1)=24\cdot(\Theta+1)\ \text{bytes},$$

and it is

$$4\cdot 3\cdot(\Theta+1)=12\cdot(\Theta+1)\ \text{bytes}$$

in the single precision format. In practice, nevertheless, values (16) are integers (strictly speaking, naturals), so they are written with the unsigned 16-bit precision at most, when they are allowed to vary between 1 and 65535. In this case the data descrambler key occupies just

$$2\cdot 3\cdot(\Theta+1)=6\cdot(\Theta+1)\ \text{bytes}.$$

If it is known beforehand that

$$\max\{M,\max\{M_\gamma\}_{\gamma=1}^{\Theta},\max\{y,x\},\max\{y_\gamma,x_\gamma\}_{\gamma=1}^{\Theta}\}<256$$

then the data descrambler key occupies half of the latter by being written with the unsigned 8-bit precision — it is $3\cdot(\Theta+1)$ bytes. The shuffler descrambling, on the other hand, needs to know matrix (17) of unique N^2 integers from 1 to N^2, which would occupy $8N^2$ or $4N^2$ bytes if the double or single precision format was used, respectively. Inasmuch as using the unsigned 8-bit precision is unlikely here, then either $2N^2$ or $4N^2$ bytes are occupied depending on whether the unsigned 16-bit or 32-bit precision is respectively used. Therefore, the memory occupation by the shuffler descrambling key may seriously affect the data transfer rate. For instance, if 1024×1024 images are shuffling-scrambled and transferred, then an additional amount of 4 megabytes of information should be transferred along or afterwards for descrambling. This is quite unacceptable due to a 1024×1024 color image represented in a 8-bit scale itself is 3 megabytes of information, whereas a 1024×1024 grayscale image is just 1 megabyte. Contrariwise, the knight-tour scrambling at the depth of, say, 5, is accompanied with only 36 bytes ensuring an acceptably low guess probability.

DISCUSSION OF THE CONTRIBUTION

In addition to the knight-tour scrambling advantages, a convention for scrambling keys can be applied to avoid sending values (16) for descrambling. Such conventions are really plausible and effective when a small group of data chunks is sent over. Theoretically, a convention for the entries of matrix (17) might be applied, too. But once the shuffler scrambling key must be unexpectedly changed (e. g., by the reason of an oncoming cyberthreat), it will be required nonetheless at the descrambling side, unless there is another convention for the case of changing the key. Anyway, an information signal about the change should be sent. Such inconvenience makes the shuffler scrambling too bulky and far inefficient.

However, a deeper shuffling still can be applied by the analogy to the scrambling of some depth. For such a scrambling, matrix (17) may be used repeatedly, or a series of such matrices is used. A twofold application of the shuffling decreases the guess probability down to N^{-4}, which becomes acceptable for images or data sets comprising at least a few hundred (numeric or symbolic) elements.

The suggested knight open tour algorithm is a significant contribution to the field of data scrambling by three reasons. First, its implementation by Algorithm 2 for scrambling and Algorithm 3 for descrambling, with Algorithm 1 for generating a knight open tour, is very simple and easy to understand. Second, the knight-tour scrambling maintains a linear time complexity. Third, its guess probability is sufficiently low if an appropriate depth of scrambling is used. Eventually, the data scrambler knight tour algorithm can be combined with other linear-time-complexity scrambling algorithms to further strengthen the data protection.

In addition to the simplicity, the data scrambler and descrambler by the knight open tour algorithm are practically symmetric. Hence, they are easy applicable yet ensuring proper security of data. Despite the knight open tour algorithm is presented for the square matrix, it is scalable to any size. After all, the chessboard matrix can be used partially for non-square data matrices. Moreover, the data can be reshaped into a vector, either row or column, comprising an odd number of entries, whereupon a part of the chessboard matrix is still used to scramble the data.

CONCLUSION

A data scrambling algorithm has been suggested based on a knight open tour problem solution, whose structure seems chaotic enough to substitute ordinary shuffling. The linear time complexity of the algorithm inspires its practical embedding mainly owing to the scrambling non-sophisticated subtlety and low guess probability. The latter is regulated by changing the scrambling depth determined by repetitive application of the chessboard matrix. The size of this matrix is usually increased as the scrambling is deepened.

The research is possible to extend and advance in the way of studying more favorable knight open tours for the given chessboard matrix. As the computation time grows in a quadratic manner by deepening the scrambling, but the guess probability is lowered far stronger, a tradeoff between the depth and re-identification risk might be ascertained. Another open question is which strategy of increasing the chessboard matrix size would be optimal to attain the tradeoff at the shallowest possible depth.

REFERENCES

1. S.A. Abdelhameed, S.M. Moussa, and M.E. Khalifa, "Privacy-preserving tabular data publishing: A comprehensive evaluation from web to cloud," *Computers & Security*, vol. 72, pp. 74–95, 2018. doi: https://doi.org/10.1016/j.cose.2017.09.002
2. N. Li, N. Zhang, S.K. Das, and B. Thuraisingham, "Privacy preservation in wireless sensor networks: A state-of-the-art survey," *Ad Hoc Networks*, vol. 7, issue 8, pp. 1501–1514, 2009. doi: https://doi.org/10.1016/j.adhoc.2009.04.009
3. L. Zhang, S. Hao, J. Zheng, Y. Tan, Q. Zhang, and Y. Li, "Descrambling data on solid-state disks by reverse-engineering the firmware," *Digital Investigation*, vol. 12, pp. 77– 87, 2015. doi: https://doi.org/10.1016/j.diin.2014.12.003
4. S. Kim, M. Kyoung Sung, and Y. Dohn Chung, "A framework to preserve the privacy of electronic health data streams," *Journal of Biomedical Informatics*, vol. 50, pp. 95–106, 2014. doi: https://doi.org/10.1016/j.jbi.2014.03.015
5. S. De Capitani di Vimercati, S. Foresti, G. Livraga, and P. Samarati, "Chapter 18 — Digital infrastructure policies for data security and privacy in smart cities," in *J.R. Vacca (Ed.)*, *Smart Cities Policies and Financing*. Elsevier, 2022, pp. 249–261. doi: https://doi.org/10.1016/B978-0-12-819130-9.00007-3
6. R. Amdouni, M. Gafsi, R. Guesmi, M.A. Hajjaji, A. Mtibaa, and E.-B. Bourennane, "High-performance hardware architecture of a robust block-cipher algorithm based on different chaotic maps and DNA sequence encoding," *Integration*, vol. 87, pp. 346–363, 2022. doi: https://doi.org/10.1016/j.vlsi.2022.08.002
7. I.C. Semanjski, "Chapter 5 — Data analytics," in *I.C. Semanjski (Ed.), Smart Urban Mobility*. Elsevier, 2023, pp. 121–170. doi: https://doi.org/10.1016/B978-0-12-820717-8.00008-7
8. P. Pandya, "Chapter 15 — Advanced Data Encryption," in *J.R. Vacca (Ed.), Cyber Security and IT Infrastructure Protection*. Syngress, 2014, pp. 325–345. doi: https://doi.org/10.1016/B978-0-12-416681-3.00015-X
9. P. Sun, "Security and privacy protection in cloud computing: Discussions and challenges," *Journal of Network and Computer Applications*, vol. 160, Article ID 102642, 2020. doi: https://doi.org/10.1016/j.jnca.2020.102642
10. N. Sa'adah, "Trusted Data Transmission Using Data Scrambling Security Method with Asymmetric Key Algorithm for Synchronization," *EMITTER International Journal of Engineering Technology*, vol. 6, issue 2, p. 217, 2018. doi: https://doi.org/10.24003/emitter.v6i2.267
11. P. Pandya, "Chapter 70 — Advanced Data Encryption," in *J.R. Vacca (Ed.), Computer and Information Security Handbook* (Second Edition). Morgan Kaufmann, 2013, pp. 1127–1138. doi: https://doi.org/10.1016/B978-0-12-394397-2.00070-2
12. T. Stapko, "CHAPTER 8 — Choosing and Optimizing Cryptographic Algorithms for Resource-Constrained Systems," in *T. Stapko (Ed.), Practical Embedded Security*. Newnes, 2008, pp. 149– 171. doi: https://doi.org/10.1016/B978-075068215-2.50009-4
13. D.S. Guamán, D. Rodriguez, J.M. del Alamo, and J. Such, "Automated GDPR compliance assessment for cross-border personal data transfers in android applications," *Computers & Security*, vol. 130, Article ID 103262, 2023. doi: https://doi.org/10.1016/j.cose.2023.103262
14. R. Mia et al., "A comparative study on HIPAA technical safeguards assessment of android mHealth applications," *Smart Health*, vol. 26, Article ID 100349, 2022. doi: https://doi.org/10.1016/j.smhl.2022.100349
15. D. Salomon, *Data Privacy and Security: Encryption and Information Hiding*. Springer-Verlag, Berlin, Heidelberg, 2003, 480 p.
16. H. Zhong, C. Gu, Q. Zhang, J. Cui, C. Gu, and D. He, "Conditional privacy-preserving message authentication scheme for cross-domain Industrial Internet of Things," *Ad Hoc Networks*, vol. 144, Article ID 103137, 2023. doi: https://doi.org/10.1016/j.adhoc.2023.103137

17. W. Wang, H. Huang, Z. Yin, T. R. Gadekallu, M. Alazab, and C. Su, "Smart contract token-based privacy-preserving access control system for industrial Internet of Things," *Digital Communications and Networks*, vol. 9, issue 2, pp. 337–346, 2023. doi: https://doi.org/10.1016/j.dcan.2022.10.005
18. N. Khalid, A. Qayyum, M. Bilal, A. Al-Fuqaha, and J. Qadir, "Privacy-preserving artificial intelligence in healthcare: Techniques and applications," *Computers in Biology and Medicine*, vol. 158, Article ID 106848, 2023. doi: https://doi.org/10.1016/j.compbiomed.2023.106848
19. W.E. Yancey, W.E. Winkler, and R.H. Creecy, "Disclosure Risk Assessment in Perturbative Microdata Protection," in *J. Domingo-Ferrer (Ed.), Inference Control in Statistical Databases*. *Lecture Notes in Computer Science*, vol. 2316. Springer, Berlin, Heidelberg, 2002. doi: https://doi.org/10.1007/3-540-47804-3_11
20. V. Torra, "Microaggregation for Categorical Variables: A Median Based Approach," in *J. Domingo-Ferrer and V. Torra (Eds.), Privacy in Statistical Databases. PSD 2004*. *Lecture Notes in Computer Science,* vol. 3050. Springer, Berlin, Heidelberg, 2004. doi: https://doi.org/10.1007/978-3-540-25955-8_13
21. J. Domingo-Ferrer and V. Torra, "A Quantitative Comparison of Disclosure Control Methods for Microdata," in *P. Doyle, J.I. Lane, J.J.M. Theeuwes, and L.M. Zayatz (Eds.), Confidentiality, Disclosure, and Data Access: Theory and Practical Applications for Statistical Agencies*. Elsevier, Amsterdam, 2001, pp. 111–133.
22. W. Wu, Q. Qi, and X. Yu, "Deep learning-based data privacy protection in software-defined industrial networking," *Computers and Electrical Engineering*, vol. 106, Article ID 108578, 2023. doi: https://doi.org/10.1016/j.compeleceng.2023.108578
23. H.M. Ghadirli, A. Nodehi, and R. Enayatifar, "An overview of encryption algorithms in color images," *Signal Processing*, vol. 164, pp. 163–185, 2019. doi: https://doi.org/10.1016/j.sigpro.2019.06.010
24. S. Yaremko, E. Kuzmina, N. Savina, D. Yaremko, V. Kuzmin, and O. Adler, "Development of a Smart Education System for Analysis and Prediction of Students' Academic Performance," in *S. Babichev and V. Lytvynenko (Eds.), Lecture Notes in Computational Intelligence and Decision Making. ISDMCI 2021*. *Lecture Notes on Data Engineering and Communications Technologies*, vol. 77. Springer, Cham, 2022. doi: https://doi.org/10.1007/978-3-030-82014-5_52
25. H. A. Yehoshyna, V. V. Romanuke, "Constraint-based Recommender system for commodity realization," *Journal of Communications Software and Systems*, vol. 17, no. 4, pp. 314–320, 2021. doi: https://doi.org/10.24138/jcomss-2021-0102
26. U. Sopaoglu, O. Abul, "Classification utility aware data stream anonymization," *Applied Soft Computing*, vol. 110, Article ID 107743, 2021. doi: https://doi.org/10.1016/j.asoc.2021.107743
27. G. Loukides, A. Gkoulalas-Divanis, "Utility-preserving transaction data anonymization with low information loss," *Expert Systems with Applications*, vol. 39, issue 10, pp. 9764–9777, 2012. doi: https://doi.org/10.1016/j.eswa.2012.02.179
28. I. Parberry, "An efficient algorithm for the knight's tour problem," *Discrete Applied Mathematics*, vol. 73, issue 3, pp. 251–260, 1997. doi: https://doi.org/10.1016/S0166-218X(96)00010-8
29. M. Singh, A. Kakkar, and M. Singh, "Image encryption scheme based on knight's tour problem," *Procedia Computer Science*, vol. 70, pp. 245–250, 2015. doi: https://doi.org/10.1016/j.procs.2015.10.081
30. S.-S. Lin, C.-L. Wei, "Optimal algorithms for constructing knight's tours on arbitrary $n \times m$ chessboards," *Discrete Applied Mathematics*, vol. 146, issue 3, pp. 219–232, 2005. doi: https://doi.org/10.1016/j.dam.2004.11.002
31. M. Valtorta, M. I. Zahid, "Warnsdorff's tours of a knight," *Journal of Recreational Mathematics*, vol. 25, no. 4, pp. 263–275, 1993.
32. J. Jeffers, J. Reinders, and A. Sodani, "Chapter 9 — Vectorization," in *J. Jeffers, J. Reinders, and A. Sodani (Eds.), Intel Xeon Phi Processor High Performance Pro-*

gramming (Second Edition). Morgan Kaufmann, 2016, pp. 173–212. doi: https://doi.org/10.1016/B978-0-12-809194-4.00009-0

33. V.V. Romanuke, "Finite uniform approximation of zero-sum games defined on a product of staircase-function continuous spaces," *Annals of the University of Craiova, Mathematics and Computer Science Series*, vol. 49, issue 2, pp. 270–290, 2022. doi: https://doi.org/10.52846/ami.v49i2.1554

Received 04.10.2023

INFORMATION ON THE ARTICLE

Vadim V. Romanuke, ORCID: 0000-0001-9638-9572, Vinnytsia Institute of Trade and Economics of State University of Trade and Economics, Ukraine, e-mail: romanukevadimv@gmail.com

Svitlana A. Yaremko, ORCID: 0000-0002-0605-9324, Vinnytsia Institute of Trade and Economics of State University of Trade and Economics, Ukraine, e-mail: s.yaremko@vtei.edu.ua

Olena M. Kuzmina, ORCID: 0000-0002-0061-9933, Vinnytsia Institute of Trade and Economics of State University of Trade and Economics, Ukraine, e-mail: o.kuzmina@vtei.edu.ua

Hanna A. Yehoshyna, ORCID: 0000-0002-2381-1231, Northwestern Polytechnic, Grande Prairie, Canada, e-mail: hyehoshyna@nwpolytech.ca

АЛГОРИТМ ЦИКЛУ ШАХОВОГО КОНЯ ДЛЯ СКРЕМБЛЮВАННЯ ДАНИХ / В.В. Романюк, С.А. Яремко, О.М. Кузьміна, Г.А. Єгошина

Анотація. Скремблювання даних у наш час залишається важливою методикою для захисту конфіденційної інформації за допомогою певного перемішування, після якого розшифрування є надважким, однак зберігається можливість легітимних дій з даними після скремблювання. Оскільки повноцінне маніпулювання діями з даними після скремблювання залишається проблемою на тлі ризику втрати даних та їх несанкціонованого розшифрування, скремблювання та дескремблювання мають виконуватись ще швидше, не збільшуючи ризики втрати та розшифрування. Алгоритм скремблювання повинен мати лінійну часову складність та ще більше мінімізувати зазначені ризики. Перспективним підходом є задача побудови відкритого циклу шахового коня, розв'язки якої виглядають наче випадкові послідовності позицій коня. Відтак формалізується алгоритм відкритого циклу шахового коня, за яким кінь наче хаотично пересувається по шаховій дошці. Ця формалізація представлена у формі відформатованого псевдокоду для подальшого його ефективного впровадження незалежно від мови програмування. На виході отримано квадратну матрицю, котра відображає відкритий цикл шахового коня. На основі матриці циклу шахового коня подано алгоритми скремблера та дескремблера даних у тому ж стилі. Ці алгоритми мають лінійну часову складність. Скремблювання на основі циклу шахового коня має досить низьку імовірність випадкової дешифрації за умови, якщо використана прийнятна глибина скремблювання, де дані повторно скремблюються. Глибина скремблювання визначається багаторазовим застосуванням матриці шахової дошки, розмір якої зазвичай збільшується з поглибленням скремблювання. Порівняно з псевдовипадковим перемішуванням даних разом зі збереженням індексів перемішування, ключ дескремблювання на основі циклу шахового коня зберігається і пересилається набагато простіше, забезпечуючи в той же час прийнятний захист даних.

Ключові слова: скремблювання даних, задача побудови відкритого циклу шахового коня, лінійна часова складність, імовірність випадкової дешифрації, глибина скремблювання.

UDC 517.9:534.1
DOI: 10.20535/SRIT.2308-8893.2024.3.04

GENERALIZED SCENARIOS OF TRANSITION TO CHAOS IN IDEAL DYNAMIC SYSTEMS

O.O. HORCHAKOV, A.YU. SHVETS

Abstract. The implementation of a new scenario of transition to chaos in the classical Lorenz system has been discovered. Signs of the presence of an implementation of the generalized intermittency scenario for dynamic systems are described. Phase-parametric characteristics, Lyapunov characteristic exponents, distributions of invariant measures, and Poincaré sections are constructed and analyzed in detail, which confirm the implementation of the generalized intermittency scenario in an ideal Lorenz system.

Keywords: ideal dynamic system, regular and chaotic attractors, generalized intermittency scenario.

ITRODUCTION

The study of the ways in which deterministic chaos arises in dynamic systems leads to the necessity to study scenarios of transition to chaos. The scenario of transition to chaos is understood as a sequence of bifurcations, as a result of which a regular steady state regime, for example a periodic one, is replaced by chaotic steady state regime. If the dynamic system is dissipative, then such steady-state regimes will be attractors of system. Despite the huge variety of dynamic systems, there are two types of scenarios for the transition from regular to chaotic modes, which are implemented in almost all dynamic systems. This is the Feigenbaum scenario, during which there is a transition from limit cycle to chaotic attractor through an infinite cascade of bifurcations of period doubling of limit cycle [1; 2]. The second typical scenario is Manneville–Pomeau intermittency [3–5]. When this scenario is implemented, the transition from limit cycle to chaotic attractor occurs in one hard bifurcation. As a result of such bifurcation, the limit cycle disappears and a chaotic attractor appears in the system. Moreover, movement along the trajectories of a chaotic attractor consists of two unpredictably alternating phases — laminar and turbulent.

Recently, a number of new scenarios for transitions to chaos have been described that generalize Manneville–Pomeau and Feigenbaum scenarios. An overview of these scenarios is given in [6]. One of these new scenarios is the so-called generalized intermittency [7; 8]. In contrast to classical intermittency, this scenario describes the transition from a chaotic (hyper-chaotic) attractor of one type to a chaotic (hyper-chaotic) attractor of another type. The implementation of the generalized intermittency scenario was discovered in a number of hydrodynamic, electro-elastic and pendulum systems [7–12], both for traditional attractors and for atypical maximal attractors.

FORMULATION OF THE PROBLEM

All implementations of the generalized intermittency scenario noted in the Introduction were discovered only in dynamic systems that were not ideal according to Sommerfeld–Kononeko or in systems with limited excitation. The fundamental feature of systems with limited excitation is the limited power of the energy source that excites the movement of a particular system. It is assumed that the power of the excitation source is comparable to the power consumed by the system itself. On the contrary, in so-called ideal systems no restrictions are imposed on the power of the excitation source. The fundamentals of the theory of systems with limited excitation were formulated in the monograph [13]. Various aspects of the dynamic behavior of various systems with limited excitation were studied in [14–18].

The main goal of this work is to demonstrate the possibility of implementing a generalized intermittency scenario in classical ideal dynamic systems (systems with unlimited excitation). The Lorenz system plays a unique role among ideal systems in chaotic dynamics. In this system in 1963, a new type of steady-state mode of a non-linear dynamic system, namely deterministic chaos, was firstly discovered.

The mathematical model of the Lorenz system can be written as a system of three differential equations [5; 19]:

$$\begin{aligned} \dot{x} &= \sigma(y - x); \\ \dot{y} &= rx - y - xz; \\ \dot{z} &= -bz + xy, \end{aligned} \tag{1}$$

here x, y, z are phase variables, and σ, r, b are some parameters. E.N. Lorenz derived a system of equations (1) at studying convection in a liquid layer, which is heated from below. In his work [19], the variable x characterizes the speed of rotation of the convection shafts, and the variables y, z are responsible for the horizontal and vertical temperature distribution, respectively. The parameter b is determined by the geometry of the convection cell, σ is the Prandtl number, which is the ratio of kinematic viscosity to the thermal diffusivity coefficient, and r is the Rayleigh number, dimensionless quantity that determines the behavior of the liquid under the influence of temperature.

Subsequently, it turned out that the Lorenz system of equations is applicable not only to the problem of convection in a layer of liquid, but also to describe the dynamics of many other physical systems. These include the convection problem in a closed loop, dissipative oscillator with inertial excitation, etc. [5; 20].

METHODS OF NUMERICAL CALCULATIONS AND MAIN NUMERICAL RESULTS

The system of differential equations (1) is nonlinear, therefore the main methods for studying the dynamic behavior of such a system are various numerical methods. Such methods are: Runge–Kutta method (both with constant and variable steps of numerical integration) for constructing phase portraits, Hénon method for constructing Poincaré sections and phase-parametric characteristics, the Benettin–

Galgani method for calculating Lyapunov characteristic exponents, computer algorithms for encoding images with shades of different brightness for constructing distributions of the natural invariant measure [5; 21; 22]. The general methodology for conducting such studies is described in [23].

A characteristic feature of the Lorenz system is the existence of pairs of symmetric attractors, which could be either regular or chaotic. When the bifurcation parameter changes, a pair of separately existing symmetric attractors can "merge" into one attractor. Then, with a further change of the bifurcation parameter, a pair of attractors may arise again. Let us illustrate this process for some specific values of parameters of Lorenz system. Let the parameters of system (1) be respectively equal

$$r = 203.1, \quad b = \frac{8}{3}.$$

We take parameter b to be the same as in [19], and choose the Rayleigh number sufficiently large. We choose the Prandtl number σ as the bifurcation parameter.

Numerical calculations have shown that for values of the bifraction parameter $9 \le \sigma \le 10$, two symmetric attractors simultaneously exist in system (1). When $\sigma > 10$ these attractors "merge" and only one attractor remains in the system. In Fig. 1, *a* are shown the phase-parametric characteristics (bifurcation trees) of system (1). The values of the bifurcation parameter σ are plotted along the abscissa axis, and the values of the phase variable x are plotted along the ordinate axis. These characteristics were constructed using the Hénon method, when the plane $z = 170$ was chosen as secant plane.

In Fig. 1, *a*, at $9 \le \sigma \le 10$, the phase-parametric characteristic of one of the attractors is plotted in gray, and the other is plotted in black. The individual branches of bifurcation trees correspond to limit cycles of system (1). The points at which new individual branches of bifurcation trees appear are clearly visible. These points correspond to period doubling bifurcations of limit cycles. We note that such of period doubling bifurcations occur for both symmetric limit cycles for the same value of the bifurcation parameter σ. And, at last, the densely gray and the densely black areas of the bifurcation trees correspond to the chaotic attractors of the Lorenz system.

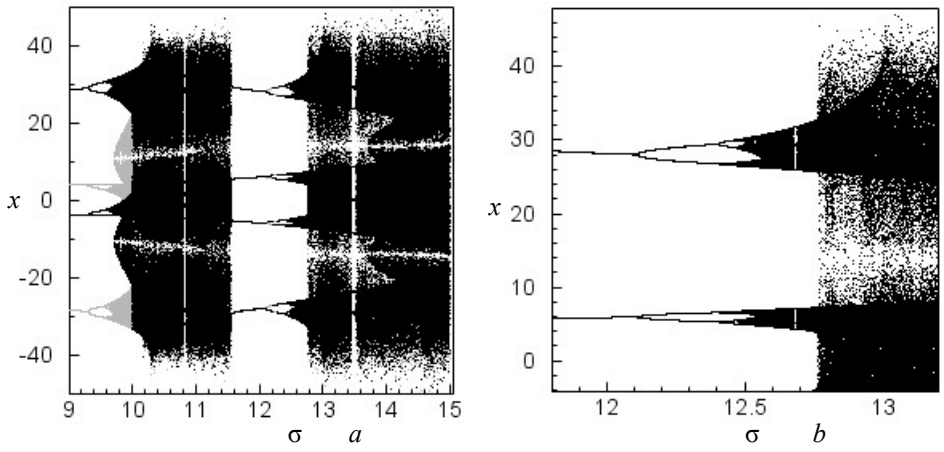

Fig. 1. Phase-parametric characteristics

In Fig. 2, *a* are constracted the phase portraits of two chaotic attractors of the Lorenz system at $\sigma = 10$. One of the attractors is plotted in gray, the other in

black. Both chaotic attractors exist simultaneously, and each of them has its own basin of attraction. The transition from limit cycles to chaos for both attractors occurs according to Feigenbaum's scenario [1; 2]. These chaotic attractors are symmetric in the phase variables x and y. Both attractors have the same spectrum of Lyapunov characteristic exponents, and the maximum characteristic exponent must be positive. This is a necessary condition for the existence of chaos.

When $\sigma > 10$, the existing two chaotic attractors merge into one. As can be seen from the consideration of the bifurcation tree, for all values of $\sigma \in (10,15)$, there is a single attractor in the system, which can be either a limit cycle or a chaotic attractor. The phase portrait of such a "united" chaotic attractor, constructed at $\sigma = 10.01$, is shown in Fig. 2, *b*. Note that the spectrum of Lyapunov characteristic exponents of this attractor is practically no different from the corresponding spectrum of attractors are shown in Fig. 2, *a*.

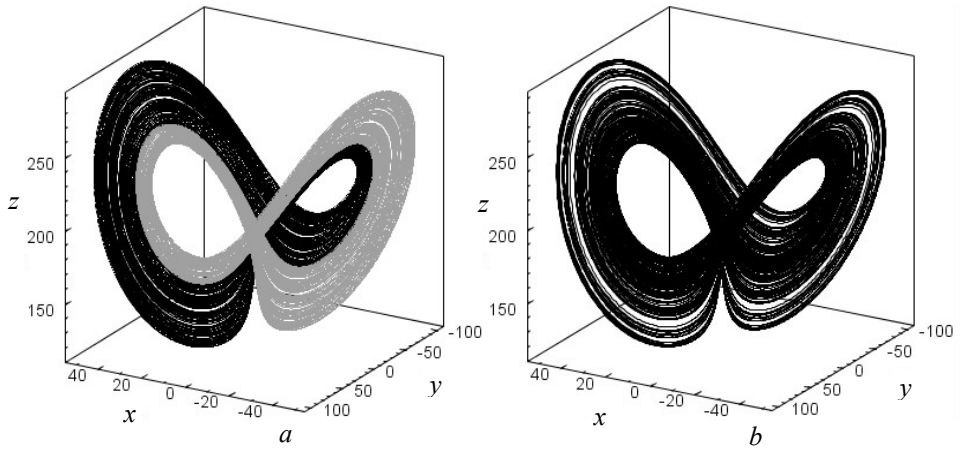

Fig. 2. Phase portrait of chaotic attractors at $\sigma = 10\,(a)$ and $\sigma = 10.01$ (b)

Since the classical scenarios for the transition from regular attractors to chaotic attractors for the Lorenz system are quite well studied [4; 5; 21; 22], we will focus on the implementation of a new scenario of generalized intermittency.

For this, consider an enlarged fragment of the phase-parametric characteristic shown in Fig. 1, *b*. Let us study this phase-parametric characteristic in neighborhood of the bifurcation point $\sigma \approx 12.764$. Both in left and right semi-neighborhood of this bifurcation point in system (1) there are exist chaotic attractors (densely black areas of the bifurcation tree). However, as can be seen from Fig. 1, *b*, area of the densely black region of localization of the points of the bifurcation tree to the right of the point $\sigma \approx 12.764$ noticeably exceeds the corresponding area to the left of the bifurcation point. This feature of the phase-parametric characteristic is one of the signs of the implementation of the generalized intermittency scenario [6–12].

In Fig. 3, *a* is constracted the distribution of natural invariant measure over the phase portrait of the attractor at value $\sigma = 12.76$. The maximum Lyapunov characteristic exponent of this attractor, calculated using the method of Benettin et al., is positive and equal $\lambda_1 = 1.289$. The positivity of the maximum Lyapunov exponent is another evidence of chaotic nature of this attractor.

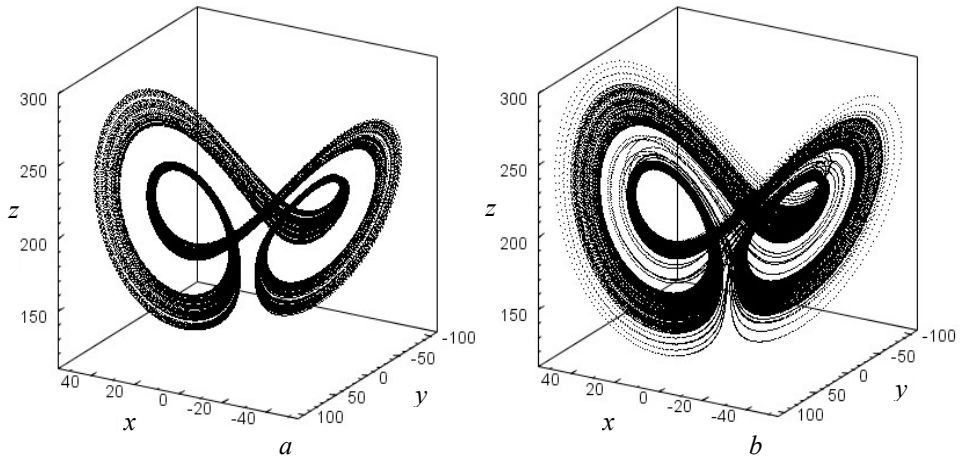

Fig. 3. Distribution of the natural invariant measure at $\sigma = 12.76\,(a)$ and $\sigma = 12.775\,(b)$

At the value of bifurcation parameter σ increases, one hard bifurcation happens at point $\sigma \approx 12.764$. After which the chaotic attractor that existed at $\sigma < 12.764$ disappears and a chaotic attractor of a different type appears in the system (1). The transition from a chaotic attractor of one type to a chaotic attractor of another type occurs according to the scenario of generalized intermittency. In Fig. 3, *b* is constructed distribution of the natural invariant measure over phase portrait of the new chaotic attractor at $\sigma = 12.775$. The attractor that arises after passing the bifurcation point has a significantly larger positive maximum Lyapunov characteristic exponent. This characteristic exponent is equal $\lambda_1 = 1.71$. Such a noticeable increase in the value of the maximum characteristic exponent after passing the bifurcation point is another sign of the implementation of the scenario of generalized intermittency. The movement of the trajectory along the phase portrait of the arising chaotic attractor consists of two phases, so called, rough laminar and turbulent. Rough laminar phase corresponds to chaotic wanderings of the trajectory in the region of localization of the disappeared chaotic attractor (densely black area in Fig. 3, *b*). For turbulent phase corresponds to departures of the trajectory to more distant regions of the phase space (gray points on the distribution of the invariant measure in Fig. 3, *b*). Such transitions from the rough laminar phase of motion to the turbulent phase occur an infinite number of times. Note that the moment of transition from the rough laminar phase to the turbulent phase and the moment of return of the trajectory from the turbulent phase to the rough laminar phase are unpredictable. Also note, the time during which the trajectory is in a rough laminar phase significantly exceeds duration of time, in which trajectory in turbulent phase.

The scenario of generalized intermittency at transitions “a chaotic attractor of one type a chaotic attractor of another type” can also be identified by studying Poincaré sections. In Fig. 4, *a*, *b*, using the Hénon method, Poincaré sections of chaotic attractors at $\sigma = 12.76$ and at $\sigma = 12.775$ are constructed. Here $z = 200$ plane is selected as the secant plane. Both Poincaré sections have a quasi-ribbon structure and represent chaotic sets of individual points. Note that the quasi-ribbon structure is typical for chaotic attractors of the Lorenz system. As can be seen from Fig. 4, *b*, the structure of the Poincaré section of this attractor includes all fragments of the Poincaré section of the chaotic attractor shown in Fig. 4, *a*.

These fragments of the Poincaré section of the attractor at $\sigma = 12.76$ form a rough laminar phase of the attractor at $\sigma = 12.775$. Accordingly, in the structure of the Poincaré section of the attractor at $\sigma = 12.775$, new points additionally appear, which form the turbulent phase.

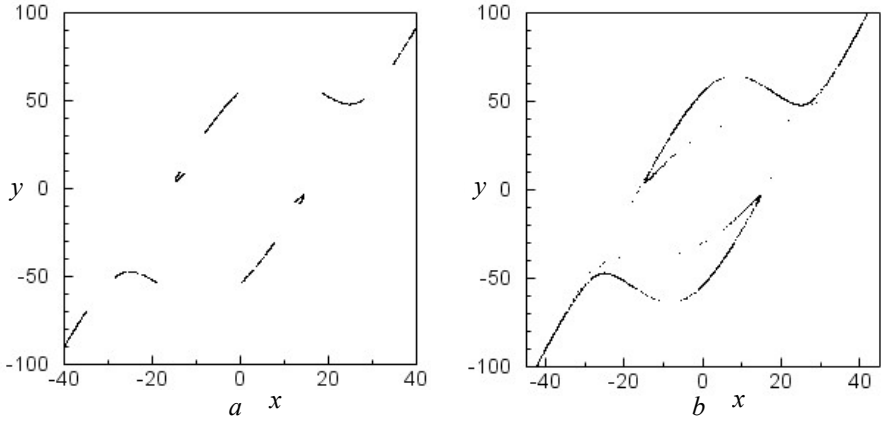

Fig. 4. Poincaré section at $\sigma = 12.76$ (*a*) and $\sigma = 12.775$ (*b*)

The implementation of the generalized intermittency scenario can be found when studying bifurcations in other parameters, in particular for r (the Rayleigh number in the classical work of Lorenz [19]). Let the parameters of system (1) be respectively equal

$$\sigma = 10,\ b = \frac{8}{3}.$$

And now we choose the Rayleigh number r as the bifurcation parameter. The technique for performing numerical calculations is similar to that used when studying bifurcations with respect to the parameter σ.

In Fig. 5, *a* are constructed parts of two phase-parametric characteristics of

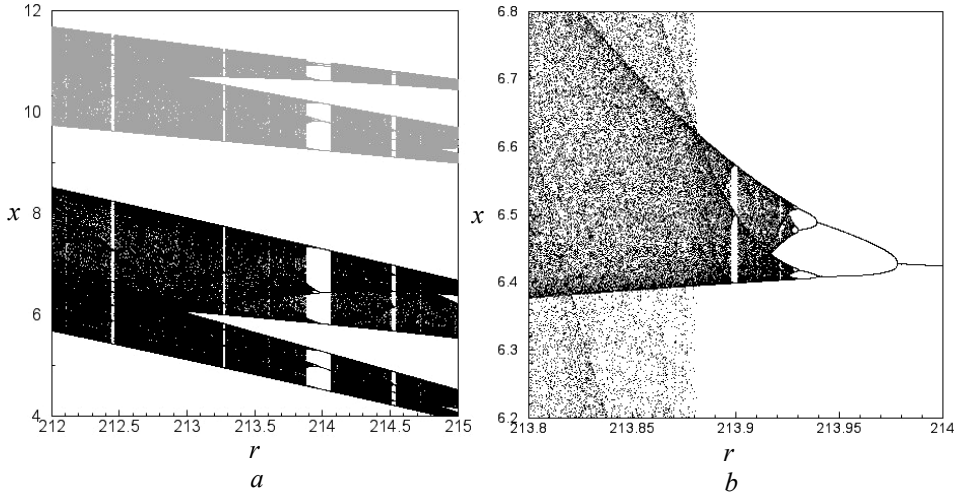

Fig. 5. Phase-parametric characteristics

system (1). These phase-parametric characteristics, “gray” and “black,” correspond to two attractors existing in the system. These two attractors exist in the system simultaneously. Moreover, the only possible situation is when either two

limit cycles or two chaotic attractors simultaneously exist in the system. A careful study of Fig. 5, *a* allows us to identify a number of transitions to chaos according to Feigenbaum's scenario, which occur as the parameter r decreases. In turn, as the parameter r increases, transitions to chaos occur according to the Manneville–Pomeau scenario. We especially emphasize that all bifurcations of these two attractors occur at the same values of the parameter r.

However, we are primarily interested in the implementation of the generalized intermittency scenario. To do this, we will construct a significantly enlarged fragment of the "black" phase-parametric characteristic. Such a fragment is shown in Fig. 5, *b*. At decreasing the values of parameter r in Fig. 5, *b* is clear visible the process of branching of individual branches of the bifurcation tree. As is known, such a process describes the transition to chaos through a cascade of bifurcations of period doubling of the limit cycles. After the appearance of a chaotic attractor, with a further decrease in the values of the parameter r, a sufficiently small window of periodicity arises in which the cascade of bifurcations of period doubling again repeats and a chaotic attractor arises again.

After the appearance of a chaotic attractor, with a further decrease in the values of the parameter r, a sufficiently small window of periodicity appears in which the period-doubling bifurcation sequence again repeats and a chaotic attractor appears again. Finally, when $r \approx 213.885$, one of the signs of the implementation of the generalized intermittency scenario can be seen on the phase-parametric characteristic. Namely, a significant increase in the region of chaos in the phase-parametric characteristic. We studied bifurcations only for one of existing chaotic attractors of the system. However, the same processes can be seen when studying an enlarged fragment of the "gray" phase-parametric characteristic, that correspond to symmetric chaotic attractor.

In Fig. 6, *a* the distributions of the natural invariant measure are plotted over the phase portraits of a pair, symmetric with respect to *x* and *y*, attractors at $r = 213.89$. These symmetrical attractors are shown in black and gray. In Fig. 6, *b* shows the distributions of the natural invariant measure over the phase portraits of another pair of symmetric attractors at $r = 213.88$. In this figure, each of the symmetrical attractors is also shown in black and gray. Both pairs of constructed attractors are chaotic attractors, since they have positive maximum Lyapunov characteristic exponents. As shown by numerical calculations carried out using the method of Benettin et al., each of the chaotic attractors shown in Fig. 6, *a* have the same maximum exponent $\lambda_1 = 0.18$. Accordingly, the second pair of chaotic attractors has maximum exponent $\lambda_1 = 0.28$. So, when passing the bifurcation point $r \approx 213.885$, the second sign of the implementation of the generalized intermittency scenario is observed, namely a significant increase of the maximum Lyapunov characteristic exponent.

For a more visual description of the phases of generalized intermittency in Fig. 6, *c*, *d*, respectively, show significantly enlarged fragments of the distributions of invariant measures for one of the attractors before and immediately after the bifurcation point. Note that for the second of the symmetric attractors we will have a similar description of the phases of generalized intermittency. The rough laminar phase in Fig. 6, *d* form thicker black areas, the shape of which is similar to the areas of distribution of invariant measures in Fig. 6, *c*. The turbulent phase is formed by individual points between the "turns" of the rough laminar phase. As

in the case of studying bifurcations with respect to σ parameter, a picture typical for generalized intermittency can also be found when studying the similarities of Poincaré sections before and after the bifurcation point $r \approx 213.885$.

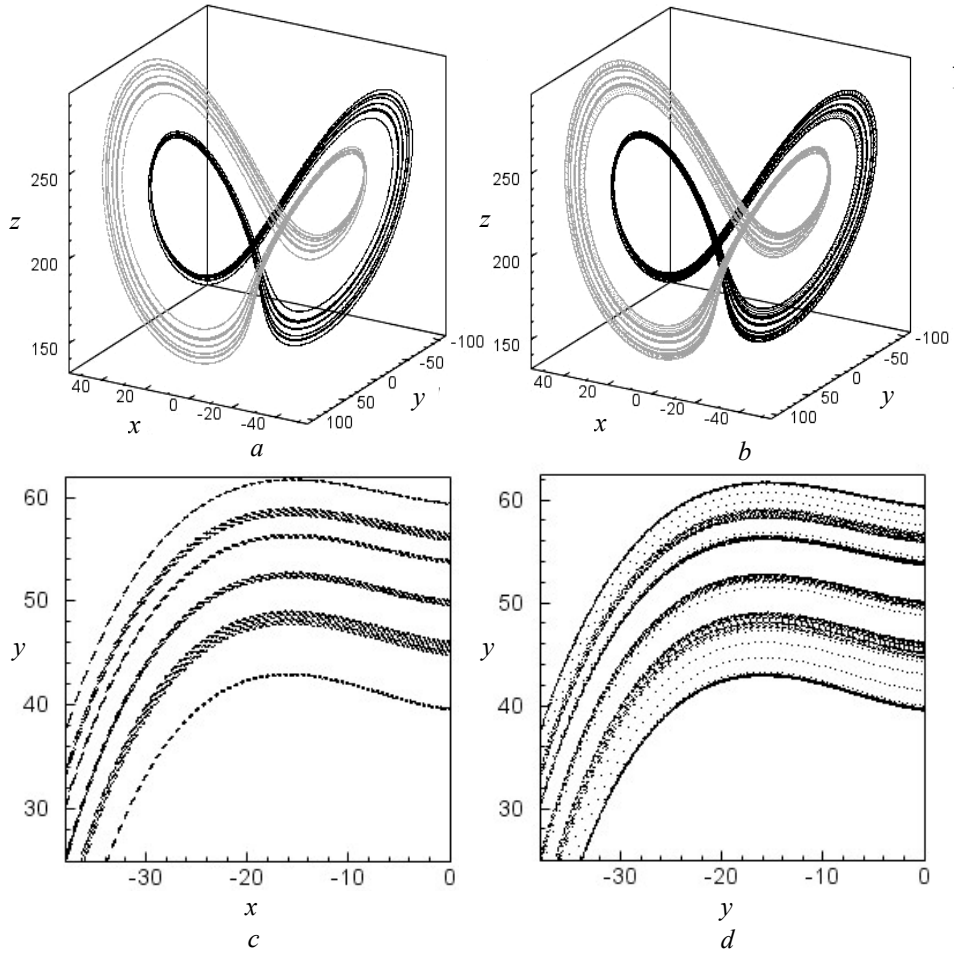

Fig. 6. Distribution of the natural invariant measure at $\sigma = 213.89\,(a)$ and $\sigma = 213.88\,(b)$; fragments of projections at $\sigma = 213.89\,(c)$ and at $\sigma = 213.88\,(d)$

CONCLUSIONS

Thus, for the classical ideal dynamic Lorenz system, the implementation of transitions from "a chaotic attractor of one type to a chaotic attractor of another type" was established according to the scenario of generalized intermittency. It is shown that such a scenario can be realized both in the case of existence of a single attractor in the Lorenz system, and in the case of existence of a pair of symmetric attractors.

REFERENCES

1. M.J. Feigenbaum, "Quantitative universality for a class of nonlinear transformations," *J. Stat. Phys.*, 19(1), pp. 25–52, 1978. doi: https://doi.org/10.1007/BF01020332

2. M.J. Feigenbaum, “The universal metric properties of nonlinear transformations,” *J. Stat. Phys.*, 21(6), pp. 669–706, 1979. doi: https://doi.org/10.1007/BF01107909
3. P. Manneville, Y. Pomeau, “Different ways to turbulence in dissipative dynamical systems,” *Physica D. Nonlinear Phenom.*, 1(2), pp. 219–226, 1980. doi: https://doi.org/10.1016/0167-2789(80)90013-5
4. Y. Pomeau, P. Manneville, “Intermittent transition to turbulence in dissipative dynamical systems,” *Comm. Math. Phys.*, 74(2), pp. 189–197, 1980. doi: https://doi.org/10.1007/BF01197757
5. S.P. Kuznetsov, *Dynamic Chaos*. M.: Fizmatlit, 292 p., 2006.
6. A. Shvets, “Overview of Scenarios of Transition to Chaos in Nonideal Dynamic Systems,” *Springer Proceedings in Complexity*. Springer, Cham, pp. 853–864, 2021. doi: https://doi.org/10.1007/978-3-030-70795-8_59
7. T.S. Krasnopolskaya, A.Yu. Shvets, “Dynamical chaos for a limited power supply for fluid oscillations in cylindrical tanks,” *J. Sound Vibr.*, 322(3), pp. 532–553, 2009. doi: https://doi.org/10.1016/j.jsv.2008.09.007
8. A.Yu. Shvets, V.A. Sirenko, “Scenarios of transitions to hyperchaos in nonideal oscillating systems,” *J. Math. Sci.*, 243(2), pp. 338–346, 2019. doi: https://doi.org/10.1007/s10958-019-04543-z
9. A. Shvets, S. Donetskyi, “Transition to deterministic chaos in some electroelastic systems,” *Springer Proceedings in Complexity*, pp. 257–264, 2019. doi: https://doi.org/10.1007/978-3-030-15297-0_23
10. A. Shvets, S. Donetskyi, “New Types of Limit Sets in the Dynamic System “Spherical Pendulum—Electric Motor,”” *Advanced Structured Materials*, 157, pp. 443–455, 2021. doi: https://doi.org/10.1007/978-3-030-75890-5_25
11. A.Y. Shvets, “Typical and Generalized Transitions to Deterministic Chaos for Atypycal Attractors of Non-Ideal Dynamic Systems,” *System Research and Information Technologies*, no. 4, pp. 141–150, 2022. doi: https://doi.org/10.20535/SRIT.2308-8893.2022.4.11
12. A.Yu. Shvets, “Nonisolated Limit Sets for Some Hydrodynamics Systems with Limited Excitation,” *J. Math. Sci.*, 274(6), pp. 912–922, 2023. doi: https://doi.org/10.1007/s10958-023-06650-4
13. V.O. Kononenko, *Vibrating system with a limited power-supply*. London: Iliffe, 1969, 236 p.
14. K.V. Frolov, T.S. Krasnopolskaya, “Sommerfeld effect in systems without internal damping,” *Soviet Applied Mechanics*, 23(12), pp. 1122–1126, 1987. doi: https://doi.org/10.1007/BF00884888
15. T.S. Krasnopol’skaya, A.Y. Shvets, “Parametric resonance in the system: Liquid in tanks + electric motor,” *Int. Appl. Mech.*, 29(9), pp. 722–730, 1993. doi: https://doi.org/10.1007/BF00847371
16. T.S. Krasnopolskaya, G.J.F. van Heijst, “Wave pattern formation in a fluid annulas with a vibrating inner shell,” *Journal of Fluid Mechanics*, vol. 328, pp. 229–252, 1996. doi: https://doi.org/10.1017/S0022112096008701
17. N.N. Verichev, “Chaotic torsional vibration of imbalanced shaft driven by a limited power supply,” *J. Sound Vibr.*, 331(2), pp. 384–393, 2012. doi: https://doi.org/10.1016/j.jsv.2011.08.022
18. M. Dimentberg, C. Bucher, “Combinational parametric resonance under imperfectly periodic excitation,”*J. Sound Vibr.*, 331(19), pp. 4373–4378, 2012. doi: https://doi.org/10.1016/j.jsv.2012.04.025
19. E.N. Lorenz, “Deterministic nonperiodic flow,” *J. Atmos. Sci.*, 20, pp. 130–141, 1963. doi: https://doi.org/10.1175/1520-0469(1963)020<0130:DNF>2.0.CO;2
20. E.N. Lorenz, “The mechanics of vacillation,” *J. Atmos. Sci.*, 20, pp. 448–464, 1963. doi: https://doi.org/10.1175/1520-0469(1963)020<0448:TMOV>2.0.CO;2

21. *Handbook of Applications of Chaos Theory*; Edited by Christos H. Skiadas, Charilaos Skiadas. Chapman and Hall/CRC, 2016, 952 p.
22. V.S. Anishchenko, T.E. Vadivasova, *Lectures on Nonlinear Dynamics*. Research Center Regular and Chaotic Dynamics, 2011, 516 p.
23. A.Yu. Shvets, T.S. Krasnopolskaya, "Hyperchaos in piezoceramic systems with limited power supply," *Solid Mechanics and its Applications*, 6, pp. 313–322, 2008. doi: https://doi.org/10.1007/978-1-4020-6744-0_27

Received 02.04.2024

INFORMATION ON THE ARTICLE

Aleksandr Yu. Shvets, ORCID: 0000-0003-0330-5136, National Technical University of Ukraine "Igor Sikorsky Kyiv Polytechnic Institute", Ukraine, e-mail: aleksandrshvetskpi@gmail.com

Oleksii O. Horchakov, ORCID: 0009-0006-3664-8812, Institute of Mathematics NAS of Ukraine, Ukraine, e-mail: jarkafres@gmail.com

УЗАГАЛЬНЕНІ СЦЕНАРІЇ ПЕРЕХОДУ ДО ХАОСУ В ІДЕАЛЬНИХ ДИНАМІЧНИХ СИСТЕМАХ / О.О. Горчаков, О.Ю. Швець

Анотація. Виявлено реалізацію нового сценарію переходу до хаосу в класичній системі Лоренца. Описано ознаки наявності реалізації сценарію узагальненої переміжності для динамічних систем. Побудовано та детально проаналізовано фазово-параметричні характеристики, показники Ляпунова, розподіли інваріантних мір та перерізи Пуанкаре, які підтверджують реалізацію сценарію узагальненої переміжності в ідеальній системі Лоренца.

Ключові слова: ідеальна динамічна система, регулярний і хаотичний атрактори, сценарій узагальненої переміжності.

UDC 004.942:537.525
DOI: 10.20535/SRIT.2308-8893.2024.3.05

COMPARISON OF METHODS FOR INTERPOLATION AND EXTRAPOLATION OF BOUNDARY TRAJECTORIES OF SHORT-FOCUS ELECTRON BEAMS USING ROOT-POLYNOMIAL FUNCTIONS

I. MELNYK, A. POCHYNOK, M. SKRYPKA

Abstract. The article considers and discusses the comparison of interpolation and extrapolation methods of estimation of the boundary trajectory of electron beams propagated in ionized gas. All estimations have been computed using root-polynomial functions to numerically solve a differential-algebraic system of equations that describe the boundary trajectory of the electron beam. By providing analysis, it is shown and proven that in the case of solving a self-connected interpolation-extrapolation task, the average error of the beam radius estimation is generally smaller. This approach was especially effective in estimating the focal beam radius. An algorithm for solving self-connected interpolation-extrapolation tasks is given, and its efficiency is explained. Corresponding graphic dependencies are also given and analyzed.

Keywords: interpolation, extrapolation, root-polynomial function, ravine function, average error, electron beam, boundary trajectory.

INTRODUCTION

The development of electron beam technologies is very important today for advanced branches of industry, including metallurgy, mechanical engineering, instrument making, and microelectronic production, as well as automotive, aircraft, and space industries [1–10]. It is caused by the advantages of the electron beam as a technological instrument, such as its high total power and power density, the simplicity of changing and controlling focal beam parameters using electric and magnetic fields, as well as providing technological operation in the medium of pure vacuum [1–10].

For example, the use of electron beams today in the electronic industry is mostly oriented toward welding contacts of electronic devices, including cryogenic ones [8–12], deposition of ceramic dielectric films for high-quality capacitors and microwave transmitters and receiver devices [9; 10; 13–15], as well as toward refining of silicon [16–19]. A special technical problem is obtaining and applying intensive electron beams in high-energy accelerators [7; 20–22].

In such circumstances, the development of electron beam technologies and the sources of electrons are provided in two main directions. The first is improving the traditional electron guns with heated cathodes, and the second is the elaboration of novel types of electron sources based on other physical principles. For example, electron sources based on gas discharges are elaborated today and successfully applied in industry.

Among this type of electron source, a special place occupied the high-voltage glow discharge (HVGD) electron guns, which are generally characterized by the stable operation in the soft vacuum in the medium of different gases, including active and noble ones, as well as by simplicity of construction [23–28]. Another well-known advantage of HVGD electron guns is their simplicity in controlling discharge current and beam power. In the paper [29], the slow aerodynamic control of HVGD current using electromagnetic valves has been considered, and the corresponding time regimes have been analyzed. Fast electric control of beam power by lighting the additional low-voltage discharge and changing the concentration of charged particles in anode plasma, as well as the corresponding time regimes for such fast regulation, have been considered in the paper [30].

Generally, the main advantage possibilities for using HVGD electron guns in industry are as follows:

1. Refining of silicon for the microelectronic industry [16–20; 31].
2. Obtaining high-quality ceramic films for microelectronic production and for power-energetic insulators. Obtaining defense films for cutting instruments and heat-protection films for engines in the automotive, aircraft, and space industries by applying HVGD electron guns is also possible [33–37].
3. Development of 3-D printing technology by metals [38–40].

Therefore, in such circumstances, the development of novel mathematical approaches for the simulation of short-focus electron beams generated by HVGD electron guns is generally necessary.

PERVIOUS RESEARCHES AND STATEMENT OF THE SIMULATION PROBLEM

The problem is that today elaboration of HVGD electron guns is mostly provided by a combination of sophisticated theoretical approaches [23; 26–30] and complex experimental works [24; 25], because simplified mathematical relations for estimation of the focal parameters of short-focus electron beams at low pressure in ionized gas don't exist [23]. Also, in part of the book [23], general approaches for the simulation of electric field distribution and the trajectories of charged particles have been systematized. Corresponding recommendations for the simulation of HVDG electron guns have also been given in [23]. But in any case, such a sophisticated approach to designing this type of guns is significantly hinders the necessary development and implementation in industry of its novel, advanced constructions. Therefore, the finding of simplified mathematical relations for interpolation, extrapolation, and approximation of the trajectories of short-focus electron beams in low-pressure ionized gas is necessary [23]. Corresponding relations for an intensive long-focus electron beam propagated in high vacuum in ion-

ized gases are well-known [1–10]. In the paper [41], simple analytical relations for estimating the depth of welding seam penetration using short-focus electron beams formed by HVGD electron guns have been proposed. Corresponding simulation results have been analyzed and compared with experimental data [41]. Therefore, it is clear that finding and analyzing the simple analytical relations for estimation of the focal parameters of short-focus electron beams propagated in ionized gas is really necessary.

In the years 2019–2020 in the papers [42–44] a simple approach for estimating the parameters of short-focus electron beams propagated in ionized gas has been proposed. Generally, this approach is based on the suggestion that, in such physical conditions, the beam boundary trajectory can be described with high precision by the ravine function, which has one global minimum, and outside the region of minimum, this dependence is similar to a linear one. Such an approach generally corresponds to the main singularities of the physics of electron beams [1–10]. In the papers [42–44], by the numerical experiments have shown that such ravine functions with the precision of fractions of a percent can be described by root-polynomial functions, written as follows [42–45]:

$$r_b(z) = \sqrt[n]{C_n z^n + C_{n-1} z^{n-1} + \ldots + C_1 z + C_0}, \tag{1}$$

where z is the longitudinal coordinate of beam propagation, $r_b(z)$ is the beam radius in corresponded cross-section by z coordinate, n is the degree of the polynomial and the order of the root-polynomial function, and $C_0 \ldots C_n$ are the polynomial coefficients.

The generally obtained results of interpolation have been systematized and analyzed in the paper [45]. In this work, analytical relations for calculation of the coefficients of root polynomial functions (1) from second to fifth order n have been obtained, and the interpolation task was solved relatively to numerical solution of the corresponded set of algebra-differential equations, which described the boundary trajectory of an electron beam propagated in ionized gas [1–10; 23; 45]:

$$f = \frac{n_e}{n_{i0} - n_e};\ C = \frac{I_b(1 - f - \beta^2)}{4\pi\varepsilon_0 \sqrt{\frac{2e}{m_e}} U_{ac}^{1.5}};\ \frac{d^2 r_b}{dz^2} = \frac{C}{r_b};\ \theta = \frac{dr_b}{dz} + \theta_s;$$

$$n_e = \frac{I_b}{\pi r_b^2};\ \ v_e = \sqrt{\frac{2eU_{ac}}{m_e}};\ \ n_{i0} = r_b^2 B_i p n_e \sqrt{\frac{\pi M \varepsilon_0 n_e}{m_e U_{ac}}} \exp\left(-\frac{U_{ac}}{\varepsilon_0 n_e r_b^2}\right);$$

$$\gamma = \sqrt{1-\beta^2};\ \tan\left(\frac{\theta_{\min}}{2}\right) = \frac{10^{-4} Z_a^{4/3}}{2\gamma\beta^2};\ \tan\left(\frac{\theta_{\max}}{2}\right) = \frac{Z_a^{3/2}}{2\gamma\beta^2}; \tag{2}$$

$$\overline{\theta^2} = \frac{8\pi (r_b Z_a)^2 dz}{n_e} \ln\left(\frac{\theta_{\min}}{\theta_{\max}}\right),\ \ \beta = \frac{v_e}{c},$$

where U_{ac} is the accelerating voltage, I_b is the electron beam current, p is the residual gas pressure, z is the longitudinal coordinate, r_b is the radius of the

boundary trajectory of the electron beam, n_e is the beam electrons' concentration, n_{i0} is the concentration of residual gas ions on the beam symmetry axis, m_e is the electron mass, f is the residual gas ionization level, B_i is the gas ionization level, ε_0 is the dielectric constant, v_e is the average velocity of the beam electrons, c is the light velocity, γ is the relativistic factor, $\theta_{\min}$ and $\theta_{\max}$ are the minimum and maximum scattering angles of the beam electrons, corresponding to Rutherford model [1–10], Z_a is the nuclear charge of the residual gas atoms, dz is the length of the electron path in the longitudinal direction at the current iteration, and $\bar{\theta}$ is the average scattering angle of the beam electrons.

In the work [45], it has also been proven that the ravine function (1) can be successfully used for interpolation of the results of solving the set of equations (2) with very small errors in the range of 0.1–8%. Corresponding dependences of interpolation error on z coordinates are given in Fig. 1 [45]. But the main conclusion that has been made is that interpolation error strongly depends on the position of the base points of interpolation, whose number is always equal to $n+1$. Generally, the ravine function, which is described by a set of relations (2), is always symmetric relatively to the plane $z = z_f$, where z_f is the location of beam focus, which should correspond to the minimum of the ravine root-polynomial function (1) [1–10]. Therefore, in [45], the symmetric position of the base point, which gives the minimal error of interpolation, has been considered. When the numerical solution is asymmetric, the error of interpolation is usually increasing several times [45]. Such estimations of asymmetric solutions also increase the error in defining focal beam parameters.

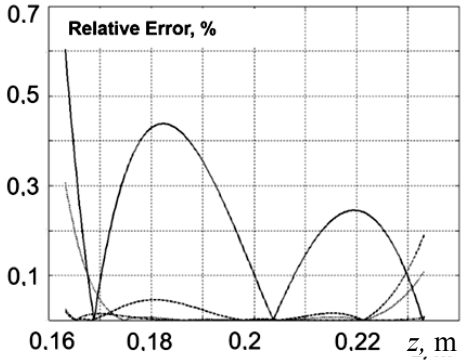

Fig. 1. Errors of interpolation of the boundary trajectory of the electron beam depend on *z* coordinate [45]

The solid line corresponded to a second-order function, the dotted line — to a third-order function, the dashed line — to a fourth-order function, and the dash-dotted line — to a fifth-order function. Model parameters: $U_{ac} = 10\,\text{kV}$; $I_b = 0.5\,\text{A}$; $p = 0.1\,\text{Pa}$.

Therefore, the transformation of the asymmetric dataset for solving the set of relations (2) into a symmetric one has been proposed, and the corresponding simulation results have been studied. In such conditions, the additional symmetric point is given to the analyzed data set, and the task of interpolation with defining the polynomial coefficients $C_0 \ldots C_n$ is solved between two symmetric points. And outside this symmetric region, the task of extrapolation for the same root-

polynomial function (1) has been solved, and the corresponding total error of interpolation and approximation has been defined. The general formulation of this task and the analysis of the obtained simulation results are given in the next sections of this article.

In the paper [46], the possibility of using third-order root-polynomial functions for approximation experimental data about the boundary trajectories of short-focus electron beams in ionized gases as well as the corresponding algorithm of approximation has been considered. Another approach for the simulation of gas discharge electron beam devices with consideration of experimental data has been proposed in the paper [20].

The provided analysis of relevant sources on methods of interpolation and extrapolation showed that other known methods for estimation of the ravine functions either give a large error or are generally not suitable for solving the problem of estimation boundary trajectories of electron beams [42–50]. For example, for polynomial interpolation and extrapolation [48; 49], eliminating unnecessary outliers of the estimated data, especially for high-order polynomials, is generally impossible. Such an estimate, with the exception of a large error, does not even provide sufficiently reliable qualitative results about the boundary trajectory of the electron beam. As a rule, the reason for these outliers is different values of the derivative of the ravine function in the region of the minimum and outside it. The main advantages of the proposed approach of interpolation using root-polynomial functions are as follows:

1. The smoothing of the estimated root-polynomial function in the region of linear variation of numerical data.

2. Obtaining, by this reason, only one global minimum in corresponded area.

Generally, even for high-order root-polynomial functions, outliers and unnecessary extremums are not observed [45].

It is for this reason that the interpolation error is significantly smaller, especially for the symmetrical ravines data sets [45]. Therefore, the main subject of the presented research is to study the possibilities of transforming asymmetric sets of numerical data into symmetric ones using appropriate numerical methods of functional analysis [58–52].

FORMALIZING INTERPOLATION AND EXTRAPOLATION TASKS FOR ASYMMETRIC RAVINE FUNCTIONS DESCRIBED BOUNDARY TRAJECTORIES OF ELECTRON BEAM

Generally, the regions of interpolation and approximation for right-hand and left-hand asymmetric ravine data functions are shown in the Fig. 2. It is clear that the main idea of this approach is to choose the position of the boundary point z_{bp}, which divides the whole range of providing calculations by z coordinate into two regions: Interpolation Region IR and Extrapolation Region ER.

By this way, the task of calculating the boundary trajectory of an electron beam comes down to the problem of interpolation of the symmetric ravine function on the region IE, which has been considered and described in the papers [42–

45]. After that, the root-polynomial function (1) with the same coefficients is used for the Extrapolation Region ER. Considering, corresponding to Fig. 2, the values of the radiuses of Start Point SP r_{start} and End Point EP r_{end}. Also considering the full set of beam trajectory coordinates (z_i, r_i), $(i \in [1; N_P])$, where N_P is the number of calculated points, has been obtained using a set of equations (2). In practice, the value of N_P is $N_P > 10^4$. On the contrary, the value of the basic points N_{BP} for solving complex interpolation-extrapolation tasks is significantly smaller: $N_{BP} = n - 1$. Also, i_0, the start value of variable i, is necessary to formalize the considered task by numerical algorithm. Using the previously described assumptions, the position of the boundary point z_{bp} is defined by following the recurrent arithmetic-logic relation [47]:

$$z_b(i) = (r_{end} > r_{start}) \cdot \left(\begin{pmatrix} r(i) < r_{start} \\ i_0 = 1;\ i = i + 1 \end{pmatrix} \cdot z(i) + \begin{pmatrix} r(i) \geq r_{start} \\ i = i + 1 \end{pmatrix} \cdot z_b(i-1) \right) +$$

$$+ (r_{start} \geq r_{end}) \cdot \left(\begin{pmatrix} r(i) < r_{end} \\ i_0 = N_P;\ i = i - 1 \end{pmatrix} \cdot z(i) + \begin{pmatrix} r(i) \geq r_{end} \\ i = i - 1 \end{pmatrix} \cdot z_b(i+1) \right). \qquad (3)$$

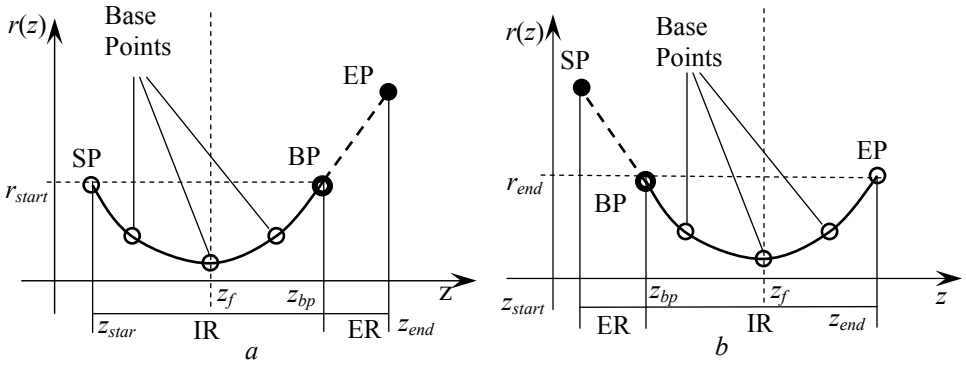

Fig. 2. Right-hand (*a*) and left-hand (*b*) asymmetric ravine functions: IR — Interpolation Region; ER — Extrapolation Region; SP — Start Point; EP — End Point; BP — Boundary Point

The formalized algorithm for solving the complex self-connected interpolation-extrapolation task using relation (1)–(3) on the different regions of longitudinal coordinate z is described by the flowchart presented in Fig. 3.

SOFTWARE FOR NUMERICAL EXPERIMENTS AND ESTIMATIONS OF ERRORS

Using the algorithm described in the previous section of the article for finding the boundary point z_b, both interpolation and self-connected interpolation-extrapolation tasks have been solved. After that, the error of estimation was analyzed. Both tasks are solved in the region $z \in [z_{\min}, z_{\max}]$. Such types of errors were considered and analyzed.

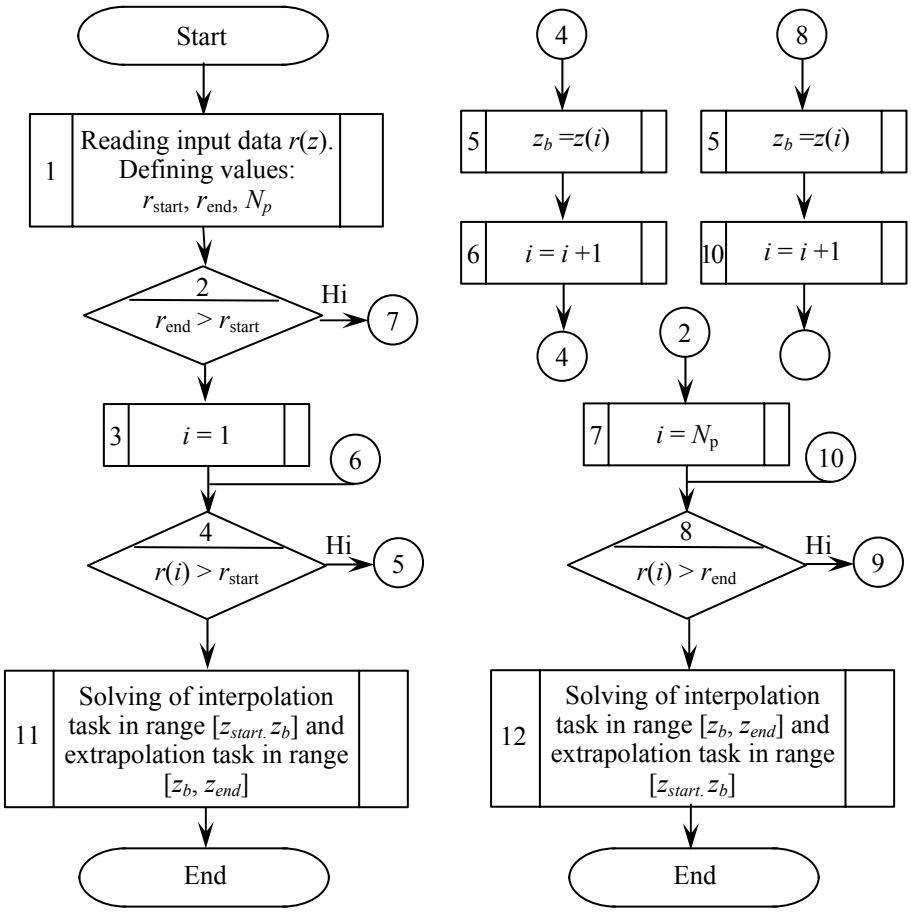

Fig. 3. Flowchart of considered algorithm for solving self-connected interpolation-extrapolation task

1. Maximal error $\varepsilon_{\max}$.

2. Average error ε_{av}, which is generally defined by the well-known method of optimization technique [48–52] and of mathematical statistics [53; 54] as follows:

$$\varepsilon_{av} = \frac{\sum_{i=1}^{N_p} |r_{est} - r_{sim}|}{N_p},$$

where r_{sim} is the radius of the electron beam, calculated numerically by the set of equations (2) using the fourth-order Runge-Kutt method [51; 52], and r_{est} is the value of the beam radius, estimated using relation (2).

3. Error on focus position ε_F.

4. Error on focal beam radius ε_{rf}.

Corresponding relations for defining the third and fourth types of errors have been considered in the papers [43–45].

Corresponding software for the simulation and estimation parameters of electron beams was realized in the Python programming language, including advanced libraries for scientific calculations and graphic libraries. For the correct

location and including these libraries, a virtual environment, virtual memory, virtual variables, and virtual disk have been created on the local computer [55; 56].

Let's consider some results of the simulation and errors in estimations.

Task 1. Acceleration voltage U_{ac} is 15 kV; beam current I_b is 8.5 A; operation pressure in the guiding channel p is 4.5 Pa; the initial radius of the electron beam r_{start} is 8.5 mm; the initial angle of convergence of the electron beam θ is 15^0; the starting point z_{start} is 0.1 m; the first end point z_{end} is 0.15 m; and symmetrical point z_b with the same radius is 0.148 m. That is, the length of the symmetrical segment for the highest interpolation accuracy: $0.148\,\text{m} - 0.1\,\text{m} = 0.048$ m.

For this example, dependence $r(z)$, defined using the set of equations (2), is presented in Fig 4.

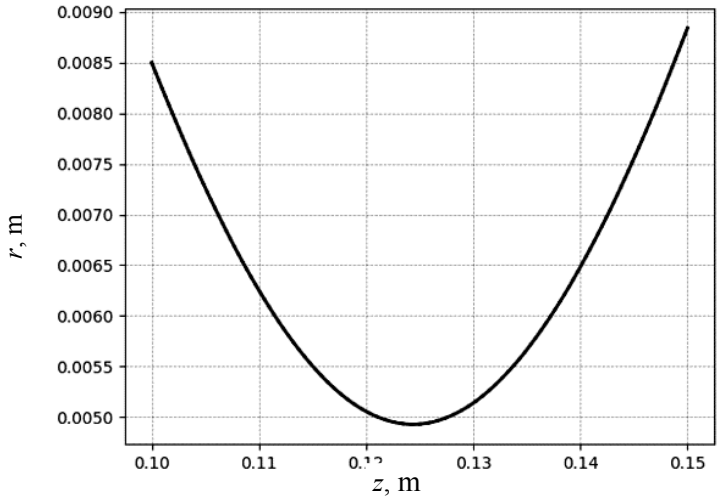

Fig. 4. Dependence *r*(*z*) for $U_{ac} = 15\,\text{kV}$, $I_b = 8.5\,\text{A}$, $p = 4.5\,\text{Pa}$, end point $z_{\text{end}} = 0.15\,\text{m}$ (screen copy)

It is clear that the dependence presented in Fig. 4 is a right-hand asymmetric ravine function. Errors in solving interpolation and self-connected interpolation-extrapolation tasks for this example are presented in Table 1. All errors have been estimated for different order of root-polynomial functions n and length of extrapolation region L_{add}. Task parameter L_{add} is given in Table 1 in absolute value, in meters, and relatively to the length of the interpolation region IR, in percents.

The dependences of estimation errors for two fourth-order root-polynomial functions that have been obtained for solving interpolation and self-connected interpolation-extrapolation tasks are presented in Fig. 5. It is clear that the level of maximal error is similar, nearly 3%, but in the case of extrapolation error in the focal region, it is generally smaller. Corresponding data from Table 1 are as follows; interpolation: $\varepsilon_F = 0.06\,\%$, $\varepsilon_{rf} = 7.56 \cdot 10^{-3}\,\%$; extrapolation: $\varepsilon_F = 0.0041\,\%$, $\varepsilon_{rf} = 1.82 \cdot 10^{-6}\,\%$. Data from Table 1 show also that if for the extrapolation task the maximal error value $\varepsilon_{\max}$ can be greater, then in the case of interpolation, the value of the average error for the extrapolation task ε_{av} is generally smaller. The dependences of the value of ε_{av} on the relative length of the extrapolation region ER for the tasks of interpolation and self-connected interpolation-extrapolation are presented at Fig. 6.

Table 1. Interpolation and extrapolation errors for Task 1

n	$\varepsilon_{\max}$, %		ε_{av}, %		ε_F, %		ε_{rf}, %		L_{add}, m / %
	Extrapolation	Interepolation	Extrapolation	Interepolation	Extrapolation	Interepolation	Extrapolation	Interepolation	
2	2.29	2.84	1.26	1.4476	0	0.08	$5.28\cdot10^{-13}$	$1.7\cdot10^{-3}$	$2\cdot10^{-3}$ / 4.2
3	5.92	6.58	3.25	3.55	0	0.02	0.6	0.635	
4	0.66	0.844	0.2734	0.31	0	0.004	$7.7\cdot10^{-11}$	$2.1\cdot10^{-4}$	
5	2.08	2.27	0.85	0.925	0	0.004	0.44	0.47	
6	0.14	0.203	0.063	0.07	0	0.02	$2.4\cdot10^{-8}$	$8.5\cdot10^{-5}$	
2	2.3	3.243	1.25	1.546	$1.11\cdot10^{-14}$	$6\cdot10^{-3}$	$4.57\cdot10^{-13}$	$6\cdot10^{-3}$	$3\cdot10^{-3}$ / 6.25
3	5.914	7.14	3.2	3.76	0	0.0041	0.629	$7.6\cdot10^{-3}$	
4	0.649	1.0	0.27	0.34	0.0041	0.06	$1.82\cdot10^{-6}$	$7.56\cdot10^{-3}$	
5	2.2	2.58	0.884	1.03	0.0041	0.02	0.48	0.53	
6	0.27	0.256	0.084	0.0654	0	0.041	$3.51\cdot10^{-9}$	$4\cdot10^{-4}$	
2	2.3	3.7	1.254	1.66	0	0.22	$1.23\cdot10^{-13}$	0.013	$4\cdot10^{-3}$ / 8.3
3	5.9	7.71	3.197	3.973	0	$4.1\cdot10^{-3}$	0.65	0.744	
4	0.86	1.17	0.2765	0.38	0.0042	0.1	$7.1\cdot10^{-7}$	$1.878\cdot10^{-3}$	
5	2.33	2.93	0.93	1.14	0.0042	0.6	0.52	0.03345	
6	0.424	0.316	0.07	0.1	0	0.067	$2.23\cdot10^{-8}$	10^{-3}	
2	2.29	4.113	1.27	1.782	$2.23\cdot10^{-14}$	0.291	$2.46\cdot10^{-13}$	0.0224	$5\cdot10^{-3}$ / 10.4
3	5.9	8.3	3.2	4.195	0	$85\cdot10^{-3}$	0.68	0.8	
4	1.15	1.35	0.288	0.4264	0	0.14	$3.38\cdot10^{-11}$	$3.86\cdot10^{-3}$	
5	2.474	3.311	1.0	1.2646	0.0043	0.047	0.5637	0.67	
6	0.56	0.383	0.08	0.1166	0	$9.376\cdot10^{-2}$	$2\cdot10^{-8}$	$2\cdot10^{-3}$	
2	4.89	6.6	1.4573	2.6	$1.11\cdot10^{-14}$	0.676	$4.39\cdot10^{-13}$	0.1263	10^{-2} / 20.8
3	9.52	11.3	3.5	5.4	0	0.02	0.8	1.1443	
4	2.97	2.45	0.42	0.76	0	0.44	$6.35\cdot10^{-11}$	$3.56\cdot10^{-2}$	
5	4.17	5.9	1.39	2.07	$4.7\cdot10^{-3}$	1.77	0.812	1.1226	
6	1.69	0.83	0.17	0.2756	0	0.34	$1.12\cdot10^{-8}$	0.0273	

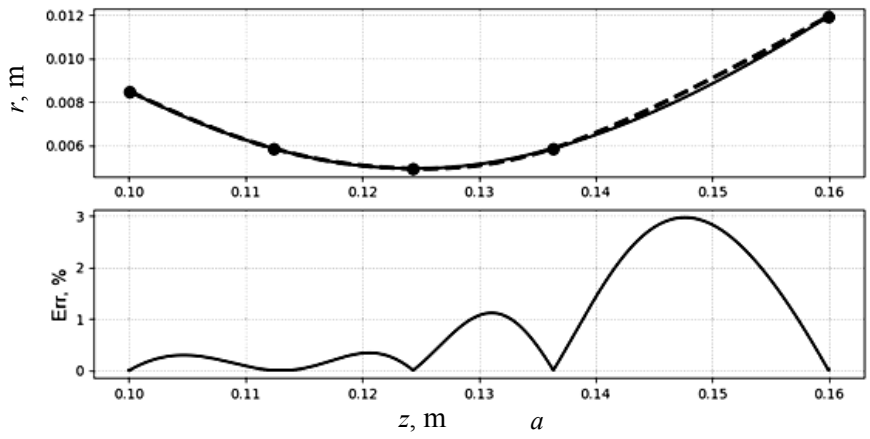

Fig. 5. Dependences of electron beam radius (top) and error of estimation (bottom) on z coordinate for the interpolation task (*a*) and the self-connected interpolation-extrapolation task (*b*). $U_{ac} = 15\,\text{kV}$; $I_b = 8.5\,\text{A}$; $p = 4.5\,\text{Pa}$; $n = 4$; $z_{\text{end}} = 0.16\,\text{m}$. On the top dependence $r(z)$, the straight line corresponds to the obtained numerical solution, and the dash line corresponds to estimations (screen copy)

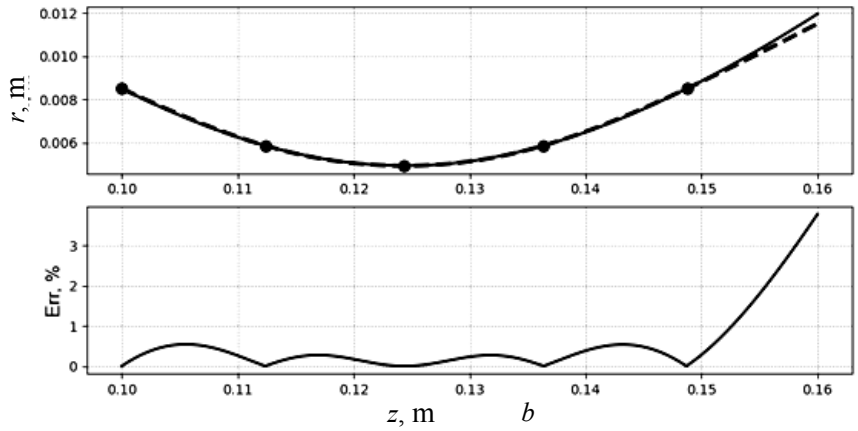

Contiued Fig. 5

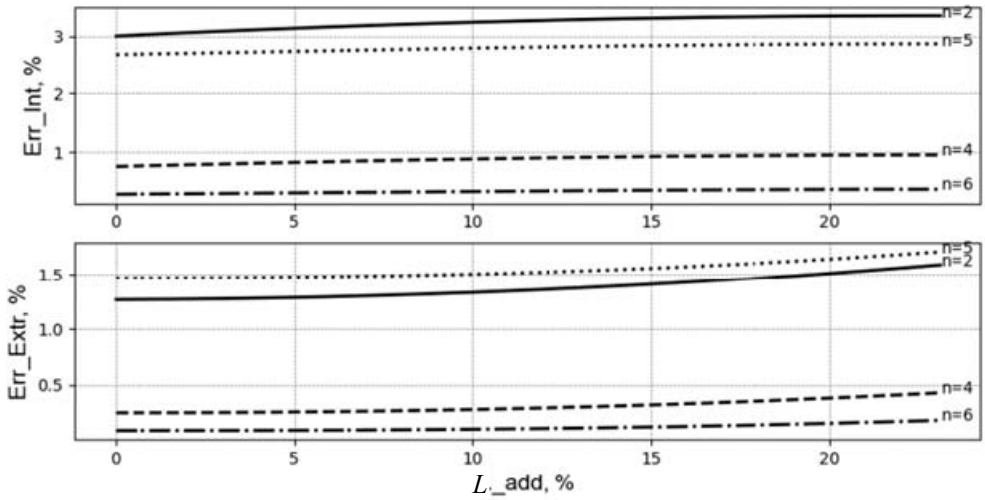

Fig. 6. Dependences of average error ε_{av} of interpolation (top) and end interpolation-extrapolation (bottom) tasks on the value of extrapolation region ER relative to interpolation region IR L_{add} for the root-polynomial functions of different order n. Right-hand ravine function, Task 1 (screen copy)

Task 2. U_{ac} is 15 kV; I_b is 5.5 A; p is 4.5 Pa; r_{start} is 10.3 mm; θ is 15^0; z_{start} is 0.1 m; and z_{end} is 0.15 m. Since in this case $r_{start} > r_{end}$, symmetrical point z_b with the same radius, as r_{end}, is $z_b = 0.101743$ m. That is, the length of the symmetrical segment for the highest interpolation accuracy:

$$0.147\text{ m} - 0.101743\text{ m} = 0.045257\text{ m},\ \text{or, in relative units:}$$

$$0.001743\text{ m} / 0.045257\text{ m} \cdot 100\,\% = 3.85\,\%.$$

In the next steps of providing the calculations, we will reduce the coordinate z_{end} of the end point of the considered interval. That is, take $z_{end} < 0.147$. Thus, we bring it closer to the extremum of the $r(z)$ ravine function, or to the position of the focus of the electron beam z_f. In this way, we will decrease the interpolation interval IR and increase the extrapolation interval ER. For this task, dependence $r(z)$, defined using the set of equations (2), is presented in Fig 7.

It is clear that the dependence presented in Fig. 7 is a left-hand asymmetric function. Errors in solving interpolation and self-connected interpolation-extrapolation tasks for this example are presented in Table 2.

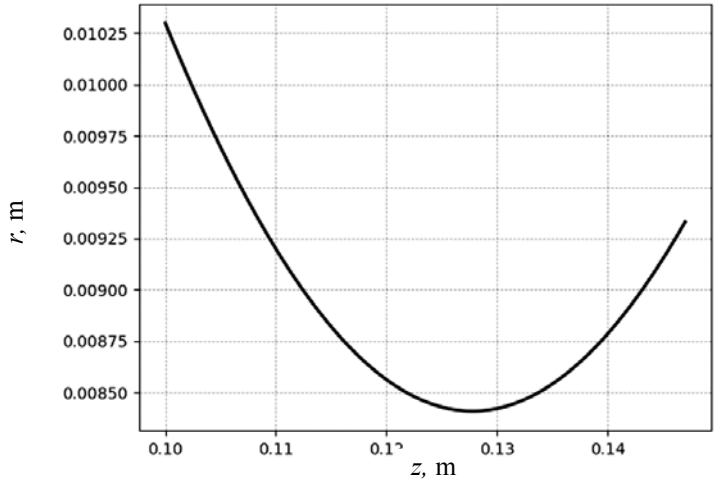

Fig. 7. Dependence $r(z)$ for $U_{ac} = 15\,\text{kV}$, $I_b = 8.5\,\text{A}$, and end point $z_{\text{end}} = 0.147\,\text{m}$ (screen copy)

Table 2. Interpolation and extrapolation errors for Task 2

n	$\varepsilon_{\max}$, %		ε_{av}, %		ε_F, %		ε_{rf}, %		L_{add}, m / %
	Extrapo-lation	Interepo-lation	Extrapo-lation	Interepo-lation	Extrap-olation	Interepo-lation	Extrapo-lation	Interepo-lation	
2	1.85	2.5215	1.0	1.224	0	0.1	$6.68\cdot10^{-13}$	$2.86\cdot10^{-3}$	$1.75\cdot10^{-3}$/ 3.8
3	4.8	5.6522	2.6	2.98	0	$3.77\cdot10^{-3}$	0.46	0.5	
4	0.497	0.7	0.2	0.247	0	$2.34\cdot10^{-4}$	$6.37\cdot10^{-11}$	0.034	
5	1.4255	1.624	0.593	0.6754	0	$7.56\cdot10^{-3}$	0.29	0.317	
6	0.1716	0.1737	$4.236\cdot10^{-2}$	$5.31\cdot10^{-2}$	0	$2\cdot10^{-2}$	$1.6\cdot10^{-8}$	$9.1\cdot10^{-3}$	
2	1.6	2.6	0.88	1.1743	$1.11\cdot10^{-14}$	0.16	$1.4\cdot10^{-13}$	$6.5\cdot10^{-3}$	$2.75\cdot10^{-3}$/ 6.35
3	4.2	5.51	2.27	2.81	0	$3.7\cdot10^{-2}$	0.4	0.45	
4	0.583	0.752	0.1722	0.236	0	$5\cdot10^{-2}$	$3.69\cdot10^{-12}$	$5.16\cdot10^{-4}$	
5	1.19	1.74	0.5	0.61	0	$7\cdot10^{-3}$	0.243	0.2764	
6	0.26	0.19	0.037	0.05	0	0.026	$1.53\cdot10^{-8}$	$1.55\cdot10^{-4}$	
2	1.686	2.68	0.782	1.1378	0	0.21	$2.28\cdot10^{-13}$	0.0112	$3.75\cdot10^{-3}$/ 9.1
3	3.6427	5.36	1.9842	2.65	0	$7.2\cdot10^{-3}$	0.346	0.41	
4	0.78	0.78	0.152	0.23	0	$6.5\cdot10^{-2}$	$8.73\cdot10^{-11}$	$8.26\cdot10^{-4}$	
5	1.13	1.3256	0.43	0.55	0	$7.236\cdot10^{-3}$	0.2	0.24	
6	0.3422	0.2	0.0343	0.05	0	$3.26\cdot10^{-2}$	$1.33\cdot10^{-9}$	$2.1\cdot10^{-4}$	
2	2.46	2.8	0.64	1.1	$1.11\cdot10^{-14}$	0.3	$6.68\cdot10^{-13}$	$2.262\cdot10^{-2}$	$5.75\cdot10^{-3}$/ 15.43
3	4.94	2.36	1.576	5.1	0	10^{-2}	0.256	0.337	
4	1.17243	0.8332	0.14	0.2293	$3.4\cdot10^{-3}$	$1.33\cdot10^{-3}$	$5.62\cdot10^{-7}$	$8\cdot10^{-2}$	
5	1.735	1.07	0.3427	0.46	0	10^{-2}	0.134	0.18	
6	0.527	0.235	$3.77\cdot10^{-2}$	$5.1\cdot10^{-2}$	0	$3.46\cdot10^{-2}$	$3.93\cdot10^{-13}$	$2.72\cdot10^{-4}$	
2	4.224	3.0	0.65	1.225	$3.34\cdot10^{-14}$	0.44	$2.81\cdot10^{-13}$	$4.74\cdot10^{-2}$	$1.075\cdot10^{-2}$ / 39.4
3	8.42	4.34	1.4	1.83	0	0.012	0.105	0.1915	
4	2.1	0.934	0.22	0.27	$3.1\cdot10^{-3}$	$8.6\cdot10^{-2}$	$7.65\cdot10^{-7}$	$1.45\cdot10^{-3}$	
5	3.354	0.86	0.39	0.327	0	$1.2\cdot10^{-2}$	$4\cdot10^{-2}$	$8\cdot10^{-2}$	
6	1.235	0.31	0.12	$6.9\cdot10^{-2}$	$3.1\cdot10^{-3}$	$3.1\cdot10^{-2}$	$3.81\cdot10^{-6}$	$2.15\cdot10^{-4}$	

The dependences for estimation error for fourth-order root-polynomial functions for interpolation and self-connected interpolation-extrapolation tasks are presented in Fig. 8. It is clear that the level of maximal error for the task of interpolation is $\varepsilon_{\max} = 0.05\,\%$, and for the self-connected interpolation-extrapolation task, it is twice as high, $\varepsilon_{\max} = 0.1\,\%$. But in this case, as in the previous example, the extrapolation error in the focal region is generally smaller. The corresponding data from Table 2 are as follows. Interpolation: $\varepsilon_F = 2.34 \cdot 10^{-4}\,\%$, $\varepsilon_{rf} = 0.034\,\%$; extrapolation: $\varepsilon_F = 0\,\%$, $\varepsilon_{rf} = 6.37 \cdot 10^{-11}\,\%$. In this task, the value of the average error for extrapolation ε_{av} is also generally smaller. The dependences of the value of ε_{av} on the relative length of the extrapolation region ER for the interpolation and self-connected interpolation-extrapolation tasks are presented in Fig. 9.

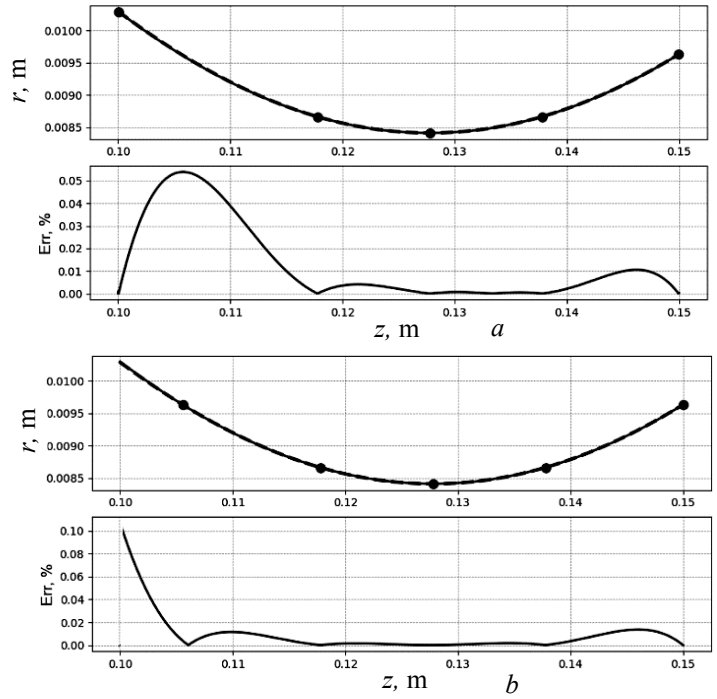

Fig. 8. Dependences of electron beam radius (top) and error of estimation (bottom) on z coordinate for the interpolation task (*a*) and the self-connected interpolation-extrapolation task (*b*). $U_{ac} = 15\,\text{kV}$; $I_b = 5.5\,\text{A}$; $p = 5.5\,\text{Pa}$; $n = 4$; $z_{\text{end}} = 0.147\,\text{m}$. On the top dependences, the $r(z)$ straight line corresponds to the obtained numerical solution, and the dash line corresponds to estimations (screen copy)

Another testing numerical experiments for right-hand and left-hand ravine numerical data, which have been provided, give the similar results of error estimation.

For the output of digital and graphic information, advanced libraries of the Python programming language have been used, such as tkinter, numpy, and matplotlib, which have been located on the virtual disk and included separately [55; 56]. A graphic interface window of elaborated software for the bookmarking "Errors of Estimation" is presented in Fig. 10. For saving and further analyzing the obtained graphic information, the bottom "Save Graph" has been provided in the interface window.

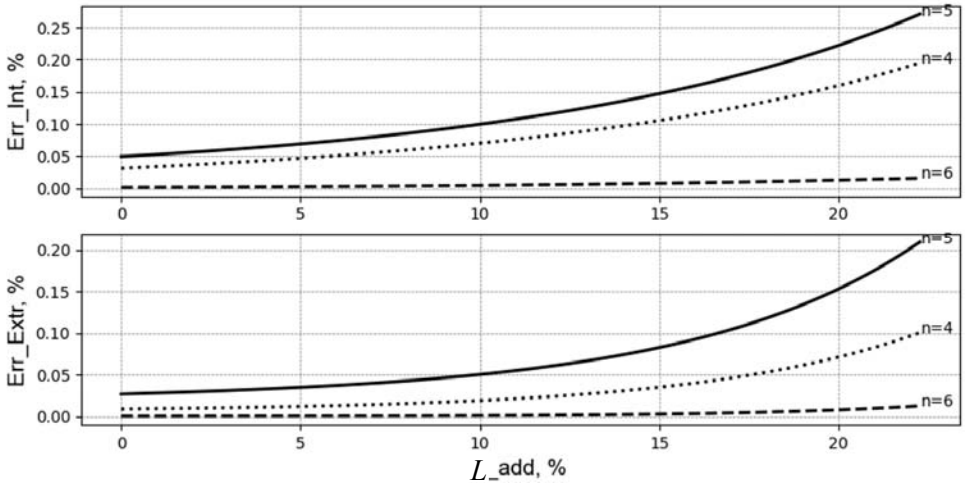

Fig. 9. Dependences of average error ε_{av} of interpolation (top) and interpolation-extrapolation (bottom) tasks on value of extrapolation region ER relative to interpolation region IR L_{add} for the root-polynomial functions of different order n. Left-hand ravine function. Task 2 (screen copy)

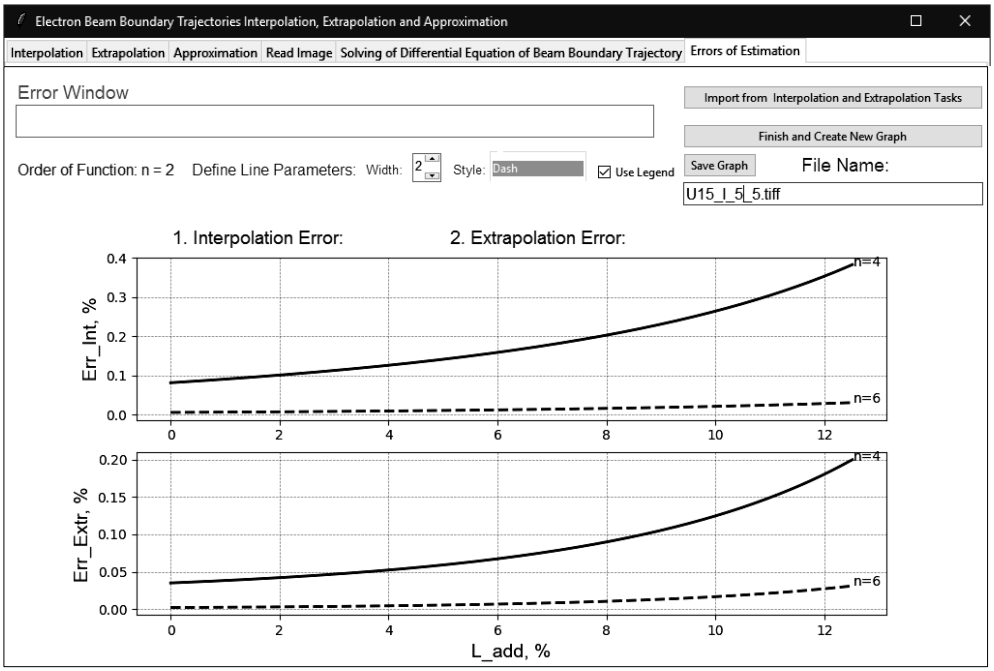

Fig. 10. Interface window for bookmarking “Errors of Estimation” in elaborated computer software

ANALYSIS OF OBTINED RESULTS AND DISCUSSION

The main conclusions about the estimation errors of interpolation and self-connected interpolation tasks are as follows:

1. Usually, the root-polynomial functions (1) of odd order have a larger error value than the functions of even order. Generally, the authors have already discussed this problem in the paper [45], and it is caused by the location of base

points. For functions of even order, the number of base points is odd, and in such a condition, one point is located in the minimum of the ravine function data, and other points are located evenly symmetrically to it. Such a location is considered optimal from the point of view of obtaining minimal interpolation error [45]. Since in the case of the odd order of the root-polynomial function and the even number of base points, this condition can't be fulfilled, the value of error, especially in the region of minimum of the ravine function, is usually greater [45]. In any case, the way to select the base points strongly influences the value of the maximal and average errors for solving interpolation and self-connected interpolation-extrapolation tasks.

2. The values of maximal and average errors for interpolation and extrapolation tasks in the cases of right-hand and left-hand asymmetric data sets are generally similar. It is generally clear by comparing the numerical data given in Table 1 and Table 2.

3. The maximal error of extrapolation increases with the enlarging of the interval of extrapolation ER L_{add}. The maximum error of extrapolation usually corresponds to the end point of this interval z_{end}. Corresponding dependences $\varepsilon_{av}(L_{add})$ are given in Fig. 6 and Fig. 9.

4. In the case of solving self-connected interpolation-extrapolation tasks, the value of the average error is generally smaller, even in cases of large values of the interval of extrapolation ER L_{add}. Corresponding digital data are given in Table 1 and Table 2.

5. In the case of solving a self-connected interpolation-extrapolation task, the values of errors in defining focal beam parameters ε_F and ε_{rf} are generally smaller. In most cases, for this task, the error of defining focus position is absent; $\varepsilon_F = 0$. Corresponding digital data are given in Table 1 and Table 2.

6. For the task of interpolation, the maximal error $\varepsilon_{\max}$ usually corresponds to the midpoint of the interval between two selected base points. Corresponding dependences $\varepsilon_{av}(z)$ are given in Fig. 5 and Fig. 8.

7. In any case, using the self-connected interpolation-extrapolation method is very effective from the point of view of obtaining the minimal error of numerical data estimation in the region of the position of the focus of an electron beam. Corresponding to Table 1 and Table 2, in some cases the error of interpolation-extrapolation estimations by the focal beam radius ε_{rf} is significantly small, resulting in a range of [10^{-13} %; 10^{-7} %].

Other features of estimating errors in solving interpolation, extrapolation, and approximation tasks for the boundary trajectory of electron beams by using root polynomial functions of the form (1), including comparison with experimental data, are the subject of separate further studies.

All research described in this paper has been provided in the Scientific and Educational Laboratory of Electron Beam Technological Devices of the National Technical University of Ukraine "Igor Sikorsky Kyiv Polytechnical Institute".

CONCLUSION

The conducted research and the obtained modeling data showed that the use of the root polynomial function (1) to solve self-connected tasks of the interpolation-extrapolation problem for ravine digital data obtained as a result of the numerical

solution of the system of algebraic-differential equations (2) and describing the boundary trajectory of a short-focus electron beam, propagating in ionized gas are very effective and provide significantly small estimation errors.

The obtained average error of estimation is in the range of $\varepsilon_{av} = 0.05 - 1.5\,\%,$ and the error of estimation of focal beam radius is in the range of $\varepsilon_F = 10^{-13} - 0.6\,\%.$ An estimations of the value of the average error on the length of the extrapolation region ER relative to the length of the extrapolation region IR are also obtained, and the corresponding graphic dependences $\varepsilon_{av}(L_{add})$ are given and analyzed. It is also significant that the average errors of solving self-connected problems of interpolation-extrapolation digital data for right-hand and left-hand asymmetric ravine functions aresimilar.

Obtained simulation results can be interesting for experts in the physics of electron beams, in the elaboration of HVGD electron guns, and in applying advanced electron-beam technologies in different branches of modern industry.

REFERENCES

1. J.D. Lawson, *The Physics of Charged-Particle Beams*. Oxford: Clarendon Press, 1977, 446 p. Available: https://www.semanticscholar.org/paper/The-Physics-of-Charged-Particle-Beams-Stringer/80b5ee5289d5efd8f480b516ec4bade0aa529ea6
2. M. Reiser, *Theory and Design of Charged Particle Beams*. John Wiley & Sons, 2008, 634 p. Available: https://www.wiley.com/en-us/Theory+and+Design+of+Charged+Particle+Beams-p-9783527617630
3. M. Szilagyi, *Electron and Ion Optics*. Springer Science & Business Media, 2012, 539 p. Available: https://www.amazon.com/Electron-Optics-Microdevices-Miklos-Szilagyi/dp/1461282470
4. S.J.R. Humphries, *Charged Particle Beams*. Courier Corporation, 2013, 834 p. Available: https://library.uoh.edu.iq/admin/ebooks/76728-charged-particle-beams---s.-humphries.pdf
5. S. Schiller, U. Heisig, and S. Panzer, *Electron Beam Technology*. John Wiley & Sons Inc, 1995, 508 p. Available: https://books.google.com.ua/books/about/Electron_Beam_Technology.html?id=QRJTAAAAMAAJ&redir_esc=y
6. R.A. Bakish, *Introduction to Electron Beam Technology*. Wiley, 1962, 452 p. Available: https://books.google.com.ua/books?id=GghTAAAAMAAJ&hl=uk&source=gbs_similarbooks
7. R.C., Davidson, H. Qin, *Physics of Intense Charged Particle Beams in High Energy Accelerators*. World Scientific, Singapore, 2001, 604 p. Available: https://books.google.com.ua/books/about/Physics_Of_Intense_Charged_Particle_Beam.html?id=5M02DwAAQBAJ&redir_esc=y
8. H. Schultz, *Electron Beam Welding*. Woodhead Publishing, 1993, 240 p. Available: https://books.google.com.ua/books?id=I0xMo28DwcIC&hl=uk&source=gbs_book_similarbooks
9. G. Brewer, *Electron-Beam Technology in Microelectronic Fabrication*. Elsevier, 2012, 376 p. Available: https://books.google.com.ua/books?idsnU5sOQD6noC&hl=uk&source=gbs_similarbooks
10. I. Brodie, J.J. Muray, *The Physics of Microfabrication*. Springer Science & Business Media, 2013, 504 p. Available: https://books.google.com.ua/books?id=GQYHCAAAQBAJ&hl=uk&source=gbs_similarbooks
11. A.A. Druzhinin, I.P. Ostrovskii, Y.N. Khoverko, N.S.Liakh-Kaguy, and A.M. Vuytsyk, "Low temperature characteristics of germanium whiskers," *Functional materials 21*, no. 2, pp. 130–136, 2014. Available: http://dspace.nbuv.gov.ua/bitstream/handle/123456789/120404/02-Druzhinin.pdf?sequence=1

12. A.A. Druzhinin, I.A. Bolshakova, I.P. Ostrovskii, Y.N. Khoverko, and N.S. Liakh-Kaguy, "Low temperature magnetoresistance of InSb whiskers," *Materials Science in Semiconductor Processing*, vol. 40, pp. 550–555, 2015. Available: https://academic-accelerator.com/search?Journal=Druzhinin
13. A. Zakharov, S. Rozenko, S. Litvintsev, and M. Ilchenko, "Trisection Bandpass Filter with Mixed Cross-Coupling and Different Paths for Signal Propagation," *IEEE Microwave Wireless Component Letters*, vol. 30, no. 1, pp. 12–15, Jan. 2020.
14. A. Zakharov, S. Litvintsev, and M. Ilchenko, "Trisection Bandpass Filters with All Mixed Couplings," *IEEE Microwave Wireless Components Letter*, vol. 29, no. 9, pp. 592–594, 2019. Available: https://ieeexplore.ieee.org/abstract/document/8782802
15. A. Zakharov, S. Rozenko, and M. Ilchenko, "Varactor-tuned microstrip bandpass filter with loop hairpin and combline resonators," *IEEE Transactions on Circuits Systems. II. Experimental Briefs*, vol. 66, no. 6, pp. 953–957, 2019. Available: https://ieeexplore.ieee.org/document/8477112
16. T. Kemmotsu, T. Nagai, and M. Maeda, "Removal Rate of Phosphorous form Melting Silicon," *High Temperature Materials and Processes*, vol. 30, issue 1-2, pp. 17–22, 2011. Available: https://www.degruyter.com/journal/key/htmp/30/1-2/html
17. J.C.S. Pires, A.F.B. Barga, and P.R. May, "The purification of metallurgically grade silicon by electron beam melting," *Journal of Materials Processing Technology*, vol. 169, no. 1, pp. 347–355, 2005. Available: https://www.academia.edu/9442020/The_purification_of_metallurgical_grade_silicon_by_electron_beam_melting
18. D. Luo, N. Liu, Y. Lu, G.Zhang, and T. Li, "Removal of impurities from metallurgically grade silicon by electron beam melting," *Journal of Semiconductors*, vol. 32, issue 3, article ID 033003, 2011. Available: http://www.jos.ac.cn/en/ article/doi/10.1088/1674-4926/32/3/033003
19. D. Jiang, Y. Tan, S. Shi, W. Dong, Z. Gu, and R. Zou, "Removal of phosphorous in molten silicon by electron beam candle melting," *Materials Letters*, vol. 78, pp. 4–7, 2012.
20. A.F. Tseluyko, V.T. Lazurik, D.L. Ryabchikov, V.I. Maslov, and I.N. Sereda, "Experimental study of radiation in the wavelength range 12.2-15.8 nm from a pulsed high-current plasma diode," *Plasma Physics Reports*, 34(11), pp. 963–968, 2008. Available: https://link.springer.com/article/10.1134/S1063780X0811010X
21. V.G. Rudychev, V.T. Lazurik, and Y.V. Rudychev, "Influence of the electron beams incidence angles on the depth-dose distribution of the irradiated object," *Radiation Physics and Chemistry*, 186, 109527, 2021. Available: https://www.sciencedirect.com/science/article/abs/pii/S0969806X21001778
22. V.M. Lazurik, V.T. Lazurik, G. Popov, and Z. Zimek, "Two-parametric model of electron beam in computational dosimetry for radiation processing, *Radiation Physics and Chemistry*, 124, pp. 230–234, 2016. Available: https://www.sciencedirect.com/science/article/abs/pii/S0969806X1530133X
23. I. Melnyk, S. Tuhai, and A. Pochynok, "Universal Complex Model for Estimation the Beam Current Density of High Voltage Glow Discharge Electron Guns," *Lecture Notes in Networks and Systems*; Eds: M. Ilchenko, L. Uryvsky, L. Globa, vol. 152, pp. 319–341, 2021. Available: https://www.springer.com/gp/book/9783030583583
24. S.V. Denbnovetsky, V.G. Melnyk, and I.V. Melnyk, "High voltage glow discharge electron sources and possibilities of its application in industry for realizing different technological operations," *IEEE Transactions on Plasma Science*, vol. 31, issue 5, pp. 987–993, October, 2003. doi: 10.1109/TPS.2003.818444
25. S. Denbnovetskiy et al., "Principles of operation of high voltage glow discharge electron guns and particularities of its technological application," *Proceedings of SPIE, The International Society of Optical Engineering*, pp. 10445–10455, 2017. Available: https://spie.org/Publications/Proceedings/Paper/10.1117/12.2280736
26. I.V. Melnyk, "Numerical simulation of distribution of electric field and particle trajectories in electron sources based on high-voltage glow discharge," *Radioelectronic and Communication Systems*, vol. 48, no. 6, pp. 61–71, 2005. doi: https://doi.org/10.3103/S0735272705060087

27. S.V. Denbnovetsky, J. Felba, V.I. Melnik, and I.V. Melnik, "Model of Beam Formation in a Glow Discharge Electron Gun with a Cold Cathode," *Applied Surface Science*, 111, pp. 288–294, 1997. Available: https://www.sciencedirect.com/science/ article/pii/S0169433296007611?via%3Dihub
28. J.I. Etcheverry, N. Mingolo, J.J. Rocca, and O.E. Martınez, "A Simple Model of a Glow Discharge Electron Beam for Materials Processing," *IEEE Transactions on Plasma Science*, vol. 25, no. 3, pp. 427–432, June, 1997.
29. S.V. Denbnovetsky, V.I. Melnyk, I.V. Melnyk, and B.A. Tugay, "Model of control of glow discharge electron gun current for microelectronics production applications," *Proceedings of SPIE. Sixth International Conference on "Material Science and Material Properties for Infrared Optoelectronics"*, vol. 5065, pp. 64–76, 2003. doi: https://doi.org/10.1117/12.502174
30. I.V. Melnyk, "Estimating of current rise time of glow discharge in triode electrode system in case of control pulsing," *Radioelectronic and Communication Systems*, vol. 56, no. 12, pp. 51–61, 2017.
31. A. Mitchell, T. Wang, "Electron beam melting technology review," *Proceedings of the Conference "Electron Beam Melting and Refining State of the Art 2000, Reno, NV, USA, 2000*, ed. R. Bakish, pp. 2–13.
32. D.V. Kovalchuk, N.P. Kondraty, "Electron-beam remelting of titanium – problems and development prospects," *Titan 2009*, no. 1(23), pp. 29–38.
33. V.A. Savenko, N.I. Grechanyuk, and O.V. Churakov, "Electron beam refining in production of platinum and platinum-base alloys. Information 1. Electron beam refining of platinum," *Advances in Electrometallurgy*, no. 1, pp. 14–16, 2008.
34. T.O. Prikhna et al., "Electron-Beam and Plasma Oxidation-Resistant and Thermal-Barrier Coatings Deposited on Turbine Blades Using Cast and Powder Ni(Co)CrALY(Si) Alloys I. Fundamentals of the Production Technology, Structure, and Phase Composition of Cast NiCrAlY Alloys," *Powder Metallurgy and Metal Ceramics*, vol. 61, issue 1-2, pp. 70–76, 2022. Available: https://link.springer.com/article/10.1007/s11106-022-00296-8
35. T.O. Prikhna et al., "Electron-Beam and Plasma Oxidation-Resistant and Thermal-Barrier Coatings Deposited on Turbine Blades Using Cast and Powder Ni(Co)CrAlY(Si) Alloys Produced by Electron-Beam Melting II. Structure and Chemical and Phase Composition of Cast CoCrAlY Alloys," *Powder Metallurgy and Metal Ceramicsthis*, vol. 61, issue 3-4, pp. 230–237, 2022.
36. I.M. Grechanyuk et al., "Electron-Beam and Plasma Oxidation-Resistant and Thermal-Barrier Coatings Deposited on Turbine Blades Using Cast and Powder Ni(Co)CrAlY(Si) Alloys Produced by Electron Beam Melting IV. Chemical and Phase Composition and Structure of Cocralysi Powder Alloys and Their Use," *Powder Metallurgy and Metal Ceramics*, vol. 61, issue 7-8, pp. 459–464, 2022.
37. M.I. Grechanyuk et al., "Electron-Beam and Plasma Oxidation-Resistant and Thermal-Barrier Coatings Deposited on Turbine Blades Using Cast and Powder Ni (Co)CrAlY (Si) Alloys Produced by Electron Beam Melting III. Formation, Structure, and Chemical and Phase Composition of Thermal-Barrier Ni(Co)CrAlY/ZrO_2–Y_2O_3 Coatings Produced by Physical Vapor Deposition in One Process Cycle," *Powder Metallurgy and Metal Ceramics*, vol. 61, issue 5-6, pp. 328–336, 2022.
38. J. Zhang et al., "Fine equiaxed β grains and superior tensile property in Ti–6Al–4V alloy deposited by coaxial electron beam wire feeding additive manufacturing," *Acta Metallurgica Sinica (English Letters)*, 33(10), pp. 1311–1320, 2020.
39. D. Kovalchuk, O. Ivasishin, "Profile electron beam 3D metal printing," in *Additive Manufacturing for the Aerospace Industry*. Elsevier Inc., 2019, pp. 213–233.
40. M. Wang et al., "Microstructure and mechanical properties of Ti-6Al-4V cruciform structure fabricated by coaxial electron beam wire-feed additive manufacturing," *Journal of Alloys and Compounds*, vol. 960. article 170943. doi: https://doi.org/10.1016/j.jallcom.2023.170943
41. I. Melnyk, S. Tuhai, M. Surzhykov, I. Shved, V. Melnyk, and D. Kovalchuk, "Analytical Estimation of the Deep of Seam Penetration for the Electron-Beam Welding Technologies with Application of Glow Discharge Electron Guns," *2022 IEEE 41-st International Conference on Electronics and Nanotechnology (ELNANO), 2022*, pp. 1–5.

42. I. Melnyk, S. Tuhai, and A. Pochynok, "Calculation of Focal Paramters of Electron Beam Formed in Soft Vacuum at the Plane which Sloped to Beam Axis," *The Forth IEEE International Conference on Information-Communication Technologies and Radioelectronics UkrMiCo'2019. Collections of Proceedings of the Scientific and Technical Conference, Odesa, Ukraine, September 9-13, 2019*. doi: 10.1109/UkrMiCo47782.2019.9165328
43. I. Melnyk, S. Tuhai, and A. Pochynok, "Interpolation of the Boundary Trajectories of Electron Beams by the Roots from Polynomic Functions of Corresponded Order," *2020 IEEE 40th International Conference on Electronics and Nanotechnology (ELNANO)*, pp. 28–33. doi: 10.1109/ELNANO50318.2020.9088786
44. I. Melnik, S. Tugay, and A. Pochynok, "Interpolation Functions for Describing the Boundary Trajectories of Electron Beams Propagated in Ionised Gas," *15-th International Conference on Advanced Trends in Radioelectronics, Telecommunications and Computer Engineering (TCSET – 2020)*, pp. 79–83. doi: 10.1109/TCSET49122.2020.235395
45. I.V. Melnyk, A.V. Pochynok, "Study of a Class of Algebraic Functions for Interpolation of Boundary Trajectories of Short-Focus Electron Beams," *System Researches and Information Technologies*, no. 3, pp. 23–39, 2020. doi: https://doi.org/10.20535/SRIT.2308-8893.2020.3.02
46. I. Melnyk, S. Tuhai, M. Skrypka, A. Pochynok, and D. Kovalchuk, "Approximation of the Boundary Trajectory of a Short-Focus Electron Beam using Third-Order Root-Polynomial Functions and Recurrent Matrixes Approach," *2023 International Conference on Information and Digital Technologies (IDT)*, Zilina, Slovakia, 2023, pp. 133–138, doi: 10.1109/IDT59031.2023.10194399
47. I. Melnyk, A. Luntovskyy, "Estimation of Energy Efficiency and Quality of Service in Cloud Realizations of Parallel Computing Algorithms for IBN," in Klymash, M., Beshley, M., Luntovskyy, A. (eds) *Future Intent-Based Networking. Lecture Notes in Electrical Engineering*, vol. 831, Springer, Cham, pp. 339–379. doi: https://doi.org/10.1007/978-3-030-92435-5_20
48. G.M. Phillips, *Interpolation and Approximation by Polynomials*. Springer, 2023, 312 p. Available: http://bayanbox.ir/view/2518803974255898294/George-M.-Phillips-Interpolation-and-Approximation-by-Polynomials-Springer-2003.pdf
49. N. Draper, H. Smith, *Applied Regression Analysis*; 3 Edition. Wiley Series, 1998, 706 p. Available: https://www.wiley.com/en-us/Applied+Regression+ Analysis,+3rd+Edition-p-9780471170822
50. C. Mohan, K. Deep, *Optimization Techniques*. New Age Science, 2009, 628 p. Available: https://www.amazon.com/Optimization-Techniques-C-Mohan/dp/1906574219
51. M.K. Jain, S.R.K. Iengar, and R.K. Jain, *Numerical Methods for Scientific & Engineering Computation*. New Age International Pvt. Ltd., 2010, 733 p. Available: https://www.google.com.ua/url?sa=t&rct=j&q=&esrc=s&source=web&cd=&ved=2ahUKEwippcuT7rX8AhUhlYsKHRfBCG0QFnoECEsQAQ&url=https%3A%2F%2Fwww.researchgate.net%2Fprofile%2FAbiodun_Opanuga%2Fpost%2Fhow_can_solve_a_non_linear_PDE_using_numerical_method%2Fattachment%2F59d61f7279197b807797de30%2FAS%253A284742038638596%25401444899200343%2Fdownload%2FNumerical%2BMethods.pdf&usg=AOvVaw0MjNl3K877lVWUWw-FPwmV
52. S.C. Chapra, R.P. Canale, *Numerical Methods for Engineers*; 7th Edition. McGraw Hill, 2014, 992 p. Available: https://www.amazon.com/Numerical-Methods-Engineers-Steven-Chapra/dp/007339792X
53. E. Wentzel, L. Ovcharov, *Applied Problems of Probability Theory*. Mir, 1998, 432 p. Available: https://mirtitles.org/2022/06/03/applied-problems-in-probability-theory-wentzel-ovcharov/
54. J.A. Gubner, *Probability and Random Processes for Electrical and Computer Engineers*. UK, Cambridge: Cambridge University Press, 2006. Available: http://www.amazon.com/Probability-Processes-Electrical-Computer-Engineers/dp/0521864704
55. M. Lutz, *Learning Python*; 5th Edition. O'Reilly, 2013, 1643 p.
56. W. McKinney, *Python for Data Analysis: Data Wrangling with Pandas, NumPy, and Jupyter*; 3rd Edition. O'Reilly Media, 2023, 579 p.

Received 02.11.2023

INFORMATION ON THE ARTICLE

Igor V. Melnyk, ORCID: 0000-0003-0220-0615, National Technical University of Ukraine "Igor Sikorsky Kyiv Polytechnic Institute", Ukraine, e-mail: imelnik@phbme.kpi.ua

Alina V. Pochynok, ORCID: 0000-0001-9531-7593, Research Institute of Electronics and Microsystem Technology of the National Technical University of Ukraine "Igor Sikorsky Kyiv Polytechnic Institute", Ukraine, e-mail: alina_pochynok@yahoo.com

Mykhailo Yu. Skrypka, ORCID: 0009-0006-7142-5569, National Technical University of Ukraine "Igor Sikorsky Kyiv Polytechnic Institute", Ukraine, e-mail: scientetik@gmail.com

ПОРІВНЯННЯ ЗАСТОСУВАННЯ МЕТОДІВ ІНТЕРПОЛЯЦІЇ ТА ЕКСТРАПОЛЯЦІЇ ГРАНИЧНИХ ТРАЄКТОРІЙ КОРОТКОФОКУСНИХ ЕЛЕКТРОННИХ ПУЧКІВ ІЗ ВИКОРИСТАННЯМ КОРЕНЕВО-ПОЛІНОМІАЛЬНИХ ФУНКЦІЙ / І.В. Мельник, А.В. Починок, М.Ю. Скрипка

Анотація. Розглянуто й обговорено порівняння методів інтерполяційного та екстраполяційного оцінювання граничної траєкторії електронних пучків, які поширюються в іонізованому газі. Оцінювання виконано з використанням коренево-поліноміальних функцій для числового розв'язання системи алгебро-диференціальних рівнянь, що описують граничну траєкторію електронного пучка. Показано та доведено, що у разі розв'язання взаємозв'язаної задачі інтерполяції-екстраполяції середня похибка оцінювання радіуса променя, зазвичай, є меншою. Особливо ефективним виявилося використання цього підходу в оцінюванні фокального радіуса променя. Наведено алгоритм розв'язання інтерполяційно-екстраполяційної задачі та пояснено його ефективність. Наведено та проаналізовано відповідні графічні залежності.

Ключові слова: інтерполяція, екстраполяція, коренево-поліноміальна функція, яружна функція, електронний пучок, гранична траєкторія.

UDC 517.925
DOI: 10.20535/SRIT.2308-8893.2024.3.06

IDENTIFICATION OF NONLINEAR SYSTEMS WITH PERIODIC EXTERNAL ACTIONS (Part I)

V. GORODETSKYI

Abstract. The problem of identifying nonlinear systems with periodic external actions is considered in the article. The number of such actions in the system is not limited, and these actions can be either additive or multiplicative. We use a time series of observed system variables to calculate unknown equation coefficients. The proven theorem allows us to separate the unknown coefficients of the system into variables and constants. The proposed computational procedure allows us to avoid possible errors caused by the discrete nature of observable time series. Identification of zero coefficients is carried out in two ways, eliminating erroneous zeroing of the terms of the equations. The method is illustrated with a numerical example of identifying a chaotic system with periodic external actions.

Keywords: identification, ordinary differential equation, external action, periodic coefficient, constant coefficient.

INTRODUCTION

Nonlinear systems with external actions occur in the study of many real objects and processes. Such systems are widespread, for example, in biology [1–3], ecology [4], epidemiology [5], mechanical engineering [6–8], and electrical engineering [9].

A significant amount of research is devoted to constructing models of non-autonomous systems, including those that involve periodic external actions. In [4], for example, non-autonomous models of the "predator-prey" type are studied for almost periodic systems that are used in bioinformatics, social networks, and wireless sensor networks. Study [6] is devoted to the analysis of the influence of external periodic force on the behavior of the model of single-degree-of-freedom vibro-impact system. In this work the conditions for the transition of the model from the chaotic to the regular regime have been studied. In paper [7], a nonlinear non-autonomous dynamic model of a quarter vehicle with nonlinear spring and damping was studied. The influences of the damping coefficient, external action amplitude and frequency on the dynamic responses were analyzed. It was established that the system could have chaotic, quasi-periodic or periodic motion. A study of a bio-reactor model with periodic nutrient forcing is presented in [10]. The paper [11] investigates the global behaviors of the logistic system with periodic impulsive perturbations. The authors formulate condition under which the system may have periodic solution. A wide class of non-autonomous models is described and analyzed in [12]. An increasing interest in non-autonomous systems was admitted in [13]. This survey introduces basic concepts and tools for non-autonomous dynamical systems and their application to various biological mod-

els. Investigation [14] is devoted to the analysis of various modes of the oscillator with periodic external action.

Additionally, extensive research has been conducted to address one of the specific instances of the inverse problem [15], which is the identification of non-autonomous systems based on the observed variables. For example, neural networks were used in [16; 17] to solve this problem. The study [18] proposes a method for constructing a nonlinear, non-autonomous model with a hyperbolic linear part. The articles [19; 20] consider various approaches to identifying systems of differential equations with an additive external action. A similar problem for systems of difference equations was solved in [21].

FORMULATION OF THE PROBLEM

In the works mentioned above, the problem of identifying a system with a known model structure and additive external action is typically addressed. We are attempting to solve a more general problem. Namely, we propose a method for finding external actions, both additive and multiplicative, without limiting their quantity. This task is complicated by the lack of information regarding which coefficients of the differential equation are constant and which are periodic (representing external actions). Also, the task can become more difficult when we study systems with deterministic chaos. As is known [22], the behavior of such systems essentially depends on the initial conditions.

Consider a system consisting of ordinary differential equations (ODEs) of the form

$$\dot{x}_i = \sum_{j=0}^{m} c_{ij}(t) f_j(\mathbf{x}), \qquad (1)$$

where $i = 1,...,n;\ \mathbf{x} = \{x_1(t),...,x_n(t)\}$. We assume that the right-hand sides of equation (1) satisfy the conditions for the existence and uniqueness of the solution on a certain time interval when $t \in [0;t_e],\ t_e > 0$.

The coefficients in equation (1) can be of three types: $c_{ij}(t) = \text{const}$, $c_{ij}(t) = 0$, and $c_{ij}(t) = p_{ij}(t)$, where $p_{ij}(t)$ is a continuous periodic function with a period T. This function represents an external action on the system. Each equation of the system can have many periodic coefficients that correspond to external actions. Moreover, all periodic coefficients in each equation have the same period. Generally speaking, the external actions of equation (1) are multiplicative. If, for example, $f_0(\mathbf{x}) = 1$, then the external action $c_{i0}(t)$ becomes additive.

A method is proposed for solving the following problem. We assume that the functions $x_i(t)$, $\dot{x}_i(t)$, and $f_{ij}(\mathbf{x})$ in equation (1) are known. It is necessary to define the following:

1. Determine which coefficients of equation (1) are periodic, which are constant, and which are zero. We assume that equation (1) has at least one coefficient of each type. At the same time, the number of coefficients of each type is limited only by the total number of coefficients in the equation, which is $m+1$.

2. Find the period of the functions $p_{ij}(t)$.

3. Find the values of the constant coefficients.
4. Find the form of the functions $p_{ij}(t)$.

METHOD

To solve this problem, we will use the following approach. Consider the case when, in equation (1), $c_{ij}(t) = \text{const} \quad \forall j \in 0,...,m$. Then, to find these coefficients, we can use a system of $m+1$ linear algebraic equations (SLAE) compiled for $m+1$ time points $t_0,...,t_m$:

$$\begin{cases} \dot{x}_i(t_0) = c_{i0} f_0(\mathbf{x}(t_0)) + c_{i1} f_1(\mathbf{x}(t_0)) + ... + c_{im} f_m(\mathbf{x}(t_0)), \\ \dot{x}_i(t_1) = c_{i0} f_0(\mathbf{x}(t_1)) + c_{i1} f_1(\mathbf{x}(t_1)) + ... + c_{im} f_m(\mathbf{x}(t_1)), \\ ..... \\ \dot{x}_i(t_m) = c_{i0} f_0(\mathbf{x}(t_m)) + c_{i1} f_1(\mathbf{x}(t_m)) + ... + c_{im} f_m(\mathbf{x}(t_m)). \end{cases} \tag{2}$$

The SLAE (2) coefficients can be calculated using the well-known relation [23]:

$$\mathbf{C} = \mathbf{A}^{-1}\mathbf{B}, \tag{3}$$

where

$$\mathbf{C} = \begin{bmatrix} c_{i0} \\ c_{i1} \\ ... \\ c_{im} \end{bmatrix}, \quad \mathbf{A} = \begin{bmatrix} f_0(\mathbf{x}(t_0)) & f_1(\mathbf{x}(t_0)) & ... & f_m(\mathbf{x}(t_0)) \\ f_0(\mathbf{x}(t_1)) & f_1(\mathbf{x}(t_1)) & ... & f_m(\mathbf{x}(t_1)) \\ ... & & & \\ f_0(\mathbf{x}(t_m)) & f_1(\mathbf{x}(t_m)) & ... & f_m(\mathbf{x}(t_m)) \end{bmatrix}, \quad \mathbf{B} = \begin{bmatrix} \dot{x}_i(t_0) \\ \dot{x}_i(t_1) \\ ... \\ \dot{x}_i(t_m) \end{bmatrix}.$$

To calculate constant coefficients using formula (3), it is sufficiently to do the following:

1. Select arbitrary moments of time $t_0,...,t_m$.

2. Form matrix $\mathbf{A}$ and vector $\mathbf{B}$ for these moments. We assume that matrix A is not singular.

3. Use formula (3) to obtain vector $\mathbf{C}$.

Note that, since in this case all the $c_{i0},...,c_{im}$ coefficients are constant, it is sufficiently to perform all the listed above operations for one set of $t_0,...,t_m$.

If at least one of the required coefficients is a function of time $c_{ij}(t) = \text{var}$, it is necessary to find its values at each point in the time interval $t \in [0;t_e]$. Using the procedure described above for some arbitrary set of $t_0,...,t_m$, we will obtain some value of coefficient $c_{ij}(t)$. At the same time, it is not known to which point in time from the interval $[0;t_e]$ this value corresponds. Thus, the function $c_{ij}(t)$ cannot be constructed. As will be shown below, to eliminate this uncertainty when calculating periodic coefficients using formula (3), it is sufficiently to impose some conditions on the moments of time for which matrix $\mathbf{A}$ and vector $\mathbf{B}$ are formed.

Let the time moments for which the SLAE (2) is formed obey the relations:

$$t_1 = t_0 + \tau, \quad t_2 = t_0 + 2\tau, \ ... \ , \quad t_m = t_0 + m\tau; \quad t_0 \geq 0, \quad \tau > 0, \quad t_m \leq t_e. \tag{4}$$

Theorem. Let equation (1) has constant coefficients and periodic coefficients with a period of T. Additionally, let the SLAE be formed in the form of equation (2) for the time moments, subject to the conditions (4) and when $\tau = T$. When solving the SLAE using relation (3), we obtain a vector $\mathbf{C}$, which consists of the values of the periodic coefficients of equation (1) at time t_0 as well as the values of the constant coefficients of this equation.

Proof. Let us first assume that in equation (1), one of the coefficients, for example, $c_{i0}(t)$, is periodic with a period T, while the remaining coefficients are constant. Then the SLAE (2) will take the following form:

$$\begin{cases} \dot{x}_i(t_0) = c_{i0}(t_0) f_0(\mathbf{x}(t_0)) + c_{i1} f_1(\mathbf{x}(t_0)) + ... + c_{im} f_m(\mathbf{x}(t_0)), \\ \dot{x}_i(t_1) = c_{i0}(t_1) f_0(\mathbf{x}(t_1)) + c_{i1} f_1(\mathbf{x}(t_1)) + ... + c_{im} f_m(\mathbf{x}(t_1)), \\ ..... \\ \dot{x}_i(t_m) = c_{i0}(t_m) f_0(\mathbf{x}(t_m)) + c_{i1} f_1(\mathbf{x}(t_m)) + ... + c_{im} f_m(\mathbf{x}(t_m)). \end{cases} \tag{5}$$

Let us form a matrix $\mathbf{A}$ and vector $\mathbf{B}$ to solve system (5). To do this, we choose the moments of time according to the condition stated in the theorem, which is condition (4). If at the same time $\tau = T$, then, since the function is periodic with a period of T, we get

$$c_{i0}(t_0) = c_{i0}(t_1) = ... = c_{i0}(t_m), \tag{6}$$

where

$$t_1 = t_0 + T,\ t_2 = t_0 + 2T, ...,\ t_m = t_0 + mT.$$

That is, in the system (5), the periodic coefficient $c_{i0}(t)$ becomes constant. Therefore, applying formula (3) to solve SLAE (5) is correct. The resulting vector of coefficients of the system (5) will include the values of the constant coefficients of equation (1) and the value of the periodic coefficient at time moments (6).

According to the conditions of the problem, all periodic coefficients of equation (1) have the same period. Therefore, the above reasoning is valid if equation (1) has more than one periodic coefficient. That is, when forming the SLAE of the form (2) and considering relations (4) at $\tau = T$, all periodic coefficients of equation (1) will have constant values that correspond to the time moment t_0. Then, by solving the SLAE (2), we can determine these constant values of the periodic coefficients of equation (1) as well as the values of the constant coefficients of equation (1). This completes the proof.

Corollary. To separate the desired coefficients into constant and periodic ones, it is sufficient to form two systems of the form (2) for two values of t_0: t_{01} and t_{02} while considering conditions (4). If $\tau = T$, $t_{01} \neq t_{02}$, and $|t_{01} - t_{02}| \neq kT$ $(k = 1,2,...)$, then when solving these two SLAEs, we obtain the same values for the constant coefficients in equation (1).

This Corollary was used to construct the identification algorithm described in the next section. It is also necessary to note an important special case that may arise with an arbitrary choice of t_{01} and t_{02} values in the proposed algorithm and which may lead to incorrectness of results. This situation will be considered in the Special case section.

NUMERICAL RESULTS

On the basis of proven Theorem and its Corollary, an algorithm was developed that can be divided into two stages. At the beginning, we can address the first three points of the formulated problem. In the second stage, the form of the functions $p_{ij}(t)$ is determined.

To illustrate the method, we used system (7), which was built based on the well-known Rössler system [24]:

$$\begin{cases} \dot{x}_1 = -x_2 - x_3, \\ \dot{x}_2 = x_1 - dx_2, \\ \dot{x}_3 = c_{30}(t) + c_{33}(t)x_3 + c_{36}(t)x_1x_3, \end{cases} \tag{7}$$

where

$$d = 0.15,\ c_{30}(t) = 0.5 + 0.4\sin\left(\frac{2\pi t}{T}\right),\ c_{33}(t) = -20,\ c_{36}(t) = 5 + 2.5\sin\left(\frac{2\pi t}{T} - \frac{\pi}{2}\right).$$

As we can see, the third equation of the system has two external actions: an additive one $c_{30}(t)$ and a multiplicative one $c_{36}(t)$. The period of external actions was taken to be $T = 2.11\,s$. The system was solved over an interval of 100 s with a step size of $\Delta t = 0.01s$. Fig. 1 shows the time series of the variables in the system (7), and Fig. 2 displays its phase trajectories.

The object of study is the third equation of the system (7). We will identify it based on the general structure of the form (8), which includes a second-degree polynomial on the right-hand side:

$$\dot{x}_3 = c_{30}(t) + c_{31}(t)x_1 + c_{32}(t)x_2 + c_{33}(t)x_3 + c_{34}(t)x_1^2 + c_{35}(t)x_1x_2 + \\ + c_{36}(t)x_1x_3 + c_{37}(t)x_2^2 + c_{38}(t)x_2x_3 + c_{39}(t)x_3^2. \tag{8}$$

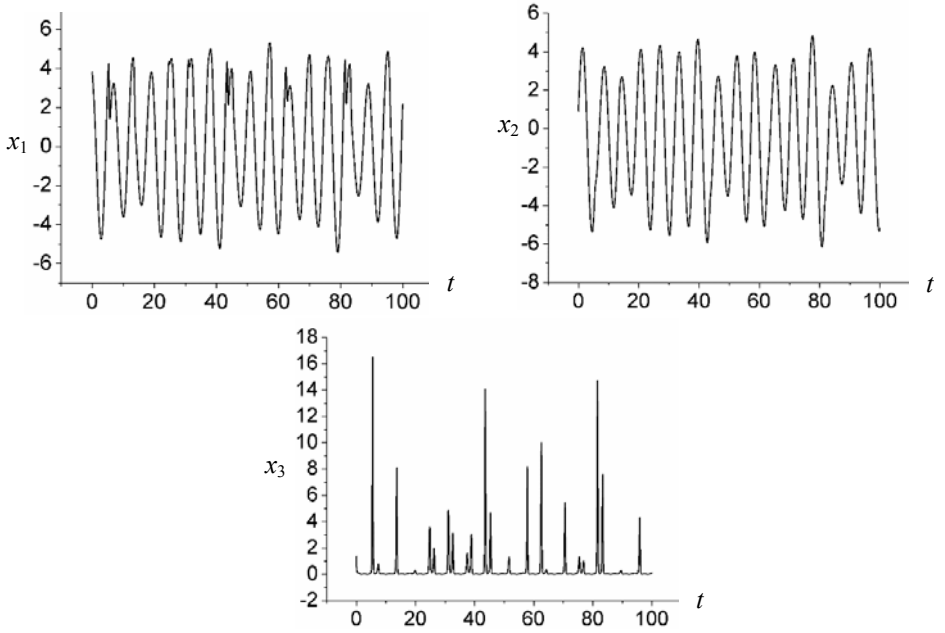

Fig. 1. Time series of system (7) variables

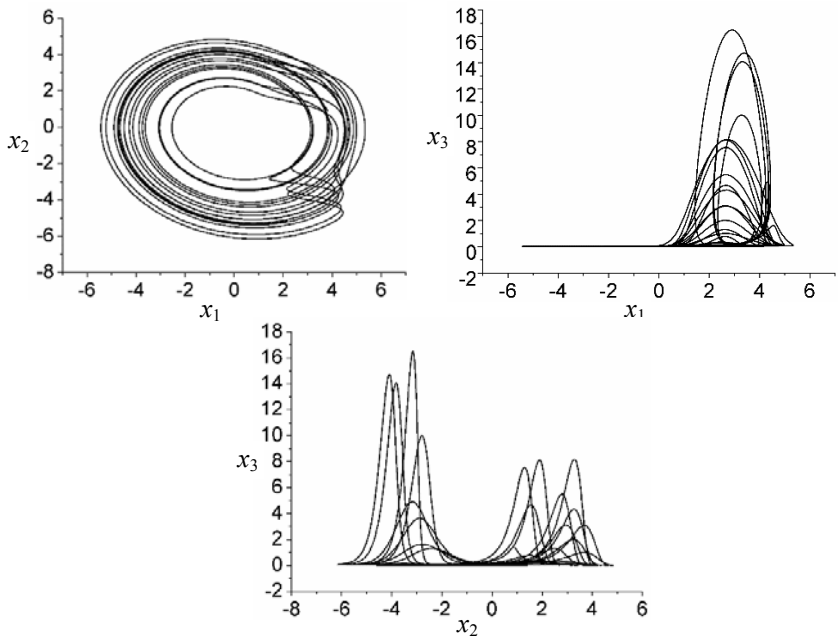

Fig. 2. Phase trajectories of system (7)

The solution to the formulated problem can be significantly simplified if it is possible to first estimate the period of external actions on the system. This possibility exists, for example, with resonance [25]. In this case, the period of external action can be estimated based on the period of oscillation of the observed variables. It is easy to show that for a chaotic system (7) such an approach will not lead to proper results. Considering that the external actions of this system are included in its third equation, then, first of all, these actions can affect the shape of the function $x_3(t)$. As a result, this function can become periodic. But, as follows from Fig. 1, this function has no periodicity. Also, the period of external actions cannot be estimated based on an analysis of the shape of the functions $x_1(t)$ and $x_2(t)$. For example, Fig. 3 shows the time series $x_2(t)$ and $v_{36}(t)$, where the latter is the variable component of the external action $c_{36}(t)$, $v_{36} = 2.5\sin(2\pi t/T - \pi/2)$. It is obvious that the quasi-period of a function $x_2(t)$ does not coincide with the period of $v_{36}(t)$ and is not a multiple. Therefore, we cannot preliminarily estimate the period of external actions and thus simplify the solution of the problem. Moreover, due to the lack of information about the existence of external periodic action, we may erroneously assume that the model has only constant coefficients. Such an initial assumption may lead to the construction of an inadequate model.

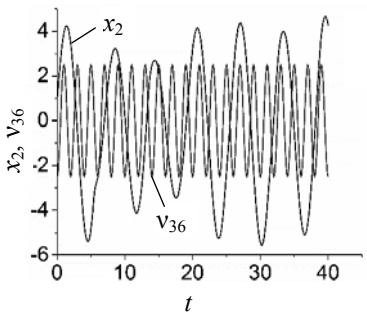

Fig. 3. Comparison of oscillation periods of functions $v_{36}(t)$ and $x_2(t)$

In general, the main steps of the first stage of the proposed algorithm in relation to equation (8) are as follows:

1. We set t_{01}, form the SLAE (2), and solve it by setting the values of τ within a certain range of $(\tau_b;\tau_e)$ which presumably includes the desired value of T. Thus, we obtain the values of all coefficients $c_{3j}(t)$.

2. Repeat step 1 for $t_{02} \neq t_{01}$.

3. For each coefficient $c_{3j}(t)$, we find a value τ at which

$$\delta_j = \sqrt{(c_{3j}^1 - c_{3j}^2)^2} \to \min, \tag{9}$$

where c_{3j}^1 and c_{3j}^2 represent the values of the coefficient $c_{3j}(t)$ obtained for t_{01} and t_{02}, respectively.

The calculations were carried out for $t_{01} = 0.15s$, $t_{02} = 0.4s$, $\tau_b = 1.0s$, $\tau_e = 11.5s$. The calculation results are shown in Table 1. The first line of Table 1 shows the τ values for which relation (9) is satisfied. Since the calculations involve discrete time series instead of continuous functions $x_i(t)$, there is a possibility of errors when calculating (9). Therefore, in order to obtain more complete information for analyzing the results, lines 2–5 of Table 1 show the τ values for which the δ_j value is closest to zero. As the line number increases, the δ_j value also increases.

Table 1. The first line shows the τ values at which δ_j takes on the least values

№	The τ values calculated for the coefficients of equation (8) at $\delta_j \to \min$									
	$c_{30}(t)$	$c_{31}(t)$	$c_{32}(t)$	$c_{33}(t)$	$c_{34}(t)$	$c_{35}(t)$	$c_{36}(t)$	$c_{37}(t)$	$c_{38}(t)$	$c_{39}(t)$
1	2.08	**8.44**	**2.11**	**8.44**	**8.44**	**2.11**	8.78	**2.11**	**8.44**	**2.11**
2	10.10	**2.11**	**8.44**	10.05	**2.11**	**8.44**	4.16	**8.44**	**2.11**	**8.44**
3	5.26	**4.22**	**10.55**	**10.55**	**4.22**	**10.55**	6.67	**4.22**	**10.55**	1.31
4	10.03	**10.55**	**4.22**	**2.11**	**10.55**	2.05	4.06	**10.55**	**6.33**	**4.22**
5	3.34	9.38	4.71	**4.22**	8.10	**4.22**	5.44	8.37	**4.22**	5.42

Based on the data presented in Table 1, the following conclusions can be drawn.

1. In the columns corresponding to the coefficients $c_{31}(t)$, $c_{32}(t)$, $c_{33}(t)$, $c_{34}(t)$, $c_{35}(t)$, $c_{37}(t)$, $c_{38}(t)$, $c_{39}(t)$, the predominant values are $\tau = 2.11s$ or multiples: $4.22s$, $6.33s$, $8.44s$ and $10.55s$ (these values are highlighted in bold in the table). Based on the corollary of the theorem, it can be argued that these coefficients are constant. Such regularity is not observed for the coefficients $c_{30}(t)$ and $c_{36}(t)$, suggesting that these coefficients are variable.

2. In addition, we can infer from the table that the search value for the period of external action is $T = 2.11s$, and consequently, $4.22s = 2T$, $6.33s = 3T$, $8.44s = 4T$, $10.55s = 5T$.

The values of the coefficients c_{3j}^1 and c_{3j}^2, which satisfy relation (9) and were used to fill the first line of Table 1, are indicated in Table 2. An examination of these values suggests that equation (8) has only one non-zero constant coefficient, c_{33}. The final conclusion can be reached after further analysis.

Table 2. Calculated values of the constant coefficients of equation (8)

t_0	Coefficients							
	c_{31}	c_{32}	c_{33}	c_{34}	c_{35}	c_{37}	c_{38}	c_{39}
$t_{01} = 0.15s$	$3.417*10^{-5}$	$5.070*10^{-5}$	-20.019	$2.399*10^{-6}$	$6.222*10^{-6}$	$3.682*10^{-7}$	$-9.514*10^{-4}$	$9.320*10^{-2}$
$t_{02} = 0.4s$	$-2.017*10^{-5}$	$-5.214*10^{-7}$	-20.022	$-1.450*10^{-6}$	$2.168*10^{-7}$	$2.094*10^{-7}$	$3.027*10^{-4}$	$4.599*10^{2}$

Moreover, it will be possible to answer the fourth point of the formulated problem, which is to determine the form of the functions $c_{30}(t)$ and $c_{36}(t)$. The second part of the algorithm is dedicated to solving this problem. With the already known value of T, the SLAE (2) is formed for t_0 varying within a certain range. By solving the SLAE at all points within this range, we can evaluate the values of all coefficients (both constant and variable) at these specific time intervals. The time series of certain coefficients, obtained from the calculation for $10\ s \le t_0 \le 30\ s$, are shown in Fig. 4. In the graphs, the calculated values of the coefficients are indicated by $c_{30}^c, c_{31}^c, \ldots$ The graphs in this figure have singularities, i.e., some points where the values of c_{ij} differ significantly from neighboring points. This occurs because the matrix $\mathbf{A}$ formed for calculating the coefficients of c_{ij}, in this case, has a determinant $\det \mathbf{A} \to 0$.

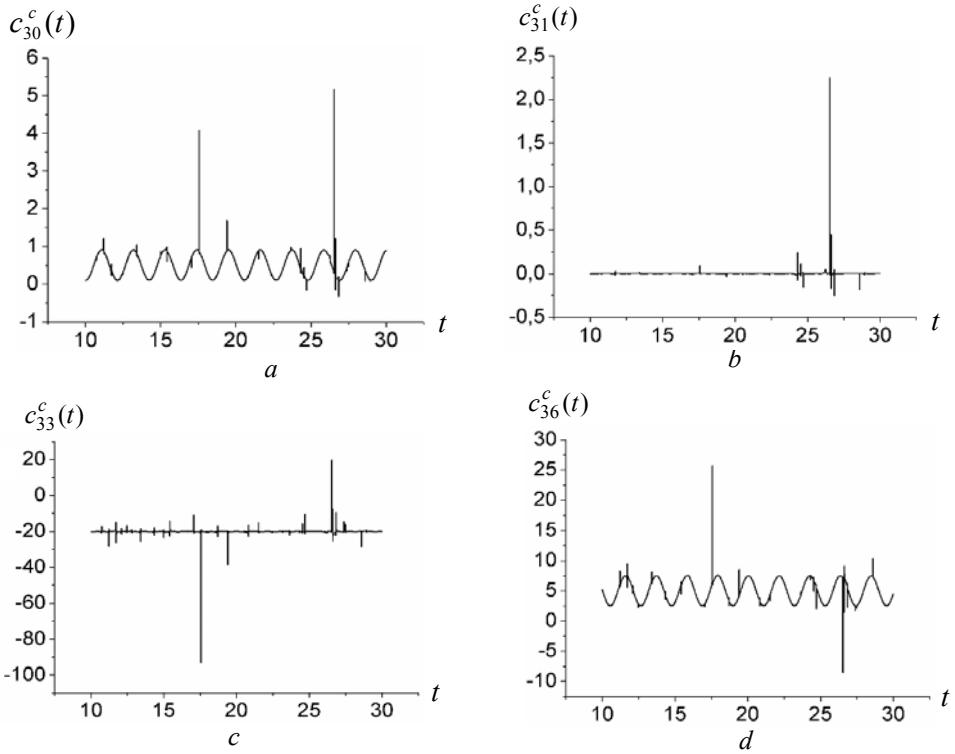

Fig. 4. Time series of $c_{30}^c(t)$, $c_{31}^c(t)$, $c_{33}^c(t)$, $c_{36}^c(t)$ obtained as a result of the calculation

We also note that, for example, in Fig. 4, *b*, $c_{31}^c \approx 0$ at points where the singularity does not occur. Here, graphs for some of the coefficients from Table 2 are not shown since all of them, except for $c_{33}(t)$, have a similar form to Fig. 4, *b*. That is, the values of these coefficients are close to zero. This fact confirms the preliminary assessment based on the data in Table 2, namely: $c_{31} = c_{32} = c_{34} = c_{35} = c_{37} = c_{38} = c_{39} = 0$.

Re-identification of equation (8) using non-zero coefficients $c_{30}(t)$, $c_{33}(t)$, $c_{36}(t)$ allowed us to obtain the time series, as shown in Fig. 5, *a*, *b*, *c*. Fig. 5, *d*

shows the original and identified time series of the $c_{30}(t)$ coefficient on the interval $21.2\,s \le t \le 22.2\,s$. This figure illustrates the proximity of these series, except for points with a singularity.

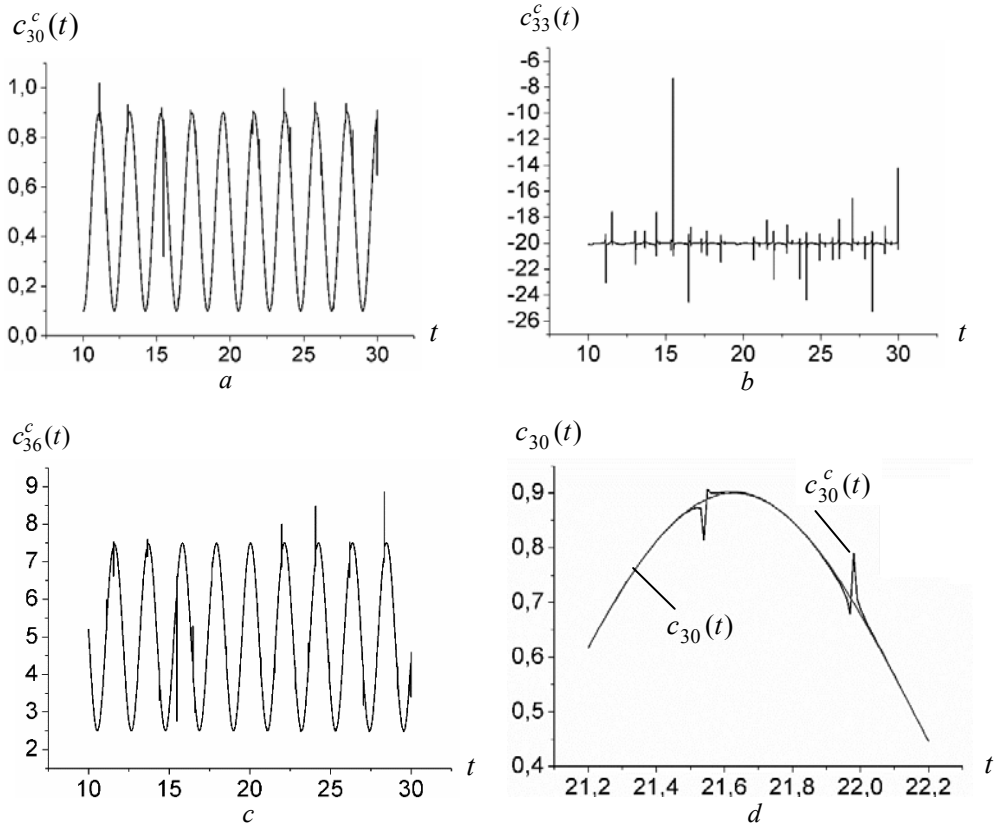

Fig. 5. Time series of calculated coefficients: a — $c_{30}^{c}(t)$; b — $c_{33}^{c}(t)$; c — $c_{36}^{c}(t)$; d — initial $c_{30}(t)$ and calculated $c_{30}^{c}(t)$ time series on the interval $21.2\,s \le t \le 22.2\,s$

Fig. 6 shows the time series of errors: $\Delta c_{30} = c_{30}^{c} - c_{30}$, $\Delta c_{33} = c_{33}^{c} - c_{33}$, $\Delta c_{36} = c_{36}^{c} - c_{36}$, which allows us to visually estimate the accuracy of identification.

SPECIAL CASE

As noted in the Method section, for a certain set of calculation parameters the result may be incorrect. This situation is possible when a periodic function $c_{ij}(t)$ has the period T and the following conditions are met

$$c_{ij}(t_{01}) = c_{ij}(t_{02}),\ \ |t_{01} - t_{02}| = \frac{T}{a},\ \ (a = 2,3,...). \qquad (10)$$

Let us illustrate the features of the algorithm application in this case with an example. Let the system (7) have the following parameters:

$$d = 0.15,\ c_{30}(t) = 1 + \sin\left(\frac{2\pi t}{T}\right),\ c_{33}(t) = -20,\ c_{36}(t) = 5,\ T = 2\,s. \qquad (11)$$

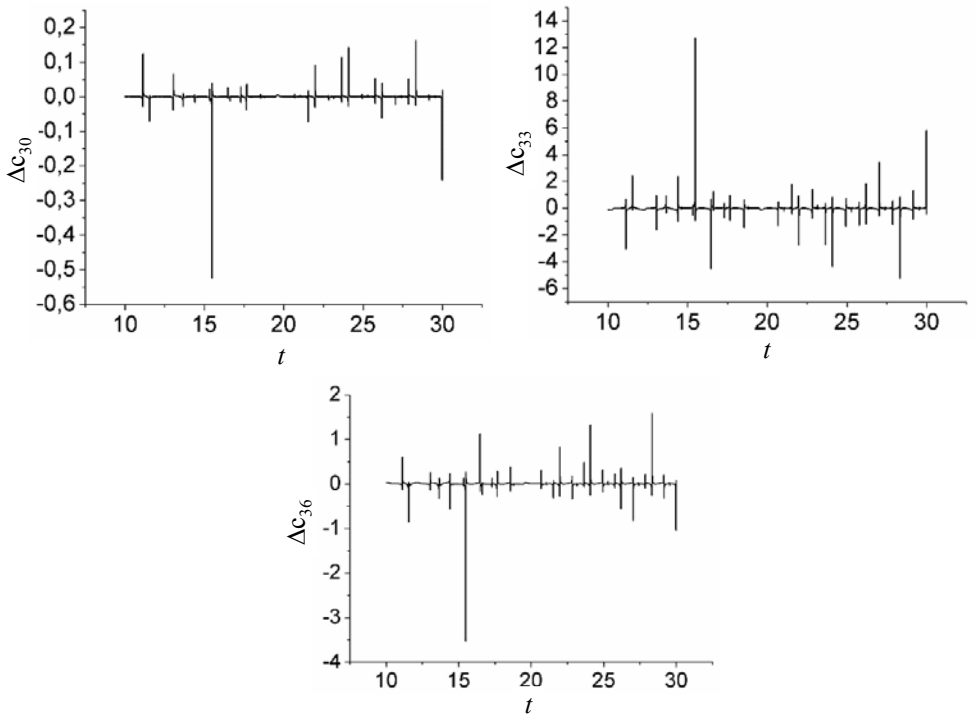

Fig. 6. Time series of errors

The system was solved over an interval of 100 s with a step size of $\Delta t = 0.01s$. Identification was carried out according to the algorithm described above for $t_{01} = 1s,\ t_{02} = 2s$. The input action graph is shown in Fig. 7. As follows from (11) and illustrated by the graph, the following relationships hold:

$$c_{30}(t_{01}) = c_{30}(t_{02}),\ \ |t_{01} - t_{02}| = \frac{T}{2} = 1s.$$

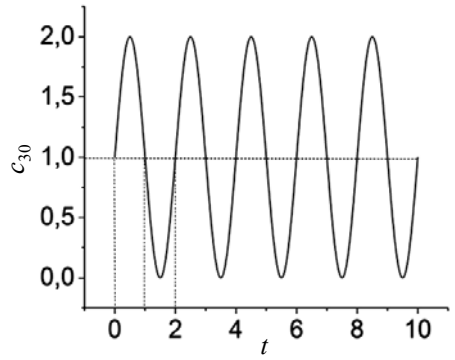

Fig. 7. Time series of external action in (11)

It can be noted that these relationships correspond to conditions (10). As a result of applying the algorithm, the data presented in Table 3 were obtained.

An analysis of these data similar to the analysis of Table 1 may lead us to incorrect conclusions.

1. Since all columns of Table 3 contain values $\tau = 1,2,...$, all the coefficients are constant.

2. We can also mistakenly assume that $T = 1s$, and the values $2s, 3s, ..., 10s$ are multiples.

Obviously, both of these conclusions are incorrect. But this result can be easily corrected by changing the calculation parameters of the algorithm to violate the conditions (10). In this case, the value $t_{02} = 2.01s$ was used instead of $t_{02} = 2s$. That is, the moment of time t_{02} was shifted by 1 step compared to the previous case. The calculation results are given in Table 4.

Table 3. The same as in Table 1 for system (7) with parameters (11)

№	The τ values calculated for the coefficients of equation (8) at $\delta_j \to \min$									
	$c_{30}(t)$	$c_{31}(t)$	$c_{32}(t)$	$c_{33}(t)$	$c_{34}(t)$	$c_{35}(t)$	$c_{36}(t)$	$c_{37}(t)$	$c_{38}(t)$	$c_{39}(t)$
1	**1.00**	**9.00**	**4.00**	**7.00**	**3.00**	**10.00**	6.07	**3.00**	**4.00**	**6.00**
2	**7.00**	**2.00**	**9.00**	**1.00**	**2.00**	**4.00**	**6.00**	**8.00**	**2.00**	5.72
3	**9.00**	**10.00**	**8.00**	**6.00**	**10.00**	**8.00**	**2.00**	**4.00**	**9.00**	5.64
4	**2.00**	**3.00**	**10.00**	**9.00**	**1.00**	**5.00**	**5.00**	**2.00**	**8.00**	5.99
5	**3.00**	**1.00**	**2.00**	**5.00**	**5.00**	**9.00**	**9.00**	**7.00**	3.42	**10.00**

Table 4. The same as in Table 3 with $t_{02} = 2.01s$

№	The τ values calculated for the coefficients of equation (8) at $\delta_j \to \min$									
	$c_{30}(t)$	$c_{31}(t)$	$c_{32}(t)$	$c_{33}(t)$	$c_{34}(t)$	$c_{35}(t)$	$c_{36}(t)$	$c_{37}(t)$	$c_{38}(t)$	$c_{39}(t)$
1	9.07	**10.00**	**4.00**	**6.00**	**2.00**	**10.00**	**2.00**	**8.00**	**4.00**	**6.00**
2	2.49	**2.00**	**10.00**	**2.00**	**10.00**	**4.00**	**6.00**	**4.00**	7.65	6.10
3	9.47	4.51	**8.00**	8.40	7.50	**8.00**	**8.00**	**2.00**	**2.00**	8.53
4	5.72	4.84	**2.00**	8.97	**8.00**	**2.00**	**4.00**	**10.00**	**8.00**	5.67
5	0.58	**8.00**	**6.00**	**8.00**	**4.00**	2.28	**10.00**	**6.00**	**10.00**	**10.00**

The data in Table 4 already allow us to draw the correct conclusions.

1. In the identified equation, the coefficient c_{30} is periodic, the other coefficients are constant.

2. The function $c_{30}(t)$ has a period $T = 2s$ and the values $4s, 6s, 8s, 10s$ are multiples.

It should be noted that in a real study, repeating the identification with changed t_{02} is not mandatory to obtain the correct result. It is sufficient to apply the last stage of the algorithm based on the data in Table 3, namely, to try to obtain the form of the input action with already known possible values of T. For this purpose, the SLAE (2) is formed taking into account the conditions (6) for t_0 varying within a certain range. By solving the SLAE at all points within this range, we can evaluate the values of c_{ij} coefficients for all these points. Thus, we obtain the function $c_{ij}(t)$.

On the contrary, when conditions (10) are met, the condition $c_{ij}(t_0) = c_{ij}(t_1) = ... = c_{ij}(t_m)$ is met only for specific t_0. If we choose $T = 1s$, then, for example, at $t_0 = 0s$ we will get according to (6) $t_1 = 1s$. As it is seen from Fig. 7, $c_{30}(0s) = c_{30}(1s)$. However, at $t_0 = 0.5s$ we will get $t_1 = 1.5s$ and $c_{30}(0.5s) \neq c_{30}(1.5s)$. Thus, we cannot construct a function $c_{ij}(t)$ for all t_0 within a given time interval.

This feature becomes apparent when we perform the second stage of the algorithm. Time series of all coefficients at $T = 1s$ were calculated. Two of them are shown in Fig. 8, *a* and 8, *b*. For comparison, Fig. 8, *c* and 8, *d* show the graphs obtained for the same functions, but at $T = 2s$. The choice of the correct T value when considering these four graphs is obvious.

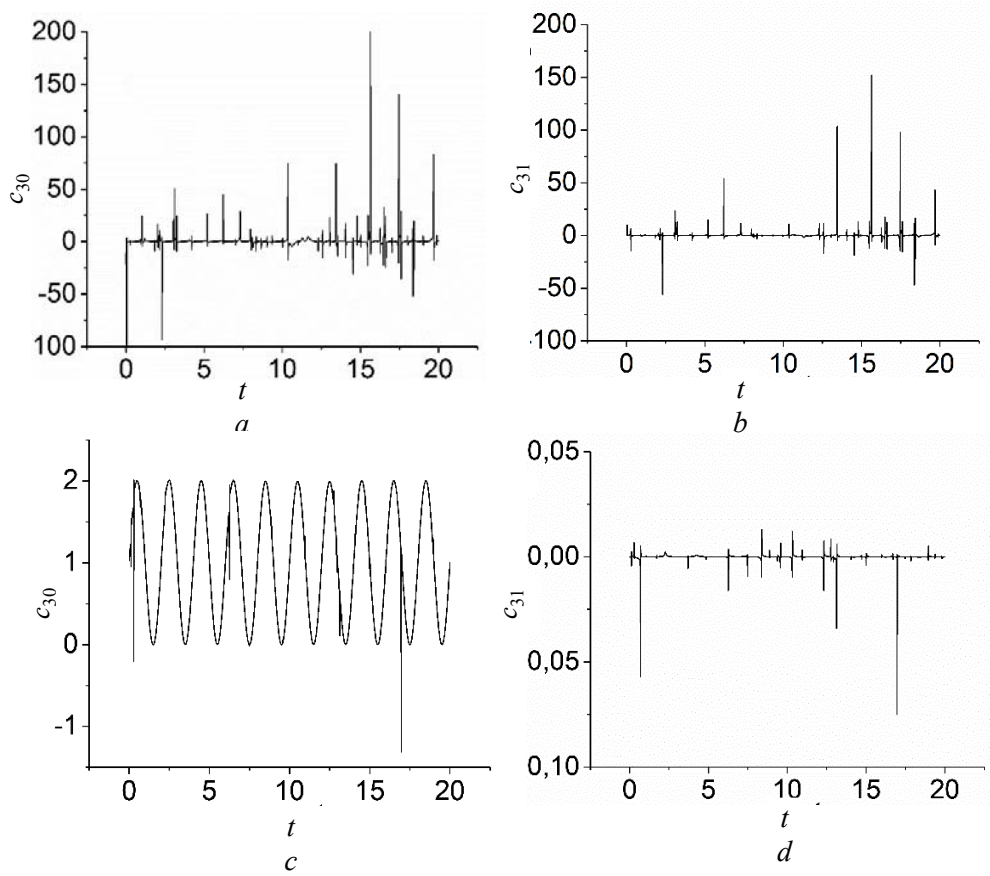

Fig. 8. Time series of calculated coefficients $c_{30}(t)$ and $c_{31}(t)$: *a* and *b* for $T = 1\ s$; *c* and *d* for $T = 2\ s$

CONCLUSIONS

The proven theorem and its corollary make it possible to solve the inverse problem with many unknowns. Such unknowns can be the number and values of constant ODE coefficients, the number, period and forms of external actions. The latter can be both additive and multiplicative. The number of external actions in each equation of the system is unlimited. The only restriction is that all the external actions in each equation must have the same period. The method allows us to detect unknown periodic actions that cannot be identified based on the form of observed variables.

To solve the formulated problem, it is not necessary to know in advance which coefficients in the ODE system's equations are variables, constants, or zeros. To use proposed method for solving formulated problem it is sufficiently to have time series of observed variables.

REFERENCES

1. T. Caraballo, X. Han, and P. Kloeden, "Chemostats with time-dependent inputs and wall growth," *Appl. Math. & Inf. Sci.*, vol. 9, no. 5, pp. 2283–2296, 2015. doi: 10.12785/amis/090509

2. Z. Zhang, S. Dey, and A. Singh, "Role of periodic forcing on the stochastic dynamics of a biomolecular clock," *European Control Conference (ECC)*, pp. 824–829, 2021. doi: 10.23919/ECC54610.2021.9654892
3. P.L. Gong, J.X. Xu, "Global dynamics and stochastic resonance of the forced Fitz-Hugh–Nagumo neuron model," *Phys. Rev. E*, vol. 63, article no. 031906, 2001. doi: 10.1103/PhysRevE.63.031906
4. J.P. Tripathi, V. Tiwari, and S. Abbas, "A non-autonomous ecological model with some applications,, in *Progress in Advanced Computing and Intelligent Engineering, Advances in Intelligent Systems and Computing*, vol. 714, pp. 557–563, 2018. doi: 10.1007/978-981-13-0224-4_50
5. M. Martcheva, "A non-autonomous multi-strain SIS epidemic model," *J. Biol. Dyn*., vol. 3, no. 2-3, pp. 235–251. doi: 10.1080/17513750802638712
6. J. Wang, H. Wang, and T. Wang, "External periodic force Control of a single-degree-of-freedom vibroimpact system," *J. Cont. Sci. Eng.*, vol. 2013, article no. 570137. doi: 10.1155/2013/570137
7. S. Zhou, G. Song, M. Sun, and Z. Ren, "Nonlinear dynamic analysis of a quarter vehicle system with external periodic excitation," *Int. J. Non-Lin. Mech.*, vol. 84, pp. 82–93, 2016. doi: 10.1016/j.ijnonlinmec.2016.04.014
8. Y. Ueda, "Randomly transitional phenomena in the system governed by Duffing's equation," *J. Stat. Phys.*, vol. 20, pp. 181–196, 1979. doi: 10.1007/BF01011512
9. M. Hasler, "Electrical circuit with chaotic behavior," *Proc. IEEE*, vol. 75, no. 8, pp. 1009–1021, 1987. doi: 10.1109/PROC.1987.13846
10. H.L. Smith, X.Q. Zhao, "Dynamics of a periodically pulsed bio-reactor model," *J. Diff. Equ*., vol. 155, pp. 368–404, 1999. doi: 10.1006/jdeq.1998.3587
11. X.N. Liu, L.S. Chen, "Global dynamics of the periodic logistic system with periodic impulsive perturbations," *J. Math. Anal. Appl.*, vol. 289, pp. 279–291, 2004. doi: 10.1016/j.jmaa.2003.09.058
12. P.E. Kloeden, M. Rasmussen, "Nonautonomous dynamical systems," *Mathematical Surveys and Monographs*, vol. 176. Providence, Rhode Island: American Mathematical Society, 2011. doi: 10.1090/surv/176
13. P.E. Kloeden, C. Potzsche, Nonautonomous dynamical systems in the life sciences," *Lecture Notes in Mathematics*, vol. 2102, pp. 3–39, 2013. doi: 10.1007/978-3-319-03080-7_1
14. A. Chithra, I.R. Mohamed, "Multiple attractors and strange nonchaotic dynamical behavior in a periodically forced system," *Nonl. Dyn.*, vol. 105, pp. 3615–3635, 2021. doi: 10.1007/s11071-021-06608-8
15. A. Tarantola, *Inverse problem theory and methods for model parameter estimation*. Philadelphia: Society for Industrial and Applied Mathematics, 2005. doi: 10.1137/1.9780898717921
16. R. Yoon R, H.S. Bhat, and B. Osting, "A non-autonomous equation discovery method for time signal classification," *SIAM J. Appl. Dyn. Sys.*, vol. 21, no. 1, pp. 33–59, 2022. doi: 10.1137/21M1405216
17. O. Schön, R.S. Götte, and J. Timmermann, "Multi-objective physics-guided recurrent neural networks for identifying non-autonomous dynamical systems," *IFAC-Papers-OnLine*, vol. 55(12), pp. 19–24, 2022. doi: 10.1016/j.ifacol.2022.07.282
18. M. Cenedese, J. Axås, B. Bäuerlein, K. Avila, and G. Haller, "Data-driven modeling and prediction of non-linearizable dynamics via spectral submanifolds," *Nature Commun*., vol. 13, article no. 872, 2022. doi: 10.1038/s41467-022-28518-y
19. T.S. Jang, H. Baek, H.S. Choi, and S.G. Lee, "A new method for measuring non-harmonic periodic excitation forces in nonlinear damped systems," *Mech. Syst. Sign. Proc*., vol. 25, no. 6, pp. 2219–2228, 2011. doi: 10.1016/j.ymssp.2011.01.012
20. B.P. Bezruchko, D.A. Smirnov, "Constructing nonautonomous differential equations from a time series," *Phys. Rev. E*, vol. 63, article no. 016207, 2001. doi: 10.1103/PhysRevE.63.016207

21. T. Sauer, “Observing periodically forced systems of difference equations,” *J. Difference Equ. Appl.*, vol. 16, no. 2–3, pp. 269–273, 2010. doi: 10.1080/10236190902870439
22. E. Glasner, B. Weiss, “Sensitive dependence on initial conditions,” *Nonlinearity*, vol. 6, no. 6, article no. 1067, 1993. doi: 10.1088/0951-7715/6/6/014
23. G. Strang, *Linear algebra and its applications*. New York, USA: Academic Press, 1976.
24. O.E. Rössler, “An equation for continuous chaos,” *Phys. Lett. A*, vol. 57, no. 5, pp. 397–398, 1976. doi: 10.1016/0375-9601(76)90101-8
25. M. Wang et al., “Fundamental limits and optimal estimation of the resonance frequency of a linear harmonic oscillator,” *Commun. Phys.*, vol. 4, article no. 207, 2021. doi: 10.1038/s42005-021-00700-6

Received 15.01.2024

INFORMATION ON THE ARTICLE

Viktor G. Gorodetskyi, ORCID: 0000-0003-4642-3060, National Technical University of Ukraine “Igor Sikorsky Kyiv Polytechnic Institute”, Ukraine, e-mail: v.gorodetskyi@ukr.net

ІДЕНТИФІКАЦІЯ НЕЛІНІЙНИХ СИСТЕМ З ПЕРІОДИЧНИМИ ЗОВНІШНІМИ ДІЯМИ (Частина I) / В.Г. Городецький

Анотація. Розглянуто проблему ідентифікації нелінійних систем з періодичними зовнішніми діями. Кількість таких дій у системі не обмежена, і ці дії можуть бути як адитивними, так і мультиплікативними. Для обчислення невідомих коефіцієнтів рівнянь використано часові ряди спостережуваних змінних системи. Доведена теорема дозволяє розділити невідомі коефіцієнти системи на змінні та сталі. Запропонована обчислювальна процедура дозволяє уникнути можливих помилок, спричинених дискретністю спостережуваних часових рядів. Ідентифікацію нульових коефіцієнтів виконано двома способами, що виключає помилкове обнулення членів рівнянь. Метод ілюстровано числовим прикладом ідентифікації хаотичної системи з періодичними зовнішніми діями.

Ключові слова: ідентифікація, звичайне диференціальне рівняння, зовнішня дія, періодичний коефіцієнт, сталий коефіцієнт.

UDC 519.652
DOI: 10.20535/SRIT.2308-8893.2024.3.07

FAIRNESS OF 2D COROTATIONAL BEAM SPLINE AS COMPARED WITH GEOMETRICALLY NONLINEAR ELASTIC BEAM

I. ORYNYAK, P. YABLONSKYI, D. KOLTSOV, O. CHERTOV, R. MAZURYK

Abstract. The goal of this paper is to further investigate the properties and advantages of corotational beam spline, CBS, as suggested recently. Emphasis is placed on the relatively simple task of drawing the spline between two endpoints with prescribed tangents. In the capacity of "goodness" of spline, the well-known notion of "fairness" is chosen, which presents itself as the integral from the squared curvature of spline over its length and originates from the elastic beam theory as the minimum of energy of deformation. The comparison is performed with possible variants of the cubic Bezier curve, BC, and geometrically nonlinear beam, GNB, with varying lengths. It was shown that CBS was much more effective than BC, where any attempt to provide better fairness of BC by varying the distances from endpoints to two intermediate points generally leads to lower fairness results than CBS. On the other hand, GNB, or in other words, the elastica curve, can give slightly better values of fairness for optimal lengths of the inserted beam. It can be explained by the more sophisticated scientific background of GNB, which employs 6 degrees of freedom in each section, compared with CBS, which operates only by 4 DoF.

Keywords: corotational beam spline, geometrically nonlinear beam, 2D, Bezier curve, fairness, transfer matrix method.

INTRODUCTION

In this paper we analyze the aesthetical quality, or in other words the fairness of the newly proposed Corotational Beam Spline, CBS [1]. For a few examples, we will also compare the CBS results with those obtained by an accurate Geometrically Nonlinear Beam, GNB, approach [2]. It is done intentionally because sometimes there is confusion as to the difference between the real beam and the beam splines. For the case of small displacements, both approaches are the same – we mean cases of explicit presentation $y = y(x)$, where for example, y is the vertical coordinate of the point, and x is the horizontal one. Yet in the case of large displacements GNB operates by 6 parameters and presents itself as the solution of the differential equation of the 6th order, whereas the explicit beam spline is always the solution of the 4th order equation.

Historically, the beams have generated splines both as technical tools initially, and later as the mathematical model [3]. For many years, starting from early AD Roman times the elastic beams (long and thin strips of wood) have been used by draftsmen to fair in a smooth curve between specified points for shipbuilding [4]. Mathematical cubic spline approximation in its present form was suggested in 1957 by Holladay [5]. He noted that for curves with modest slopes,

the cubic spline became identical to the bending of a straight beam. The latter operates by four degrees of freedom – displacement, angle of rotation (first derivative), bending moment (second one), and transverse force (third one). To apply the beam spline the positions of consecutive points should be known and one additional boundary condition should be specified at each end. The beam spine is called the natural one if the second derivative is taken as zero. In beam theory, this corresponds to simply supported end, when displacement is fixed, and moment is zero.

The language and technique of the beam theory were fruitfully employed later. Mention only a few ideas. First of all, in analogy to beam the different end conditions can be considered [3; 6]. They are: free end conditions, when second and third derivatives (moment and force) are equal to zero and the position is unknown; the clamped one, when the position and angle (first derivative) are prescribed; zero force condition (third derivative is additionally equal to zero). Another finding of the beam theory is the employment of the tensed beam model to use in beam spline – this is to make the spline straighter [7] at the expense of increased curvature at the prescribed positions (control points). Instead of the 3rd-order polynomial the 1st-order polynomial and two exponential functions, $\exp(\pm kx)$, are used, where coefficient k is proportional to the square root of the prescribed axial force (used in addition to the usual transversal one) [8]. Note, that if $k \to 0$ we get the usual beam spline. Also note, that 4 parameters tensed beam model is a simplification of 6 parameters planar beam problem (analog of the elastica).

Mention some additional beam features suggested during the "golden age" of the beam domination in the spline development. Very effective is the application of the beam on the elastic support model instead of the usual rigid ones, where the curve was suspended by springs attached to its control points for smoothing the errors of measurements [9]. The spring stiffness controls how closely the beam interpolates these points [10]. Asker [11] introduces several approaches to overcome wiggles [12]. The variable beam stiffness is in a piecewise constant fashion and in a piecewise linear fashion, which allows to change locally the spline behavior while keeping the same control points. As noted in [12] these methods are equivalent to the weighted spline of Salkauskas [13].

The main drawback of 'classical' beam splines is that they are suitable only for interpolation to plane curves, which turn through an angle of less than 180° [14]. The reason is the explicit presentation of the form $y = f(x)$, which is axis dependent and is not able to represent multiple-valued functions, and cannot be used where a constraint involves an infinite derivative [15].

So, generally, for any geometry, the implicit representations of the form $f(x, y) = 0$, and parametrical representation of the form $y = f(t)$ and $x = g(t)$, where t is an additional parameter, are used for curve splines [15]. As to beam splines in particular, Ferguson [16] introduces the parametric cubic spline curve by applying the cubic spline function for each coordinate by employing the independent curve parameter t, by prescribing for each consequent vector point (x, y) the non-decreasing value of parameter t. Their drawback is in the arbitrariness of the parameter t, the choice of which leads to different configurations [17], especially in smoothing the sharp corners [18], or in general, in case of large curvature [19]. Of course, it can be 'repaired' by imposing the additional re-

quirement to transverse force (third derivative), by changing the positions of corner points [18], but it implies additional complications. So, the parametric beam spline is rarely used nowadays.

Very popular now are splines based on Bezier curves, B-splines, and NURBS [15]. Their peculiarities are that they are formed by special polynomial or rational functions, and the sum of them in each control point is equal to 1. Other kinds of curves are used very often, too [19; 20]. Nevertheless, despite of present less usability, the cubic beam splines have tremendous historical significance and a large impact on the development of the spline theory. We can formulate, at least, three of their salient contributions.

1. The quantitative notion of the curve aesthetic measure or 'fairness'. The number of curves passing through a set of points is infinite, thus the interpolation problem is by nature ill-posed [21]. So convenient criteria for the best curve must be formulated. Of course, the notion of a fair curve appeared long before the origin of cubic beam spline, and various qualitative formulations were abundantly employed in literature [12; 21]. However, the first mathematically exact definition was based on the analogy with the elastic beam theory, where the energy of deformation E is given by expression [5; 8]:

$$E = \int_0^L \kappa^2(l)dl \,, \tag{1}$$

where κ is the curvature, l is an element of length, and L is the length. So, the curve is deemed to be the best, if it provides the minimum of energy E. In the context of CAD, this integral becomes one of the standard criteria for the fairness of a planar spline curve [22]. Note, that cubic splines give the minimum energy only in case of small deflections.

The expression (1) for the energy E very often is supplemented by other components, which also have the 'beam' origin. For example, for a 3D beam, it is common to introduce the 'stretch' energy, which is proportional to the 'elongation' of the beam and is the integral from the squared first derivative, or the 'twist' energy, which is found as the integral from the squared third derivative (rotation of the beam) [23]. For approximation spline, the control points are often considered as the springs [10], and the extension or compression of which makes the additional contribution to the elastic energy. So, an additional term for each "spring' (control) point is considered, which is proportional to the squared difference between the position of the spring and smoothened points [24]. Such curves are named minimal energy curves, MEC, [12].

Of course, the beam-based energy criteria are not unique mathematical formulations for defining the best curve. Other formulations are widely used, too, but they were either inspired by the energy criteria analogy or emerged as a result of the drawback of MEC for the best curve construction. Explain this. When the length of the spline is not restricted, the best MEC (mathematically) may be attained for the spline of infinite length and minimal curvature [25].

So, in general, MEC does not correspond to the common requirement of Farin [26], that a curve's curvature plot must be almost piecewise linear, continuous, and with only a small number of segments. So, a different functional, which satisfies Farin's criteria, the so-called minimum variation curve, MVC, was proposed in [12]. Instead of $\kappa^2(l)$ in functional (1) the square of the derivative of

curvature $\left(\frac{d\kappa(l)}{dl}\right)^2$ is used. In contrast to the MEC which bends as *little* as possible, the MVC bends as uniformly or as smoothly as possible [12]. Yet the MVC has no clear physical sense, it is not as flexible as the MEC to account for other constraints, for example, for the required proximity to the control points at approximation.

So, the MEC are still widely used in the usual continuous [22] or discrete form [27], where the energy is accounted for integrally in the control points as the sum of squared angular misalignments. The minimization of functional can give an aesthetically pleasant curve, which is stable for relatively slowly changing angles between neighboring control points. Very often the energy minimization is applied as a polishing tool for curves, which are derived by other kinds of splines. For example, in many works, energy minimization is applied to Bezier curves [28; 29], cubic spline curves [30], biarck splines [31], B-splines [32], for Hermite splines [33], and many others.

2. Development of the technique of construction of *elastica* and promotion of its popularity. The notion of elastica originated at the end of the 17th century due to the efforts of the Bernoulli brothers [34]. The elastica is the free-form deformation of the elastic beam, whose shape is such that its squared curvature (1) was minimized. It was an interesting mathematical task, and many famous scientists contributed to its solution and application to different problems, to mention only Euler, Laplace, Kirchhoff, Max Born, Love, etc [34].

The practical resurrection of interest in elastica originated in the works of Schoenberg [34] in 1946, where the spline was defined as a variational problem that minimizes the functional (1) but makes the small-deflection approximation. The basic shortcoming of the works of Schoenberg and Holliday [34] was underlined by Birkhoff and de Boor in 1965 [35], where it was noted that linearized interpolation schemes are not invariant under rigid rotation. So, they suggested replacing linearized spline curves with non-linear splines (or "elastica"). Furthermore, they obtained the differential equation for curvature functions $\kappa(l)$, which satisfy to minimum energy requirement (1):

$$\ddot{\kappa}(l) + \frac{1}{2}\kappa^3 = 0 . \qquad (2)$$

This curve was treated as a free elastic curve as it refers to a planar elastic curve without length constraints. This result was extended in work [36], where it was shown that equation (2) can be applied for segmented curvature function with natural end conditions that pass through a prescribed set of control points. Other generalization of these results consists in the justification of the validity of equation (2) when the end conditions are given in the form of prescribed tangents [37].

Based on these general results the various algorithms of elastica construction were proposed. The first work on the numerical construction of elastica was proposed by Glass in [38], where the discrete points on the curve were specified iteratively. Technically this algorithm was later improved by Malcolm [39]. Mehlum [40] used circular arc approximation of arbitrary precision. Mehlum uses these methods in the Autokon system for curve and surface design, which became the first commercial CAD software, and underlined the tight relation between

free-form shape representations and physically inspired mathematical functions [41]. Another technique of nonlinear spline construction was suggested in [22], where the looking for function is presented as a piecewise polynomial curvature function.

Among the many early works on nonlinear elastica, we see the work of Horn [42], where it was carefully studied a specific MEC segment, defined by two points on a baseline with a vertical tangent constraint specified at each point. The approach consists of a presentation of the looking-for curve as a set of circular arcs with a minimization of energy. Starting from one arc, then two or more arcs up to sixty-four were considered, while the resulting curve resembles a croquet hoop. The resulting energy was as small as 0.913953% of the semicircle. Then the elliptical curve with minimal energy was constructed and energy was equal to 93.42% of the semicircle, and for the Cornu spiral the energy was as low as 0.9178%. Then Horn computes closed-form expressions for the energy, arc length, and maximum curvature of his subject curve and the lowest value is equal to 0.913893. MEC has at least two principal shortcomings: the first cause it to fail a very desirable property for splines such as roundness [21], and another one, is that energy depends on an unspecified length of elastica. So, in the works of Kallay [43; 44] the theoretical substantiation and numerical method are elaborated for computing that shape, given the positions and directions of the endpoints and the total length. In this case, the notion of energy and the goal of optimization become clearer and are related to the fixed length. In work [45] the elastica is constructed by the elastic curve segments which are expressed in a closed form via the elliptic functions. The method depends on the good initial guess for the approximating curve with subsequent application of gradient-driven optimization.

On the other hand, the analytical solution for Euler's Elastica motivated within the structural mechanical community the development and application of one-dimensional theories for the deformation of elastic slender bodies [46] and especially the elaboration of the comprehensive and efficient numerical formulation [47]. Geometrically nonlinear computational models of the beam under finite rotation are obtained from three basic approaches: total Lagrangian, updated Lagrangian, and Co-rotational [47]. It is beyond the goal of the paper to discern them in detail.

We only mention that technically they often are reduced to solution by the transfer matrix method, TMM, either within the Lagrangian approach [48] or in the corotational formulation [49]. The transfer matrix, which relates the set of governing parameters at any point of the element including its end with those at the beginning of the element, is called the field transfer matrix, FTM. It is derived by the solution of physical differential equations. The continuity relations between the parameters of two neighboring elements at the border between them are given by the point transfer matrix, PTM. Sometimes the method is called in literature as a method of initial parameters [50]. The transfer matrix method is a very effective tool, which allows to eliminate the intermediate unknowns of inner elements, thus while keeping a large number of degrees of freedom, technically it reduces the ultimate matrix to the size determined only by the number of real points [51].

3. Employment of local coordinates system for each element. In structural mechanics, this approach is called a corotational approach [52; 53]. Here, the total

configuration of a beam is presented as the sum of two components: straight elements position and pure deformational displacement of points. The deformation is measured from a rotating frame attached to the straight element, and linearized formulation solutions are employed in the numeric incremental procedure. The nonlinearity is accounted for by the rotation matrix between the elements. So, the discontinuous angles of rotation between elements are the key parameters of the corotational scheme. Note that the geometrically nonlinear beam model of work [2] is the enhanced corotational approach, where the reference geometry is part of a circle and already contains build-in deformation (basic solution), which is supplemented by smoothing solution derived by integration of governing linear differential equations written in curvilinear (polar) coordinates.

Within the computer graphics world, the looking for curves are usually presented as continuous ones at every stage (iteration) of computation. The only known exception is the Fowler–Wilson method [54], which was based on usual cubic beam splines in a local two-dimensional coordinate system. The Fowler-Wilson scheme is a transition from the explicit presentation of spline $y = f(x)$ to the implicit one $g(x, y) = 0$. It was very popular till the beginning of the 21st century and was used in many industries around the world [55]. So, initially, the spline is given by a set of straight sections, which determine the tangent vector and normal vector. Local sections of the spline are calculated along the normal to the section. The main requirement is to provide the continuity of slope and curvature at the borders between points. The nonlinear equations of continuity are obtained and iteratively solved.

Now return to the goal of this paper. The corotational beam spline of our work [1], among other ideas, uses the idea of straight initial sections drawn between control points, which determine the local system of coordinates. So, the purpose of splines is to smooth out the so-called misalignment (gap) angles. This resembles the idea of Fowler–Wilson. As to the task of interpolation, the main differences in our work [1] consist of two peculiarities. First, from the very beginning, our spline is constructed in a linearized statement, which is usual for the theory of beam:

$$\operatorname{tg}\theta \approx \sin\theta \approx \theta\,, \tag{3}$$

where θ is the calculated angle of rotation, this noticeably simplifies the calculations [56; 57]. Second, to suppress the errors induced by (3) we introduce the notion of auxiliary ‘imaginary’ points. So, we consider that control points are of two kinds. Points of the first kind are of the real kind, where the outer constraints are explicitly given. Points of the second kind are imaginary ones, which are arbitrarily placed between the real ones, their positions are not specified and naturally refined during the calculation process. They are intended to: a) make the length of the straight section approximately equal to the length of the spline section; b) decrease the maximal calculated angle θ within each section to provide better accuracy of (3). Another enhancement of the method is of technical significance and consists of the employment of the transfer matrix method, which allows keeping the resulting matrix for spline with imaginary points of the same dimension as without them. Besides, the geometrically exact definition of curvature is used.

The goal of the paper is to analyze the aesthetical quality or energy (1) of the CBS and compare it with GNB for example a simple task defined by two end-

points with a tangent constraint specified at each point. This choice is taken because: 1) similar tasks were considered in old theoretical investigations of elastica [42; 44]; 2) the fairness of such curve can be easily assessed visually; 3) it is a practical task for thin deformable wire held at each end by a robotic gripper [58] and for applications of robotic hot-blade cutting [45; 59].

THEORETICAL FOUNDATION OF CBS AND GNB

Short introduction to CBS

Note, that very simplified logic, designations, and equations of more general paper [60] are outlined here. The main reason for simplification is that here we consider only the task of interpolation, so many enhancements related to consistency with the task of approximation will be omitted. Note, that the solution process is organized according to the transfer matrix method, TMM, methodology.

Let we have enumerated consequently both the exactly measured (real) points and the inserted between them (in any number) imaginary points, $A_m(X_m, Y_m)$, where m is the point number, and X_m, Y_m are their Cartesian coordinates in the absolute coordinate system. Usually, we do not discern between them and name them as the control points, because referring to the transfer matrix method, TMM, the field transfer matrix, FTM, is the same for any element placed between any two neighboring points. The difference exists only for the point transfer matrix, PTM, and depends on whether the considered point is a real or imaginary one. So, in this case, the points will be discerned by using the additional lower indexes: *"r"* for real points, and "*i*" for imaginary ones. For example, $A_{m,r}$ means that point A_m is the real, and $A_{m,i}$ is the imaginary one.

Connect the consequent points A_m by straight lines and get the open or closed polygon. Consider the particular straight beam section, named as m section, which is placed between control points A_{m+1} and A_m, Fig 1. Introduce the notion of iteration number, k. The real points retain the same position at each iteration; however, the imaginary points change their position. Furthermore, the algorithm envisages that new imaginary points might be inserted during the iteration process. This is controlled by the maximal value of calculated angle θ, as to condition (3). If the angle is large enough, say, larger than $\frac{\pi}{30}$, we insert a new imaginary point. This provides the accuracy as to (3) within 0.2%. So, the insertion of a new imaginary point may change the general enumeration. Thus, the numeration is iteration dependent, and control points should be presented as $A_m^k(X_m^k, Y_m^k)$, where k is the iteration number. Nevertheless, in most cases, the upper index k will be omitted.

The vectorial length of each beam section is designated as $\vec{l}_m$:

$$\vec{l}_m = \vec{A}_{m+1} - \vec{A}_m = (X_{m+1} - X_m)\vec{i} + (Y_{m+1} - Y_m)\vec{j}\,. \qquad (4)$$

For each straight section introduce the local coordinate system (s_m, w_m) and basic vectors $\vec{t}_m$ and $\vec{n}_m$. The tangent local vector $\vec{t}_n$, is derived from (4):

$$\vec{t}_m = \frac{\vec{l}_m}{\left|\vec{l}_m\right|} = a_m\vec{i} + b_m\vec{j},$$

where

$$\left|\vec{l}_m\right| = l_m = \sqrt{(X_{m+1} - X_m)^2 + (Y_{m+1} - Y_m)^2}.$$

The normal vector $\vec{n}_m$ is perpendicular to $\vec{t}_m$ and rotated clockwise concerning it, Fig 1. Local coordinate system (s, w) is related to the basic vectors, where s is counted from $\vec{A}_m$ in the direction of $\vec{t}$, and w is directed as $\vec{n}$. Vector $\vec{n}_m$ is presented as:

$$\vec{n}_m = c_m\vec{i} + d_m\vec{j},$$

where

$$\begin{pmatrix} c_m \\ d_m \end{pmatrix} = \begin{pmatrix} \cos(-\pi/2) & -\sin(-\pi/2) \\ \sin(-\pi/2) & \cos(-\pi/2) \end{pmatrix} \begin{pmatrix} a_m \\ b_m \end{pmatrix} = \begin{pmatrix} 0 & 1 \\ -1 & 0 \end{pmatrix} \begin{pmatrix} a_m \\ b_m \end{pmatrix}.$$

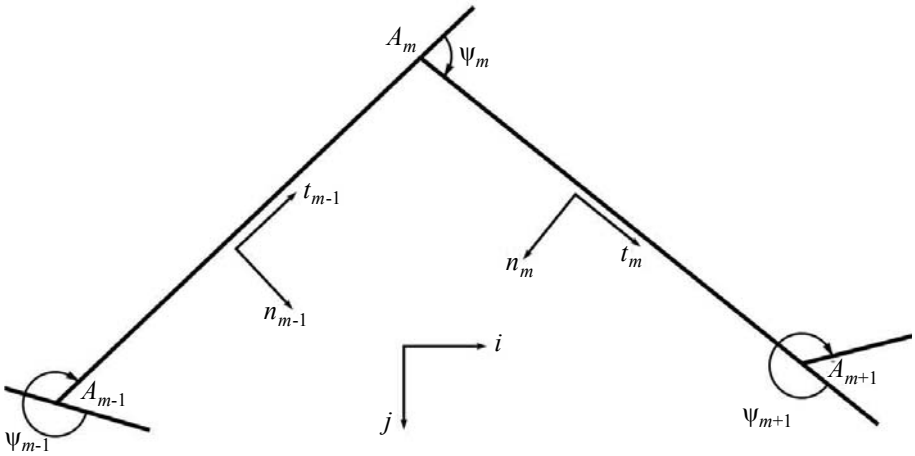

Fig. 1. The global cartesian vectors and local corotational basis for each element

Important in the model is the misalignment angle between two adjacent straight beam sections: m and $m-1$, denoted as ψ_m, Fig. 1. It is counted clockwise from vector $\vec{t}_{m-1}$ to vector $\vec{t}_m$. The angle of misalignment ψ_{m-1} is found from the scalar and vector products of these two vectors:

$$\sin(\psi_m) = \vec{t}_{m-1} * \vec{t}_m, \quad \cos(\psi_m) = \vec{t}_{m-1} \cdot \vec{t}_m. \tag{5}$$

Application of both rules is needed to establish the correct angle quadrant.

Now describe the calculation model. Consider the simplest beam model for an initially straight beam. Each straight beam section is characterized by the vector of state $\vec{Z}(s)$, which is formed by 4 scalar functions of length coordinate s:

$$\vec{Z}(s) = \text{column}\,\{W(s);\ \theta(s);\ M(s);\ Q(s)\},$$

where following the beam traditions we operate by four physical values: $W(s)$ is displacement directed along the local normal vector $\vec{n}$; $\theta(s)$ is the angle of (de-

formational) rotation of the beam axis concerning initial vector $\vec{t}$, directed clockwise; $M(s)$ is the bending moment; $Q(s)$ is the transverse force. The direction of the two latter parameters is chosen so, that the following differential dependencies between all parameters are positive [1]:

$$\frac{dW(s)}{ds} = \theta(s); \quad \frac{d\theta(s)}{ds} = \frac{M(s)}{EI}; \; \frac{dM(s)}{ds} = Q(s); \; \frac{dQ(s)}{ds} = 0, \tag{6}$$

where EI is the constant of the beam, taken below as 1. The solution of the system (6) can be presented in matrix form suitable for the application of TMM:

$$(\vec{Z}_m(s)) = [p_{i,j}(s)](\vec{Z}_{m,0}), \tag{7}$$

where $\vec{Z}_0 = \vec{Z}(s=0)$ is the vector of state in the initial point of the section considered, and the coefficients of the transfer matrix are the following:

$$[p_{l,j}(s)] = \begin{bmatrix} 1 & s & \frac{s^2}{2} & \frac{s^3}{6} \\ 0 & 1 & s & \frac{s^2}{2} \\ 0 & 0 & 1 & s \\ 0 & 0 & 0 & 1 \end{bmatrix}.$$

Note, that equations (7) can give the values of each parameter at the endpoint of each element through the initial parameters at this element by letting $s = l_m$, i.e.:

$$(\vec{Z}_m(l_m)) = (\vec{Z}_{m,1}) = [p_{i,j}(l_m)](\vec{Z}_{m,0}),$$

where lower indexes “0” and “1” mean the beginning and the end of a section, correspondently.

To formulate the calculation scheme, we need to supplement the FTM (7) with PTM equations, which relate the vector of state at the border between the end of the previous and the beginning of the next sections. For real control point, we have the following PTM relations:

$$W_{m,0} = W_{m-1,1}, \tag{8}$$

$$\theta_{m,0} = \theta_{m-1,1} - \psi_m, \tag{9}$$

$$M_{m,0} = M_{m-1,1}, \tag{10}$$

$$Q_{m,0} = Q_{m-1,1} + P_m, \tag{11}$$

$$W_{m,0} = 0. \tag{12}$$

Here P_m is an unknown force in the beam support (real control point). Generally speaking, this force is determined from condition (11), or put more correctly, the introduction of additional unknown P_m requires one additional condition (12). When compiling the system of governing the equation (11) (and unknown P_m) is not used. Condition (8) means that displacement (deviation of

position from the initial straight line) should be the same. Condition (9) is to provide the tangent continuity of the deformed contour, where the deformational angles compensate for the initial misalignment angle. Condition (10) is the equality of approximate beam curvatures. Condition (12) requires that the position of the considered control point should not change during the iteration, i.e., it is fixed.

The point transfer matrix in the case of the imaginary point is slightly different. They require continuity up to 3rd order, i.e., including the transverse force. So, we have:

$$W_{m,0} = W_{m-1,1},$$

$$\theta_{m,0} = \theta_{m-1,1} - \psi_m,$$

$$M_{m,0} = M_{m-1,1},$$

$$Q_{m,0} = Q_{m-1,1}.$$

Or in matrix form

$$(\vec{Z}_{m,0}) = [I](\vec{Z}_{m-1,1}) + \vec{C}_{m,i},$$

where $\vec{C}_i$:

$$\vec{C}_{m,i} = \text{column}\{0; -\psi_m; 0; 0\}.$$

In this case, the PTM does not contain any additional unknowns.

Let's go to the organization of the calculation process by TMM. It is convenient to start with an introduction of four unknown parameters for both the beginning and end of each element. It means we have 8 unknowns for each element. If the number of elements is M, then the number of unknowns is $8 \cdot M$. There are 4 FTM equations for each element, thus at the whole, there are $4 \cdot M$ FTM equations. On the other hand, there are $M-1$ borders between elements for open polygon, for which $4(M-1)$ PTM can be written. So, for an open polygon, $8 \cdot M - 4$ equations should be supplemented by 2+2 boundary conditions on each boundary. One of them is the condition of zero displacement, while another is either the requirement to the angle value, or requirement to curvature (moment), or to transverse force. When the contour (polygon) is closed we have no boundary conditions, but instead, one additional PTM (four conditions) is to be written at the point where the last section meets the first one.

At first glance, accounting for possibly a large number of imaginary points in this CBS technique requires too many unknowns and can be very slow. First, show that imaginary points and related unknowns actually can be removed from consideration. Consider two adjacent sections which are separated by imaginary points. According to the procedure of elimination [51] write three transfer matrixes between them:

$$(\vec{Z}_{m,1}) = [p_{i,j}(l_m)](\vec{Z}_{m,0}), \tag{13}$$

$$(\vec{Z}_{m+1,0}) = [I](\vec{Z}_{m,1}) + \vec{C}_{m,i}, \tag{14}$$

$$(\vec{Z}_{m+1,1}) = [p_{i,j}(l_{m+1})](\vec{Z}_{m+1,0}). \tag{15}$$

Substituting (14) into (15) and later (13) in the resulting equation we formally can get the matrix equation:

$$(\vec{Z}_{m+1,1}) = [p_{i,j}(l_{m+1}, l_m)](\vec{Z}_{m,1}) + \vec{D}_{m,i}, \tag{16}$$

where elements of matrix $p_{i,j}(l_{m+1}, l_m)$, and free terms vector $\vec{D}_{m,i}$ are easily calculated from (13)–(15). The matrix equation (16) is FTM for the combined element, which starts at the point $\vec{A}_m$ and ends at point $\vec{A}_{m+2}$, thus eliminating the imaginary point $\vec{A}_{m+1}$. So, two FTM and one PTM are substituted by one FTM. Second, for the remaining real points the number of unknowns can be reduced to unknown moments in them only, as it is usually given in the textbooks [8].

Note, that calculated values of Mc have dimension of curvature and the meaning of curvature in beam theory formulation. Yet they are not exact geometrical curvatures. So, the additional procedure of refining the values of curvature based on exact differential geometry formulation was established in [1] and will be used in the presentation of the results.

Main equations of GNB

The principal distinction of GNB from spline is that it operates by a real object with real properties and, especially it has a given length, L. In calculations, it is broken into a necessary number of elements. For each element, m, the notions of the Basic, $\vec{B}_m(s)$, and Smoothing, $\vec{S}_m(s)$, solutions are introduced [2; 61], where s is a curvilinear abscissa of any point of element. Then, the looking for Ultimate solution, $\vec{U}^k(s)$, is the sum of these two constituents:

$$\vec{U}^k = \vec{B}^{k-1} + \vec{S}^k. \tag{17}$$

Here the upper index k means the iteration number. So, as follows from presentation (17) the basic solution is a result of the previous iteration $i-1$. Note, that, where possible, the lower and upper indexes m and k will be omitted.

The main aim of the basic solution, BS, is to principally account for all nonlinearities, while the smoothing solution, SS, is a linearized analytical correction to BS. Another purpose of BS is that it gives the system of local curvilinear coordinates and directions concerning which the SS is derived. On the other hand, BS is permanently refined from iteration to iteration as a result of accounting for the present SS. New BS is refined according to the following rule:

$$\vec{B}^k = \vec{B}^{k-1} + g \cdot \vec{S}^k, \tag{18}$$

where g, $0 < g \le 1$ is the so-called retardation coefficient, which restricts the absolute change of BS and accounts for whether the process of solution is convergent (m can be increased) or divergent (m should be decreased). The rule (18) is schematic because not all components of SS are used in BS. For the 2D case, BS geometrically presents itself the part of a perfect circle, the radius of which R_m^k, (or curvature $\kappa_m^k = 1/R_m^k$) and current length l_m^k are related with basic (embedded in) bending moment and axial force [61].

SS solution is formulated for each element in the local curvilinear system of coordinates, Fig. 2. It operates by six governing parameters, as opposed to a

straight beam (cubic spline). They are: two force parameters – transverse force Q and axial force N, bending moment M, angle of rotation θ, and two displacement parameters — normal one w, and tangential one u. These parameters are related by six differential equations:

$$\frac{dQ}{Rd\phi}+\frac{N}{R}=P_n;\ \ \frac{dN}{Rd\phi}-\frac{Q}{R}=P_t;\ \ \frac{dM}{Rd\phi}=Q;$$

$$\frac{d\theta}{Rd\phi}=\frac{M}{EI};\ \ \frac{du}{Rd\phi}-\frac{w}{R}=-\frac{N}{EF};\ \ \frac{dw}{Rd\phi}+\frac{u}{R}=\theta.$$

In the subsequent application below we will not consider the action of outer distributed forces P_n and P_t, and neglect the axial elongation, i.e., take $\frac{1}{EF}=0$.

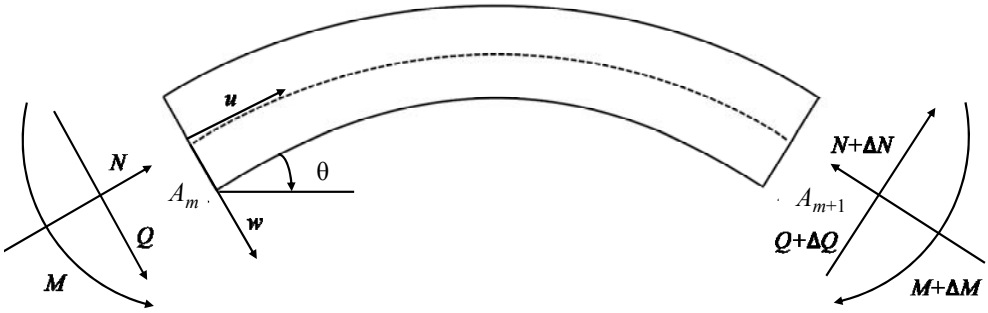

Fig. 2. General scheme of 2D curvilinear beam

The general solution of (5) for SS can be presented in the form suitable for the application of TMM [61], and schematically is given below. For FTM it can be written as [61]:

$$(\vec{Z}_m(s))=[p_{i,j}(s)](\vec{Z}_{m,0}),$$

where elements of matrix $p_{i,j}(s)$ are the solution of the differential equations (5), and the vector of state in any point s is:

$$\vec{Z}(s)=\text{column}\,\{w(s);u(s);\theta(s);M(s);Q(s),N(s)\}.$$

For PTM a similar equation can be written [61]:

$$(\vec{Z}_{m,0})=[H](\vec{Z}_{m-1,1})+\vec{C}_{m,i}.$$

In this case, the matrix $[H]$ is not an identity matrix, due to the vectorial essence of two force and two displacement parameters and different local vectorial basis used. As to the vector of free terms $\vec{C}_{m,i}$, its all components are nonzero due to the discontinuity of the basic solution (so-called gaps [61]). Note that the GNB approach requires three boundary conditions at each end of the beam.

The aim of this short introduction to GNB is twofold. First, to show that the technical solution of GNB can be similarly organized by TMM, with formal elimination of all points (sections) that do not contain the real constraints. Second, the variety of tools and possibilities of GNB analysis by numerical TMM is much richer than in the traditional elastica approach. Hint the few possible

opportunities. If one wants to make the solution "more tensed", it can be very easily done by introducing the normal pressure P_n. To "tense" or to "relax" the particular section it needs to increase or decrease the bending stiffness EI, or to make it variable. The length of particular sections or the beam as a whole can be controlled by axial stiffness EF.

Calculated curvatures in each curved section are presented as the sum of basic curvature (constant) and those induced by calculated bending moment $M_m^k(s)$:

$$\kappa_m^k(s) = \frac{1}{R_m^k} + \frac{M_m^k(s)}{EI}.$$

Four points-based Bezier spline

Consider set of four consequent control points $A_1(X_1,Y_1)$, $A_2(X_2,Y_2)$, $A_3(X_3,Y_3)$, $A_4(X_4,Y_4)$, or in vectorial form:

$$\vec{A}_m = X_m\vec{i} + Y_m\vec{j}; \quad m = 1,2,3,4.$$

They can be used for the construction of a third-order Bezier curve, $\vec{P}(x,y)$ [15]:

$$\vec{P}(x,y) = P_x\vec{i} + P_y\vec{j} = \vec{i}\cdot\sum_{m=1}^{4} X_m\cdot K_m(t) + \vec{j}\cdot\sum_{m=1}^{4} Y_m\cdot K_m(t); \quad 0\le t\le 1,$$

where $K_m(t)$ are the Bernstein's functions

$$K_1(t) = (1-t)^3, \quad K_2(t)(t) = 3t(1-t)^2, \quad K_3(t) = 3t^2(1-t), \quad K_4(t) = t^3.$$

Bezier splines have the following properties [15], important to our task:

1. The first and last points on the curve are coincident with the first and last points of the control polygon.

2. The tangent vectors at the ends of the curve have the same direction as the first and last polygon spans, respectively.

So, our subsequent task is to construct a spline, which starts in point $\vec{B}_1$ at the angle φ_1 with a horizontal axis and ends in point $\vec{B}_2$ directed at angle φ_2. Introduce the unitary tangent vectors $\vec{\eta}_1$ and $\vec{\eta}_2$ in these boundary points. They can be written as:

$$\vec{\eta}_1 = \vec{i}\cdot\cos\varphi_1 + \vec{j}\cdot\sin\varphi_1; \vec{\eta}_2 = \vec{i}\cdot\cos\varphi_2 + \vec{j}\cdot\sin\varphi_2.$$

So, four consequent points of cubic Bezier splines can be chosen as follows:

$$\vec{A}_1 = \vec{B}_1, \quad \vec{A}_4 = \vec{B}_2, \quad \vec{A}_2 - \vec{A}_1 = D_1\cdot\vec{\eta}_1; \quad \vec{A}_4 - \vec{A}_3 = D_2\cdot\vec{\eta}_2,$$

where D_1 is an absolute distance from point $\vec{A}_2$ to point $\vec{A}_1$, and D_2 from $\vec{A}_4$ to point $\vec{A}_3$.

Our next task is to obtain the element of length in each point, $ds(t)$, and the curvature $\kappa(t)$. According to differential geometry rules, we can write:

$$ds = \sqrt{(P_x')^2 + (P_y')^2}\,dt\,, \quad \kappa(t) = \frac{P_x'' P_y' - P_y'' P_x'}{\left(\sqrt{(P_x')^2 + (P_y')^2}\right)^3}\,.$$

These expressions will be used in the calculation of the Brazier spline quality.

EXAMPLES OF CALCULATION

Several similar problems will be calculated and compared here. In some cases, the well-known Bezier curve will be used too. We will consider the relatively simple task, which is defined by two endpoints with a tangent constraint specified at each endpoint.

Example task 1

First point B_1 is placed in point $(X = 0, Y = 0)$, second point B_2 has coordinates $(X = 150, Y = 0)$, the tangent in point B_1 is directed vertically, i.e., the angle (in the clockwise direction) with the horizontal axis is equal $-90°$, and in point B_2 the angle is equal to $90°$. It is the famous Horn task [42], which has demonstrated that minimization of energy is not always a solution for the best curve, and eventually led to the appearance of other criteria, say minimization of squared derivative from curvature [12].

Intuitively, the best curve is the semi-circle of diameter equal to 150. Its length, L_0 is $L_0 = \pi\frac{150}{2} = 235.62$. Calculate the quality (energy) of the ideal semi-circle. According to (1) it is equal to $E_0 = \left(\frac{2}{150}\right)^2 \frac{\pi 150}{2} \approx 0.041888$.

Construct the splines according to different techniques, Fig. 3. Designation BZ 110 relates to the Bezier spline, where two intermediate points on the prescribed tangent are placed at a distance of 110 from either endpoint. Similarly, the BZ 115.5 curve employs one point on distance 115.5 on each tangent. GNB depends on the prescribed length of the beam, so the designation GNB 230 means that the length of the beam is equal to 230. Many variants of BZ spline and GNB can be obtained. As to CBS, it gives only one possible configuration.

Analyze the results. First of all, note that CBS gives the ideal semi-circle. As to other curves, at first glance, they can approach the ideal figure very well, and each seemingly is capable of depicting the ideal circle.

With this respect, the more informative are graphs of curvature versus the length coordinate for each spline shown in Fig. 4. More definite conclusions can be drawn from it. First, note that CBS is indeed capable of giving the ideal circle. The wavy character of the graph is a reflection of an insufficient number of imaginary points — the more points, the smoother the curvature. Second, Bezier splines give noticeable deviation from the ideal circle for all parameters of optimization (distances from endpoints). Third, GNB is a very powerful technique, which depends on the chosen length of the beam. In case, when the prescribed length of GNB coincides with the length of the ideal circle, it actually gives this ideal circle.

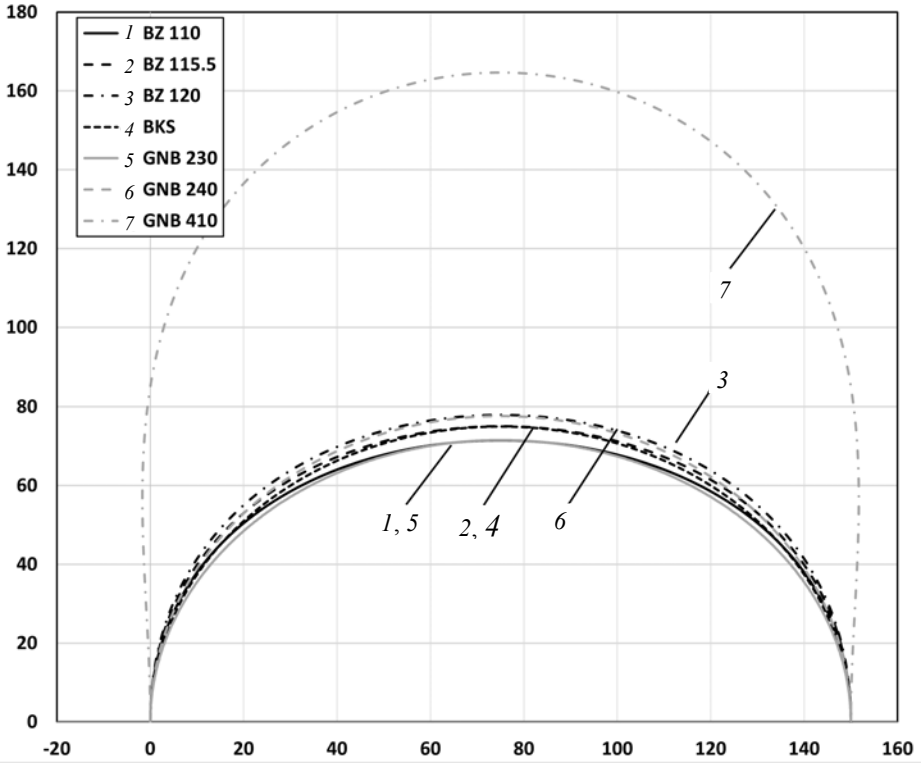

Fig. 3. Several calculated splines according to the Bezier method (4 points), BCS, and GNB

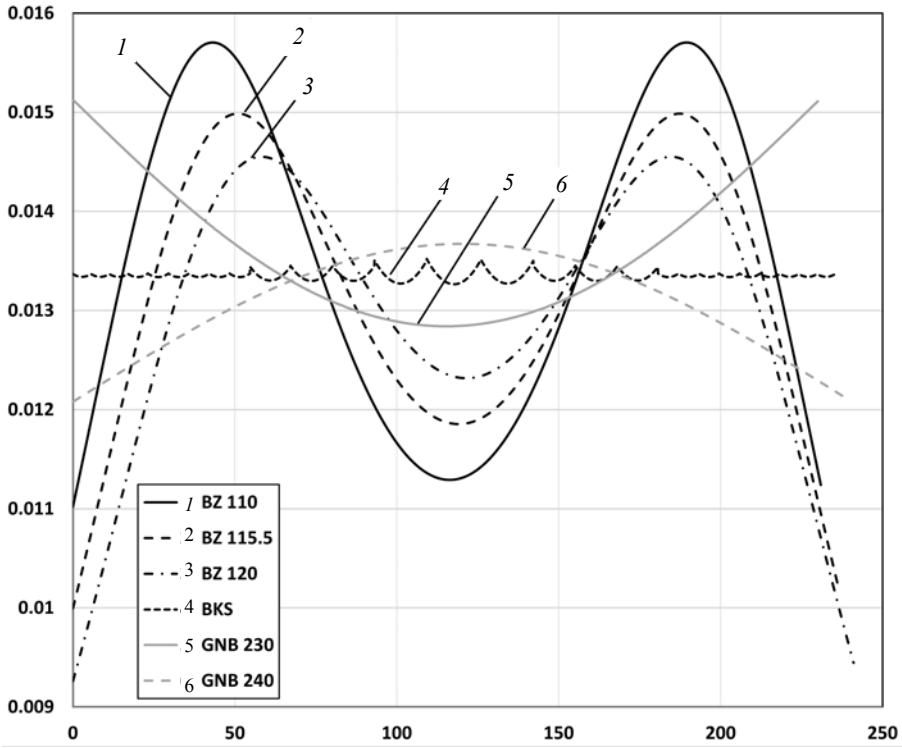

Fig. 4. The graphs of curvatures obtained by different splines for Task 1

Compare the quality (energy) of each depicted curve. The results of its calculation are given in Table 1, where the absolute value of energy, as well as the reduced value of it (divided by the ideal semi-circle value of 0.41888), are presented. The result for CBS is slightly different from the ideal circle due to a smaller number of imaginary points (only 28 points are employed here). As to Bezier's results, they are close to 1 in the considered range of chosen distances of additional points, and the lowest result is attained for the BZ 120 curve.

Table 1. Calculated energies for different splines for Task 1

Curve	BZ 110	BZ 115.5	BZ 120	BCS	GNB 230	GNB 240	GNB 410
Quality	0.04305	0.04190	0.04113	0.04190	0.043024	0.041181	0.037927
Reduced quality	1.02774	1.0003	0.9818	1.0003	1.04475	0.98312	0.90544

Evidently, the notion of energy cannot be the sole criterion of fairness. Note, that splines, which "embrace" the ideal semi-circle give the lesser values of energy. Concerning the results of Table 1 it is interesting to recall the results of Horn [42]. Remind that for this task 1 the "best" value of energy equal to 0.91383 was obtained [42]. So, plot the graph of the energy concerning beam length by GNB approach, Fig. 5. Interesting to note, that in the vicinity of the ideal semi-circle configuration ($L = L_0 = 235.6$) the quality of the curve linearly decreases with length. Yet in the range of length $310 < L < 340$, it attends the local "plateau". The calculated quality in this range is approximately equal to 0.03828 (at $L = 320$). Dividing this value by 0.041888 (ideal semi-circle) we get the reduced value equal to 0.9138, which is very close to Horn's theoretical value. This testifies to the high efficiency of the GNB approach [2]. Further increase of L beyond this range leads to a permanent slow decrease of energy, which was not predicted in Horn analysis [42]. This is related to the outward deviation of the calculated figure from the vertical lines $x = 0$ and $x = 150$, which is evident from Fig. 3 for GNB 410. For $L \to \infty$ the energy tends to zero.

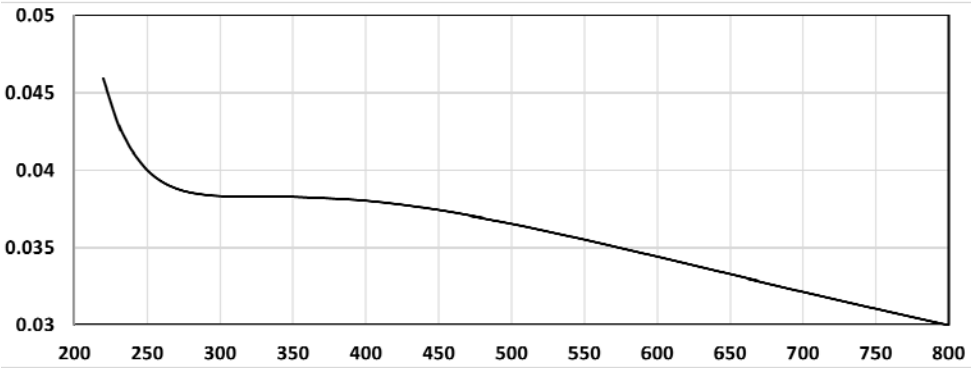

Fig. 5. Quality of GNB spline concerning the beam length for Task 1

Example task 2

This task is very similar to symmetrical Task 1. The only difference is that in first point B_1 the tangent angle is inclined to $-60°$ concerning the horizontal axis, and in second point B_2 the angle is equal to $60°$.

Intuitively, the best expected (ideal) curve is the semi-circle. From geometrical consideration, its diameter should satisfy the following relation $D/2\cos 30° = 75$, where one can get that $D = 173.20$. So, the length of the ideal figure is equal to 181.37. As to energy (1) of the ideal curve, it is equal to 0.02418.

Construct the splines according to different techniques, Fig. 6. As above CBS gives the ideal semi-circle. Bezier spline gives very close results at a distance equal to 67. When this distance is smaller, than Bezier curve lies below the ideal circle, and when the distance is larger it is situated above the ideal curve. A similar picture is for GNB splines. When their lengths are lesser than the ideal circle length, it is placed below, and above otherwise.

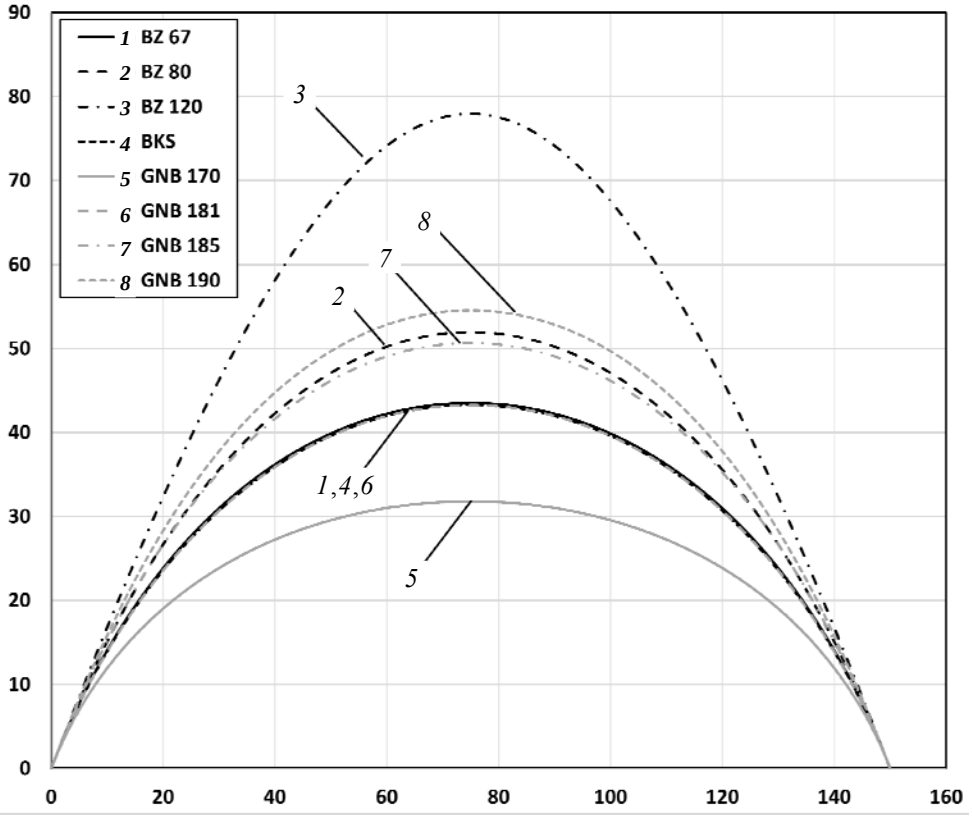

Fig. 6. Several calculated splines according to the Bezier method, BCS, and GNB, Task 2

The informative is a graph of curvatures for each spline, shown in Fig. 7. The best Bezier spline, BZ 67, is very close to the ideal circle, and its curvature is almost ideal. The same can be said about the BCS and GNB 185. Compared with CBS for Task 1 (Fig. 4), the curvature for CBS for Task 2 is much smoother: we use here as many as 120 imaginary points. Graphs of curvature are very important to judgment about the quality of different splines.

Compare the quality (energy) of each depicted curve. The results of its calculation for Task 2 are given in Table 2. That results in differently-looking curves that sometimes are very close. This means, that energy cannot be the sole criterion of the construction of the curve nor for the assessment of its fairness.

T a b l e 2 . Calculated energies for different splines for Task 2

Curve	BZ 67	BZ 80	BZ 120	BCS 181	GNB 170	GNB 181	GNB 190
Quality	0.0241	0.0246	0.0408	0.0242	0.0303	0.0242	0.0243

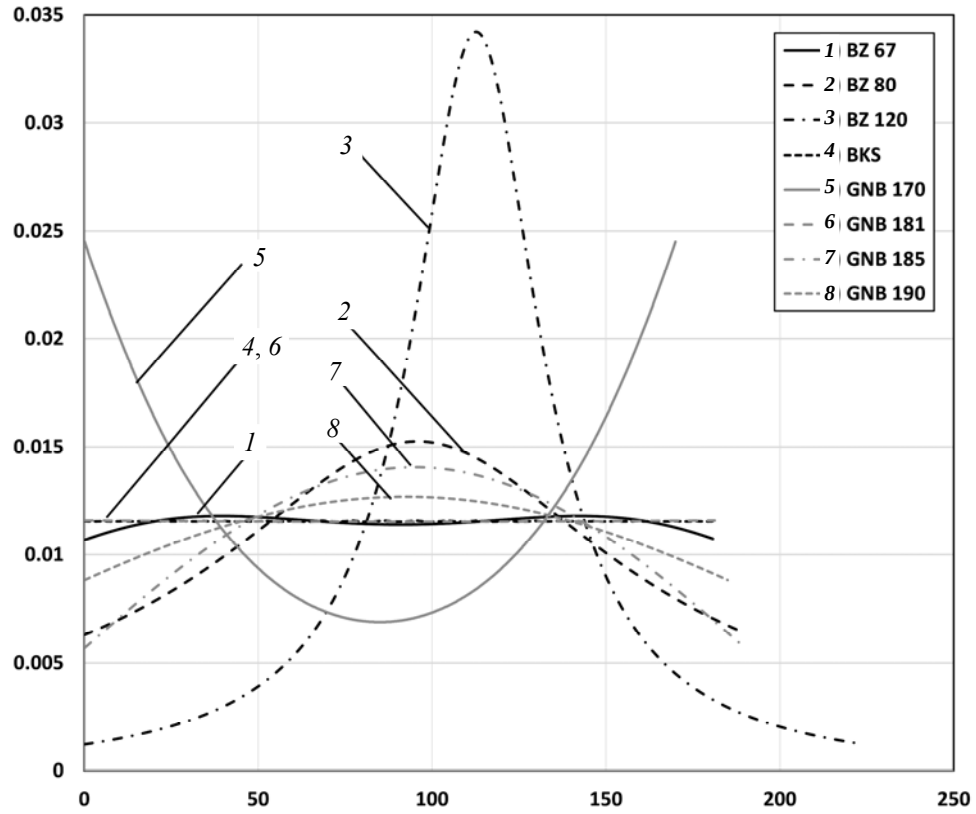

Fig. 7. The graphs of curvatures obtained by different splines for Task 2

Example task 3

This task is a more complicated one and relates to the construction of anti-symmetrical geometry. Point B_1 has coordinates $(X=0,\ Y=0)$, second point B_2 has coordinates $(X=150, Y=150)$, the tangent in point B_1 is directed at an angle *of* $60°$, while in point B_2 the angle is equal to $60°$, too.

The best solution cannot be formulated intuitively, so here we will subjectively assess the best solution below.

Construct the splines according to different techniques, Fig. 8. Look on the CBS, which does not require any auxiliary parameters. The general subjective impression is that it is visually pleasant, and its calculated length is about 294. So, chose the auxiliary parameters in other spline methods to approach this spline. It is not always possible for the Bezier splines. If we take the distance to be very small – it would resemble the straight line between two endpoints, and, of course, it should be rejected. If we take the distance in the Bezier spline too large, the graph will be placed well beyond the vertical range of $-150 < y < 150$. So, we chose subjectively the distances equal to 120, 150, and 180 as the candidates for

the best Bezier curve. Nevertheless, they are not pleasantly looking, and this can be supported by graphs of curvatures, Fig. 9. As to GNB it completely coincides with CBS, if we take its length as large as 294, Fig. 8. The increase or decrease of length leads to more loose or tight geometry, respectively.

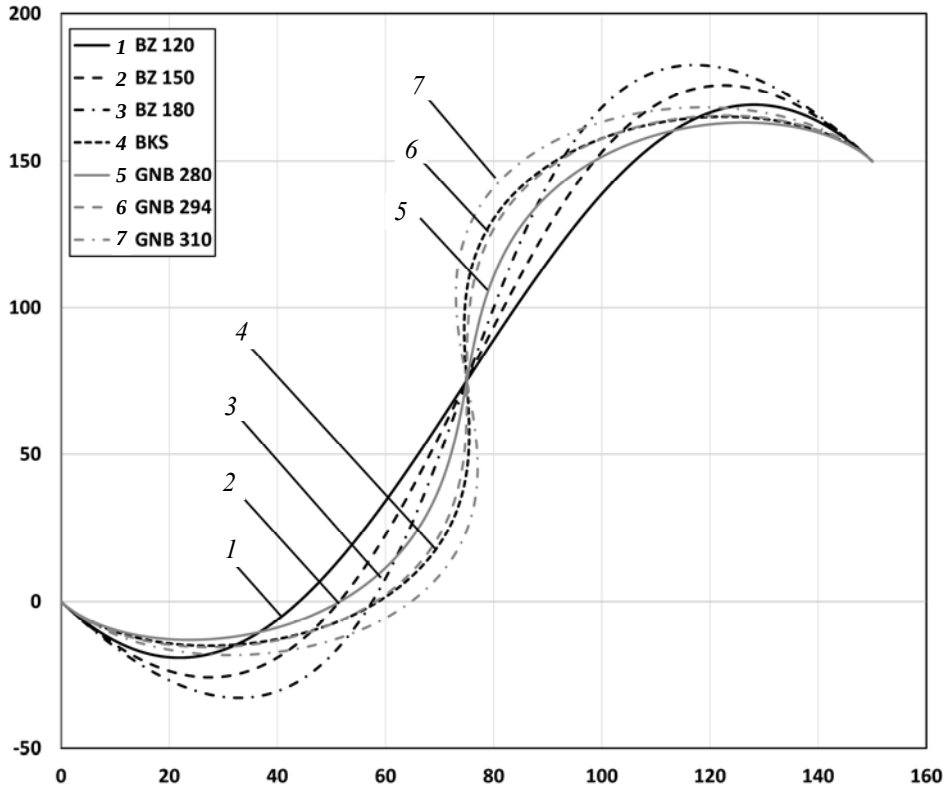

Fig. 8. Several calculated splines according to the Bezier method, BCS, and GNB, Task 3

More informative are the graphs of curvatures concerning the current length coordinate, Fig. 9. The curvature of CBS is very smooth, it is a straight line (small fluctuations are due to a limited number of imaginary points). So, an important conclusion can be drawn from its visual presentation. The CBS is a Cornu spiral, and this can be explained by the third differential equation of (6). On each small straight section $P = \text{const}$, so the moments (curvature) change linearly. In case, if intermediate points are the imaginary ones, the force does not change between them, so the whole section between any real points is a Cornu spiral.

As one can see, the GNB completely coincides with the CBS, in case its length is equal to the length of CBS. If GNB is shorter than CBS, then its curvature is larger than that of CBS. And vice versa, for longer GNB its curvature is smaller. As to the Bezier curve, it demonstrates the large local curvatures for all three considered distances chosen. As we see, the Bezier curve is ineffective for anti-symmetric cases.

Compare the energy for each curve. The results of its calculation for Task 3 are given in Table 3. The results for Bezier curves are very poor. So, the very big difference in energy can testify to the deficiency of the curve. As to GNB, the results for it are close to CBS because their lengths are similar. In any case, by varying the length of GNB the quality of it can always be better than that of CBS.

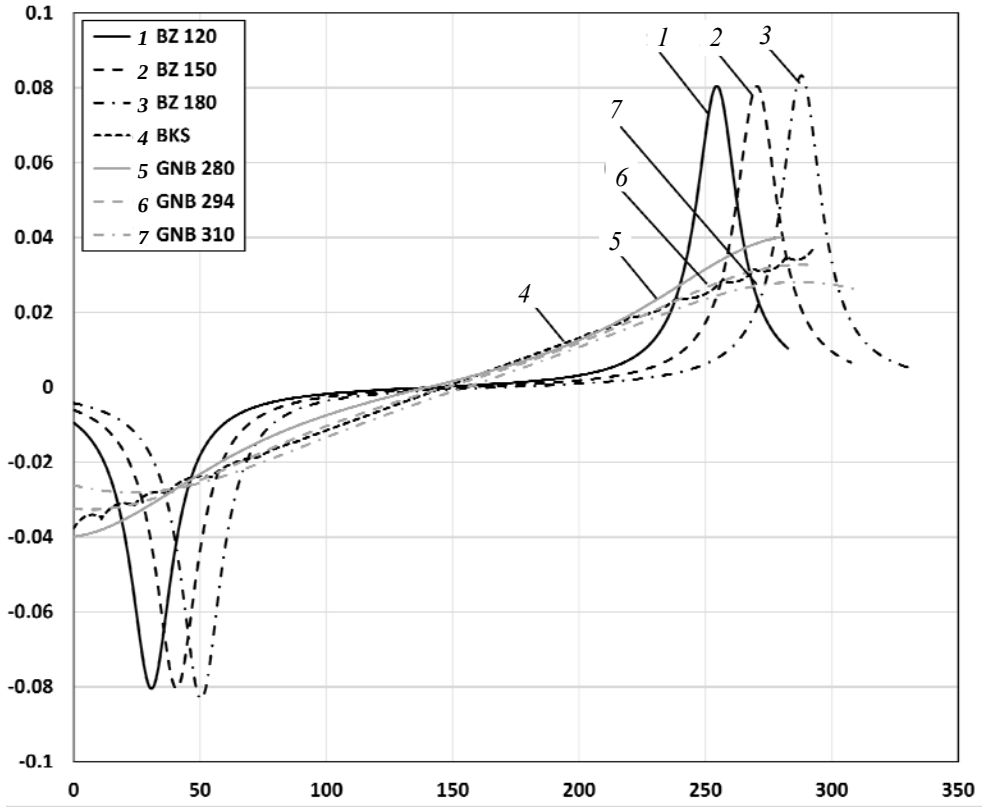

Fig. 9. The graphs of curvatures obtained by different splines for Task 3

Table 3. Calculated energies for different splines for Task 3

Curve	BZ 120	BZ 150	BZ 180	BCS	GNB 280	GNB 294	GNB 310
Quality	0.2080	0.2092	0.2173	0.1286	0.1373	0.1284	0.1225

Example task 4

This task is similar to the previous one but is not an antisymmetric. Point B_1 has coordinates $(X = 0, Y = 0)$, second point B_2 has coordinates $((X = 150,$ $Y = -150)$, the tangent in point B_1 is directed at an angle — $60°$, while in point B_2 the angle is equal to $0°$.

The best solution cannot be formulated intuitively, so here we will subjectively assess the best solution below.

Construct the splines according to different techniques, Fig. 10. As to CBS, the general subjective impression is that it is visually pleasant, and its calculated length is about 260. So, chose the auxiliary parameters in other splines as to approach this spline. As in Task 3, it is not possible for the Bezier splines – they deflect from CBS for any chosen parameter of distance. So, the results for Bezier splines are shown for three subjectively chosen distances – 100, 125, and 150. Nevertheless, they are not pleasantly looking, and this impression can be

supported by graphs of curvatures, Fig. 11, which has large local peaks of curvature, which is prohibited for "fair" spline [12]. As to GNB it completely coincides with CBS if we take its length as 260, Fig. 10. The increase or decrease of length leads to more loose or tight geometry, respectively.

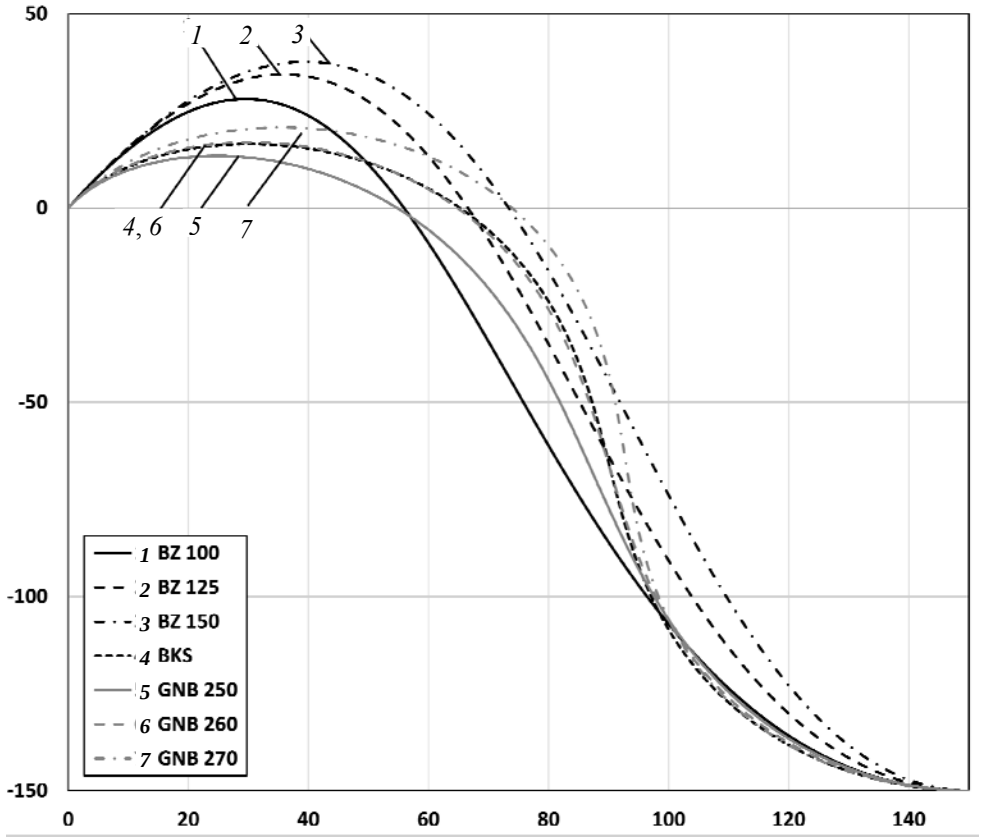

Fig. 10. Several calculated splines according to the Bezier method, BCS, and GNB, Task 4

Informative are the graphs of curvatures concerning the current length coordinate, Fig. 11. The curvature of CBS is a straight line (small fluctuations are due to a limited number of imaginary points), so evidently CBS is a Cornu spiral.

As in above Task 3, note that GNB completely coincides with CBS in case, its length is equal to the length of CBS and can be more tight or loose depending on whether the length of GNB is shorter or longer than the length of CBS. Bezier curve demonstrates the large curvatures for all three distances chosen.

Compare the energy for each curve. The results of its calculation for Task 4 are given in Table 4. The results for Bezier curves are very poor and testify to the deficiency of the curve. As to GNB, the results for energy are close for CBS because their lengths are similar. In any case, by varying the length of GNB the quality of it can always be better than that of CBS.

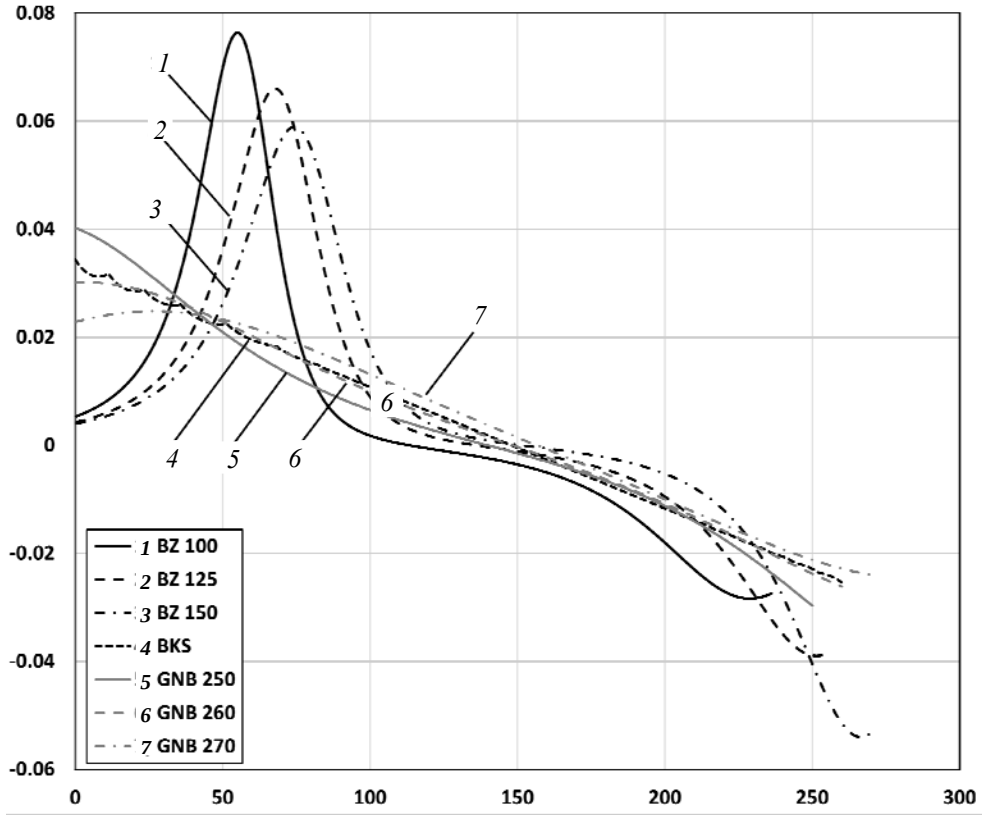

Fig. 11. The graphs of curvatures obtained by different splines for Task 4

Table 4. Calculated energies for different splines for Task 4

Curve	BZ 100	BZ 125	BZ 150	BCS	GNB 250	GNB 260	GNB 270
Quality	0.1156	0.1114	0.1153	0.0781	0.0835	0.0778	0.0753

CONCLUSION

The main attention of the paper is paid to the discussion of the advantages of CBS. On one hand, it is the four degrees of freedom simplified version of GNB, which operates by 6 degrees of freedom at each point. The beam theory origin of CBS gives a wide prospect for its modernization and application. On the other hand, the presented here version of CBS for the task of interpolation is reduced to the new original technique of construction of the Cornu spiral, which is widely recognized as one of the most aesthetic curves for the geometrical design purpose [62]. The application of the methodology of linear TMM makes this technique very simple and effective.

In detail, the method and its comparison with Brazier spline and GNB is made on the example of two endpoints that are connected by spline with prescribed tangent values. Several local conclusions can be drawn out.

1. As to the Brazier spline with the employment of four points (two intermediate ones can be chosen arbitrarily to optimize the geometry), it generally demonstrates poorer results. The resulting curvatures, especially for geometries, when

it changes the sign, behave very unsmoothly and exhibit very high local peaks. In this case, the calculated value of energy (1) is much higher than for CBS.

2. CBS for all 4 tasks considered gives very pleasant results. In all cases, the curvature is either constant (symmetric cases) or linearly changes with the spline length coordinate. The only technical requirement for its realization is the insertion of a sufficient number of imaginary points.

3. GNB is the most effective technique for spline construction as well as for modeling the deformation of real flexible beams. Its drawback for the geometrical design is that the justified length of the beam should be chosen in advance. The value obtained by the CBS solution is a good initial approximation for further GNB application. The accuracy of the GNB technique is demonstrated in the example of the well-known Horn task [42].

4. Energy criteria of fairness (1) cannot be considered as a sole criterion for the spline construction. On the other hand, a very big value of it testifies to the drawback of the applied technique.

REFERENCES

1. I. Orynyak, D. Koltsov, O. Chertov, and R. Mazuryk, "Application of beam theory for the construction of twice differentiable closed contours based on discrete noisy points," *System Research and Information Technologies*, no. 4, pp. 119–140, 2022. doi: https://doi.org/10.20535/SRIT.2308-8893.2022.4.10
2. I. Orynyak, R. Mazuryk, and A. Oryniak, "Basic (discontinuous) and smoothing up (conjugated) solutions in transfer matrix method for static geometrically nonlinear beam and cable in plane," *Journal of Engineering Mechanics*, vol. 146, no. 5, 2020. doi: https://doi.org/10.1061/(ASCE)EM.1943-7889.0001753
3. J.H. Alberg, E.N. Nilson, and J.L. Walsh, *The theory of splines and their applications*. New York: Academic, 1967.
4. G. Farin, "History of Curves and Surfaces in CAGD," *Handbook of CAGD*, G. Farin, M.S. Kim, and J. Hoschek (Eds), 2002. doi: https://doi.org/10.1016/B978-044451104-1/50002-2
5. J.C. Holladay, "A smoothest curve approximation," *Math. Tables Aids Comput*., 11, pp. 233–243, 1957. doi: https://doi.org/10.2307/2001941
6. R.H. Bartels, J.C. Beatty, and B.A. Barsky, *An introduction to splines for use in computer graphics and geometric modeling*. Morgan Kaufmann, 1995.
7. Daniel G. Schweikert, "An Interpolation Curve using a Spline in Tension," *Journal of Mathematics and Physics*, 45, pp. 312–317, 1966. doi: https://doi.org/10.1002/sapm1966451312
8. S.P. Timoshenko, *Strength of Materials: Part II Advanced Theory and Problems*. D. Van Nostrand, 1956.
9. Even Mehlum, "A Curve-Fitting Method Based on a Variational Criterion," *BIT*, 4, pp. 213–223, 1964.
10. P.H. Wagner, X. Luo, and K.A. Stelson, "Smoothing curvature and torsion with spring splines," *Computer-Aided Design*, 27, pp. 615–626, 1995. doi: https://doi.org/10.1016/0010-4485(95)99798-d
11. Asker Bengt, "The Spline Curve, A Smooth Interpolating Function Used in Numerical Design of Ship-Lines," *BIT*, 2, pp. 76–82, 1962.
12. H.P. Moreton, "Minimum curvature variation curves, networks, and surfaces for fair free-form shape design," Doctoral dissertation, University of California, Berkeley, 1992.
13. K. Salkauskas, "C1 Splines for Interpolation of Rapidly Varying Data," *Rocky Mountain Journal of Mathematics*, 14, pp. 239–250, 1984.
14. G. Birkhoff, H. Burchard, and D. Thomas, *Nonlinear Interpolation by Splines, Pseudosplines, and Elastica*. General Motors Research Laboratories Report 468, 1965.

15. D.F. Rogers, *An introduction to NURBS: with historical perspective*. Morgan Kaufmann, 2001.
16. James Ferguson, "Multivariable Curve Interpolation," *Journal of the Association of Computing Machinery*, 11, pp. 221–228, 1964.
17. M.P. Epstein, "On the influence of parametrization in parametric interpolation," *SIAM Journal on Numerical Analysis*, 13(2), pp. 261–268, 1976.
18. J.A. Kjellander, "Smoothing of cubic parametric splines," *Computer-Aided Design*, 15(3), pp. 175–179, 1983.
19. J. Ye, R. Qu, "Fairing of parametric cubic splines," *Mathematical and Computer Modelling*, 30(5-6), pp. 121–131, 1999. doi: https://doi.org/10.1016/S0895-7177(99)00152-1
20. A. Binninger, O. Sorkine-Hornung, "Smooth Interpolating Curves with Local Control and Monotone Alternating Curvature," in *Computer Graphics Forum*, vol. 41, no. 5, pp. 25–38, 2022. doi: https://doi.org/10.1111/cgf.14600
21. R. Levien, C.H. Séquin, "Interpolating splines: Which is the fairest of them all?" *Computer-Aided Design and Applications*, 6(1), pp. 91–102, 2009. doi: https://doi.org/10.3722/cadaps.2009.91-102
22. G. Brunnett, J. Kiefer, "Interpolation with minimal-energy splines," *Computer-Aided Design*, 26(2), pp. 137–144, 1994. doi: https://doi.org/10.1016/0010-4485(94)90034-5
23. R.C. Veltkamp, W. Wesselink, "Modeling 3D curves of minimal energy," in *Computer Graphics Forum*, vol. 14, no. 3, pp. 97–110. Edinburgh, UK: Blackwell Science Ltd., 1995. doi: https://doi.org/10.1111/j.1467-8659.1995.cgf143_0097.x
24. L. Fang, D.C. Gossard, "Multidimensional curve fitting to unorganized data points by nonlinear minimization," *Computer-Aided Design*, 27(1), pp. 48–58, 1995. doi: https://doi.org/10.1016/0010-4485(95)90752-2
25. G. Birkhoff, C.R. de Boor. "Piecewise Polynomial Interpolation and Approximation," in *Approximation of Functions*, ed. H.L. Garabedian, pp. 164–190. Elsevier, New York/Amsterdam, 1965.
26. G. Farin, G. Rein, N.S. Sapidis, and A.J. Worsey, "Fairing Cubic B-Spline Curves," *Computer Aided Geometric Design*, pp. 91–103, 1987. doi: https://doi.org/10.1016/0167-8396(87)90027-6
27. Alfred M. Bruckstein, Robert J. Holt, and Arun N. Netravali, "Discrete elastica," *Applicable Analysis*, 78, 3-4, pp. 453–485, 2001. doi: https://doi.org/10.1080/00036810108840945
28. G. Xu, G. Wang, and W. Chen, "Geometric construction of energy-minimizing Béezier curves," *Science China Information Sciences*, 54, pp. 1395–1406, 2011. doi: https://doi.org/10.1007/s11432-011-4294-8
29. D. Brander, J.A. Bærentzen, A.S. Fisker, and J. Gravesen, "Bézier curves that are close to elastic," *Computer-Aided Design*, 104, pp. 36–44, 2018. doi: https://doi.org/10.1016/j.cad.2018.05.003
30. C. Zhang, P. Zhang, and F.F. Cheng, "Fairing spline curves and surfaces by minimizing energy," *Computer-Aided Design*, 33(13), pp. 913–923, 2001. doi: https://doi.org/10.1016/S0010-4485(00)00114-7
31. D.B. Parkinson, D.N. Moreton, "Optimal biarc-curve fitting," *Computer-Aided Design*, 23(6), pp. 411–419, 1991. doi: https://doi.org/10.1016/0010-4485(91)90009-L
32. G. Xu, Y. Zhu, L. Deng, G. Wang, B. Li, and K.C. Hui, "Efficient construction of B-spline curves with minimal internal energy," *Computers, Materials & Continua*, 58(3), pp. 879–892, 2019. doi: https://doi.org/10.32604/cmc.2019.03752
33. J. Li, "Combined internal energy minimizing planar cubic Hermite curve," *Journal of Advanced Mechanical Design, Systems, and Manufacturing*, 14(7), 2020.
34. R. Levien, *The elastica: a mathematical history*. Electrical Engineering and Computer Sciences University of California at Berkeley, Technical Report No. UCB/EECS-2008-103, 2008.
35. Garrett Birkhoff, Carl R. de Boor, "Piecewise polynomial interpolation and approximation," *Proc. General Motors Symp. of 1964*, pp. 164–190.
36. E.H. Lee, G.E. Forsythe, "Variational study of nonlinear spline curves," *SIAM review*, 15(1), pp. 120–133, 1973. doi: https://doi.org/10.1137/1015004

37. G.H. Brunnett, "Properties of minimal-energy splines," in *Curve and surface design*; Society for Industrial and Applied Mathematics, pp. 3–22, 1992. doi: https://doi.org/10.1137/1.9781611971651.ch1
38. J.M. Glass, "Smooth-curve interpolation: A generalized spline-fit procedure," *BIT Numerical Mathematics*, 6(4), pp. 277–293, 1966. doi: https: //doi.org/10.1007/BF01966089
39. M.A. Malcolm, "On the computation of nonlinear spline functions," *SIAM Journal on Numerical Analysis*, 14(2), pp. 254–282, 1977. doi: https://doi.org/10.1137/0714017
40. Even Mehlum, *Curve and Surface Fitting Based on Variational Criteria for Smoothness*. Central Institute for Industrial Research, Oslo, Norway, 1969.
41. E. Cohen, T.Lyche, and R.F. Riesenfeld, "MCAD: Key historical developments,' *Computer methods in applied mechanics and engineering*, 199(5-8), pp. 224–228, 2010. doi: https://doi.org/10.1016/j.cma.2009.08.003
42. B.K. Horn, "The curve of least energy," *ACM Transactions on Mathematical Software (TOMS)*, 9(4), pp. 441–460, 1983. doi: https://doi.org/10.1145/356056.356061
43. M. Kallay, "Plane curves of minimal energy," *ACM Transactions on Mathematical Software (TOMS)*, 12(3), pp. 219–222, 1986. doi: https://doi.org/10.1145/7921.7924
44. M. Kallay, "Method to approximate the space curve of least energy and prescribed length," *Computer-Aided Design*, 19(2), pp. 73–76, 1987. doi: https://doi.org/ 10.1016/S0010-4485(87)80048-9
45. D. Brander, J. Gravesen, and T.B. Nørbjerg, "Approximation by planar elastic curves," *Adv. Comput. Math.*, 43, pp. 25–43, 2017. doi: https://doi.org/10.1007/ s10444-016-9474-z
46. O.M. O'Reilly, *Modeling nonlinear problems in the mechanics of strings and rods*, pp. 187–268. Cham: Springer International Publishing, 2017. doi: https://doi.org/10.1007/978-3-319-50598-5
47. C. Meier, A. Popp, and W.A. Wall, "Geometrically exact finite element formulations for slender beams: Kirchhoff–Love theory versus Simo–Reissner theory," *Archives of Computational Methods in Engineering*, 26(1), pp. 163–243, 2019. doi: https://doi.org/10.1007/s11831-017-9232-5
48. Y. Goto, Y. Morikawa, and S. Matsuura, "Direct Lagrangian nonlinear analysis of elastic space rods using transfer matrix technique," *Proc. of JSCE, Struct. Eng./Earthquke Eng.*, 5(1), 1986.
49. A. Rosen, O. Gur, "A transfer matrix model of large deformations of curved rods," *Computers & Structures*, 87(7-8), pp. 467–484, 2009. doi: https://doi.org/10.1016/ j.compstruc.2008.12.014
50. I.V. Orynyak, S.A. Radchenko, "A mixed-approach analysis of deformations in pipe bends. Part 3. Calculation of bend axis displacements by the method of initial parameters," *Strength of materials*, 36, pp. 463–472, 2004. doi: https://doi.org/10.1023/B:STOM.0000048394.98411.4f
51. F. Leckie, E. Pestel, "Transfer-matrix fundamentals," *International Journal of Mechanical Sciences*, 2(3), pp. 137–167, 1960. doi: https://doi.org/10.1016/0020-7403(60)90001-1
52. J.H. Argyris et al., "Finite element method—the natural approach," *Computer Methods in Applied Mechanics and Engineering*, 17, pp. 1–106, 1979. doi: https://doi.org/10.1016/0045-7825(79)90083-5
53. M.A. Crisfield, "A consistent co-rotational formulation for non-linear, three-dimensional, beam-elements," *Comput. Methods Appl. Mech. Eng.*, 81, pp. 131–150, 1990. doi: https://doi.org/10.1016/0045-7825(90)90106-V
54. A.H. Fowler, C.W. Wilson, *Cubic Spline, a Curve Fitting Routine*, Report No. Y-1400, Contract No. W-7405-ENG-26, Nuclear Division, Union Carbide Corp., Oak Ridge, Tenn., 1962, pp. 1–41.
55. W.D. Birchler, S.A. Schilling, *Comparisons of Wilson–Fowler and Parametric Cubic Splines with the Curve-Fitting Algorithms of Several Computer-Aided Design Systems (No. LA-13784)*. Los Alamos National Lab. (LANL), Los Alamos, NM (United States), 2001. https://doi.org/10.2172/776180
56. I.V. Orynyak, I.V. Lokhman, and A.V. Bogdan, "Determination of curve characteristics by its discrete points measured with an error and its application to stress analysis

for buried pipeline," *Strength of Materials*, 44, pp. 268–284, 2012. doi: https://doi.org/10.1007/s11223-012-9380-7

57. I.V. Orynyak, A.V. Bohdan, and I.V. Lokhman, "The 2d Spring Splines procedure application with prescribed accuracy for determination of the global (pipe centerline) as well as the local (dent) curvatures," *International Pipeline Conference*, 12, pp.171–181, 2012. doi: https://doi.org/10.1115/ipc2012-90127
58. A. Borum, T. Bretl, "The free configuration space of a Kirchhoff elastic rod is path-connected," in *2015 IEEE International Conference on Robotics and Automation (ICRA)*, pp. 2958–2964. doi: https://doi.org/10.1109/ICRA.2015.7139604
59. David Brander et al., "Designing for hot-blade cutting: Geometric Approaches for High-Speed Manufacturing of Doubly Curved Architectural Surfaces," in *Advances in Architectural Geometry 2016*, pp. 306–327. doi: https://doi.org/10.3218/3778-4_21
60. S.P. Timoshenko, *Strength of materials: Part 1: Elementary theory and problems*. N.-Y.: Robert E. Krieger, 1958.
61. I. Orynyak, R. Mazuryk, "Application of method of discontinuous basic and enhanced smoothing solutions for 3D multibranched cable," *Engineering Structures*, 251, 113582, 2022. doi: https://doi.org/10.1016/j.engstruct.2021.113582
62. K.T. Miura, G. Ru, "Aesthetic curves and surfaces in computer-aided geometric design," *International Journal of Automation Technology*, 8(3), pp. 304–316, 2014. doi: https://doi.org/10.20965/ijat.2014.p0304

Received 26.04.2024

INFORMATION ON THE ARTICLE

Igor V. Orynyak, ORCID: 0000-0003-4529-0235, National Technical University of Ukraine "Igor Sikorsky Kyiv Polytechnic Institute", Ukraine, e-mail: igor_orinyak@yahoo.com

Petro M. Yablonskyi, ORCID: 0000-0002-1971-5140, National Technical University of Ukraine "Igor Sikorsky Kyiv Polytechnic Institute", Ukraine, e-mail: ypn@ukr.net

Dmytro R. Koltsov, ORCID: 0000-0002-0396-7255, National Technical University of Ukraine "Igor Sikorsky Kyiv Polytechnic Institute", Ukraine, e-mail: koltsovdd@gmail.com

Oleg R. Chertov, ORCID: 0000-0003-0087-1028, National Technical University of Ukraine "Igor Sikorsky Kyiv Polytechnic Institute", Ukraine, e-mail: chertov@i.ua

Roman V. Mazuryk, ORCID: 0000-0003-4309-824X, National Technical University of Ukraine "Igor Sikorsky Kyiv Polytechnic Institute", Ukraine, e-mail: r.mazuryk.ua@gmail.com

ДОБРОТНІСТЬ 2D КОРОТАЦІЙНОГО СПЛАЙНУ ПРОМЕНЯ ПОРІВНЯНО З ГЕОМЕТРИЧНО НЕЛІНІЙНО ПРУЖНИМ ПРОМЕНЕМ / І.В. Ориняк, П.М. Яблонський, Д.Р. Кольцов, О.Р. Чертов, Р.В. Мазурик

Анотація. Метою статті є подальше дослідження властивостей і переваг нещодавно запропонованого коротаційного балкового сплайну (КБС). Акцент зроблено на розгляді досить простої задачі проведення сплайну між двома кінцевими точками із заданими дотичними в них. Як критерій «хорошості» сплайну обрано відоме поняття «добротності», яке являє собою інтеграл від квадрата кривини сплайну по його довжині, що походить із теорії пружної балки як енергія деформації. Порівняння «добротності» КБС виконано з деякими варіантами кубічної кривої Безьє (КБ) і геометрично нелінійної балки (ГНБ) зі змінною довжиною. Показано, що КБС є набагато ефективнішим, ніж КБ, для якої будь-яка спроба забезпечити кращу «добротність» КБ шляхом зміни відстані від кінцевих точок до двох проміжних точок, як правило, призводить до гірших результатів порівняно з КБС. З іншого боку, ГНБ, або іншими словами, крива «еластика», здатна давати дещо кращі значення «добротності» для оптимальної довжини балки. Це можна пояснити більш складною методологічною основою ГНБ, яка використовує 6 ступенів вільності в кожному перерізі порівняно з 4-ма ступенями вільності в КБС.

Ключові слова: коротаційний балковий сплайн, геометрично нелінійна балка, плоска задача, крива Безьє, добротність, метод початкових параметрів.

UDC 004.89:004.3
DOI: 10.20535/SRIT.2308-8893.2024.3.08

THE ROLE OF GENERATIVE ARTIFICIAL INTELLIGENCE (GAI) IN SCIENTIFIC RESEARCH

A.I. PETRENKO

Abstract. The emergence and growing capabilities of Generative Artificial Intelligence (GAI) are profoundly transforming scientific research. Although AI extends human intelligence by automating certain tasks, it complements rather than replaces human creativity. This article discusses the implications of AI for the scientific process, including ethical considerations and the need for a balanced approach that combines the strengths of human and artificial intelligence in the process of discovering knowledge and solving complex problems. The discussion extends to the need for universities to adapt their curricula to prepare future researchers for the AI era, emphasizing scenario-based thinking and uncertainty management as important skills for the future.

Keywords: Generative Artificial Intelligence, hypothesis analysis and testing, searching scientific data sources, research planning, writing and editing scientific manuscripts, organizing and presenting results.

THE FUNCTIONS OF GSI SERVICES IN SCIENTIFIC RESEARCH INVESTIGATION

At the end of last year 2023 a number of leading Ukrainian universities (including Igor Sikorsky Kyiv Polytechnic Institute, Kherson State University, Zaporizhzhia Polytechnic National University and others) developed and adopted recommendations on the use of artificial intelligence in learning, teaching and research [1–3]. Based on these recommendations, we will try to detail and illustrate the possibilities and consequences of using Generative Artificial Intelligence (GAI) in conducting research and presenting the results, taking into account the aspects of Open Science [4].

Based on the experience gained, it is recommended to use artificial intelligence in research for the following activities:

- automated generation of hypotheses and concepts based on data analysis;
- analysis and testing of hypotheses and iteration of research processes;
- finding sources of scientific data, reviewing, interpreting and citing them;
- searching for and extracting specific data from large databases, which significantly speeds up the information retrieval process;
- building a plan/structure for a project/qualifying thesis;

- gathering and processing information related to the topic of the project/assignment;
- analyzing and processing large data sets, identifying patterns, templates and correlations in them;
- translating, editing and summarizing texts;
- organizing and comparing the results obtained;
- bridging the gaps between different fields of research by providing explanations and combining concepts from different disciplines by finding common trends and patterns;
- writing scientific reports;
- writing articles (grammar, translation, paraphrasing, summarizing) according to the requirements of scientific journals;
- automatically generate graphs, charts and other visual representations of data, including video, to illustrate key findings and trends;
- plagiarism checking;
- converting spoken information into printed text (natural language processing);
- summary generation.

These activities can be considered as functions of the respective GAI services. They require changes in the training of future scientists and professionals and are a powerful means of personalizing education by adapting content and experiences in ways that were previously impossible. Developing future-oriented skills in future scientists, such as scenario thinking, systems thinking, and managing uncertainty and complexity, requires more than memorizing or even managing large data sets.

THE GENERATION AND TESTING OF RESEARCH HYPOTHESES FORM THE BASIS OF SCIENTIFIC RESEARCH

GAI is already influencing the development of science, going beyond simple automation and becoming an active participant in the pursuit of knowledge and understanding. However, in scientific research, the use of artificial intelligence represents a significant shift in paradigm, enabling active collaboration between machines and humans to formulate research hypotheses and questions. Artificial intelligence systems have traditionally been powerful tools for data analysis. However, their evolution now enables them to generate hypotheses based on patterns that may escape human observation. GAI algorithms can sift through massive amounts of data much quicker than humans, identifying interesting patterns or unique connections. This can lead to new hypotheses for scientists to investigate further. The combination of machine-driven hypotheses and human experience shows promise for scientific advancement. It is important to maintain human control over the scientific process and interpretation of results.

However, the ability of artificial intelligence to generate hypotheses raises questions about the nature of creativity in research. Can artificial intelligence truly exhibit creativity in hypothesizing, or are they restricted to pattern recognition in available data?

Additionally, the intersection of artificial intelligence and research extends beyond hypothesis generation to encompass the formulation of research questions. Active collaboration between machines and researchers can expand the

scope and depth of scientific research by identifying gaps in knowledge and suggesting profound questions. This approach emphasizes the indispensable role of human understanding in forming the research program. Although GAI has great potential, integrating it into hypothesis formation is not without issues. One significant problem is the "black box" nature of many advanced GAI algorithms. The "black box" issue arises as the complex nature of GAI makes it difficult to understand how it generates ideas. AI can be compared to a chef who creates a secret recipe without disclosing the ingredients. To trust AI, it is important to understand its thought process, which can be challenging.

As these systems become more complex, it becomes increasingly difficult for human researchers to understand the reasoning behind the non-traditional hypotheses generated by the GAI. Large language models such as ***Copilot*** (ChatGPT-4) (https://www.bing.com/chat), ***Gemini*** Ulta (https://gemini.google.com/) or ***Cloud-3*** (https://claude.ai/) can exacerbate this issue. Figure 1 contains a fragment of Gemini's answer on the question about examples of GAI-powered hypotheses in Computer Science.

Gemini Advanced

Hypotheses on GAI EnhancingSpecific Tasks:

1. **Automated Code Generation:** GAIs will outperform the best human programmers in generating error-free, efficient code across multiple programming languages when given a clear problem specification.
2. **Network, Security:** GAI-powered intrusion detection systems will have a significantly lower false-positive rate and higher detection rate of novel cyberattracks compared to current state-of-the-art systems.
3. **Natural Language Understanding:** GAI models will achieve human-level performance on complex natural language understanding tasks like reading comprehension, text summarization, and nuanced sentiment analysis.
4. **Data Compression:** GAI-designed data compression algorithms will consistently achieve higher compression ratios with minimal loss of information copared to existing methods on diverse data types.

Fig. 1. Illustration of talk with Gemini about its ability to generate hypotheses

The results of talk on the same topic with ChatGPT-4 and Cloud-3 are shown on Fig. 2 and Fig. 3 respectively.

Generative AI (GAI) has gained prominence in various fields, including computer science. Here are a few hypotheses related to GAI applications in this domain:

Enhanced Code Generation: GAI models, such as Generative Pretrained Transformers (GPT), could be leveraged to automatically generate high-quality code snippets, improving software development efficiency and reducing human effort.

Data Augmentation: GAI techniques can create synthetic data samples, augmenting existing datasets for training machine learning models. This could enhance model generalization and performance.

Natural Language Understanding: GAI models excel at understanding and generating natural language. They could be used to improve chatbots, virtual assistants, and sentiment analysis systems.

Drug Discovery: GAI can assist in drug discovery by generating molecular structures with desired properties, potentially accelerating the search for new medications.

Art and Creativity: GAI-generated art, music, and literature could inspire new creative works or even lead to novel artistic styles.

Fig. 2. Illustration of talk with ChatGPT-4 about its ability to generate hypotheses

Here are some concrete hypotheses related to potential applications of Artificial General Intelligence (AGI) in computer science:

AGI systems could autonomously **develop new algorithms and data structures** that are more efficient and scalable than those designed by human programmers.

AGI systems could **seamlessly integrate and optimize different areas of computer science**, such as machine learning, computer vision, natural language processing, and robotics, leading to more sophisticated and versatile applications.

AGI systems could **automatically debug and optimize legacy software systems**, improving their performance, security, and maintainability.

AGI systems could **dynamically allocate and manage computing resources** (e.g., CPU, memory, storage) across distributed systems, leading to more efficient utilization of hardware resources.

AGI systems **could autonomously explore and generate novel computational architectures, programming paradigms, and programming languages** that are better suited for specific tasks or domains.

AGI systems could **automatically translate high-level specifications or requirements into efficient and robust software implementations**, facilitating rapid prototyping and development of complex systems.

AGI systems could **continuously monitor and adapt software systems to changing environments**, user behaviors, and security threats, enabling self-healing and self-optimizing systems.

AGI systems could **autonomously discover and exploit patterns and insights in large-scale data**, leading to breakthroughs in areas such as bioinformatics, computational finance, and scientific computing.

AGI systems could **dynamically synthesize and integrate knowledge from multiple domains**, enabling the development of interdisciplinary applications that leverage insights from diverse fields.

AGI systems could **autonomously explore the vast search space of potential software solutions**, leading to the discovery of novel and innovative approaches to complex computational problems.

These hypotheses span various areas of computer science, including algorithm design, software engineering, distributed systems, programming languages, and interdisciplinary applications. However, it's important to note that the realization of these hypotheses would depend on significant advancements in AGI research and the development of robust and reliable AGI systems.

Fig. 3. Illustration of talk with Cloud-3 about its ability to generate hypotheses which is the most meaningful

It seems that GAI can't actually generate a new thought, rather than repeat something from the training array, or substitute the most likely answer from the same training array. There is a very thin line between creating new thoughts (hypotheses) and just looking for information from an existing array. The lack of interpretation and concretization can hinder the acceptance of hypotheses generated by artificial intelligence in the scientific community. In addition, the datasets on which GAI models are trained can contain inherent prejudices that may influence the generated hypotheses. If this bias is not addressed, it can distort the development of perspectives in science. It is important to recognize that although artificial intelligence can process vast amounts of information, it cannot discern subtleties [5; 6].

Nevertheless, at the beginning of October 2023, researchers gathered in Stockholm, who under led by Hiroaki Kitano, a biologist and CEO of Sony AI,

considered questions about the introduction of *Nobel prizes for developers of artificial intelligence and artificial cooperation intelligence and people* who made an outstanding scientific contribution [7]. And it's fair, because GAI is on its own influence on the development of scientific research can be rightly considered as a quality fundamental direction of modern science.

As GAI plays a more active role in hypothesis formation, ethical considerations become a priority. The responsible use of GAI requires constant vigilance to prevent undesirable consequences. Researchers must be vigilant in detecting and mitigating biases and one-sidedness in the training datasets, ensuring that the system of artificial intelligence does not preserve or strengthen existing inequalities in the adequacy of generated solutions for various branches and tasks.

In addition, the ethical implications of hypotheses generated by GAI, particularly in sensitive areas such as genetics or social sciences, require careful consideration. Transparency in the decision-making process regarding GAI hypotheses is crucial for building trust within the scientific community and society as a whole. Striking the right balance between innovation and ethical responsibility is an ongoing challenge that demands constant attention, as collaboration between humans and GAI continues to evolve [8]. Accurate thinking, creativity, and understanding of context play a vital role in improving and testing hypotheses generated by the GAI.

However, despite their intelligence, GAI cannot replace human scientists. It is still necessary for people to carefully consider the suggestions made by AI and interpret their true meaning. Good teamwork among different experts, such as computer scientists, ethicists, and researchers, is essential to ensure the best use of AI. Researchers must act as critical evaluators, questioning the assumptions made by artificial intelligence algorithms and ensuring that the proposed hypotheses are consistent with available knowledge. This will not only improve our understanding of the underlying processes but also ensure that the hypotheses meet ethical and scientific standards.

The integration of artificial intelligence into the hypothesis generation process is an ongoing journey with enormous potential. The combined efforts of humans and machines hold the promise of accelerating scientific discovery, generating new ideas and solving complex problems facing humanity. However, this journey requires a balanced approach that recognizes the strengths of artificial intelligence while respecting the unique skills and ethical considerations that humans bring to the table.

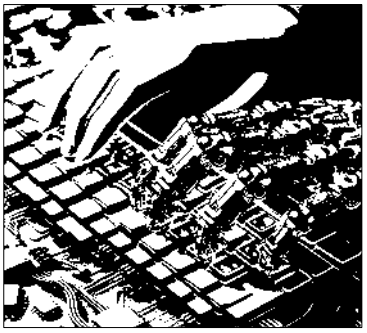

Fig. 4. Symbol of human-machine partnership generated by GAI

For example, the transformative power of GAI in hypothesis generation is changing the landscape of scientific research. However, this would not be possible without a joint and dynamic partnership between humans and machines, which has the potential for unprecedented advances and opens up a new era of scientific research and understanding that is inherent in Industry 5.0 technologies (Fig. 4).

PRIORITY SERVICES FOR STUDENTS TO LEARN MODERN RESEARCH METHODOLOGY

With the increasing use of GAI in scientific research, it is important for universities to prepare future researchers to work in this era. While some may argue that the use of artificial intelligence in fundamental scientific research is too complex for higher education purposes, it is still important for students to learn modern research methodology. It may be argued that not all students are capable of understanding modern advanced research methods. Empirical research can be conducted through student projects to test their scientific development abilities and the consequences of using artificial intelligence in the learning process. Modern university curriculums worldwide include some traditional aspects of scientific research.

The use of GAI in scientific research involves various aspects, including experimentation, data collection and interpretation, modelling, and automation of design. Therefore, the question of prioritizing certain GAI services for inclusion in educational programs arises. Developing educational adaptations of professional GAI services can help teach future scientists about the ethics of using GAI in scientific research and instil in them a sense of responsibility. However, teachers should not only be trained to use artificial intelligence tools and data, but also to understand the rapidly changing landscape of modern science in the era of artificial intelligence. It is important to develop individual solutions for each specialty to ensure the appropriate selection of basic GAI services.

Regulatory documents of universities [1–3] provide recommendations for using existing GAI services, which now number in the thousands. It is important to note that there are many options available for choosing GAI services. GAI services have become popular due to their ability to democratize GIS (Geographic information systems) applications, making them accessible to people without technical training. Each GAI service learns from a specific set of data that determines its effectiveness in performing specialized tasks. It is crucial to accurately determine and select the service that best meets your needs to get the most out of these GAI services. As a first step in implementing university policies for the use of artificial intelligence in academic activities, we have selected and demonstrated five effective interdisciplinary GAI services below. Their selection was based on an attempt to ensure their uniqueness and to avoid describing many of the GAI services that can be found in most publications. They serve as tools to support different aspects of the research process.

Semantic scholars. Search and Discovery of Scientific Information

Semantic Scholar (https://www.semanticscholar.org/) is a GAI service that provides access to a huge database of more than 211 million articles from all fields of science, making it one of the largest repositories of scientific literature. This comprehensive collection covers a wide range of subjects including: physics, chemistry, biology, medicine, history, computer science, etc. From cutting-edge research papers to historical publications, *Semantic Scholar* has a wealth of resources to

support researchers in their pursuit of knowledge. One of the key features of *Semantic Scholar* is its powerful search and filtering capabilities based on artificial intelligence.

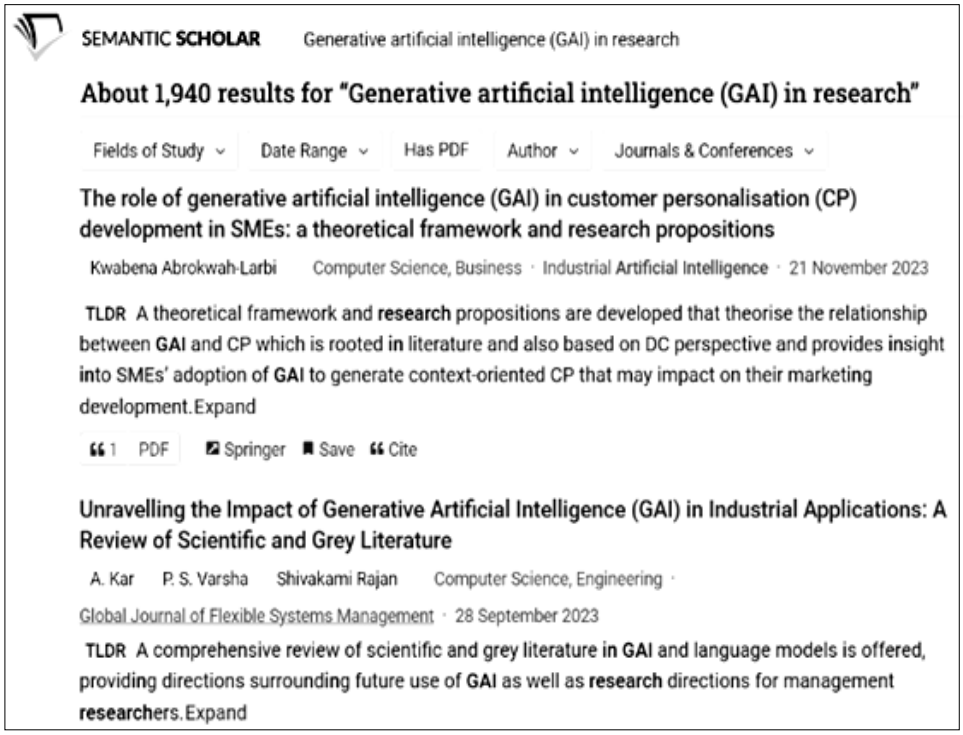

Fig. 5. A fragment of selected literature (1940 sources in English and 3 in Ukrainian)

The service uses natural language processing and machine learning algorithms to analyze the content of articles and extract relevant information. This allows users to perform advanced searches by specific keywords, authors, journals, publication dates, and other parameters, enabling accurate and efficient article retrieval [10]. The selection of literature sources on the topic of this article made by the service is illustrated in Fig. 5.

It is interesting to compare received results with those obtained from a Google search engine based on the user's query. Often, the data obtained from such searches do not correspond to the search goal and return simple URLs of sites and fragments of content that are not always relevant. Developers must check website content, filter out irrelevant information, and optimize it according to constraints. Fig. 5 shows that the Semantic Scholar's results differ from Google's. It mainly consists of published articles, each providing detailed information on its significance (through the number of citations) and direction (topic). The article can be sorted by different criteria, including the number of authors and sources used to build it (*References*), related papers such as images and publications (*Related Papers*), publication date (*Recency*), number of citations (*Citation Count*), importance (*Most Influential Papers*), and relevance to the topic (*Relevance*).

Please note that this service has 56 alternative purpose-specific services, such as *Scholarcy, OpenRead, Elicit, Scispace, Scite, Research Buddy, Mirrorthink, and Epsilon*. A comparison of their results with Semantic Scholar is available on the website https://theresanaiforthat. com/ai/semanticscholar/.

***Explain a paper*. Extracting and understanding information from sources**

Explain Paper (https://www.explainpaper.com/) is an AI service designed to work with scientific publications from any field, including natural sciences, social sciences, humanities, etc. However, it works best with materials that are complex in technical and scientific jargon. The explanations aim to cover the main concepts and key findings as accurately as possible. However, it is always advisable to refer to the original article for technical details. You should think of an AI explanation as a "tutor friend" pointing out the main ideas. The Explain Paper service accepts PDF documents from any source — journals, preprint servers, university websites, etc. You can set the depth of explanation from basic to very detailed (expert). This service is designed for researchers and scientists seeking to broaden their knowledge beyond their respective fields.

The Explain GAI service is designed for:

- *researchers and scientists* who want to extend their knowledge beyond their own field. Artificial intelligence explanations help them to quickly understand key ideas in papers from other fields;
- *graduate students and researchers* who need to process large volumes of dense, complex documents, as simplified explanations allow for faster reading;
- *industry professionals* in technical positions who want access to the latest research and ideas, as the service makes the most recent article more accessible;
- *lifelong learners and knowledge seekers* who want to keep up to date, because Explain Paper makes complex documents accessible.

Downloading the content of Gemini's answer about examples of AI-powered hypotheses in Computer Science (Fig. 2) and selecting part of the text to get the GAI-generated explanation is shown in Fig. 6.

According to the ExplainPaper website, users can save time and improve the accuracy of their work by using this service [11]. This service has 63 alternatives, including Ask Your PDF, Brevity, HeyScience, Skimlt.ai, Summatity, SummaryBox, Docu-Ask, SciSpace Copilot, AI Next Assistant, Doks.ai, PDFAI.io, and others (https://topai.tools/alternatives/explainpaper).

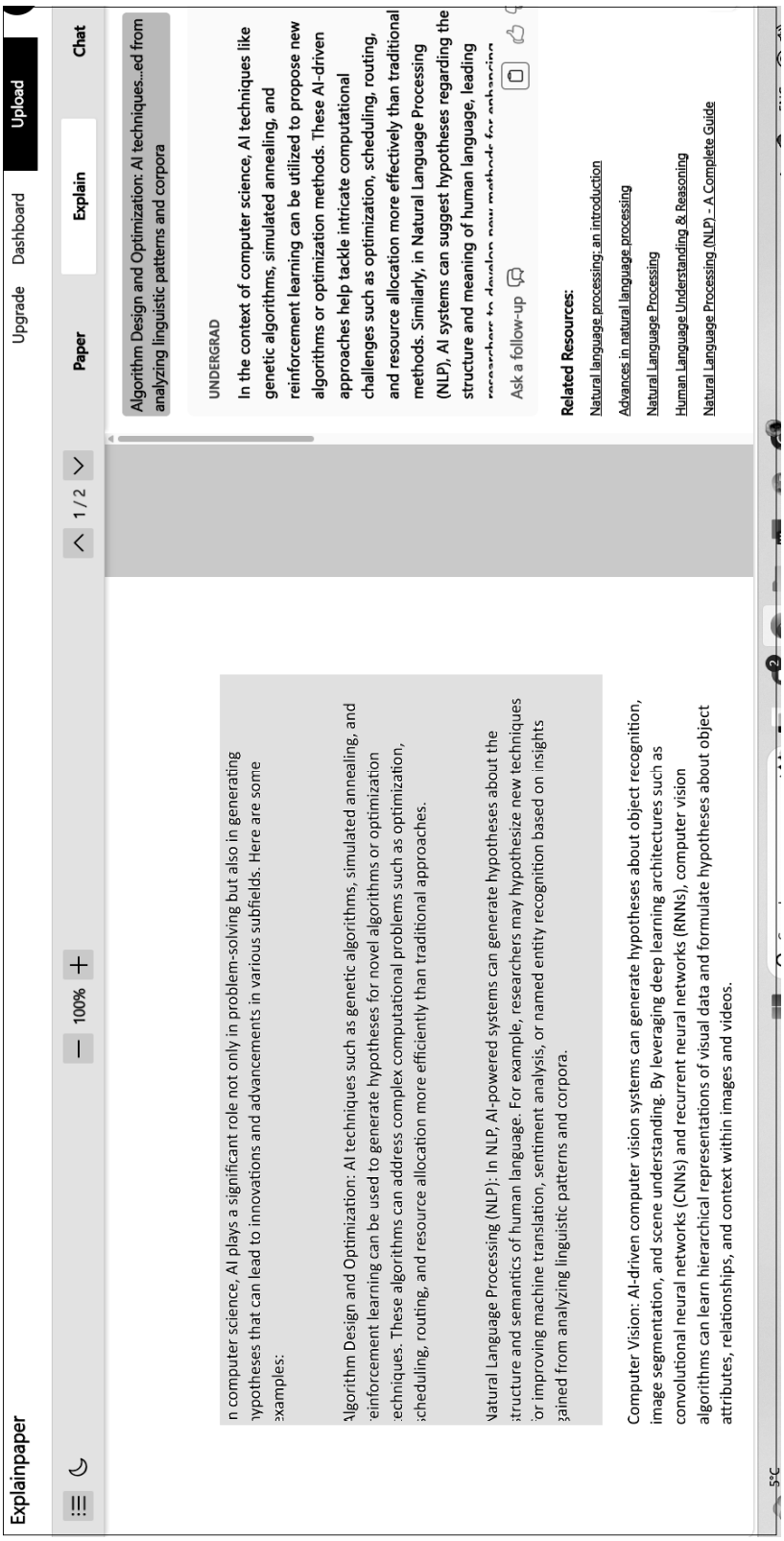

Fig. 6. Highlight a section of text in an article and its explanation

IntelliConsult. Project consulting/engineering

IntelliConsult (https://intelliconsultai.com/) uses the power of artificial intelligence to analyze project data and provide valuable information and recommendations for project optimization [12]. It can be used to easily create project plans, allocate resources and set realistic timeframes. *IntelliConsult* is easy to use thanks to its user-friendly interface. It guides you through the entire consulting process, making it easy to access the features and support you need. Fig. 7 shows the input interface for entering a description of the project for which the plan was developed (Fig. 8).

Fig. 7. The input interface for entering the project description

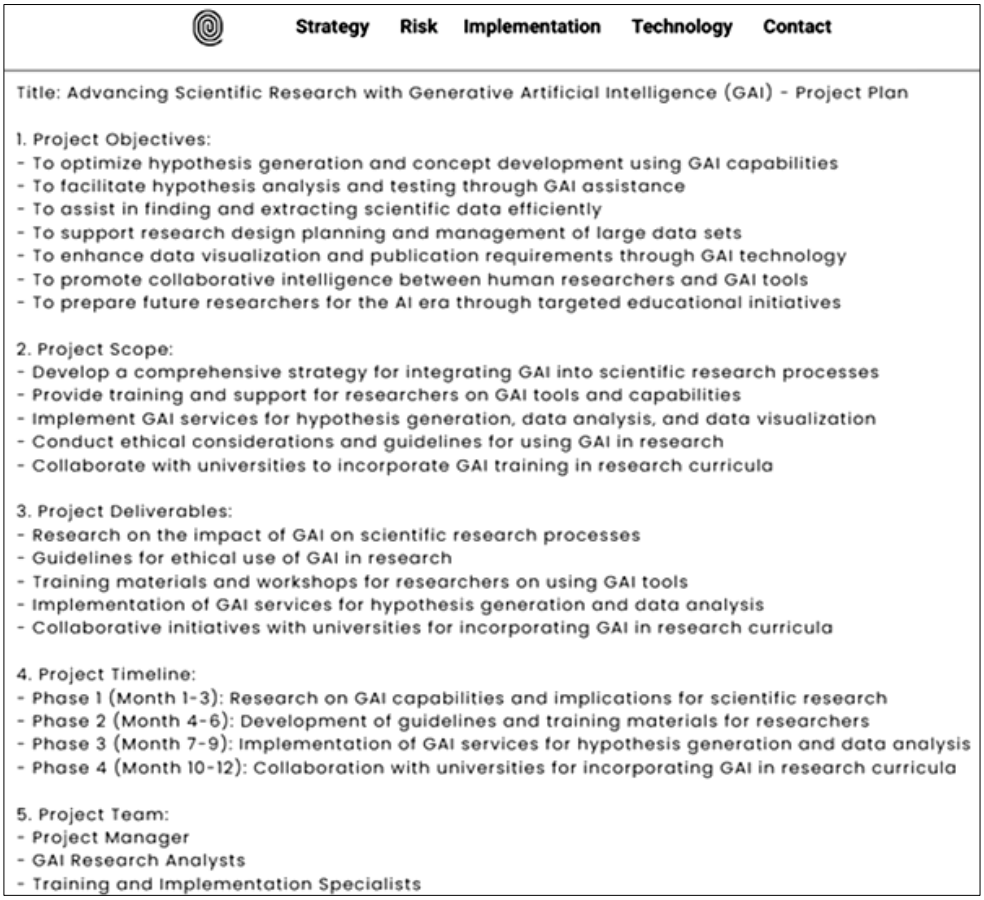

Fig. 8. Illustration of the results of developing individual strategies and justifying project decisions

The *IntelliConsult* service is a guide for achieving excellence in projects. It offers strategic project management and planning, risk analysis and management, project result optimization, and inspiration for innovation. This service provides project planning and strategic support throughout the entire project life cycle, thanks to the latest artificial intelligence technology.

According to https://theresanaiforthat.com/ai/intelliconsult /, *IntelliConsult* has 43 competitors, including *Wolfe, Gitsul Group, AI-Engageme, Consultant in, Strategic Mind, ProfitGPT, My Consultant, Peter Drucker, ai revolution, ConsultGPT, and AI Transform*.

Academic GPT. Writing scientific papers

AcademicGPT (https://academicgpt.net/) is an GAI service that helps professionals with the complex process of writing scientific papers [13]. Its artificial intelligence algorithms excel at generating annotations and concise abstracts, providing users with a significant increase in productivity. This service allows professionals to upload their papers in PDF format and use the power of GAI algorithms to improve their work. However, it is important to remember that while *AcademicGPT* is a powerful service, it should complement, not replace, thoughtful research writing.

First, a user uploads a draft of a research paper to *AcademicGPT* and selects one of three sections*: Write, Feedback* or *Explain*. In the drop-down menu "Choose which type of paper section the AI should write" (Fig. 9), you can select the type of task for which AcademicGPT should create content.

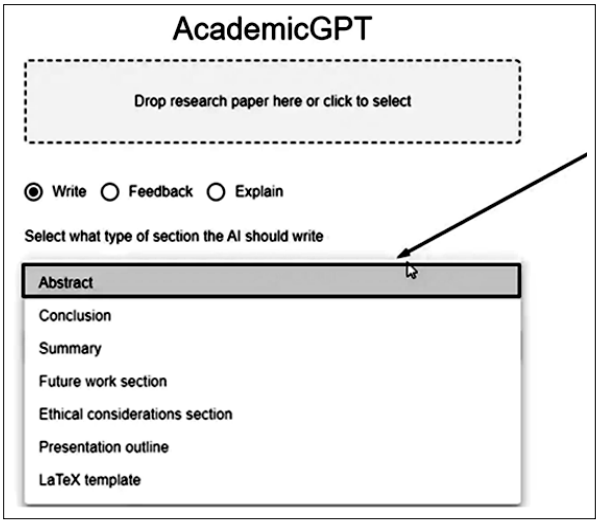

Fig. 9. Selecting a task in the "Write" section: abstract, conclusions, summary, future manuscript sections, ethical considerations section, online presentation, LaTeX format)

Next, in the "Feedback" and "Explain" sections, the user selects clear instructions or key points that AcademicGPT should follow when creating the content of his or her paper. In the Feedback section, the following instructions can be selected: Strength of Argument, Language, Coherence, Originality, Citation, and in the Explain section: Simple and Short, Simple and Long, Complex and Long, Complex and Short.

After entering the instructions, clicking on the Create button allows AcademicGPT to use its GAI capabilities to generate an abstract or any other appropriate academic section based on the requirements. Fig. 10 shows an example of an abstract for this article "The use of generative artificial intelligence (GAI) in scientific research".

Fig. 10. Illustration of the abstract been generated by GAI

If necessary, users can review or expand the generated content by reusing the *AcademicGPT* service and providing additional instructions or adjusting the initial input. Once the user is satisfied with the generated content, they can export it in the required format or copy and paste it into their research paper.

It is important to note that there are many alternative services available for this purpose, such as *Shutterstock, Grammarly, Gamma AI, CrushOn.AI, Runwayml, You, DeepAI, PixAI - AI Art Generator, MaxAI.me, and Simplified*. A comparison of their results with AcademicGPT is provided on the website https://www.toolify.ai/alternative/academicgpt.

***SlidesGPT*. Presentation/Publication of results**

SlidesGPT (https://slidesgpt.com/) is a GAI service that makes it easy to create slides for Google presentations, for example, the results of a research paper. To create a slide, you need to prepare a presentation plan or content source, then simply paste the text and get a presentation in seconds. It is possible to review the draft slides and make corrections or additions. Instead of just starting with a prompt, you can also ask the service to convert a PDF or web page into a presentation outline. With an intuitive interface, the service understands the user's presentation needs and helps them design slides that are both informative and attractive. It is ideal for professionals who need to quickly create powerful presentations, teachers who want to make educational content more engaging, or students preparing for academic projects.

Fig. 11 shows 4 out of 10 slides generated by *SlidesGPT* using the annotation from this article in Ukrainian.

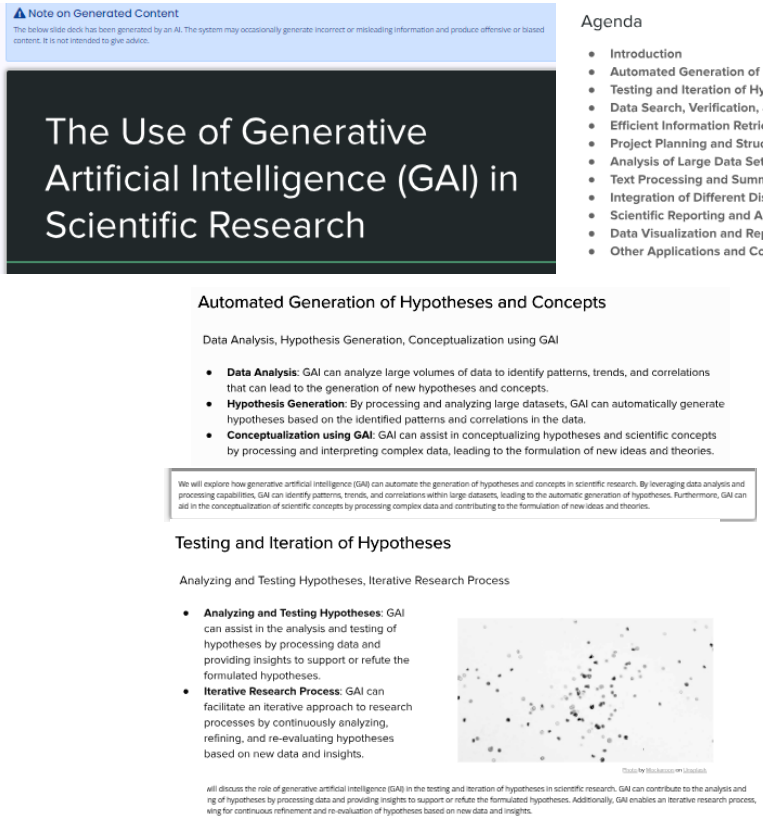

Fig. 11. Illustration of generated slides on the topic "The use of Generative Artificial Intelligence (GAI) in scientific research"

After viewing the generated presentation, the user has the opportunity to customize it according to their specific needs. They can edit the content, replace images, rearrange slides and make any necessary changes. *SlidesGPT's* GAI service is capable of creating doctoral-level presentations, including detailed, factual and specific information. It can integrate user-provided data into presentations, ensuring that the source data is accurate and up-to-date. Among the many alternative presentation services, *MagicSlides[14], SlidesAI, AhaSlides, SlidesGo, Beautiful AI, Invideo, Canva, Tome, Hitch, Gamma, Prezi and Syis* (https://ahaslides.com/blog/slides-ai-platforms/) are worth mentioning.

These five GAI services are valuable for both students and teachers, as they can enhance productivity and work quality while reducing the time and effort required for important tasks. In the fast-changing technological landscape and with the growing demands on the competencies of future professionals, clarity is especially crucial.

CONCLUSIONS

Generative Artificial Intelligence (GAI) is transforming scientific research. GAI offers a range of services to optimize hypothesis generation and concept devel-

opment, facilitate hypothesis analysis and testing, assist in finding and extracting scientific data, assist in research design planning, manage large data sets, perform translations and editing, meet journal publication requirements, create data visualizations, check for plagiarism, transcribe audio recordings, and generate summaries [15]. Expanding research capacity in this way improves personalized education by shifting from rote learning to critical thinking and problem-solving [8; 9]. Future research in this field should aim to develop methodologies for evaluating GAI-generated hypotheses that are both innovative and scientifically rigorous. One potential avenue for exploration is the design of GAI systems with explainable algorithms, which would offer transparency in their reasoning processes and make their hypotheses more understandable and acceptable to the scientific community.

The use of Generative Artificial Intelligence (GAI) in research and academia has both significant benefits and challenges. Tools such as *AcademicGPT* and *SlidesGPT* demonstrate the potential to empower people by simplifying the creation of scientific documents and presentations. With the help of AI services such as *Semantic Scholar* and *Explain Paper*, researchers can increase their access to knowledge, improve understanding and develop new hypotheses. However, despite these benefits, the implementation of GAI should be approached with caution, taking into account ethical considerations and the risk of data bias. Scientific institutions need to develop and refine guidelines for the responsible use of GAI, ensuring that it serves as a complement to human intelligence, not a replacement [16–19]. Many universities mentioned in [18] are equipped by GAI detection tools (e.g. *GPTZero, Turnitin, GPTKit, Winston AI*, etc.) [20]. By striking a balance between innovation and maintaining academic integrity, GAI can become a powerful ally in the pursuit of scientific progress and the evolution of educational practices.

REFERANCES

1. *Policy on the use of artificial intelligence for academic activities at Igor Sikorsky KPI*. Available: https://osvita.kpi.ua/sites/default/files/downloads/polityka-vykorystannia-shtuchnogo-intelektu_2023.pdf
2. *The policies for using artificial intelligence in education, teaching, and research at Kherson State University*. Available: https://www.kspu.edu/ File-Download.ashx?id=00653012-555c-46b2-bb64-05ba9bf26773
3. *The principles for using generative artificial intelligence at Zaporizhzhia Polytechnic National University*. Available*:* https://zp.edu.ua/uploads/pubdocs/2023/ Dekl_pro_pryn_vykor_heneratyvnoho_shtuchnoho_intelektu.pdf
4. M. Marienko, V. Kovalenko, "Artificial Intelligence and Open Science," *Physical and Mathematical Education*, vol. 38, no. 1, pp. 48–53, 2023. doi: 10.31110/2413-1571-2023-038-1-007
5. "AI is transforming how science is done. Science education must reflect this change," *SCIENCE*, vol. 382, issue 6677, 21 Dec 2023. doi: 10.1126/science.adm9788
6. Uttkarsha Bhosale, *AI-Driven Hypotheses: Real world examples exploring the potential and challenges of AI-generated hypotheses in science*. Available: https://www.enago.com/academy/ai-generated-research-hypothesis/
7. Tim Keary, *Artificial Superintelligence (ASI)*. Available: https://www. techopedia.com/definition/31619/artificial-superintelligence-asi
8. *Generative AI in Academic Research: Perspectives and Cultural Norms*. Available: https://research-and-innovation.cornell.edu/generative-ai-in-academic-research/

9. Yueqiao Jin, Lixiang Yan, Vanessa Echeverria, Dragan Gašević, and Roberto Martinez-Maldonado, *Generative AI in Higher Education: A Global Perspective of Institutional Adoption Policies and Guidelines*, arXiv:2405.11800v1 [cs.CY], 20 May 2024. Available: https://arxiv.org/pdf/2405.11800
10. *Semantic Scholar*. Available: https://www.wikidata.uk-ua.nina.az/Semantic_Scholar.html
11. *Enhance Your Research Paper Understanding with Explain Paper*. Available: https://www.toolify.ai/ai-news/enhance-your-research-paper-understanding-with-explain-paper-1069228
12. *IntelliConsult*. Available: https://www.stork.ai/ru/ai-tools/intelliconsult
13. *TopAI.tools*. Available: https://topai.tools/t/academicgpt
14. *Magic Slides*. Available: https://www.popularaitools.ai/tools/magic-slides
15. *Best Practices for Generative AI in Research*. Available: https://www.aje.com/arc/best-practices-generative-ai-in-research/
16. F. Miao, W. Holmes, *Guidance for generative AI in education and research*. 2023. Accessed on: February 5, 2024. Available: https://unesdoc.unesco.org/ark:/48223/pf0000386693
17. L. Yan et al., "*Practical and ethical challenges of large language models in education: A systematic scoping review*," British Journal of Educational Technology, 55, pp. 90–112, 2024.
18. B.L. Moorhouse, M.A. Yeo, and Y. Wan, "*Generative AI tools and assessment: Guidelines of the world's top-ranking universities*," Computers and Education Open, 5, 100151, 2023. Available: https://www.sciencedirect.com/science/ article/pii/S2666557323000290
19. M. Sullivan, A. Kelly, and P. McLaughlan, "*ChatGPT in higher education: considerations for academic integrity and student learning*," J. Appl. Learn. Teach., 6 (1), 2023. Available: https://doi.org/10.37074/jalt.2023.6.1.17
20. *9 Best Free AI Detectors for Teachers in 2024*. Available: https://www.classpoint.io/blog/best-free-ai-detectors-for-teachers

Received 30.05.2024

INFORMATION ON THE ARTICLE

Anatolii I. Petrenko, ORCID: 0000-0001-6712-7792, Educational and Research Institute for Applied System Analysis of the National Technical University of Ukraine "Igor Sikorsky Kyiv Polytechnic Institute", Ukraine, e-mail: tolja.petrenko@gmail.com

ВИКОРИСТАННЯ ГЕНЕРАТИВНОГО ШТУЧНОГО ІНТЕЛЕКТУ (ГШІ) В НАУКОВИХ ДОСЛІДЖЕННЯХ / А.І. Петренко

Анотація. Поява та зростаючі можливості генеративного штучного інтелекту (ГШІ) глибоко трансформують наукові дослідження. Хоча ГШІ розширює людський інтелект шляхом автоматизації певних завдань, він радше доповнює, ніж замінює людську креативність. Розглянуто наслідки ГШІ для наукового процесу, включаючи етичні міркування та необхідність збалансованого підходу, який об'єднує сильні сторони людського та штучного інтелекту в процесі відкриття знань і вирішення складних проблем. Обговорення поширюється на необхідність для університетів скорегувати навчальні програми для підготовки майбутніх дослідників до епохи ГШІ, підкреслюючи сценарне мислення та управління невизначеністю як важливі навики майбутнього.

Ключові слова: генеративний штучний інтелект, аналіз і тестування гіпотез, пошук джерел наукових даних, планування дослідження, написання і редагування наукових рукописів, упорядкування і презентація результатів.

UDC 004.852
DOI: 10.20535/SRIT.2308-8893.2024.3.09

REDUCING RISK FOR ASSISTIVE REINFORCEMENT LEARNING POLICIES WITH DIFFUSION MODELS

A. TYTARENKO

Abstract. Care-giving and assistive robotics, driven by advancements in AI, offer promising solutions to meet the growing demand for care, particularly in the context of increasing numbers of individuals requiring assistance. It creates a pressing need for efficient and safe assistive devices, particularly in light of heightened demand due to war-related injuries. While cost has been a barrier to accessibility, technological progress can democratize these solutions. Safety remains a paramount concern, especially given the intricate interactions between assistive robots and humans. This study explores the application of reinforcement learning (RL) and imitation learning in improving policy design for assistive robots. The proposed approach makes the risky policies safer without additional environmental interactions. The enhancement of the conventional RL approaches in tasks related to assistive robotics is demonstrated through experimentation using simulated environments.

Keywords: assistive robotics, reinforcement learning, diffusion models, imitation learning.

INTRODUCTION

Care-giving and assistive robotics are some of the most promising potential applications for AI systems. For decades already, it has been an active research field. This is certainly unsurprising, given the growing number of people who need care, which at some point may not be difficult to sattisfy in some countries [1; 2].

Moreover, given the circumstances of war actions in Ukraine, the demand will constantly grow. Tens of thousands of people will require rehabilitation, and some of them will require physical assistance for very long periods. To satisfy that demand, some amount of automation is certainly necessary. Although given the high costs of assistive devices, not everybody can afford them, the technological progress and drastic simplification of development and hardware requirements will help to democratize them and make them affordable.

One of the biggest concerns of that progress is safety [3]. At the moment, most devices employ sophisticated manually-designed policies and mechanisms to ensure robustness and safety. Since assistive robots interact with humans, it is desirable to reduce the risk, or in other words, improve the success rate.

One way of automating the policy design process is machine learning. For instance, reinforcement learning (RL) allows for policy learning from data of interaction with humans, which are difficult to rigorously model and predict [3; 4]. Manually designed policies have difficulties with such cases, as it's difficult to make them robust to the modeling errors.

This problem is amplified when humans can demonstrate only limited cooperation, such as in the case of people with disabilities. Cheap robotic arms (which

are more affordable) are also difficult to rigorously model, which makes vendors choose expensive hardware instead.

RL already has been applied to tasks that involve difficult-to-model physical tasks, such as ziplock bag manipulation [5] or cable manipulation [6]

However, RL policies often require millions of time steps for full convergence, and while the explored good trajectories are produced much earlier, it takes a while for the policies to stop breaking them for the sake of exploration.

In this paper, a way of not taking the burden of training an algorithm until full convergence, but rather collecting those first successful trajectories and using them to fit a robust policy is considered. This allows for reducing the risk of fairly non-robust policies without any additional interactions with the environment. It is demonstrated that this approach outperforms the bare model-free RL method in the tasks of assistive robotics, simulated using Assistive Gym [7].

PRELIMINARIES

Markov Decision Process (MDP) M is a tuple (S, A, r, T), where S — state space; A — action space; $r : S \times A \to R$ — reward function, $T = P(s_{t+1} \mid s_t, a_t)$ — probability that an environment will transition to the state s_{t+1} given that the current state is s_t and the action taken a_t.

Reinforcement Learning algorithm takes MDP M and searches for a policy π, that maximizes the discounted return objective:

$$\pi^* = \arg\max_\pi \mathrm{E}_{\tau \sim p(\cdot)} \sum_{t=0}^{\infty} \gamma r(s_t, a_t).$$

Here τ is a trajectory $(x_0, a_0, x_1, a_1, \ldots x_T)$ usually sampled by applying a policy π.

Model-free reinforcement learning algorithms are considered, namely Actor–Critic, which learns a value function $v(s)$ and a policy function $\pi(a \mid s)$. The latter is often minimized using the former for the advantage estimation. There are multiple instances of the Actor–Critic algorithm. For instance, Proximal Policy Optimization [8] or A3C [9].

Also diffusion models for policy fitting are considered. Namely, Denoising Diffusion Probabilistic Models (DDPM), which are generative models based on Stochastic Langevin Dynamics [10].

The idea is to fit a noise-predicting network ε_θ, that predicts a gradient $\nabla E(x)$. This gradient is computed and applied repeatedly

$$x' = x - \gamma \nabla E(x)$$

to recover an input x_0 from its noised version x_K. These models are trained on a set of inputs and then are used to generate novel inputs from pure noise. This approach to imitation learning is a focus of [11]

For assistive robotics, Assistive Gym [7] is used. It is modified it to be more suitable for using it with diffusion policies. See the Experimental Validation section for details.

METHOD

First, a model-free reinforcement learning algorithm is employed to discover successful trajectories. Proximal Policy Optimization (PPO) algorithm is chosed in this paper, as it is widely used and is very easy to apply. That algorithm collects the trajectories by interacting with an environment and fits its policy function by minimizing the following loss:

$$L_{PPO}(\phi) = \mathrm{E}_{\tau \sim p_{\phi}(\cdot)} \min(r_t A_t, clip(r_t, 1-\varepsilon_t, 1+\varepsilon_t) A_t) .$$

Specifically, a fully connected network with ReLU activation functions is used to approximate the policy/value functions. This decision was made because a low dimensional state is being observed instead of images (Fig.1).

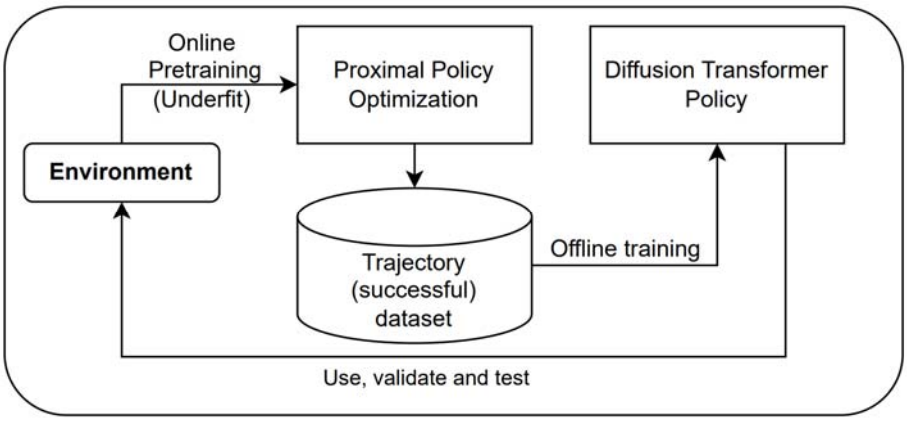

Fig. 1. A diagram schematic of a proposed algorithm. First, a baseline online RL policy is pretrained, then successful trajectories are sampled, and a diffusion policies algorithm is fine-tuned on those in an offline manner

A PPO is trained as a baseline. The problem with PPO is that it requires a lot of samples, which is often too expensive (in computing) or dangerous (when applied in the real-world setting). Therefore, it is trained for a fixed number of time steps, stopping it often way before the full convergence.

When applied to assistive robotics tasks, PPO produces high-risk policies, as evidenced by experiments (see EXPERIMENTAL VALIDATION section).

To reduce the risk, successful trajectories produced by high-risk PPO-based policies are selected and imitation learning techniques based on diffusion models are applied.

$r_s(s_i)$ is defined as a new reward function, which may be different from the original and is binary, meaning it is either 1 or 0. For instance, in the Assistive Feeding task, success is defined like a predicate “The food on a spoon is safely placed in the mouth of a human within 10 seconds”. This sparse reward is given right before the episode’s termination. For brevity, denote

$$r_s(\tau) = \sum_{s_i \in \tau} r_s(s_i) .$$

Also, define $\pi_\theta(a \mid s, success)$ as a policy conditioned on (a, s) being a part of the successful trajectory. This approach is inspired by control as inference problem statement [12].

Suppose a PPO policy π_θ is trained. If one takes

$$p_\phi(\tau \mid success) = p(s_0)\prod_{i=1}^{T}\pi_\phi(a_i \mid s_i, success)p(s_i \mid s_{i-1}, a_{i-1})$$

and fits the Diffusion Policy on $(s,a) \sim p_\phi(\tau \mid success)$, they'd arrive to a much more robust policy, given the assumption that the set of successful trajectories is enough to cover the stochasticity and uncertainty of the environment. For the robotics tasks considered, this assumption tends to be true in practice.

The diffusion policy is approximated using a diffusion transformer architecture, proposed in [11]. It is simplified a bit for the environments with shorter trajectories. Also, it has been found that U-Net-based architectures give almost the same results, so it is not include them in this study.

Algorithm. Let's summarize an algorithm described earlier.

1. Train a PPO policy for T_{PPO} time steps.
2. Sample a dataset of trajectories using a pre-trained PPO policy
$$D = \{\tau_i, i = 1,...,N \mid \tau_i \sim p_{PPO}(\tau)\}.$$
3. Sample a dataset of successful trajectories
$$D_{succ} = \{\tau \mid \tau \in D, r_s(\tau) = 1\}.$$
4. Initialize the weights of a neural net θ.
5. Repeat for M epochs:

retrieve a batch of trajectories B from the dataset

$$B = \{(s_k, a_k, ..., s_{k+T}, a_{k+T})_i, i = 1,...,N_B\};$$

following [11] set $A = (a_k, ..., a_{k+T})$ and $O = (s_k, ..., s_{k+T})$, and minimize the DDPM training loss:

$$L_{DDPM}(B) = MSE(\varepsilon^k, \varepsilon_\theta(O_t, A_t + \varepsilon^k, k)); \quad \theta' = \theta - \gamma\nabla L_{DDPM}(B);$$

update neural networks' parameters:

$$\theta' \leftarrow \theta;$$

Here:

T_{PPO} — num timesteps for the PPO to be trained on;

N — number of all samples from the PPO policy;

N_B — batch size for the diffusion model;

γ — learning rate;

T — Diffusion Policy horizon. Can also be different for actions and observations. Actions of this horizon are predicted conditioned on observations.

For a neural network architecture, the Diffusion Transformer [11] architecture is used (Fig. 2).

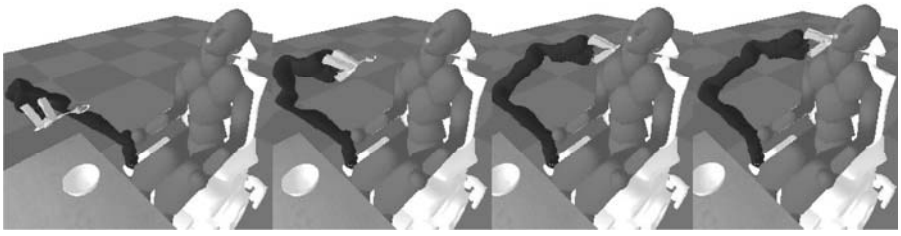

Fig. 2. A trajectory produced by the policy trained using the proposed method. The task — Assistive Feeding

EXPERIMENTAL VALIDATION

For experimental validation, Assistive Gym [7] simulation benchmark is used. The observation space usually contains a low dimensional arm state, human head state, and some other task- or tool-related statistics. All the tasks are done using the simulated Jaco robot arm. The proposed method is evaluated on the following tasks:

1. **Assistive Feeding**. A task where a robotic arm uses a spoon full of food to feed a person. The task is considered successful if 75% of food is in the person's mouth. The resulting trajectory is depicted in Fig. 2.

2. **Assistive Drinking**. A task where a robotic arm uses a cup full of water to assist a person with drinking. The task is considered successful if 75% of water is in the person's mouth.

3. **Assistive Bed Bathing**. A task where a robotic arm uses a sponge to wash a person. The task is considered successful if the necessary spots of a person's surface are touched with a sponge.

4. **Assistive Arm Manipulation**. A task where a robotic arm is used to reposition a person's arm. The task is considered successful, if the arm is successfully repositioned.

First, a PPO baseline is trained until it is sufficient for a policy to produce successful trajectories. In the study, 1000 successful trajectories have been collected for each task. It has been found, that for many tasks, the number of trajectories less than 300 degrades the performance of the method.

After that, sample successful trajectories are sampled from the PPO policy, as described in Algorithm 1, and a diffusion policy is fit on those.

The results are given in Table.

Results of fine-tuning the PPO policies with the proposed method

Task	**Success (%)**	
	PPO risky, %	Fine-tuned (proposed), %
Arm Manipulation	19	71
Bed Bathing	2	12
Drinking	10	56
Feeding	33	86

Arm Manipulation and Drinking PPO is trained for 1 million steps. Bed Bathing PPO is trained for 2 million steps (to get any reasonable policies). Feeding PPO is trained for 400k steps. Please note, in order to improve baseline and diffusion performance, episodes are terminated if success is achieved. Originally, termination only occurred when the number of steps exceeded a limit. It's been found that this affects the method's performance

As one may observe, the resulting policy outperforms the underfit ones, but also performs as good or better than the long-trained PPO policy. Remarkably, this is achieved without any additional environment steps, just using the offline data. One may also sample those trajectories during the training of a baseline, thus removing the need to sample them afterward.

The results that good could be explained by the properties of the modern imitation learning techniques, such as diffusion policy, used in this paper. It has

been observed, that these methods demonstrate interesting out-of-distribution generalizations [5].

It is also apparent, that the Bed Bathing benchmark though is improved, but still is not beaten. It is hypothesized, that this is due to a low diversity of the collected trajectories, insufficient to cover the entire distribution.

In addition to generalization, it is hypothesized, that since the PPO itself balances exploration and exploitation, this may prevent it from fast convergence on successful trajectories, continuously trying to look for other modalities.

Another interesting observation is that when the PPO baseline is trained until full convergence using up to several million steps, it usually gets on-par performance with the fine-tuned version. Although, on the Feeding benchmark fully converged PPO got an 87% success rate, while its fine-tuned version achieved 98%. But even without that, it's still a much worse result than the fine-tuned approach, since it requires additional millions of time steps.

CONCLUSION

In this paper, a novel approach to reduce risk in assistive reinforcement learning policies using diffusion models is proposed. The proposed method leverages the strengths of both model-free reinforcement learning and imitation learning techniques based on diffusion models to improve policy robustness without additional interactions with the environment.

The effectiveness of the proposed approach is demonstrated through experimental validation on various assistive robotics tasks simulated using Assistive Gym. By fine-tuning policies obtained from a baseline PPO algorithm with offline data, significant improvements in success rates are achieved across different tasks. Importantly, the method outperformed risky policies generated directly by PPO.

The results indicate the potential of diffusion-based imitation learning techniques in enhancing the safety and reliability of assistive robotics systems.

Future work could explore additional refinements to the diffusion-based policy fitting process and include re-exploration iteration for diffusion policies, to make the process iteratively switch between fine-tuning and exploration.

REFERENCES

1. D.M. Taylor, "Americans with disabilities: 2014," *US Census Bureau*, pp. 1–32, 2018.
2. J. Broekens et al., "Assistive social robots in elderly care: A review," *Gerontechnology*, vol. 8, no. 2, pp. 94–103, 2009.
3. R. Ye et al., "Rcare world: A human-centric simulation world for care-giving robots," in *2022 IEEE/RSJ International Conference on Intel-ligent Robots and Systems (IROS), IEEE, 2022*, pp. 33–40.
4. J.Z.-Y. He, Z. Erickson, D.S. Brown, A. Raghunathan, and A. Dragan, "Learning representations that enable generalization in assistive tasks," in *Conference on Robot Learning, PMLR, 2023*, pp. 2105–2114.
5. Z. Fu, T.Z. Zhao, and C. Finn, "Mobile aloha: Learning bimanual mobile manipulation with low-cost whole-body teleoperation," *arXiv preprint*, 2024. doi: https://doi.org/10.48550/arXiv.2401.02117
6. J. Luo et al., "Serl: A software suite for sample-efficient robotic rein-forcement learning," *arXiv preprint*, 2024. doi: https://doi.org/10.48550/arXiv.2401.16013

7. Z. Erickson, V. Gangaram, A. Kapusta, C.K. Liu, and C.C. Kemp, “Assistive gym: A physics simulation framework for assistive robotics,” in *2020 IEEE International Conference on Robotics and Automation (ICRA), IEEE, 2020*, pp. 10 169–10 176.
8. J. Schulman, F. Wolski, P. Dhariwal, A. Radford, and O. Klimov, “Proximal policy optimization algorithms,” *arXiv preprint*, 2017. doi: https://doi.org/10.48550/arXiv.1707.06347
9. V. Mnih et al., “Asynchronous methods for deep reinforcement learn-ing,” in *International Conference on Machine Learning, PMLR, 2016*, pp. 1928–1937.
10. M. Welling and Y.W. Teh, “Bayesian learning via stochastic gradient langevin dynamics,” in *Proceedings of the 28th International Conference on Machine Learning (ICML-11), Citeseer, 2011*, pp. 681–688.
11. S. Levine, “Reinforcement learning and control as probabilistic infer-ence: Tutorial and review,” *arXiv preprint*, 2018. doi: https://doi.org/10.48550/arXiv.1805.00909
12. C. Chi et al., “Diffusion policy: Visuomotor policy learning via action diffusion,” *arXiv preprint*, 2023. doi: https://doi.org/10.48550/arXiv.2303.04137

Received 05.02.2024

INFORMATION ON THE ARTICLE

Andrii M. Tytarenko, ORCID: 0000-0002-8265-642X, Educational and Research Institute for Applied System Analysis of the National Technical University of Ukraine “Igor Sikorsky Kyiv Polytechnic Institute”, Ukraine, e-mail: titarenkoan@gmail.com

ЗНИЖЕННЯ РИЗИКІВ СТРАТЕГІЙ НАВЧАННЯ З ПІДКРІПЛЕННЯМ ДЛЯ ДОГЛЯДУ ІЗ ДИФУЗІЙНИМИ МОДЕЛЯМИ / А.М. Титаренко

Анотація. Допоміжна робототехніка для догляду, що розвивається завдяки досягненням штучного інтелекту, являє собою перспективу для вирішення зростаючого попиту на догляд, особливо в контексті збільшення кількості осіб, які його потребують. Ефективні та безпечні допоміжні пристрої могли б стати корисними, особливо в контексті підвищеного попиту через травми, пов'язані з війною. Хоча вартість є бар'єром для доступності, технологічний прогрес може зробити їх більш доступними. Безпека є найважливішою проблемою, особливо з огляду на модельну складність взаємодії між роботами та людьми. Досліджено застосування навчання з підкріпленням та навчання імітацією для поліпшення процесу проєктування стратегій для асистентних роботів. Запропонований підхід допомагає зробити неробастні стратегії підвищеного ризику більш безпечними без додаткових взаємодій із середовищем. Шляхом експериментів у симульованих середовищах продемонстровано перевагу, яку цей підхід дає в поєднанні з традиційними методами навчання з підкріпленням у завданнях, пов'язаних з допоміжною робототехнікою.

Ключові слова: допоміжна робототехніка, навчання з підкріпленням, дифузійні моделі, навчання імітацією.

ВІДОМОСТІ ПРО АВТОРІВ

Городецький Віктор Георгійович,

доцент, кандидат фізико-математичних наук, доцент кафедри автоматизації електротехнічних та мехатронних комплексів Навчально-наукового інституту енергозбереження та енергоменеджменту КПІ ім. Ігоря Сікорського, Україна, Київ

Горчаков Олексій Олександрович,

аспірант Відділу математичних проблем механіки та теорії керування Інституту математики НАН України, Київ

Єгошина Анна Анатоліївна,

доцент, кандидат технічних наук, викладач комп'ютерних наук Північно-західної політехніки, Канада, Гранде Преері

Кольцов Дмитро Романович,

магістр, аспірант кафедри прикладної математики КПІ ім. Ігоря Сікорського, Україна, Київ

Кузьміна Олена Михайлівна,

доцент, кандидат технічних наук, доцент кафедри економічної кібернетики та інформаційних систем Вінницького торговельно-економічного інституту Державного торговельно-економічного університету, Україна, Вінниця

Мазурик Роман Володимирович,

магістр, аспірант кафедри прикладної математики КПІ ім. Ігоря Сікорського, Україна, Київ

Малий Олександр Юрійович,

доцент, кандидат технічних наук, в.о. завідувача кафедри інформаційних технологій електронних засобів Національного університету «Запорізька політехніка», Україна, Запоріжжя

Мельник Ігор Віталійович,

професор, доктор технічних наук, професор кафедри електронних пристроїв та систем факультету електроніки КПІ ім. Ігоря Сікорського, Україна, Київ

Мороз Гаррі Володимирович,

старший викладач кафедри радіотехніки та телекомунікацій Національного університету «Запорізька політехніка», Україна, Запоріжжя

Ориняк Ігор Володимирович,

професор, доктор технічних наук, професор кафедри прикладної математики КПІ ім. Ігоря Сікорського, Україна, Київ

Петренко Анатолій Іванович,

професор, доктор технічних наук, професор кафедри системного проектування ІПСА КПІ ім. Ігоря Сікорського, Україна, Київ

Починок Аліна Володимирівна,

кандидат технічних наук, старший науковий співробітник Науково-дослідного інституту електроніки та мікросистемної техніки КПІ ім. Ігоря Сікорського, Україна, Київ

Романюк Вадим Васильович,

професор, доктор технічних наук, професор кафедри економічної кібернетики та інформаційних систем Вінницького торговельно-економічного інституту Державного торговельно-економічного університету, Україна, Вінниця

Скрипка Михайло Юрійович,

аспірант кафедри електронних пристроїв та систем факультету електроніки КПІ ім. Ігоря Сікорського, Україна, Київ

Титаренко Андрій Миколайович,

аспірант ІПСА КПІ ім. Ігоря Сікорського, Україна, Київ

Фарафонов Олексій Юрійович,

доцент, кандидат технічних наук, доцент кафедри інформаційних технологій електронних засобів Національного університету «Запорізька політехніка», Україна, Запоріжжя

Федін Сергій Сергійович,

професор, доктор технічних наук, професор кафедри інформаційних систем і технологій Національного транспортного університету, Україна, Київ

Флис Ігор Михайлович,

доцент, кандидат технічних наук, професор кафедри наземної артилерії Національної академії Сухопутних військ імені гетьмана Петра Сагайдачного, Україна, Львів

Фурманова Наталія Іванівна,

доцент, кандидат технічних наук, декан факультету інформаційної безпеки та електронних комунікацій Національного університету «Запорізька політехніка», Україна, Запоріжжя

Чертов Олег Романович,

професор, доктор технічних наук, завідувач кафедри прикладної математики КПІ ім. Ігоря Сікорського, Україна, Київ

Швець Олександр Юрійович,

професор, доктор фізико-математичних наук, професор кафедри математичної фізики та диференціальних рівнянь фізико-математичного факультету КПІ ім. Ігоря Сікорського, Україна, Київ

Яблонський Петро Миколайович,

доцент, кандидат технічних наук, доцент кафедри нарисної геометрії, інженерної та комп'ютерної графіки КПІ ім. Ігоря Сікорського, Україна, Київ

Яковенко Вадим Віталійович,

старший науковий співробітник, доктор технічних наук, професор кафедри управління діями підрозділів десантно-штурмових військ та морської піхоти Військової академії, Україна, Одеса

Яремко Світлана Анатоліївна,

доцент, кандидат технічних наук, доцент кафедри економічної кібернетики та інформаційних систем Вінницького торговельно-економічного інституту Державного торговельно-економічного університету, Україна, Вінниця